

FACULDADE DE ENGENHARIA DA UNIVERSIDADE DO PORTO

Timing Analysis of Real-Time Systems Considering the Contention on the Shared Interconnection Network in Multicores

Dakshina Dasari



Doctoral Programme in Electrical and Computer Engineering

Supervisor: Dr. Vincent Nélis

May 14, 2014

**Timing Analysis of Real-Time Systems Considering
the Contention on the Shared Interconnection
Network in Multicores**

Dakshina Dasari

Doctoral Programme in Electrical and Computer Engineering

May 14, 2014

Abstract

Multicore technology has been heralded as one of the course-changing computing technologies, providing new levels of energy-efficient performance, enabled by advanced parallel processing and miniaturization techniques. This is evident by the fact that every leading chip designer has a multicore processor as a part of its product offerings and also by witnessing the proliferation of this technology across the entire range of embedded devices. Real-time embedded systems are no exception to this trend either. By definition, a key requirement for real-time embedded systems is to be able to deliver their functional behaviour within specific time bounds. However, while the computational capabilities of multicores are indisputable, they must be assessed for their predictability before employing them to host real-time applications which have strict timing requirements. While the study of timing analysis for uniprocessors is in its mature stages, given the decades of research dedicated to it, the timing analysis in the domain of multicores is still in its nascent stages.

The broader focus of this thesis is to address the timing analysis challenge in multicores: specifically on determining the impact of shared resources like the shared bus (or NoC's in many-core systems) on the execution time of the real-time tasks, when deployed on these multicores. To elaborate, in typical implementation of multicore systems, multiple cores access the main memory via a shared channel (like the front side bus). This often leads to contention on this shared channel, which results in an increase of the execution time and the response time of the tasks. Computing the upper bounds on these timing parameters is a vital prerequisite for the deployment of real-time tasks on these multicores and is an relatively new area of research. The work in this thesis aims at meeting this objective of providing and validating methods for the timing analysis of applications executed on multicore and many-core platforms which inherently do not guarantee predictability.

The main contributions include proposing a model to derive the memory profile of tasks and the memory request profile of a core for a given time interval. This is extended further to propose a general framework to model the availability of the shared bus, using the memory profile of the analyzed task in finer granularity and to be able to deal with different bus arbitration mechanisms. This work has also been extended to the realm of the "Many-Core" systems, by proposing a method to derive the worst-case traversal time for a mesh-based interconnect network. The thesis also delves into memory controller analysis and as an interesting case study provides temporal analysis of Phase change memory based multicore systems, which unlike DRAM based systems, have noticeably different read and write latencies.

Resumo

As tecnologias baseadas em sistemas multi-processador estão a mudar os sistemas computacionais, proporcionando novos níveis de desempenho na eficiência energética, devido à utilização de técnicas avançadas de processamento paralelo e miniaturização dos componentes. Isto é evidenciado pelo facto de todos os principais construtores de processadores terem nas suas linhas de produtos, processadores baseados na arquitectura multi-processador. Também se tem verificado uma massificação da utilização deste tipo de processadores em sistemas embebidos, em geral, e, mais especificamente, também nos sistemas embebidos utilizados em sistemas de tempo real. Por definição, um sistema de tempo real deve produzir correctamente os resultados dentro de um limite temporal, isto é, os resultados só são válidos se forem disponibilizados dentro intervalos de tempo bem definidos. Apesar de os sistemas multi-processador não suscitarem muitas dúvidas em relação à sua capacidade de processamento, estes devem ser estudados e avaliados por forma a garantir que as restrições temporais (apresentadas pelos sistemas de tempo real) são garantidas. Enquanto que o estudo da análise temporal para sistemas uni-processador está num estado considerado maduro, fruto da várias décadas de investigação dedicadas a este tipo de sistemas, a análise temporal para sistemas multi-processador está ainda num estado inicial.

Em sentido lato, nesta dissertação são endereçados os desafios associados à análise temporal para sistemas multi-processador. Em detalhe, é determinado o impacto dos recursos partilhados, como por exemplo o barramento de acesso à memória partilhado pelos vários processadores, no tempo de execução das tarefas (constituintes do sistema de tempo real). Tipicamente, num sistema multi-processador, os vários processadores acedem à memória principal através de um único canal (ou barramento), logo é partilhado por todos. A utilização deste canal é exclusiva, o que implica que estes processadores disputam-no sempre que pretendem aceder à memória principal. Ora, isto tem impacto quer no tempo de execução quer no tempo de resposta das tarefas. Determinar os limites temporais máximos associados, por exemplo, à utilização do canal de acesso à memória é um pré-requisito vital para assegurar que as restrições temporais das tarefas são garantidas. E desta forma assegurar o correcto desempenho de um sistema de tempo real numa arquitectura multi-processador. O trabalho apresentado nesta dissertação tem como objectivo definir e validar métodos de análise temporal para aplicações de tempo real a executar em arquitecturas multi-processador. Para tal foi criado um sistema genérico que permite modelar a disponibilidade do canal partilhado (com baseperfis de memória das tarefas) independente da política usada no acesso ao canal partilhado.

As principais contribuições incluem a proposta de um modelo para derivar perfis de uso da memória por parte das tarefas e perfis dos pedidos de acesso à memória por parte dos processadores num determinado intervalo temporal. Com a informação obtida por esse modelos é possível efectuar uma análise baseada no tempo de resposta das tarefas.

Este trabalho foi também estendido para suportar sistemas multi-processador cuja interligação entre os processadores e a memória é baseada numa rede com uma configuração em malha. No decorrer do trabalho desenvolvido no contexto desta dissertação foi efectuada uma análise de controladores de memória e como caso de estudo é apresentada uma análise temporal para sistemas baseados PCM (*Phase-Change Memory*) em arquitecturas multi-processador, que contrariamente aos sistemas baseados em DRAM (*Dynamic Random Access Memory*), tem diferentes latências nas operações de leitura e escrita.

Acknowledgments

Feeling gratitude and not expressing it is like wrapping a present and not giving it.

William Arthur Ward

Reaching this milestone would have not been possible without the support of many people. An exceptional friend and advisor, Vincent Nélis to whom I offer my heartfelt gratitude for his excellent guidance, patience, constructive reviews and for unconditionally standing by me throughout this journey. I would like to thank Eduardo Tovar who went the extra mile to ensure a conducive research environment and was always approachable. I have had the privilege of collaborating with Arvind Easwaran, Bjorn Andersson, Stefan M. Petters, Borislav Nikolic, Daniel Mosse and Benny Akesson along with Vincent at different phases of my research. I will forever treasure the interactions with them; their energy, technical acumen and enthusiasm was contagious and the teamwork saw us through various obstacles.

I would like to acknowledge Paulo Baltarejo Sousa for translating the abstract of the thesis in Portuguese. Thanks to the administration and the technical staff at CISTER for handling all the related glitches and providing a smooth work environment.

I feel lucky to be sharing my workspace with Boris, Artem, Ali, Kos, Guru and Jose, who were competitive, worked hard and partied harder – with these people around, it was always great to be at the lab. The drabness and monotony in life were superseded by the increased fun quotient during this phase, thanks to colleagues and friends, especially Patrick, Geoffrey, Vikram, Ali, Shashank, Ganga, Sujit, Anuj, Kiran and Kritika – I will always cherish the delicious dinners and board-game evenings!

My family has been extremely supportive of my work and I could not be here without them. Finally, these acknowledgements would be incomplete without whole heartedly thanking Guru, my husband, colleague, my best friend. Life has been a joyful roller-coaster ride with you around. Thanks for the wonderful dinners you made whenever I had deadlines and arrived late. Thanks for just being there for me and with me, whenever I needed you.

This work was partially supported by FCT (Fundação para a Ciência e Tecnologia) under the individual doctoral grant SFRH / BD / 71169 / 2010.

List of Author's Publications

This is a list of papers and publications that reflects the results achieved during the development of the research work presented in this dissertation. A significant part of this thesis is compiled from these papers and publications.

Journals

- Dakshina Dasari, Borislav Nikolic, Vincent Nélis and Stefan M. Petters, “NoC Contention Analysis using a Branch and Prune Algorithm”, *ACM Transaction on Embedded Computing* (Accepted for publication).

Conferences

- Dakshina Dasari, Vincent Nélis and Daniel Mosse, “Timing analysis of PCM Main Memory in Multicore Systems”, *In Proceedings of the 19th IEEE International Conference on Embedded and Real-Time Computing Systems and Applications (RTCSA 2013)*.
- Dakshina Dasari, Benny Åkesson, Vincent Nélis, Muhammad Ali Awan, Stefan M. Petters, “Identifying the Sources of Unpredictability in COTS-based Multicore Systems”, *In Proceedings of the 8th IEEE International Symposium on Industrial Embedded Systems (SIES 2013)*,
- Dakshina Dasari and Vincent Nélis, “An Analysis of the Impact of Bus Contention on the WCET in Multicores”, *In Proceedings of the 9th IEEE International Conference on Embedded Software and Systems (ICESS-2012)*,
- Dakshina Dasari, Björn Andersson, Vincent Nélis, Stefan M. Petters, Arvind Easwaran and Jinkyu Lee, “Response Time Analysis of COTS-Based Multicores Considering The Contention On The Shared Memory Bus”, *In Proceedings of the 8th IEEE International Conference on Embedded Software and Systems (IEEE ICES-11)*,

Under Submission

- Dakshina Dasari, Vincent Nélis, and Benny Åkesson, “Unified Framework for Bus Contention Analysis in Multicores”

Contents

1	Introduction	1
1.1	Introduction to Embedded systems	1
1.2	Real-Time Embedded Systems	3
1.3	Paradigm shifts in the design of embedded systems	9
1.4	Computing Platforms	11
1.5	Overview of a typical many core system	16
1.6	Problems addressed in this thesis	19
1.7	Motivation and Relevance of this work	22
1.8	Thesis Organization	28
2	Background and Related work	31
2.1	Timing Analysis	31
2.2	Timing Analysis: Uniprocessors to Multicore systems	34
2.3	Related Work	48
2.4	Scope for further work	53
3	Computing Per-Task and Per-Core Memory Request Profiles	57
3.1	Introduction	57
3.2	System and Task Model	61
3.3	Per-Task Cache Analysis	62
3.4	Per-Task Memory Profile Analysis	64
3.5	Per-Core Memory Profile Analysis	69
3.6	Computation of the Per-Core Request Profile	73
3.7	Correctness and properties of the $PCR\mathcal{P}_p(t)$ function	78
3.8	Optimization and Computational Complexity	81
3.9	Adaptations of $PCR\mathcal{P}()$ and Integration with existing work	83
3.10	$PCR\mathcal{P}$ case study: WCET analysis	86
3.11	System wide Analysis	88
3.12	Performance Comparison: Simulations	89
3.13	A method to obtain the parameters experimentally	94
3.14	Chapter Summary	97
4	Unified Framework for Bus Contention Analysis in Multicores	99
4.1	System and Task Modeling	100
4.2	Overview of Approach	103
4.3	Step 1: Modeling the Availability of the Bus	107
4.4	Step 2: Find the maximum cumulative delay for a given request-set mapping	111
4.5	Step 3: Finding the worst-case assignment	112

4.6	Step 4: Region-Wise Analysis	125
4.7	Related Work	129
4.8	Experimental Results	130
4.9	Conclusion	133
5	Bus Contention Analysis of Phase Change Memory based Multicores	135
5.1	Introduction to Phase Change Memory	135
5.2	Related Work	137
5.3	Model of computation	138
5.4	An Initial Approach to the Problem	141
5.5	An Upper Bound on the external interference	142
5.6	Summary of the evaluations	152
5.7	Chapter Summary	156
6	NoC Contention Analysis of Many Core Systems	157
6.1	Introduction to many-core systems	157
6.2	Related Work	159
6.3	System Model	162
6.4	Input Traffic Characterization Functions	167
6.5	Conceptual description of existing RC based methods	169
6.6	Proposed method for tighter WCTT	170
6.7	The Branch and Prune Algorithm	173
6.8	A more efficient algorithm: Branch, Prune and Collapse	179
6.9	Simulations and Results	183
6.10	Conclusions	192
7	Thesis Summary, Reflections and Future Work	193
7.1	Summary of the work	194
7.2	Limitations of current work and future directions	197

Chapter 1

Introduction

“Technology is the campfire around which we tell our stories.”

Laurie Anderson

1.1 Introduction to Embedded systems

A host of scientific inventions in the past decades have been vital in transforming the world from one inhabited by mankind to one which is strewn around with electronic and computing systems. The prevalence of these devices in our lives is so ubiquitous that it would not be far-fetched to state that we live in a world dominated by computing devices – from simple ones like a pre-set alarm in a cell-phone which heralds the dawn, pacemakers implanted within the human body to regulate and monitor heartbeats, to high end systems like space-ships which can literally transport us to another world. As an informed and curious species that we claim to be, an insight into these co-habiting devices is therefore warranted to understand their inner workings. Given the whole range of these systems, we shall focus on a specific set of these which are called “embedded systems”.

Although it belongs to the broader category of systems called computing systems or computers, the key differentiator between embedded systems and other computers is the range of activities that they are designed for. In contrast to the more popularly known “computers” which are built with general purpose processors designed to carry out varying functions, the processor of an embedded system is pre-programmed to deliver a specific functionality. Although no standard and rigorous definition exists in literature, we shall refer to the following:

Definition 1. *“Embedded Systems are electronic systems that contain a microprocessor or a micro controller, but we do not think of them as computers – the computer is hidden or embedded in the system.” – Todd D. Morton [1]*

Definition 2. *An embedded system is some combination of computer hardware and software, with either fixed or programmable capabilities, that is specifically designed for a particular kind of application device.*

1.1.1 Examples of embedded systems

It is interesting to know that embedded systems were primarily designed to cater to large, safety-critical applications like rocket and satellite control, energy production control, telephone switches, flight control. But with time, they have been employed in other fields thereby addressing a wider range of functionalities spanning transport systems (avionics, space, automotive, trains), electrical and electronic appliances (cameras, toys, televisions, home appliances, audio systems, and cellular phones), process control (energy production and distribution, factory automation and optimization), telecommunications (satellites, mobile phones and telecom networks), energy (production, distribution, optimized use), security (e-commerce, smart cards), health (hospital equipment, mobile monitoring), etc and have become indispensable to our daily lives. Given the aforementioned examples, we can without loss of generality say that embedded systems typically execute control functions, finite state machines, and signal processing algorithms. In addition they are also employed to detect and react to faults in both the computing and surrounding electromechanical systems besides manipulating application-specific user interface devices.

1.1.2 Requirements of embedded systems

As seen above, given the multitude of larger systems that embedded systems reside in and the demand for integrating multiple functionalities into smaller compact systems, the resources available to these systems is highly constrained. It seems apt at this point to quote Peter Thompson, System Architect of Military and Aerospace, GE Intelligent Platforms [2]:

“It has become a recurring customer mantra: ‘We want more capability than we had previously – but using less Size, Weight, and Power (SWaP) than the older systems used to.’” Embedded computers typically have tight constraints on both functionality and implementation. In particular, they may need to conform to one or more constraints including size and weight limits, power consumption, satisfy safety and reliability requirements, guarantee real-time operation and be reactive to external events while meeting tight cost targets.

Koopman et.al [3] have described the specific requirements of embedded systems, which are summarized here. The size, weight and form factor constraints specifically hold for embedded computers which are physically a sub-component in bigger systems. Therefore, these constraints are inherently dictated by aesthetics, form factor requirements, or having to fit into limited spaces among other mechanical components. To optimize fuel usage and portability in the automotive domain, systems with smaller weight are desirable. Safety and reliability constraints are posed by systems which have obvious risks associated with

failure. An example is mission-critical applications such as aircraft flight control systems, in which severe personal injury or equipment damage could result from a failure of the embedded computer.

For embedded systems that do not operate in a controlled environment, the main requirement is to continue operating in harsh conditions. Excessive heat is often a problem, especially in applications involving combustion (e.g., many transportation applications) or devices that are embedded in human beings (e.g, pacemakers). Additional problems faced by these systems is a need for protection from vibration, shocks, lightning, power supply fluctuations, water, corrosion, fire, and general physical abuse.

Most embedded systems must operate in real-time – the required behaviour must not only conform to the functional correctness, but also be delivered within preset time bounds. In many cases, the system design must take into account the worst-case performance. Predicting the worst case may be difficult on complicated architectures, leading to overly pessimistic estimates. Apart from all this, though embedded computers have stringent requirements, cost is always an important issue.

An embedded systems designer must therefore consider not only meeting the basic functional requirements like correct behavior but also address non-functional (more rightly called extra-functional) requirements like low power consumption, small form factor and weight, besides security, reliability and robustness. In addition, most embedded systems have to meet specific timing constraints and must deliver the correct behavior within a specified time limit – these systems belong to a specialized category of systems called *real-time embedded systems* (RTES). Such systems are a focus of this work and hence we shall explore them further in the next section.

1.2 Real-Time Embedded Systems

In simple terms, embedded systems which must adhere to certain temporal requirements and deliver the expected functionality within pre-defined time bounds are called “real-time embedded systems”. In this section we shall discern in detail the meaning, categorization and properties of these real-time systems. In a real-time system, the correctness of the system behavior depends not only the logical results of the computations, but also on the physical instant of time at which these results are produced. The key differentiator is the dimension of time — a given response is deemed correct and useful only if it delivered in conformance with some temporal requirements. From a system perspective, a real-time system is essentially a set of subsystems i.e., the controlled object, the real-time computer system and the human operator or interfacing unit. It is reactive in nature i.e., it reacts to stimuli from the controlled object (or the operator) within time intervals dictated by its environment.

1.2.1 Real-time Taxonomy

Most interactions (stimuli and responses) in real-time systems are recurrent in nature. Therefore these systems are typically modeled as finite collections of simple, highly repetitive entities or abstractions called *tasks* each of which releases a sequence of *jobs* at different rates depending on the nature of the application [4]. While the task is an abstraction, the jobs constituting it are the actual active instances of the task which perform the required actions by using the resources of the execution platform. In other words, a job is the unit of work that is scheduled and executed by the system.

Definition 3. *A real-time task is a sequence of real-time jobs that are semantically related.*

An example of the abstract nature of the task is the “maintain constant altitude” task for aeroplanes. This task will consist of a set of jobs that execute to allow the aeroplane to fly at a constant altitude. Formally we may define a job as follows:

Definition 4. *A real-time job defines a basic request for execution. When such a request is made, C units of processor time must be allocated to this job over the next D time units. C represents the execution requirement, and D the relative deadline of the job.*

Note that the deadline of a job is relative to its release time and hence is called the *relative* deadline. To re-iterate, a job is characterized by certain functional parameters which define its behaviour, temporal parameters to express its timing properties and constraints (like its deadline) and resource parameters which define its execution requirements.

1.2.1.1 Classification based on job release patterns

Depending on the release patterns of the jobs by a task, we can classify tasks as follows [5]:

- Periodic tasks: Jobs of a periodic task are released by the task at constant intervals of fixed duration known as the “period” of the task.
- Sporadic tasks: Jobs of a sporadic task are released by the task at arbitrary points in time, but with defined minimum inter-arrival times between two consecutive releases.
- Aperiodic tasks: Jobs of an aperiodic task do not have any pre-defined bounds on their releases. In other words, an aperiodic task is a stream of jobs released by a task at irregular intervals, with no pre-defined pattern of release.

In this work, we focus only on *sporadic tasks*

1.2.1.2 Soft, hard and firm real time systems

Every real-time system is associated with some timing constraints, called the *relative-deadline* in formal real-time terminology. The system may consist of one or more tasks

that must be executed to deliver the required behaviour. The deadline denotes the time by which the each (job of a) task in the system must complete its execution in order to provide the desired output. In other words, the job(s) of the task must be also given the required resources for their execution i.e., C_i time units of execution must be completed within D_i time units of their release. Failure to meet these deadlines can have varying repercussions depending on the system. Based on the different consequences of missing their deadlines, real-time systems are classified as soft, hard and firm real-time systems [6].

- **Soft real-time systems:** In these systems, missing a deadline leads to a degraded performance. The desired functionality (result), if produced after the pre-set deadline retains its utility (inspite of the degradation) and the system keeps functioning. On-line transaction systems, airline reservation systems are examples of soft real-time systems. In other words, non-adherence to the timing requirements is tolerated to certain levels.
- **Hard real-time systems:** Systems in which missing the deadlines leads to a catastrophe, like loss to human life, fall under the category of hard real-time systems. The system moves to a “failed” state in such cases. In other words, given the dire consequence, non-adherence to the timing requirements is not acceptable in these systems. Industrial process controllers, pacemakers and air traffic control systems are examples of hard real-time systems.
- **Firm real-time systems:** In these systems, if the desired functionality (result) is produced after the pre-set deadline, the result has zero utility. Unlike hard real-time systems, even when a firm real-time task does not complete within its deadline, the system does not fail. The late results are merely discarded. In other words, the utility of the results computed by a firm real-time task becomes zero after the deadline. A video conferencing application which simply discards those frames which arrive after their deadlines, but continues processing the next frame is an example of a firm real-time system.

In this work, we focus only on *hard real-time* systems.

1.2.1.3 Scheduling: Preemptive and Non Preemptive

We stated earlier, that the jobs of a task needs some execution resources from a processing element (processor). The scheduler is a specialized service of the operating system kernel responsible for deciding which job should be executing at any particular time. In other terms, the scheduler arbitrates the access to the processing element. The order of granting accesses to jobs of tasks is decided by the scheduling algorithm. Scheduling algorithms may be either preemptive or non preemptive. In non-preemptive scheduling, a job *must* be executed to completion once it starts execution, in preemptive scheduling, on the other

hand, it is permitted that an executing job may be interrupted prior to completion and its execution may be resumed later [7]. The process of suspending the job of one task and activating the other involves a switch of the job execution context. The entire state of the suspended job must be saved to enable its seamless resumption at a later point of time. The delay in saving this context of a job leads to the context switching delay, which must be taken into consideration during analyzing the system.

In this work, for simplicity, we focus only on *non-preemptive schedulers*

To facilitate easy readability, in the rest of the document, we use tasks and jobs interchangeably to denote the unit of execution.

1.2.1.4 Global and Partitioned Scheduling

If the host platform offers multiple processing elements, then jobs of a task can be scheduled to execute on any of them. The process of mapping jobs to the processing elements is called *task assignment*. Partitioned scheduling refers to a *static* task assignment in which each task is assigned to a processor and all of its jobs must execute on that processor. In contrast, a global scheduling policy allows for jobs of a task to migrate between processors and there is no strict affinity between a task and a processor. Task migrations have their own overheads, which are non-trivial to compute. Additionally, dealing with partitioned scheduling in itself in the context of this research poses numerous challenges and we believe that as a basic step, it deserves considerable research effort on its own.

In this work, we focus only on *partitioned schedulers*

1.2.2 Desired properties of real-time systems

There are two main terms frequently associated with real-time systems: predictability and composability [8]. Real-time systems must exhibit *predictable* behaviour – the temporal behaviour of a system should be known in advance. Designing for predictability therefore involves analyzing the sub-systems that impact the temporal behaviour and assessing at design time, the various uncertainties that may arise due to different system states. This analysis is carried to derive specific bounds on the timing behaviour or performance, for example to find an upper bound on the time to access to a resource.

Secondly, another desirable property is that the components constituting a real time system must be *composable*. A composable system inherently provides temporal and functional isolation of tasks co-executed on it. As a result, the on line behaviour of tasks when run in conjunction with other tasks remains the same, as when run in isolation. This in turn helps ascertaining at design time, the temporal properties of tasks by analyzing the task in isolation and avoids the problem of analyzing the impact of other sub-systems. As an

additional benefit, components with composable properties can be individually developed and tested, which reduces non-recurring engineering costs.

Since the precision of the results and the efficiency of the analysis methods are dependent on the predictability of the execution platform, they must be designed to cause minimal variation of the instruction timing, cause no interference between components provide predictable behavior and provide comprehensive documentation to help in the derivation of reasonable estimates on the execution behaviour [9].

Next we shall introduce the standard notations commonly used in the real-time system literature.

1.2.3 Notations used to model real-time applications

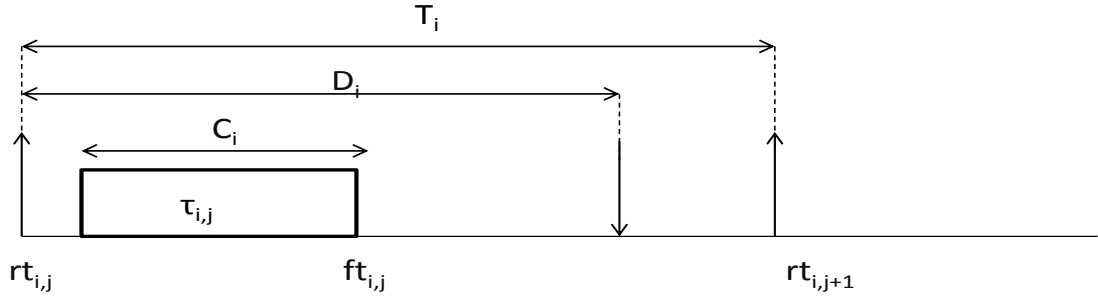


Figure 1.1: Illustration of the job parameters. Upward arrows indicate job arrivals and downward arrows indicate job-deadlines

A real-time application is modeled as a static set of n tasks $\tau = \{\tau_1 \dots \tau_n\}$. Each task τ_i releases a sequence of k jobs $\{\tau_{i,1} \dots \tau_{i,k}\}$, where k is a non-negative number and potentially $k \rightarrow \infty$. Each task τ_i is characterized by a three-tuple (C_i, T_i, D_i) . The term C_i is used to denote an upper bound on the execution time required by a job of task τ_i to complete its required functionality, without being interrupted and is called the worst-case execution time. The symbol T_i denotes the frequency at which jobs of task τ_i are released in the system. While T_i is used to denote the period for periodic tasks, it is used to denote the minimum inter-arrival time for sporadic tasks. The relative deadline denoted by D_i , is the time by which $\tau_{i,j}$ (this notation means the j^{th} job of task τ_i) must complete its execution.

Depending on the relation between the deadline and the period of tasks, a task set τ , can be categorized as follows.

Definition 5. An *implicit-deadline task-set* is characterized by the property that the relative deadline of each task τ_i is equal to its period, i.e., $(D_i = T_i)$.

Definition 6. A *constrained-deadline task-set* is characterized by the property that the relative deadline of each task τ_i in the task set is no greater than its period i.e., $(D_i \leq T_i)$.

Definition 7. An *arbitrary-deadline task-set* is characterized by the property that there is no such constraint on any task τ_i in the task-set, that is D_i can be less than, equal or greater than T_i .

In this work, we focus only on *constrained-deadline task-sets*

Each job $\tau_{i,j}$ becomes ready to be executed at release time $rt_{i,j}$ and continues until finishing (or completion) time $ft_{i,j}$. The duration of this time interval is said to be the response time $r_{i,j} = ft_{i,j} - rt_{i,j}$ and the response time, R_i of task τ_i is defined as being the maximum response time of all its jobs ($R_i = \max_{j=1}^k(r_{i,j})$). The response time of a job denotes the time between its arrival and its completion and the worst-case response time of a task is the maximum amongst the response time of all the jobs released by the task.

1.2.3.1 Timing Parameters

As noted earlier, meeting deadlines is especially key for hard real-time systems, as failing to do so may result in fatal consequences. The notion of meeting deadlines further translates to the fact that each task must deliver its functionality within the given deadline. A task typically shows a certain variation of execution times depending on the input data or different behavior of the environment. The upper bound on the execution time is called the worst-case execution time (WCET) [10]. Formally we can define the WCET as follows:

Definition 8. *“The worst-case execution time of a task indicates an upper bound on the execution time amongst all of its job releases, assuming that its execution is not interrupted”.*

Note the term “upper bound” in the definition. It is very inefficient, or even impossible to obtain the *exact* maximum value by simulating all possible combinations of input parameters [9]. This is due to the fact that the execution time is dependent on the current state of the environment and the inputs. For example, the execution time of a program is dependent on the speed of the processor it is executed on, the speed of the memory, communication channels, the current input to the program, the state of the caches and various other factors. The execution times of two consecutive program runs may differ due to changes in the cache states, inputs, changes in processor speed (owing to some background power management modes) and a host of other factors.

Therefore, an upper bound on the maximum value called the worst-case execution time is computed. These computed values have to be *safe*, in that they must not underestimate the actual upper limit. Moreover, they should be *tight*, i.e. they should be as close as possible to the exact maximum values (which in general are not computable). Similar to the WCET, another key parameter is the worst-case response time (WCRT) of a task.

Definition 9. *The response time of a job denotes the time between its arrival and its completion and the WCRT of a task is the maximum amongst the response time of all the jobs released by the task.*

The computation of parameters like the WCET and WCRT is a part of the process referred to as the *timing analysis*. The aim of timing analysis is to give an estimate for

the time a given program will take to execute under all feasible system states. Execution time estimates are used in real-time systems development to perform scheduling and schedulability analysis, to determine whether deadlines are met for tasks, to check that system-features like interrupts complete their routines in bounded times, etc.

An offline analysis of the task behavior to determine the key parameters like the upper bounds on the execution time or the WCET is vital to ensure compliance with the timing requirements of the system. Hence it is equally important to understand the parameters which can influence it and the challenges that the deployment environment poses in deriving such upper bounds. In the context of the task deployed on a computing platform, the variations in the execution time are greatly influenced by the platform's architecture. For a holistic analysis, understanding the execution environment is thereby of vital importance. In the later part of the chapter, we will focus on the processor platforms on which these real-time systems are hosted, but before that it is important to understand the driving factors behind the choice a given platform. For this, an insight into the recent trends in the embedded systems is warranted and is explained in the following section.

1.3 Paradigm shifts in the design of embedded systems

1.3.1 Shift from federated architectures to integrated architectures

The ever-increasing computing demands of emerging embedded applications has driven designers to shift from federated architectures towards integrated architectures. A *federated architecture* is characterized in that every major function of an embedded system is allocated to a dedicated hardware unit [11]. In an embedded system with evolving functionalities, this implies that adding a new function is tantamount to adding a new computational node.

As a classical case, consider the automotive domain: the number of Electronic control units (ECUs) in cars has doubled over the last decade, with upto 70 to 100 ECUs in high-end vehicles [12]. Traditionally, system designers have followed the “one function per ECU” paradigm, which scaled for systems with few ECUs in terms of the communication architecture (wiring), power consumption and maintenance costs. However with increased functionality required in applications (like navigation and infotainment features in automotive systems), the number of ECUs required increased significantly. To add to the complexity, fault-tolerance, a feature highly desired in some embedded systems, is achieved by provisioning redundant units leading to a further significant increase in the number of nodes and networks.

The increased efforts required to manage this increased complexity, while keeping power consumption at an acceptable level has led system designers to the *integrated* architecture which is based on the principles of adopting a shared computing, communication and I/O resource pool that is partitioned for use by multiple system functions [13]. The avionics field has been adopting this design paradigm which is known as the *Integrated Modular Avionics*

(IMA) architecture. The IMA concept, which replaces numerous separate processors with fewer, more centralized processing units, has witnessed significant weight reduction and maintenance savings in the new generation of commercial airliners. Boeing said by using the IMA approach it was able to reduce 2,000 pounds off the avionics suite of the new 787 Dreamliner, versus previous comparable aircrafts [13]. In alignment with these design requirements, multicores have emerged as a natural choice for system designers. They facilitate the integration of multiple functionalities onto one chip and provide major cost and performance benefits besides reducing the communication infrastructure and also the number of units to be maintained. Considering the example of the automotive domain it may be said that depending on the integration levels, future vehicles may have around 10 to 20 multicore domain control units instead of having 100 ECUs. Applications with high computing demands like navigation, telematics and infotainment can be co-hosted on these chips and can leverage the potential of these multicore platforms. To cater to the stringent needs of embedded systems, chip vendors have developed multicore systems with reduced SWaP (size, weight and power) properties. As a result, multicores have been ubiquitously used in the field of embedded systems.

Besides the shift to integrated architectures, another popular trend has been the adoption of Commercially available off the shelf (COTS) components. The next section provides an insight into the factors behind this shift.

1.3.2 RTES: The shift towards using COTS components

In-lieu of the strict timing requirements of hard real-time systems, real-time embedded systems were traditionally assembled from scratch using custom built hardware and software components, specifically designed for such systems. The entire product development cycle was long and expensive especially when used in massive systems (e.g. aircrafts): Each of the individually developed components had to be designed, developed and unit-tested and then finally integrated with the rest of the system. But with time, products got more complex and there has been a push towards using COTS components for their development.

The key driving factors for the adoption of readily available COTS components, rather than the in-house development of the entire system have been presented in [14]. For completeness, we re-state these factors here. Firstly, the growing competition among product designers to deliver more reliable systems in shorter time frames has driven them towards using COTS components. Secondly, the demand for larger and more complex solutions, cannot be effectively implemented in a timely manner by a single vendor, pushing designers to look at readily available components in the market. Also, product designers wanted to harness the benefits of highly available, reusable and fully tested COTS components. COTS component design has matured over the times and currently there is an increased degree of standard compliance among COTS products. This has been another

major driving factor for their adoption, since the adherence to standards-based development enables reduction of product integration time. Also, the increasing research in better software component “packaging” techniques and approaches have helped designers in the integration process and debugging any subsequent problems.

The adoption of COTS-based multicores in particular was also driven with the fact that previously distributed functionalities of multiple cores are now available as a single chip. In earlier systems in which functionalities were deployed in isolated chips, inefficiencies of working with multiple support environments and programming models led to a longer time-to-market and increased long-term support costs. Building and maintaining systems with multiple chips, power supply units, memories, and I/O interfaces to support the different processors adversely impacted system component manufacturing and maintenance costs.

Although COTS components provide plenty opportunities for embedded system designers, they are not without their own demerits.

1.3.3 Problems with adopting COTS components for designing real-time systems

COTS components are already used in real-time systems with low criticality (also called soft real-time systems), but they are not yet typically employed for hard real-time. The reason is that COTS components are primarily designed towards increasing the average case performance. In contrast, the key requirement for most hard real-time systems are components that collaborate together to provide *predictable* and reliable behavior. The components must provide enough documentation to derive tight upper bounds on the required parameters. But in existing COTS systems, most often only a brief description of its functionality is provided. Also, these components do not carry any guarantee of adequate testing for the intended hard real-time system environment. For example, a processor manual may report that the average time to access main memory is “x” cycles – but what is required is the worst-case estimates. Further-more only a limited description of the quality of the component is provided and the quality must be re-assessed in relation to its intended use. In most cases, the designer does not have access to the source code of the component and this inhibits easier modifications to the current design – Many COTS components are therefore “black boxes” without their source code or other means of introspection available.

Next, let us gain an insight into the COTS-based computing platforms which are employed in embedded systems.

1.4 Computing Platforms

This section defines a multicore processor, delves in the architectures and cites examples of commercially available systems.

1.4.1 Introduction to Multicore systems

With the increase in the number of functionalities provided by embedded systems, platforms that provide high computational capabilities while consuming less power together with a reduced form-factor have been highly sought after by system designers. In the past decades, chip designers addressed these demands by developing faster and faster uniprocessors by increasing the raw clock speed. However the techniques in designing memory systems did not catch up with the CPU speeds as memory access latencies were non-negligibly high leading to large processor stalls. Latency hiding techniques were then employed by designers by building in concurrency within the processor via instruction level parallelism techniques including out-of-order execution, pipelining and branch prediction. The aim was to reduce process stall times (due to memory fetch delays) and thereby maximize the processor utilization. The trend of increasing CPU speeds hit a threshold and could not scale further owing to the physical and the electromechanical limits imposed by increased transistor scaling, power requirements (the power wall), and heat dissipation [15], [16]. Monolithic unicores reached a plateau of clock frequency and chip manufacturers shifted towards the design in which multiple, sleeker, simpler, slower processors were fabricated on a single chip, which collectively not only enhanced the resulting computational power but also did so at a lower watt/instruction per cycle (IPC). These systems are now commonly referred to as as *multicore processors* or *multicore systems* or simply *multicores*. Some of the current multicores like the Niagara processor from Sun Microsystems or Intel's Larrabee [17] processors have simple processors with in-order execution.

A multicore processor is generally defined as an integrated circuit onto which two or more independent processors (called cores) are fabricated. An informal definition from Techopedia [18] is presented here:

Definition 10. *“Multicore refers to an architecture in which a single integrated circuit called a die, is used to package or hold multiple processors. The objective is to create a system that can complete more tasks at the same time, thereby providing better overall system performance.”*

Note that this term is distinct from but related to the term multi-CPU, which refers to having multiple CPUs which are not attached to the same integrated circuit.

1.4.2 Example Multicore systems

There is no doubt that the multicore transition in the microprocessor world is all but complete. The road maps of all the leading chip vendors indicate that their future products incorporate architectures that feature multiple CPU cores on the same chip. Example Multicore processors from different chip vendors include [16]:

- Intel: Core Duo, Core 2 Duo, Core 2 Quad, Core i3, i5, i7, i7 Extreme Edition family, Itanium 2, Pentium D, Pentium Dual-Core, Polaris, Xeon

- AMD: Opteron, Phenom, Turion 64, Radeon, and Firestream
- IBM: POWER4, POWER5, POWER6, PowerPC970, Xenon (X-Box 360)
- Azul Systems: Vega 1, Vega 2, Vega 3
- Cavium Networks: Octeon; ARM: MPCore
- Freescale Semiconductor: QorIQ; Analog Devices: Blackfin

Classification of multicore systems Based on their characteristics of the instruction sets and processor speeds, these systems are categorized as identical, uniform and heterogeneous multicores. Identical multicores, as the name suggests are symmetrical in the instruction set architecture (ISA) and the speeds of the processors. In a uniform multicore setting, each of the cores have the same ISA, but may be executing at different speeds. In contrast to the above, the cores in a heterogeneous system may have a different ISA and may be specialized for different functionalities.

In this thesis, we consider *identical* multicore systems only.

1.4.3 Overview of a typical multicore

The architecture of a typical COTS-based multicore system is illustrated in Figure 1.2. Although the figure is aligned to the Intel processor [19], but it is for illustration purposes only and the discussion will cater to the majority of the multicores in general. It depicts a single chip which contains 4 processing elements or processors (or central processing units (CPU)) and 2 levels of caches – the L1 cache (private to each core) and a shared L2 cache connected over a communication channel to access the main memory. A tiered memory hierarchy is generally employed with smaller faster memories (caches in this context) which are integrated on the same chip and a larger and slower external off-chip memory. These caches are employed to hide the latency in accessing the slower large main memory. The rationale behind the need for caches is that frequently accessed data must be kept closer to the processing source or “cached”, to reduce processor stall cycles. On the first access to a particular address (the cache is looked up and the data is not found therefore called a “cache miss”), the required data or instruction is fetched from the off-chip main memory and a copy is also stored on the local caches. On subsequent accesses to the same address, the cache is checked and if the data is found (called a “cache hit”), it is retrieved from the cache itself without incurring the (high) latency to fetch the data all the way from the memory to the processor. This is possible since most programs exhibit some kind of temporal and spatial locality. In most multicore designs, each core of a multicore chip has a private level-1 cache and may share a level-2 cache (and more levels down like a level-3 cache).

The multicore chip is connected to the memory controller (called the North-Bridge (NB) in Intel terminology) over an interconnection network. In our example COTS-based architecture depicted in Figure 1.2 this interconnection network is a single shared bus, usually called Front-Side Bus (FSB). The FSB is the electrical interface that connects the processor to the main chipset (which consists of integrated chips like the memory and I/O controller chips). The FSB is also referred to as the processor system bus or simply the system bus. All interrupt messages, memory, coherency traffic and I/O transactions flow between the cores and the chipset through the FSB. Since the FSB is the only path from all the cores to the memory, in case of simultaneous requests from different cores, it has an additional responsibility to decide (or “arbitrate”) the order of request transmission. This is done using an arbitration mechanism, like a round-robin mechanism, a priority driven mechanism or other mechanisms. To ensure low waiting times, most bus arbiters are “work-conserving”: If there is a request to be served, the bus has to serve it and cannot be idle.

We shall discuss the arbitration policies in the next chapter.

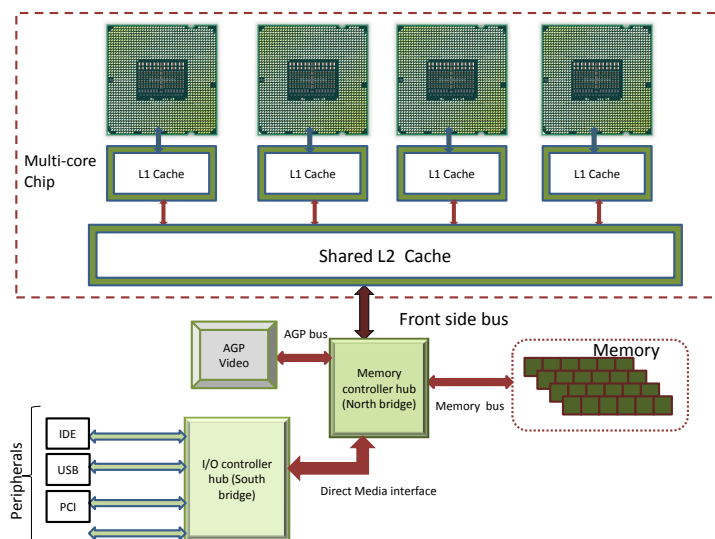


Figure 1.2: A typical COTS-based multicores architecture.

It is important to note that in this model, all the cores have the same view of the memory and requests issued by any of them (in isolation) will take the same time to reach the memory. Such a model conforms to a Uniform Access Memory (UMA) model and will be followed in the rest of the analysis of multicore systems. The North-Bridge typically handles communications between the CPUs, the system main memory (RAM), the Accelerated Graphics Port (AGP) bus to the AGP video cards and the South-Bridge (SB). The main memory is thus shared between multiple entities over the North-Bridge, which we shall henceforth refer to as “agents”, i.e., the main agents that access the system memory are the multicore chip, the graphics controller and the SB unit. The communication between

the main memory and the other agents is handled by a memory controller and a memory arbiter, both directly incorporated into the North-Bridge. Generally, a graphics controller is connected to the NB (or is sometimes integrated into the NB as well depending on the chipset design).

The South-Bridge, often referred to as the I/O Controller Hub, handles communication with the peripherals such as the hard-disk, keyboard, printer, etc., over a variety of buses like the PCI) and PCI express. The peripherals can be connected in various ways depending on the chipset design. Typically, the SB is connected to the NB via a Direct Media Interface (DMI) channel. All the Direct memory access (DMA) traffic (arising from the peripherals) is also channeled through the south bridge.

Our multicore model: *single shared bus with private caches only*

After gaining an overview on the architecture of a multicore which clearly shows the presence of shared resources like the shared bus, it is important to understand their impact of execution behaviour of tasks hosted on them.

1.4.4 Contention for the shared hardware resources in multicore systems

In contrast to the uniprocessor design in which a single core had access to the cache, the bus and the memory controller, the same low-level hardware resources are shared amongst different cores in a multicore system. Resources are mainly shared to minimize cost, energy, and increase the performance, while conforming to the design parameters of the end product, like the size, weight and power requirements. The problems in the timing analysis of multicores can be mainly attributed to the interference on these shared resources.

Consider a scenario in which there are several tasks assigned to each core in a multicore system and all the cores are active. Under such a scenario, when a specific task suffers a cache miss and has to access the main memory over an interconnection network (like the shared memory bus), its request may be blocked by the requests issued from tasks executing on the other cores. Specifically, the core hosting that task is stalled, waiting for the data to be fetched. As the number of cores that use the same front side bus (FSB) increase, the traffic on the FSB increases and this shared bus becomes the main bottleneck. This means that the processor needs to stall for a longer time, waiting on the data and hence more processor cycles are wasted. The extra delay incurred due to the bus contention is non-negligible and hence the resulting execution time of a task can be significantly increased. It was shown by Zuravlev et.al [20] that FSB contention accounts for as much as 60%- 80% of the performance variation that tasks experience on multicore processors. Additionally, in some multicore systems, the caches are shared among the cores; this further exacerbates the problem; tasks running simultaneously on two different cores may evict each other's cache lines, thereby increasing the number of cache misses,

leading to additional requests to memory and adding to the traffic on the shared bus. Hence, any timing analysis for hard real-time systems in the context of multicore systems cannot ignore the impact of the shared hardware resources. The requesters of a shared resource may often access the resource at arbitrary times, which are difficult to discern at design time. As a result, different access sequences may result in different states of the resource. The combination of different resource-states and access patterns complicates the analysis. The lack of spatial and temporal partitioning and the barely analyzable worst-case timing behaviour of performance-enhancing features render the validation of claims about the dependability and correct timing of applications on current powerful multi-cores extremely difficult to defend and prove.

1.4.5 From multicores to many-cores

Just as the technical community was getting used to the idea of multicore processors in systems on chips (SoCs), advancements in semiconductor technology propelled chip designers to further push the limits. On a casual note it may be said that, processor cores are replacing transistors as the building blocks of the current computing hardware. The multicore is becoming *many-core*; the number of processor cores closely coupled at the hearts of SoCs is rising from 4 to 8, 16 and currently chips with 256 cores are already present in the market. The Tile-Gx72 with 72 cores from Tileria [21], Kalray with 256 cores [22], Epiphany with 64 cores from Adapteva, Intel Xeon co-processor [23] with 60 cores and the 48-core Single-Chip-Cloud computer [24] are just some examples of such many-core architectures. These systems, like Kalray's MPPA (Multi-Purpose Processor Array) have been optimized to address the demand of high performance, low power embedded systems and therefore these architectures must be analyzed. The next section provides an overview of such an architecture.

1.5 Overview of a typical many core system

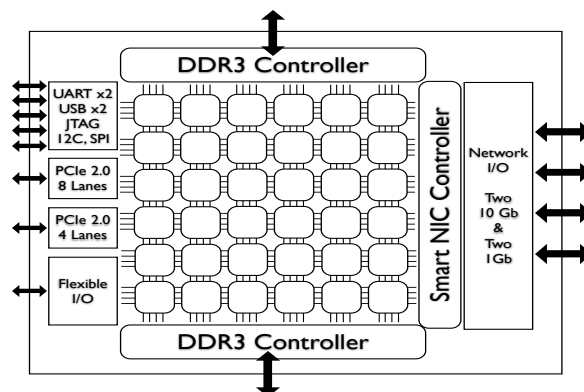


Figure 1.3: Tileria architecture. (Diagram taken from [21])

Figure 1.3 illustrates a many-core system based on the Tiler Platform. Without loss of generality we shall discuss this particular platform to gain the basic understanding. As seen in the figure, the architecture of a many-core system is visibly different from multicores, considering the number of cores, the interconnection mechanism between different cores and the positioning of the peripherals and the memory controllers. It was seen that the traditional shared bus/ring architecture (c.f. left plot of Figure 1.4) that serves as the interconnect between the cores cannot not scale beyond some number of cores (typically 8 cores is the limit). The shared bus, instead becomes a bottleneck leading to substantial increase in the access time to the off-chip memory thereby offsetting the benefits of high computing power provided by the cores. The increase in the number of cores forced a shift in the earlier design paradigm towards a more scalable interconnection medium: the Network on Chip architecture [25]. Longer wires connecting all the cores were replaced by routed interconnects using switches. This design conforms to the distributed architecture, while still being integrated on a single die.

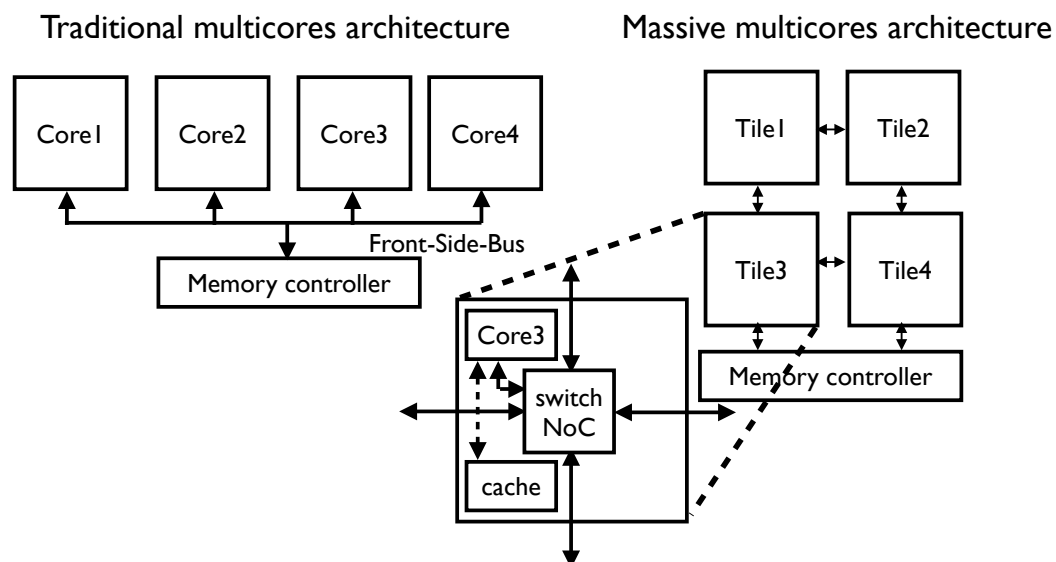


Figure 1.4: Multi-core vs. many-core architectures

Organization of the cores: One of the base principles of the many-core technology is the division of the processing elements (cores) into “tiles” interconnected by a NoC. Each tile is thus a basic modular unit, composed of a processor core, a private cache subsystem and a network switch and these tiles are homogeneous across the entire chip. The tiles are laid out in a two dimensional grid and the switch connects the tile to its neighboring tiles located in the cardinal directions, thereby forming a 2D-mesh (c.f. right plot of Figure 1.4). The NoC serves as a communication channel among the cores and between the cores and other off-chip subsystems, e.g. the main memory. The off-chip subsystems like the peripherals and the main memory are connected to the tiles on the periphery of the grid. Note that

absence of a centralized single shared cache in this architecture, since it is distributed across the tiles.

1.5.1 Contention of shared resources in NoC based many-cores

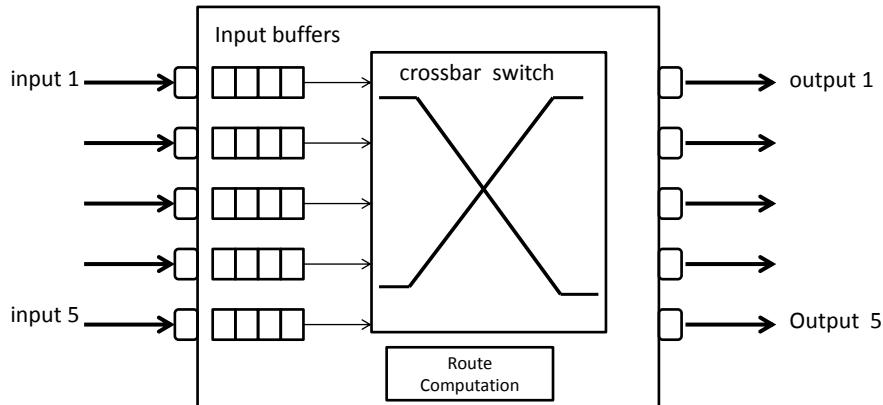


Figure 1.5: Illustrating the switch, the physical links and buffers

Figure 1.5 gives some more details regarding the switch, in which the 5 physical links incident on the input ports represent communication channels from each of the cardinal directions connecting the given tile to its neighbors in the north, south, east and west direction and a fifth link that facilitates the connection to the core present on that tile itself. Similarly, the data leaves the switch from the output links. In this diagram we have illustrated a single set of buffers which hold data from a given input port — in practice there may be many buffers and therefore many *virtual channels*. The buffers act as storage areas of finite capacities or placeholders for data in transit, until the required output port (and the corresponding output link) is busy. In this work, we assume a single virtual channel. As seen in this diagram, the main shared resources in a NoC are these buffers and the physical links.

At any given time, tasks running on different cores may release packets over the network independently and asynchronously. All the packets are transmitted over the same underlying interconnection network and share the available network resources. When several packets try to access the same resource at the same time and if resources are insufficient, it leads to a contention — for example, a router in the network may be able to only serve one packet and suspend the others based on some arbitration policy. Additionally, a packet that is blocked at one link, can in-turn block other packets waiting on previous links and the effects can cascade leading to a congested network, thereby causing a significant delay in the packet's traversal time. Thus the time to transmit a packet depends on the current load of the network, which in-turn is determined by the number of packets generated by the tasks executing on the other cores. Other factors like the routing mechanism employed also impacts the traversal times as it influences the path taken by the packets to reach

their destination — this in-turn decides whether they would directly or indirectly block the analyzed packet by contending for the same resources.

To summarize, the number of parameters contributing to the unpredictability combined with the large number of cores poses a challenging problem to designers aiming to determine an upper bound on the traversal time of a (message/memory/ IO) packet. This traversal delay can be large and can increase the execution time of the task issuing these packets. If real-time tasks are to be hosted on such many-core platforms, pre-assessing this delay at design time is crucial. In this thesis we aim to compute such an upper bound which is referred to as the worst-case traversal time (WCTT).

We are now equipped with the necessary background to understand the problems addressed in the thesis.

1.6 Problems addressed in this thesis

At the level of the processor, a task is generally a sequence of instructions which operate on some data. Once the data is available to the processor, it performs the required computations. The instructions and data reside in some level of memory (L1 cache or L2 cache or the main memory itself) within the memory hierarchy. Therefore, the total execution time of a task can be demarcated as the computational phase and the communication phase, between which an executing task keeps alternating. Then a simple way to compute the execution time is given by,

$$\text{Execution time} = \text{time for computation} + \text{time for communication}$$

- The computational phase is the time during which the task consumes resources of the processor or the *on-core* resources like access to the arithmetic logic units for computations. In a multicore/manycore system, for a task that is assigned to a processor, this component of the execution time is *independent* of the tasks executing on the other cores.
- The communication phase represents the time to fetch the required instructions and data from the memory, write the data back to memory or the time to communicate between the cores. In this phase, the task consumes resources *off the chip*, which include the bandwidth available on the interconnection network which connects the processing elements to the memory. In a multicore system, in which these off-chip resources are shared by the other cores, the communication delay *is dependent* on the utilization of the same resources by tasks executing on the other cores. Similarly in a many-core system the time to send or receive data across the shared interconnection network is dependent on the data traffic introduced by other cores.

Each data transfer constitutes a request for the interconnect mechanism (the shared bus in multicores or the interconnected mesh network in many-cores). Consider task τ_i which

needs C_i processing units (its WCET in isolation) and generates N_i requests. Assume that request i needs w_i units to be served, which implies that the core is stalled for the same time, due to which the final execution time of the task in contention C'_i is given by

$$C'_i = C_i + \sum_{i=1}^{N_i} w_i \quad (1.1)$$

In the broader context, the main aim of this thesis is to derive the delay incurred by the executing task due to contention for the shared interconnect. Towards this aim the thesis, explores related problems and subproblems, and we focus on three main areas:

1. Analysis of the impact of the shared bus on the execution time of a task in multicore systems.
2. Analysis of the impact of the interconnection network on the traversal time of a packet in many-core systems.
3. Analysis of multicore systems considering memory systems like Phase Change memory in which the read and write latencies differ to a great extent.

We have enlisted the assumptions earlier, but will re-state them here for completeness.

1.6.1 Bus Contention Analysis of multicores

Problem statement: Given a multicore system, in which cores do not share cache space, tasks are assigned a priori to all the cores and given the execution time of each task in isolation, determine an upper bound on the increased execution of a task when it is run in conjunction with other tasks co-executing on other cores. This analysis takes into consideration the contention between co-executing tasks on all the cores for the single system bus. The analysis assumes that tasks are sporadic, non-preemptive and the scheduler does not allow tasks to migrate between cores. The main aim of the problem is to arrive at a *unified framework* for computing the WCET of a task, for any given arbitration mechanism employed by the bus. The main problem is tackled by solving the following sub-problems:

1. To analyze the delay caused due to contention on the bus on a given task, a prerequisite is to analyze the memory traffic injected by tasks executing on other cores. Hence the first problem to be solved is *modeling the memory access pattern of tasks* and deriving the maximum traffic generated by the *tasks* in a given time interval.
2. Given the memory profile of every task on a core, the next problem to be solved is deriving the maximum traffic generated by the *cores* in a given time interval. Being able to do so will provide an abstract interface that takes into consideration all possible patterns of task arrivals and returns the maximum traffic that can be injected into the shared bus by any core in a given time interval.

3. A pre-requisite to analyze the maximum delay incurred by a request on the bus is to understand the underlying arbitration mechanism. The order of servicing the requests by the bus is based on its arbitration mechanism and the next step in the analysis is *modeling the availability of the bus*– to demarcate the time intervals during which the bus is busy handling traffic (from the contending tasks) and the time at which the bus is potentially available to serve the requests of the analyzed task.
4. The next problem is to develop a method of scheduling the requests (of the analyzed task) on the available free bus slots with the objective of maximizing the waiting time of each request and thereby computing the maximum delay that the task incurs. It is very difficult to derive at design time, the exact release time of every request and we can only derive the number of requests that can be released over a period of time. Given this coarse grain request distribution, we must be able to schedule requests in a manner to generate the worst-case delay.

1.6.2 Network contention analysis of many-core systems

Problem statement: Given a many-core system in which the cores are arranged in a mesh topology, and communicate with each other via an interconnection network, and data is assembled into packets, compute an upper bound on the traversal time of the packet, considering the contention for the finite links and buffers on the interconnection network. The computed parameter is referred to as the worst-case traversal time (WCTT) for a NoC based many-core system. The main problem is tackled by solving the constituent sub-problems.

1. The first important problem is to characterize the application’s flow pattern and compute the delay incurred by a packet in isolation.
2. A packet may incur delay at each intermediate router when contending with other packets issued by other flows. The next problem is to formulate a delay analysis by considering the routing and switching mechanisms employed by the interconnection network.
3. Given that packets may originate from different flows in different orders, a method to construct different flow sequences (scenarios) in order to generate that sequence which can pose the maximum delay to the analyzed packet, is warranted.
4. To avoid an exhaustive enumeration during the generation of these scenarios, an important concern is to reduce the number of investigated scenarios. This is done by applying packet release constraints to the scenarios and pruning infeasible scenarios.

Other major design issue when many-core systems are concerned, is providing scalable mechanisms that can cater to systems with large number of cores and can provide tight bounds, efficiently even when the network is heavily loaded.

1.6.3 Analysis of Phase Change Memory (PCM) based multicores

A significant part of the total delay incurred in serving requests of a given task, can be attributed to the latency imposed by the memory sub-system. Unlike the timing analysis of multicores where we consider a system for which the memory latencies for a read and write request are the same, newer memory systems with asymmetric latencies like Phase Change Memory (PCM) have been proposed. PCM is non-volatile, unlike Dynamic Random Access Memory (DRAM), consumes lesser power and is sought after by embedded system designers. We discuss more about PCM in detail in Chapter 5.

However, due to the intrinsic properties of PCM [26], the time to complete a read and write operation differs greatly; completing a write operation may take upto 10 times the time to complete a read request. If reads and writes are treated in the same manner by the memory controller, it may lead to huge processor stall times, especially during very slow write operations. To mitigate these delays, researchers have proposed different scheduling policies to be adopted by the memory controller: like prioritizing reads over writes in order to reduce program stall times. It is interesting to explore such memory systems with asymmetric read and write latencies and as a part of the thesis we also analyze such a system for its temporal behaviour.

Problem statement: Given the WCET and the memory profile of a task in isolation, compute the increase in the WCET when it runs in conjunction with other tasks deployed on a multicore system in which Phase Change Memory (replaces Dynamic Random Access Memory and) forms the main memory.

In addition to the analysis of the shared bus, the problem consists of analyzing the PCM controller. This problem involves modeling the memory controller, computing the bus availability for the analyzed task and then finding a tight upper-bound on the cumulative delay that memory requests may incur in the FSB and PCM controllers, considering that the time to serve a write request is much higher than the time to service a read request. We shall revisit this problem in detail in Chapter 5.

1.7 Motivation and Relevance of this work

The architecture of the execution platform decides if the timing analysis (static or measurement based) is practically feasible at all and whether the most precise obtainable results are precise enough. This influence of the architectural features has been of concern to both the developers of timing-analysis tools and the consumers. With the shared resource architectural paradigm supported by multicores, the problem has reached a new level of severity. Multicores are thus not yet hard real-time ready – While multicores are deployed in soft-real time embedded systems, their uptake in the hard real-time arena is limited. Anecdotal evidence from practitioners suggests that multicores are being used in hard real-time systems, with all but one core disabled, reducing it effectively to a single core platform [27]. Hence, methods which could analyze the extra execution time due to

contention on a shared bus would be valuable (much better than the current default alternative). The stark reality is that without addressing issues of shared resource contention, highly robust hard real-time systems will not be deployable and the industry will be unable to leverage the complete potential of emerging multicore systems.

1.7.1 The hardware solution: Building predictable multicores?

One solution would be to develop multi-core architectures that have features that make them predictable and hence analyzable. Temporal and spatial isolation of components should ideally be provided by the hardware itself. Spatial partitioning ensures that an application in one partition is unable to change private data of another. Temporal partitioning, on the other hand, guarantees that the timing characteristics of an application, such as the worst-case execution time (WCET), are not affected by the execution of an application in another partition. If present, these features reduce the time, effort and cost involved in the analysis of these systems, since the temporal properties of each component can be validated independently. For example, the use of partitioned (or partitionable) caches, TDMA driven buses with guaranteed time allocations to cores and peripherals would be advantageous. In these architectures, the resources would be temporally and spatially partitioned making analysis easier.

The underlying problem however is that the safety-critical market is very small compared with the consumer mass market (needing high performance systems) that is driving chip development. The design paradigm of the current and future generation of processors is inclined towards increasing the performance and as a consequence, there is no traction in the industry towards building predictable and analyzable systems. Development of multi-cores based on a reference architecture dedicated to safety critical applications and more amenable to certification is likely to be prohibitively expensive unless cross domain applications needing real-time support are large enough to force chip designers to build analyzable systems. There is thus an opportunity to bring different domains together, aerospace, automotive, rail etc. to develop multi-core devices that are built from scratch to be easily analyzable.

An alternative is to develop methodologies and toolsets that allow existing commercial off-the-shelf devices to be utilized in safety-critical applications. There is a need to satisfy safety-requirements and provide time predictability. This will require further developments in the underlying theoretical analysis of such systems and more importantly that the developed tools to support this analysis, should be cost efficient. Here there is a risk of fragmentation across sectors due a wide spectrum of multi-core architectures being developed. But we believe that unless the industry designs multicores which are real-time friendly, developing methodologies to analyse the temporal properties is a crucial step. As a logical step, it is of prime interest to understand the contribution of timing analysis within the entire process.

1.7.2 Missing link in the entire analysis process

While decades of active research have been spent in the *timing* analysis of uniprocessor systems, the same cannot be said for multicores. Research is still in its nascent stages and there are ample opportunities for improvement and filling in the missing link in the analysis cycle. To clarify, let us consider Figure 1.6 which depicts an iterative design/analysis process suitable for tasks that do not migrate from one core to another at run-time. The first step in this process involves modeling the number of cache misses that a given task suffers in isolation and computing its WCET. There is considerable research in this area of WCET computation and the interested reader can refer to [10] for a compilation of techniques to achieve this. The next step is assigning tasks on each core: this problem has also been studied in detail and the existing research literature offers mature algorithms for this particular activity [16]. Once tasks are assigned, we need to recompute the WCET considering the contention on the shared resources. This is a key input to the next step of “schedulability analysis”, after which we can ensure whether tasks meet their deadlines – this is an open problem and the “missing link” in the entire design process. Hence it is important and relevant to study this problem. Although some research has been carried out, it has been done so with a lot of strong assumptions –however they do serve as the building blocks in the final solution. We shall take a look in detail about the existing work in the upcoming chapter which is totally dedicated to it. There are enough open venues for improvement and this current research is aimed at addressing those issues to be able to actually develop end-to-end solutions that will be accepted by the industry.

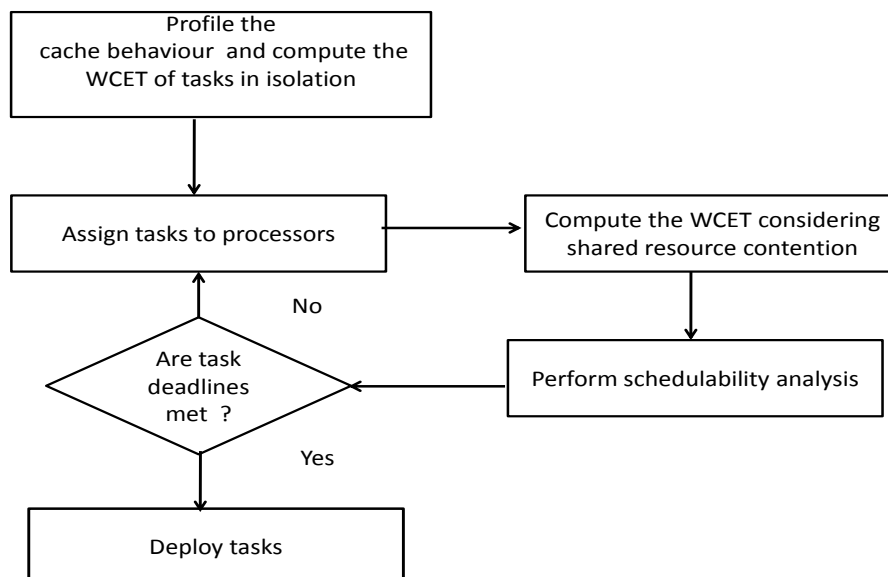


Figure 1.6: Flow Diagram for Analysis

The need for timing analysis is further driven by the facts that systems must be *certified* prior to their deployment – it would be informative to understand the gist of the

certification process.

1.7.3 Certification requirements and guidelines

A special class of hard real-time systems are safety-critical in nature. These systems operate under strict timing requirements and may cause significant damage or loss of life and/or property if they do not operate in conformance with their pre-set functional and non-functional specifications. Examples of these systems include flight and traffic control, railway interchanges, nuclear facility control systems, medical equipment and implanted devices. In order to ensure safe products, governments and international agencies took the initiative in establishing certain certification standards to regulate the quality of the final products.

Definition 11 (Certification). *“Certification is the process of issuing a certificate to indicate conformance with a standard, a set of guidelines, or some similar document.” – Neil.R.Storey [28]*

Certification norms are applicable to processes and products. Different safety standards have been established across different domains. Some of them are mentioned here:

- IEC 61508 is to ensure functional safety of electrical/electronic/programmable electronic safety-related (E/E/PE) systems.
- EN 50128 is to ensure safety norms in the railway industry
- RTCA/DO 178B and DO 254 for civil aircrafts in the avionics domain
- ISO 26262 is a functional safety standard, titled "Road vehicles – Functional safety" targeted towards the automotive domain.
- IEC 61511, IEC 62061 are safety standards for the factory automation domain

Before safety critical real-time applications can be deployed on multicores, timing guarantees must be ensured at design time and the entire system must be certified. Researchers have proposed various scheduling algorithms over the last decades, together with associated “schedulability analyses”, that enable certification authorities to verify whether the system will always fulfill all its timing requirements at run-time. In practice, each and every task of the system is assigned a “Safety Integrity Level” (SIL) reflecting the level of “criticality” of the task and the rigorousness of the certification process varies according to the SIL of the task under scrutiny. When deployed on the same multicore system, tasks of different SILs can co-exist and share some low-level hardware resources such as cores, cache subsystems, communication buses and main memory. It is of *chief importance* to understand that, *unless these tasks of different SILs are shown to be sufficiently independent*, the standards require that the hardware and software are developed at the highest SIL among the SILs of all these tasks, which is very expensive. This requirement is clearly stated in

the automotive domain (req. 7.4.2.3 of ISO 26262-4 [29]), as well as in the international standard (req. 7.6.2.10 of IEC 61508 [30]). This is why substantial efforts are put to (i) render the tasks of a same SIL as independent and isolated as possible from the tasks with different SILs and (ii) *upper-bound the impact that the execution of the tasks of a same SIL may have on the execution behavior of the tasks of different SILs, with the objective of certifying each subset of tasks at its own SIL level.*

As described earlier, by design constraints, complete isolation of tasks by partitioning at the hardware level has its limit. In most multicores, the cores are typically connected to a shared off-chip main memory by a single shared communication channel (which does not conform to the “total-isolation” paradigm). Sharing is either present at the level of the caches or/and for the interconnection network or/and for the memory subsystem. Hence in -line with the requirements, the work aims at providing upper bounds on the execution time of tasks in the presence of a shared memory bus.

Additionally, to cater to these requirements, international standards also typically favor simple and safe designs are recommended in [30] (Annex F, page 103). These include (i) partitioned scheduling (tasks do not migrate when once assigned to a given core), (ii) time-triggered architectures in which jobs are activated only at already known pre-set time instants (iii) partitioned caches and cyclic scheduling algorithms (CSA) in which the exact order of task arrivals is known at run time. In line with this requirements and the complexity in analyzing data caches, the analysis in this work considers multicores with *partitioned caches*. To summarize, analysis of multicores for their temporal behaviour is a pre-requisite for certification and is a motivating factor for this thesis.

1.7.4 Industry and Academic interest in multicores

Increased industry interest in adopting multicores for hard real-time systems is another driving factor for this research. There has been clear evidence of a strong trend toward using multicore processors in embedded systems that require hard real-time performance. The industry is also increasingly collaborating with the academia to achieve this aim.

As a result, many related projects have been initiated at the European Union level, some of them being:

1. RECOMP - Reduced Certification Costs Using Trusted Multicore Platforms [31]
2. MERASA - Multicore Execution of Hard Real-Time Applications Supporting Analyzability [32]
3. ARAMiS - Automotive, Railway and Avionics Multicore Systems [33].
4. ACROSS - ARTEMIS CROSS-Domain Architecture [34]
5. CESar - Cost-efficient methods and processes for safety relevant embedded systems [35]

Given the gravity of the problem, researchers across the world have contributed in solving different parts of the entire problem. We shall present the state-of-the-art in the next chapter. The above facts are instrumental in driving the need for analysis. But it is also necessary to understand the hardness of the problem to be solved and the need for a dedicated research effort in this direction.

1.7.5 Challenges in bus contention-aware timing analysis

To determine the WCET of a given task executing on a particular core considering the contention on a shared memory involves an assessment of the incoming (request) traffic from the other cores. Firstly, the combination of parameters like the scheduling algorithm, the memory profile of the co-scheduled tasks and their characteristics (like arrival patterns) together increase the resulting search space, making design time analysis a non-trivial exercise. Secondly, memory requests from tasks generally do not follow a predictable pattern which can be analyzed at design time - they are dependent on various factors including the input to the task and whether or not the requested data was found in the cache. It is difficult to determine bounds for a shared bus employing a predictable arbitration mechanism like TDMA, as the arrival of requests to the shared memory may not align in time with the availability of the bus slot. With non-predictable bus arbitration policies, the problem is further magnified. Thirdly, COTS-based buses are generally designed with performance enhancing features (like pipelining requests, facilitating split transactions) which effectively decrease the access latencies and reduce processor stall times –but this complicated design makes it difficult to analyze or adapt it to real-time systems, especially in the absence of the required documentation (e.g details of the arbitration mechanisms involved) and tunable interfaces (to change the existing arbitration policy). To summarize, currently existing static analysis methods are restrictive, given the huge state space that needs to be explored and measurement based methods need to consider the architectural influences in extreme detail to obtain tight bounds on the obtained WCET values. Resolving the challenges of augmenting current designs and architectures to gain the benefits of multicores for hard real-time systems can be daunting.

1.7.6 Contributions of this thesis

As seen above, the thesis addresses the constituent sub-problems of modeling the request profiles of the task and the core, modeling the bus availability and dealing with request latencies imposed by the memory subsystem. While the major portion of the thesis focuses on multicore platforms, a part of the thesis is also dedicated to the analysis of many-core systems which communicate among themselves over a network. The main contributions of this thesis are described here.

1. A basic requirement for computing the memory interference generated by a *task* is to understand its memory access pattern. The thesis address this issue and a method for

task profiling has been provided, which computes the maximum number of requests a task can generate in a given time frame. We demonstrate using simulations that the analysis provides tighter bounds than the state of the art techniques.

2. The next contribution is a method that enables to compute the maximum number of requests that a *core* can issue, which takes into consideration the set of tasks executing on that core. The method is novel in its kind to compute the per-task profiles and we also demonstrate using simulations that the analysis provides tighter bounds than the state of the art techniques.
3. On the basis of the aforementioned methods, a unified framework is proposed to compute the increased execution time, which can handle different arbitration bus policies. We believe that this is the first kind which provides a common interface to handle different bus arbitration policies and computes the increased worst-case execution time of a task by modeling the availability of the memory bus.
4. The thesis delves into the memory controller design and proposes a method to analyze the increase in execution time for memory systems with asymmetric latencies like Phase-change memory based systems. It takes into consideration the request scheduling policies in the memory controller. This is the first work which analyses memory systems with asymmetric latencies and considers the scheduling of requests in the memory controller to derive the worst-case execution time.
5. The thesis also provides a method to analyze many-core systems in which the cores organized as a grid, communicate over a network on chip infrastructure. A method to compute the traversal time of a data packet is provided. The method identifies the sources of pessimism in the existing state of the art and improves upon it by proposing techniques which not only provide tighter bounds but can also scale to handle the contention when the network is heavily loaded —i.e. there is a large amount of network traffic.

Each of these contributions will be explained in detail in the forthcoming chapters.

1.8 Thesis Organization

The document is organized as a sequence of chapters. Chapter 2 explains the background of timing analysis and details the earlier work carried out on timing analysis of multicores. The key focus of Chapter 3 is to address the problem of deriving upper bounds on the number of requests that a task can generate when run in isolation (per-task interference). This memory profile is leveraged to compute naive upper bound on the interference from each core (per-core interference). In chapter 4, a unified framework for timing algorithms which can be applied to different arbitration mechanisms is established by defining certain abstractions. At this point we deviate from analyzing the memory-bus and gain a deeper

insight into the memory subsystems with asymmetric read and write latencies. This is the main focus of Chapter 5, which motivates the adoption of Phase Change Memory (PCM) in embedded systems and analyses the temporal behaviour of tasks these multicores. After analyzing multicores with a shared memory-bus, the thesis proceeds with the analysis of many-core systems in which the cores communicate on a NoC. The communication channel is designed as a mesh of links between cores which communicate over this network and the data to be transmitted is encapsulated in packets. Chapter 6 explores this area in which we identify the sources of contention on such a Network-On-Chip and study the worst-case traversal time of a given packet. The work done in the thesis is discussed in the concluding chapter 7 and the possible directions of research are laid out.

Chapter 2

Background and Related work

We study history in order to intervene in the course of history

Adolf von Harnack

In the previous chapter, we gave an overview of the problem of computing the increased delay in the execution of a task due to the contention for shared resources like the shared bus in a multicore system. This chapter is intended to provide the necessary background before discussing the actual proposed solution. To facilitate this, the chapter is organized as follows. Section 2.1 introduces the prevalent methods in timing analysis. Next, Section 2.2 describes the necessity of a newer analysis framework for multicore systems which takes into consideration the impact of the shared resources and thereby introduces in detail these shared resources. The work carried out by contemporary researchers towards solving this problem has been summarized in Section 2.3. The chapter concludes in Section 2.4 which enlists the avenues for improvement and further research in the given domain.

2.1 Timing Analysis

The computation of the parameters like the worst-case execution time is a part of the process referred to as *timing analysis*. The aim of timing analysis is to give an estimate for the time that a given program will take to execute under all feasible system states. Although the work in this thesis is *not* focused on the computation of the worst case execution time in isolation, the basics of timing analysis are presented here for the sake of completeness.

2.1.1 Why is timing analysis required

By definition, hard real-time systems must satisfy timing constraints and must be validated before deployment by a method called schedulability analysis. Analyzing a set of tasks for schedulability verifies if all the tasks will meet their deadlines when deployed on the target

hardware. A vital input to this analysis requires safe and tight bounds on the execution time of each task in the system. Different methods have been proposed to compute such estimates in *uniprocessors* and can be mainly classified as static, measurement based and hybrid techniques [36]. We will briefly describe these methods in the following sub-sections.

2.1.2 Static Analysis

Static analysis methods analyze the task by constructing the program (task) flow model, the model of the target hardware and the inputs to the program. These techniques rely on having a precisely accurate model of the timing behaviour of the target hardware, including modeling features like pipelines, caches, memory, buses that affect the execution time of the executing task [37]. The attempt is to derive safe bounds *without* actually executing the program on the target hardware, while still considering the influence of the state changes in the underlying hardware [38]. State changes could imply a cache line being evicted, a pipeline being totally flushed out, etc. The method computes the worst-case execution path by considering constructing a control flow-graph from a given program and considering each of the paths in the graph. Loop bounds and other annotations provided to the analysis tool help in facilitating the analysis. The timing analysis framework besides analyzing the main program structure, is complemented by other modules like tools for cache analysis and pipeline analysis that help in deriving estimates considering the specifics of the target hardware. The modeling framework adopted by static analysis lends itself to formal proofs which helps in establishing whether the obtained results are safe. Today, static WCET tools are commercially available, including aiT [39] and Bound-T [40]. There also exists several research prototypes, including Chronos [41], Heptane [42], and SWEET [43].

The safety and tightness bounds achieved by the static approaches are highly dependent on the assumed abstract model of the target hardware. Earlier the embedded market was traditionally dominated by simple and predictable processors, which were easy to model and thereby derive safe and tight bounds. But within the increased computational needs of modern embedded systems, designers have moved to complex processors which are mainly designed for performance and not for predictability. In such a case, all the intricacies contributing to unpredictability should be captured by the abstract model to provide acceptable bounds. Hardware modeling relies on the chip manufacturers to publish the details of the internal workings, which is generally not provided for different reasons (intellectual property and to be ahead in the competition). The models must be therefore verified to ensure that it indeed reflects the target hardware. Failing to capture inherent performance enhancing features may result in overestimations of the execution times and the resulting bounds are not tight enough. Capturing all system states in a complex machine may lead to unacceptably high analysis times. Additionally, building and verifying the timing model for each processor variant is expensive, time consuming, and error prone. This is reflected in the high cost of commercial static analysis tools. Custom variants

and different versions of processors often have subtly different timing behaviors rendering timing models either incorrect, or unavailable.

2.1.3 Measurement based techniques

The basic principle of this method follows the mantra that “*The processor is the best hardware model*”. The program is executed on the actual hardware, *in isolation* and the execution time is measured by instrumenting the code at different points [44]. The major task in this analysis is running the program to ensure coverage of all the paths by feeding-in the representative set of inputs. Several thousands of program runs are carried out to capture variations in execution time due to the fluctuation in system states during the entire process. The maximum time recorded over all the runs, to which a safety margin is added is then reported as the WCET of the program.

This method is clearly unsafe because it is difficult to prove that path coverage ensures the worst-case execution path has been indeed taken. Another issue is whether the extra safety margin provably provides a safe bound, since it is based on some informed estimates and cannot be acceptable for safety critical systems. A very high margin will result in resource over-dimensioning, leading to very low utilization and while a small margin could lead to an unsafe system. The integrity of the actual code to be deployed in the target hardware is somehow depleted by the addition of the intrusive instrumentation code to measure the time. Although, still a popular choice in the industry, measurement based methods, have their drawbacks due to the aforementioned reasons.

2.1.4 Hybrid Approach

The hybrid approach, as the name suggests, assimilates the merits of the static analysis and the measurement based approaches. The approach uses measurements to extract timing for smaller program sections, and static analysis to deduce the final WCET estimate from these timings. The approach identifies certain flow paths using static analysis and the execution time of these flow paths is measured on real hardware or by cycle-accurate simulators. Finally, the information of the flow paths is combined with techniques from the static approach to determine the longest path. The advantage of the hybrid approach is that it does not rely on complex abstract models of the hardware architecture. However, the uncertainty of covering the worst-case behavior by the measurement remains since a safe initial state and worst-case input can not be assumed in all cases. Moreover, instrumented code is required which may not be allowed in particular certification. Example tools include Rapitime [37] and MTime.

Given that these tools exist for uniprocessors, an interesting question is whether they can be used for multicore analysis. The next section explains the need for a newer analysis framework.

2.2 Timing Analysis: Uniprocessors to Multicore systems

Most of the improvements in performance in uniprocessors is achieved by employing methods like pipelining, branch prediction, and out-of-order execution in the processor and off-chip caches. While caches are used to bridge the gap between processor speed and the access time of main memory, pipelines enable acceleration by overlapping the executions of different instructions. Control speculation (out of order execution, branch predictions) is used to avoid pipeline stalls caused by conditional jumps. These *on-chip subsystems* were the main focus of the uniprocessor timing analysis and a detailed survey of the work in this domain is presented in [10]. As a result of the extensive research, WCET analyzers which are adopted by the industry are already available for uniprocessors. Examples are aiT [10, 39], SWEET [10, 43] and RAPITime [10, 37].

2.2.1 Need for a new analysis paradigm

The key differentiator between multicores and their predecessors, the uniprocessors has not been in the basic processor design, but the packaging of these multiple cores, *sharing the same hardware resources*. The number of cores have been increased to boost the computing power, but the same resources that were dedicated to a uniprocessor systems are now shared by many cores in the case of multicores. The impact of sharing leads to considerable variations in the execution time of tasks, which cannot be overlooked. Although the earlier timing analysis tools developed for uniprocessors have robust methods to provide the WCET of tasks in isolation, the absence of an analysis of the impact of shared resources has become a very evident drawback in these tools, warranting an additional analysis framework to provide a holistic solution.

While the WCET of task in isolation is an inherent property of a task, the WCET of a task when co-executing with other tasks largely depends on their access patterns to the shared memory. Therefore a task τ_i running on Core π_p executing with task τ_j on Core π_q , sharing the same memory via a shared bus may have completed at time say C_{i1} , whereas the same task τ_i on Core π_p that executes concurrently with task τ_k assigned to Core π_q may complete at a different time C_{i2} ($\neq C_{i1}$). This change in execution behaviour must be captured by the newer analysis framework. As a logical progression, the current research for analyzing the temporal behaviour of tasks in multicores is now inclined towards studying the impact of these shared resources. To summarize, while there is enough research available on computing the WCET of a task in isolation, with all resources dedicated to it for uniprocessors, it cannot be adopted as is and will need to factor-in the impact of the extra delay due to contention on the shared resources.

As described earlier, the main focus of this work is the analysis of the shared resources, namely shared bus, caches and the memory. We shall next focus on each of this.

2.2.2 Background on the system bus (front side bus)

A bus in general refers to a bi-directional communication channel that transfers data between components inside a computer, or between computers. This expression covers all related hardware components (wire, optical fiber, etc.) and software, including communication protocols [45].

In multicore systems, the system bus or the front-side bus (FSB in the Intel's terminology) provides the communication channel between the processing units and the memory. All interrupt messages, memory, coherency traffic and I/O transactions flow between the cores and the chipset through the system bus. It is important to note that we do not deal with the I/O bus which connects with peripherals to the memory controller.

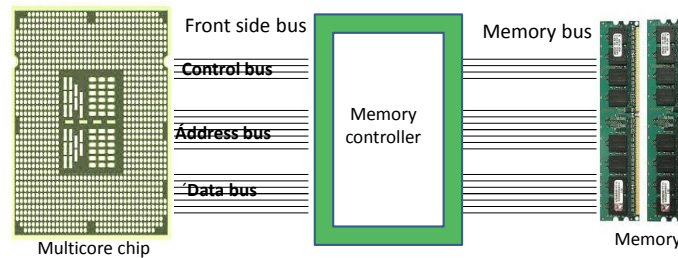


Figure 2.1: System bus (Front side bus)

Figure 2.1 illustrates the positioning of the FSB w.r.t the processing chip and the memory. Buses, in general consist of separate channels to transmit the data and the address of the memory location from where data is to be fetched from or written to. These channels are accordingly called the data bus and the address bus. Additionally there is a control bus which is used to transmit control signals across communicating units. The number of bits transmitted by the data bus (say 32 bits or 64 bits) represents its *width*. If the size of the data exceeds the bus-width, it is sent in multiple transfers. The size (or width) of the address bus indicates the maximum amount of memory a processor can address. Another property of the bus is the speed (clock frequency) at which it transfers data [46], expressed as number of cycles per second or Hertz (Hz). Bus clock speeds of 400 MHz, 533 MHz, 667 MHz, 800 MHz, 1066 MHz, or 1333 MHz are very common in modern processors.

Another important term associated with the bus is the *bandwidth* or maximum theoretical throughput which represents the amount of data it can transfer per time unit.

$$\text{Bandwidth} = \text{width} \times \text{clock frequency} \times \text{transfers per cycle}$$

The bandwidth is thus determined by the product of the width of its data path, its clock frequency (cycles per second) and the number of data transfers it performs per clock cycle [46]. For example, a 64-bit (8-byte) wide FSB operating at a frequency of 100 MHz

that performs 4 transfers per cycle has a bandwidth of 3200 megabytes per second (MB/s). This value is computed as $8B \times 100 \text{ MHz} \times 4 \text{ transfers/cycle} = 3200 \text{ MB/s}$.

2.2.3 Bus Transactions

Bus operations are performed on messages and transactions. We describe these terms here.

- **Message:** A message is a logical unit of information; for example, a write message contains a memory address to which the data must be written, control signals and the data to be written. A message requires a number of clock cycles to be sent from sender to receiver over the bus.
- **Transaction:** A transaction consists of a sequence of messages which together form a transaction. For example, a read transaction consists of a memory read message containing the address which must be read and a corresponding reply with the requested data.

Bus transactions can be carried out in several ways:

1. **Atomic bus transaction:** The simplest way to perform a non-split or atomic transaction is to implement a shared bus with an *atomic bus protocol*. In such a mechanism a transaction is modeled as an indivisible request-reply pair. A given request cannot be serviced before the bus transmits the response to the prior request. While this is simple to implement, the bus is underutilized and there is a performance hit considering that the next request is served only after the response to the previous request is obtained. In order to improve the throughput of the bus, designers have implemented mechanisms like *pipelining* and *split transactions* [47].
2. **Bus pipelining:** A bus transaction is divided into multiple stages (like arbitration, bus request, error reporting, snoop, reply, data). For example, the control bus handles sub-operations like the arbitration, request, error reporting, while the data bus is responsible for transmitting the data written to or read from memory. Since each part of the transaction does not use the same bus signals, a pipelining mechanism which entails overlapping multiple transactions that do not use the bus components simultaneously, is employed to increase the throughput (number of requests served in a given time). For example, the data bus is not used during address cycle, and address bus is not really needed during data cycles. Then the utilization of the bus can be improved by overlapping the address cycle of each transaction with data cycles of previous transaction. In general, any two phases of a transaction that use a separate set of physical signals (wires) can be pipelined.
3. **In a split-transaction bus,** a transaction is demarcated into two sub-transactions: a request transaction and a reply transaction. Both transactions (requests and replies) have to compete for the bus by arbitration. In such a mechanism, when a core places

a memory request on the bus, that core then immediately releases the bus, so that other requesters can use the bus while the memory request is in the process of being served. When the memory request is completed, the memory module involved will then acquire the bus, place the results on the bus (the read value in the case of a read request, an acknowledgment in the case of a write request), and also place on the bus the identity number of the core that made that request. The memory response is tagged with the identity of the core and the bus controller redirects the response to the corresponding core.

A pipelined bus provides responses in the order in which the requests were sent, while with split transaction buses, responses may be served in an order which does not match the order of requests issued. The advantage of a split-transaction bus over a pipelined bus is that a low-latency response does not have to wait for a high latency response to a prior request. The disadvantage (of a split transaction bus) is that both the request and the response phases must arbitrate for the bus and must be tagged with the identity of the requester. An atomic bus and a pipeline bus, by design are examples of in-order buses, while a split-transaction bus is an example of an out-of order bus.

We assume a shared-bus with an in-order, atomic transaction protocol

Another way to minimize the stall times in the processor is by a hardware initiated prefetching mechanism.

Hardware Prefetching Modern processors also provide hardware pre-fetching as a memory-latency hiding mechanism. The prefetcher predicts the next memory addresses to be accessed and pro-actively fetch this data from the main memory to the last-level caches based on observing memory access patterns. Processors based on the Intel NetBurst micro-architecture provide two prefetch mechanisms through the BIOS: Automatic hardware prefetch and Adjacent Cache Line Prefetch [48]. The Automatic hardware prefetcher prefetches streams of data and instructions from memory into the unified L2 cache on detecting successive L2 cache misses and a stride in the access pattern, as in accessing successive elements in an array, leveraging the property of locality of reference in program access patterns. The Adjacent Cache-Line Prefetch mechanism, when enabled through the BIOS, always fetches two 64-byte cache lines, irrespective of whether the additional cache line has been requested or not. However, there are two main problems when real-time tasks are concerned. Firstly, the prefetch requests consume bus bandwidth and may delay important demand requests issued by real-time tasks. Secondly they can lead to cache pollution by prefetching lines that are not required by the tasks and evicting re-usable cache lines belonging to real-time tasks. When enabled, this OS-transparent prefetching can run in the background at arbitrary times, resulting in variations experienced by the currently executing tasks. Many processors, e.g. from Intel, allow programmers to disable

this feature (see [48]) and it is important to do so to minimize the variations in temporal behavior.

In this work, we assume that hardware prefetching is disabled

2.2.4 Contention on the system bus

As described earlier, multiple cores access the main memory via a shared bus. This often leads to contention on this shared channel, which results in an increase of the response time of the tasks. Analyzing this increased response time, considering the contention on the shared bus, is challenging on COTS-based systems mainly because:

- bus arbitration protocols are often undocumented and the implementation of arbitration protocols is hidden
- the exact instants at which the shared bus is accessed by the tasks are not explicitly controlled by the operating system scheduler; they are instead a result of cache misses, TLB misses, coherency traffic, etc.
- requests are not tagged with any task priority information and thus, although the cores may enforce this prioritization and give preferential access to tasks with higher priorities, the bus may re-order the memory requests based on its internal prioritization and request scheduling mechanisms. As a consequence, requests issued by higher-priority tasks may be served later than those from lower-priority tasks.

To complicate matters, the FSB in modern processors may be an out-of-order bus (e.g., the Intel Itanium Processor Family) and employ other performance-enhancing mechanisms, including split transactions and pipelining. If pipelined buses are employed, the time for several bus transactions is not tightly bounded by simply adding the execution times of the individual transactions, since the phases within a transaction (typically arbitration, request, error, snoop, response, optional data phase) may be overlapped. For example, the Intel 4 Chipset Family boards [19] have a 12-deep in-order queue to support up to twelve outstanding pipelined requests on the FSB. In principle, the extra overhead due to the FSB is attributed to two main factors: the communication delay on the bus, which depends on the speed and data width of the bus and the time until a free slot is available on the bus. If requests are served in-order, then the first overhead can be upper bounded, since the required parameters are generally documented. The second factor is largely dependent on the bus arbitration mechanism which we shall explore next. The shared-bus architecture is appealing to chip designers given its simple topology, low area cost and the ease of implementation. The disadvantages of shared bus architecture are larger load per data bus line, longer delay for data transfer, larger energy consumption, and lower bandwidth [49].

When multiple requesters compete to access a common resource, like a shared memory, a networking switch fabric or a computational element (processor), an arbiter is required

to determine the order in which the shared resource is granted access to the requesters. In the next part, we will look at different arbitration mechanisms.

2.2.5 Bus arbitration policies

Associated with every bus is a protocol that defines the order of access by the devices attached to the bus (arbitration), the rules that the attached devices must follow to communicate over the bus (handshaking), and the signals associated with the various bus lines. Bus arbitration is based upon devices being classified as either master devices or requesters (devices that can initiate a bus transaction) or slave devices (devices which can only gain access to a bus in response to a master device's request like the bus controller). In the case of a shared bus, the bus arbiter controls the access of multiple cores to the shared memory. In the case of simultaneous requests for access to the bus, the arbiter resolves these access conflicts by serializing the requests from the different cores according to a set of rules which constitute the arbitration policy. This arbiter can grant the bus to a requester for a fixed number of bus *slots*, where each bus slot may span over a number of bus cycles.

Arbitration policies can be primarily categorized as dynamic and static arbitration policies. A dynamic arbitration policy resolves simultaneous accesses at runtime, while a static arbitration policy strictly defines the access pattern at design time. Fixed priority arbiters, first-in first-out (FIFO) and round-robin arbiters are examples of the dynamic arbitration policy, while Time Division Multiplexing (TDM) is a classical example of a static arbitration policy. Fixed-priority arbitration may be used in platforms with diverse response time requirements, TDM in platforms that require robust partitioning between applications, and round robin when a simple notion of fairness between cores is required.

In the *fixed-priority* arbitration policy, each requester is assigned a unique priority, and the grant is given to the active requester with the highest priority. The key shortcoming of priority arbiters is that, if high priority tasks are highly memory intensive, then requests from lower priority tasks may starve and may need to wait indefinitely before receiving a grant to access the bus.

A *round-robin arbiter* on the other hand, is a fair scheme and allows every active requester to access the bus in-order. It is also called the rotating priority scheme, in which the requester that is most recently granted the bus receives the lowest priority, while the next requester receives the highest priority. The basic algorithm dictates that once a requester has been served it would "go around" to the end of the pending request queue and be the last to be served again.

A specialized version called the *weighted round-robin* arbiter first assigns different *weights* to requesters and grants them bus cycles proportional to their weights; a higher weight means a higher number of cycles. This weight assignment is done repeatedly after N cycles. For example, if three requesters are assigned weights 1, 2 and 3, then they get $N/6$, $2N/6$ and $3N/6$ cycles every N cycles periodically whenever they access the bus [49].

In the *First-in First-out* arbitration scheme, a queue is maintained that stores a list of master devices (or processor cores) that are ready to use the bus in the order of bus requests. The access to the bus is thus serialized by a mechanism in which the cores that had to transmit earliest are placed at the front of the queue while later requesters are added at the end of the queue. One main drawback is the possibility of the arbiter not intervening if a single master at the front of the queue maintains control of the bus, never completing and not allowing other masters to access the bus.

A *Time Division Multiplexing* arbiter works by periodically repeating a schedule, or frame, with fixed size. Each core is allocated a pre-computed number of slots in the frame at design time. Requests from a core are only scheduled during slots allocated to that core. Empty slots or slots allocated to other cores without pending requests are hence not utilized. This type of policy makes the timing behavior of memory requests of tasks scheduled on different cores completely independent.

TDM arbitration, is therefore by design a composable and predictable arbitration scheme; predictable since the maximum time of access to a resource is bounded and composable because the access time is independent of other requesters. The round robin arbiter on the other hand is predictable, as the maximum time of access to a resource is bounded, but not composable, since the access to the shared resource (the bus here) depends on the number of other active requesters. A fixed priority arbiter, is neither predictable nor composable as the time for access to a resource cannot be upper bounded until there is sufficient knowledge about the access patterns of the higher priority requesters.

Some of the bus standards for the system buses include (i) Advanced Microcontroller Bus Architecture standard from ARM which defines the Advanced System Bus in their earlier processors and the AHB (Advanced High-performance Bus) in the more recent versions (ii) CoreConnect from IBM which it refers to as Processor Local Bus and (iii) the Front Side bus from Intel. The buses from ARM and IBM also apply for System-on-chip designs where the main memory and the cores reside on a single chip.

Bus Topology Multiple cores can be connected to each other in different ways as seen in Figure 2.2.

In this thesis, we analyze cores connected by a shared bus and mesh topologies.

After studying the basics of the shared bus, let us understand another resource, which plays a vital role in execution time of the task: the cache.

2.2.6 Caches and cache analysis

In most of the existing multicores, the large gap between the core speed and the memory is bridged by keeping the most frequently accessed data closer to the cores. In simple terms a cache is a storage area which buffers the most recent memory accesses. In the overall

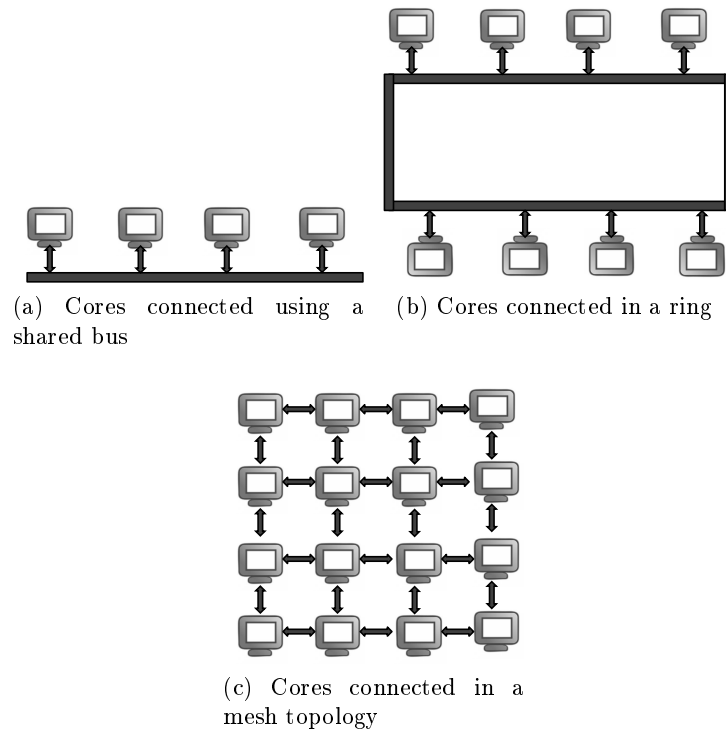


Figure 2.2: Bus Topologies

system architecture, caches are organized as stacked hierarchy; the CPU is at the top, followed by layers of one or more caches and then the main memory. In this multi-level hierarchy, caches are quantified by their level. The cache closest to the CPU is called level one, L1 for short— caches increase in level until the main memory is reached.

Cache Line A cache line or cache block is the smallest unit of memory that can be transferred to or from a cache. The essential elements that quantify a cache are called the read and write line widths. These signify the minimum amount of data the cache must read or write from the memory or cache below it. Frequently, these quantities are the same, so caches often are quantified simply by the line width.

Cache Size The next property that quantifies a cache is its size. This number is an indication of how much data could be stored in the cache.

Inclusive and Exclusive caches A multilevel cache can be either inclusive or exclusive. In an exclusive cache, a particular cache line may be present in exactly one of the cache levels. Alternatively in an inclusive cache, the cache line may be present simultaneously in more than one level of the cache.

In this work, we make no assumptions on the inclusivity

Write policy The write policy determines the time at which the modified cache line is written back into memory. In a *write-through* cache the main memory is made consistent with the modifications in the cache line immediately after a cache-line write. In contrast, in a write-back cache the process of updating the main memory is deferred to a later time, until the given cache line is evicted. The status of the cache line is however marked *dirty* in order to signal that the memory copy and the cache-copy are not coherent with each other.

In this work, we assume *write-through caches*

Cache associativity In general, caches consist of several “sets”, each of which consists of k “ways”: k is called the “associativity”, and is usually 1, 2, 4, 8 and is higher (16 way is not uncommon these days) in modern day processors. Caches are called direct mapped for $k = 1$, and set associative otherwise. Each way can hold one line from memory. The entries stored in the caches are not single words but, instead, “lines” of several contiguous words. In early caches these lines were 32 bytes long; now the norm is 64 bytes – and the terminology used is that the cache line size is 64 bytes. The relationship of all these values to the cache size is

$$\text{Cache Size} = \text{Cache line size} \times \text{associativity} \times \text{number of sets}$$

Thus a cache with associativity 8 with a cache line of 64 bytes containing 512 cache sets has cache size of 256k bytes.

Cache replacement policies: On cache updates, the replacement strategy determines the cache-way which must be evicted to store the current cache-line. Common strategies for replacement are pseudo-least recently used (PLRU), LRU (in older processors), first-in first-out (FIFO) and random replacement. LRU replacement conceptually maintains a queue of length k for each cache set, where k is the cache associativity [50]. If an element (a memory block) is accessed that is not in cache (a miss), it is placed at the front of the queue. The last element of the queue, the LRU element, is then removed if the set is full. At a cache hit, the element is moved from its position in the queue to the front, in this respect, treating hits and misses equally. LRU replacement is used in the Freescale PPC603E core and the MIPS 24 K/34 K. FIFO cache sets can also be seen as queues: New elements are inserted at the front, evicting elements at the end of the queue. In contrast to LRU, hits do not change the queue. FIFO is used in the Intel XScale and some ARM9 and ARM11-based processors. PLRU is a tree-based approximation of the LRU policy. It arranges the cache lines at the leaves of a tree with $(k - 1)$ “tree bits” pointing to the line to be replaced next (for an in-detail explanation of PLRU, consider [51]). It is used in the PowerPC 75x and the Intel Pentium II, Pentium III and Pentium IV processors. The precision and efficiency of cache analysis strongly depend on the predictability of the

employed replacement policy. The LRU replacement policy is most predictable of the known policies. Employing other policies, like PLRU or FIFO yield less precise WCET bounds, because fewer memory accesses can be precisely classified.

In this work, we make no assumptions on the replacement policy

2.2.7 Problem with shared Cache Analysis

An important step in timing analysis of a given task is its cache analysis, which tries to classify memory accesses as hits or misses. Memory accesses that cannot be safely classified as a hit or a miss have to be conservatively accounted for by considering both possibilities. Apart from the high associativity and the write policies, the predictability of cache behavior is largely influenced by the replacement policy, which is usually pseudo least-recently used (PLRU) in many multicore platforms from Intel and Infineon. The impact of these replacement policies on predictability has been presented in [51].

In uniprocessor systems, the problem of sharing the cache among tasks that could pre-empt each other (pre-emptive scheduling) on the same core is intricate [52] and the analysis to compute this extra cache-related pre-emption delay is already non-trivial. The problem is further exacerbated in multi-cores when co-executing tasks on other cores share and contend for the same cache lines, thereby increasing the possibility of cache-line evictions. Although the higher capacity of the caches was provided to decrease the accesses to main memory and thus reduce the stall time of executing tasks, non-ownership of these shared cache lines by the cores can lead to unregulated cache evictions and cache thrashing. This defeats the very purpose of providing a larger cache as it leads to increased memory requests. Additionally, bounding the number of memory requests that a particular task may generate in an interval is challenging at design time, since memory requests from tasks do not arrive periodically and the order in which tasks are executed is dependent on the on-core scheduling policy. In fact, the number of varying patterns of task arrivals on other cores, replaceable cache lines and memory request patterns result in a combinatorial explosion of possibilities. As seen above, given the complexity of the caches present in modern day processors, it is extremely challenging to derive tight estimates for shared caches. In [53], the authors clearly demonstrate that cache partitioning provides an effective means of bounding and controlling interference patterns in shared cache on a multicore system. In particular, WCETs can be bounded and controlled much more tightly when the cache is partitioned. This allows system designers to set relatively tight, yet safe, execution time budgets, thereby maximizing system utilization. The impact on bounding WCETs is more pronounced when the working set size of the task fits within the cache partition assigned to the core. That said given that embedded, real-time applications tend to have relatively small working set sizes, it is expected that cache partitioning will benefit most applications. In lieu of these facts, it may be said that hard real-time systems are more likely to be developed on processors with private caches or by either disabling or

partitioning the shared cache, if present. Hence in our analysis we consider *non-shared* caches only.

In this work, we assume non-shared caches

After an insight into the caches and the interconnection network, the document next proceeds to study the contention at the next level: the memory sub-system.

2.2.8 The Memory Device

As described earlier, requests from the cores and the peripherals (including DMA requests) are eventually directed to the Dynamic Random Access (DRAM) main memory via the memory controller. The unpredictability in DRAMs stem from their internal architecture, which is designed to deliver high volume storage at low cost per bit. To reduce area and power, it additionally tries to minimize the number of off-chip pins by using a bi-directional data path. A contemporary COTS-system typically contains many DDR3 (Dual Data Rate) DRAM chips [54] connected in parallel on a dual in-line memory module (DIMM) to form a 64-bit data path to the memory. The chips may be organized in one or more ranks that share the same interface to increase its utilization without increasing the number of pins.

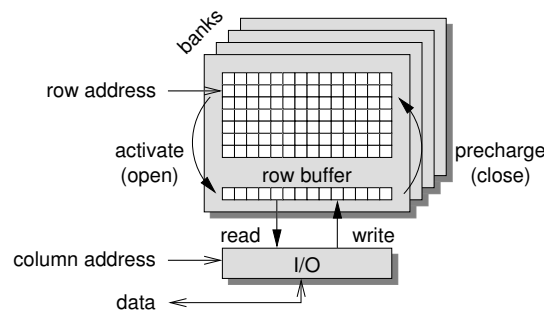


Figure 2.3: Illustration of a DRAM chip.

As illustrated in Figure 2.3, each DRAM chip comprises several banks that can be accessed in parallel. Each bank contains a matrix-like memory array of rows (also called pages) and columns. In addition, each bank has a row buffer that can store the contents of one row. On a DRAM access, the target row must first be activated (opened) by copying its contents from the memory array to the row buffer before read or write operations can be issued to the word-sized column elements. Once there are no more read or write operations, the row is precharged (closed) and the contents of the row buffer are copied back to its original place in the memory array [55]. The operations like activate row, precharge row, read from or write to the memory constitute the DRAM commands which are issued by the memory controller.

The DRAM architecture makes the response time of memory requests and the provided bandwidth highly variable for three reasons:

1. a request targeting an open row can be served immediately, while it otherwise needs the current row to be closed and the required row to be opened (details follow in the next sub-section),
2. the bi-directional data path requires several cycles to switch from read to write and vice versa,
3. to prevent data loss, the memory must occasionally be refreshed before executing the next request and the added refresh time may be longer than the time to serve the request itself.

The impact of these three factors may cause the execution time of e.g. a 64 Byte memory request to vary by an order of magnitude from a few clock cycles to a few tens of cycles. DRAM memories can hence be considered highly unpredictable resources by nature and are challenging to work with in the context of real-time systems.

2.2.9 Memory Controller

The memory controller connects the system to the off-chip DRAM and is responsible for scheduling memory accesses according to the system requirements. In a COTS system, the memory controller achieves this by maximizing the average bandwidth and minimizing the average latency, while limiting power consumption. This typically implies maximizing the utilization of the data path, possibly subject to different priorities of memory streams, when there are pending requests and make efficient use of power-down modes in the memory device when there is idle time. Overall, there are three factors that affect the response time of memory requests in the memory controller: i) the page policy, ii) the scheduling algorithm, and iii) the power-management policy. We proceed by discussing each of these in turn.

Page policy The page policy determines when precharge commands should be issued by the memory controller [56]. Currently, there are two prevalent page policies: open page and close page.

The open-page policy tries to improve the average performance of the memory controller by exploiting locality among memory requests. This is achieved by speculatively keeping activated rows open after memory accesses, hoping that the following requests to the banks target the same rows, thereby eliminating the latency and power overhead of activating and precharging the banks [55]. The drawback of this approach is a latency penalty in case the following request requires different rows in the banks, as this results in precharging and activation while the request is stalling. The open-page policy works well in case there is

sufficient locality in the memory stream to generate enough row hits to make a net gain in average performance despite this penalty.

In contrast to the open-page policy, the close-page policy always closes the active rows immediately after each memory access to minimize the overhead of opening another row in the same bank. This policy is beneficial when there is not sufficient locality within the memory stream of an application, or when locality is destroyed when memory streams from different applications are multiplexed in the memory controller to access the single off-chip memory. This policy is typically favored by memory controllers for hard real-time systems [57, 58, 59], since they are unable to guarantee any locality in the worst case due to fine-grained sharing of the memory, and hence prefer to reduce the miss penalty.

Hybrid policies that combine properties of open- and close-page policies have also been proposed. To improve performance of their systems, Intel proposed an adaptive page policy [60] that dynamically switches between open- and close-page policies based on the locality in the memory streams. In the context of real-time systems, a conservative open-page policy [61] has been proposed. The key idea is to partially exploit locality by keeping active rows open as long as possible without negatively impacting the worst-case response time of memory requests. This approach works well if there is locality in the memory traffic and if requests arrive close enough together to enable row hits to be detected early.

In our analysis, we do not delve deeply into the memory subsystem. Any page policy that facilitates the computation of upper bounds on the time for a memory access can be modeled in our analysis.

We make no specific assumptions on the page policies

Scheduling algorithm The memory scheduler is responsible for ordering incoming memory requests and generating DRAM commands (like activate row, precharge row, read row) that are scheduled according to the timing constraints of the memory. This may involve a two-level scheduler, one level for memory requests and a second one for DRAM commands, although it is possible to integrate the two. The memory scheduler is often very dynamic and uses information about the memory state when scheduling to improve average bandwidth or reduce average latency. Optimizing bandwidth may involve preferring requests that target an open row in a bank [62, 56, 63], requests that fit with the current direction of the data path [64, 65, 66], or a combination of the two [67, 68, 69]. Example mechanisms that reduce average latencies is to prefer reads over writes [63], which is beneficial if reads are blocking while writes are posted, or let high-priority memory clients preempt lower priority clients [69]. Another technique to reduce latency is presented in [62] that schedules memory bursts belonging to the same requests simultaneously thereby unblocking the stalling processor earlier. It is also proposed in [70] to try to schedule refresh operations during idle cycle cycles when there are no requests pending or even executing multiple refresh operations in sequence when idle to amortize overhead [71]. The problem

with these dynamic memory schedulers is that the interactions between the request and command schedulers are complex, especially in the presence of the aforementioned mechanisms. Thus, neither of the above memory controllers provide bounds on bandwidth or latency, making them difficult to use in the real-time context.

Power policies DRAM memories have several power-down modes [54], e.g. power-down with fast exit, power-down with slow exit, and self-refresh. These modes have increasingly large transition times in and out of the low-power state, while the current through the memory is decreasing, thus offering different trade-offs depending on the length of the idle periods and the maximum tolerable wake-up penalty. A consequence of the sometimes substantial wake-up penalties is that the worst-case memory latency does not happen when the memory controller is maximally loaded, but when there are sudden bursts of memory requests while the memory is in self-refresh. Determining the critical instance for the memory controller may hence be difficult without information about the power-management policy, further complicating the process of estimating memory latencies with both analytical and measurement-based techniques.

Summary The time to serve a memory request is *highly variable* and strongly depends on the architecture of the memory itself, as well as the scheduling algorithm and page- and power policies used in the memory controller. All this information is generally *not* divulged for COTS systems, hence it is difficult to obtain an accurate estimate of the memory latency. The memory controller may offer configuration options to disable dynamic features, such as reordering mechanisms, which makes the scheduler easier to analyze. However, these options are not exposed to developers through the middleware (BIOS) in COTS systems. Instead, the only visible options are to reduce timing constraints of the memory to reduce latencies at the expense of reliability. These problems lead us to conclude that to improve the suitability of COTS systems in the context of real-time systems, more information is required about the scheduling algorithm and page- and power policies. The possibility to disable dynamic features of the controller must furthermore be exposed to developers through the middleware. This will enable researchers to accurately determine memory latencies using analytic or measurement-based approaches. We *do not* focus on analyzing the internals of a DRAM memory system in detail. However we will analyze a simple memory controller in Chapter 5. Given the complexity in analyzing the delay in each of the sub-components from the path from the core to the memory, we assume an upper bound on the time for accessing the memory.

In this work, we assume an upper bound on the memory access time

After looking into the workings of the shared bus, caches and memory subsystems it is important to recollect the work done during and prior to the duration of the thesis. We present the related work in the next section.

2.3 Related Work

2.3.1 Work on bus contention

Amongst different bus arbitration policies, Time Division Multiple Access (TDMA) arbitration policies have been studied by the academic community in great detail. The policy is designed for timing predictability and composability and thus simplifies the timing analysis to some extent. Systems employing TDMA can be analyzed compositionally (individual components are analyzed in isolation, and the system is deemed feasible, if all its components are feasible). Interference is eliminated through explicit temporal isolation by allocating the shared resource (in this case, the shared front side bus) in different slots. The following subsection will cite some noteworthy papers in this area.

2.3.1.1 Approaches employing TDMA bus arbitration

Rosen et al. [72] describe a solution to implement predictable real-time applications on multiprocessors. They propose a bus scheduling policy based on TDMA based on a previously statically defined scheduling policy. Different time slots to access the bus are allocated to different processors by static scheduling. This schedule is stored in a dedicated memory directly connected to the bus arbiter. This solution prevents any deadline miss due to bus conflicts. However, the approach used assumes a table-driven bus arbiter, which is typically not available in COTS-based systems. The method also needs to know the workload a priori, which is the whole set of tasks that run on the system at any given time, in order to avoid situations where the bus contention increases the memory access latency and hence is not flexible.

In a TDMA-based scheme proposed by Chattopadhyay et al. [73] and Kelter et al. [74], the effect of shared instruction caches and a bus is analyzed assuming separate buses and memories for both code and data (uncommon for commodity hardware) and the method does not address data accesses to memory and hence has a limited applicability.

In a related work by Schranzofner et al. [75], a TDMA based framework is developed for analyzing the worst-case response time of real-time tasks. This was followed by their work on resource adaptive arbiters in [76]. The authors proposed a task model, where tasks are sequences of superblocks. A superblock is a functional block that has a unique entry and exit point. However, different execution paths inside a superblock are possible. As a result, the sequential order of superblocks remains the same for any execution instance of a particular task. Each superblock is associated with its corresponding worst-case execution time (WCET) and its worst-case number of access requests to a shared resource. Superblocks are further specified by phases, where phases can represent implicit communication (fetching or writing data to/from memory), computation (processing the data), or both. These phases are called the acquisition, execution and replication phases. Given these phases different task models were proposed depending on the flexibility of the model in allowing memory accesses. The dedicated model confines accesses to the shared memory

to their respective acquisition and replication phases. In the general model, computation and accesses to shared resource can happen anytime and in any order and just has one phase called a general phase. In the hybrid model, there are dedicated communication phases and a general phase. Modeling tasks to fit in these models, like the dedicated model requires studying their memory access pattern to prefetch the required data for the computation phase in a burst. Superblocks are executed in some statically pre-defined order and these communication phases must be synchronized with the availability of the bus slot for that task, which may not hold for even a predictable arbiter employing TDMA. This requires major program intervention, compiler assistance to prefetch data besides being suited only to TDMA protocols. With many tasks executing on each core, finding the superblock sequence and the bus availability resulting in the worst-case execution time is computationally expensive. The problems of eviction by superblocks of other tasks are not explained in detail in this analysis.

The TDMA bus arbitration is predictable and composable, allowing tasks to be analyzed in isolation, making it a real-time friendly protocol. But it is non work-conserving and hence the bus is idle when the core owning a time-slot does not have any requests to be served. Although it is favored in the research community, existing COTS-based systems (which are designed for high performance) do not employ it.

2.3.1.2 Methods using Timed Automata

A method to model request patterns and the memory bus using timed automata is proposed by Mingsong et al. [77]. The authors use Abstract Interpretation (AI) to analyze the local cache behavior of a program running on a dedicated core. Based on the cache analysis, they construct a Timed Automata (TA) to model the precise timing information of the program on when to access the memory bus (i.e. when a cache miss occurs). They also model the shared bus using timed automata. But the drawback is that it handles only *instruction* accesses and may have a problem of state-space explosion when applied to data accesses.

Another method employing Timed Automata was proposed by Gustavsson et al. [78] in which the WCET is obtained by proving special predicates through model checking. This approach allows for a detailed system modeling, but does not scale and suffers the same problem as the previous approach: all system states have to be explored during the WCET analysis and this may lead to a state-space explosion.

2.3.1.3 Non-TDMA models of bus arbitration

In [79], Pellizzoni et al. compute an upper bound to the contention delay incurred by a task, by deriving arrival curves for different memory access patterns. Tasks are divided into superblocks and are run in *pre-assigned* time slots. The drawback is that the solution does not scale and practical deployment seems infeasible for a large number of tasks or cores.

Schliecker et al. [80] have proposed a method to address the issue of bounding the shared resource load for multiprocessor systems using a general event based model. They assume a set of tasks executing on a set of processing elements, all accessing a global shared resource. Accesses to the shared resource are defined as event models, defining the maximum and minimum accesses in a time window. The worst-case interference is then computed in an iterative process. Each transaction takes a certain amount of time to be processed, and therefore the maximal interference that can happen due to higher priority tasks can be derived from the event models. Priorities are assigned statically, and therefore interferences on one task propagate to all lower priority tasks. There are two main issues in their approach: their assumption of a minimum interval of time between two accesses to a shared resource leads to an over-approximation of the number of requests. Also they do not propose a scalable method to pack tasks to generate the maximum number of requests.

In [79], the authors compute an upper bound to the contention delay incurred by a task, for systems comprising any number of cores and any number of peripheral buses sharing a single main memory, for time triggered (periodic) tasks, using a restrictive pre-emption model. Tasks are split into superblocks. Each superblock can include branches and loops, but superblocks must be executed in sequence. Multiple tasks executed on the same processing core are scheduled according to fixed time slots, with a given set of superblocks assigned to each slot. The cache profile is computed for all the superblocks. To ensure that the worst case pattern of cache misses is captured, cache misses are packed as tightly as possible, so as to have maximum cache misses in the smallest time window. Peripherals are represented as buffered flows and an arrival curve is computed for each peripheral. The arrival curve provides an upper bound to the amount of memory traffic issued by the source (cores or peripherals) in any interval of time. All tasks running on the same core are aggregated into an unbuffered flow (stall while waiting to be serviced) and an arrival curve is defined for them. The delay of the task under analysis is computed based on the delays caused by all buffered flows and unbuffered flows from all other cores. This method relies on accurate cache profile computations, suitable assignment of time-slots to superblocks and imposes a restriction on where the tasks can be pre-empted. The analysis does not cater to non-periodic tasks and does not apply to real-time systems deployed on multicores with shared caches.

Several probabilistic models and corresponding analysis methods have been proposed to estimate the average-case latency of memory instructions (e.g [81]). This however does not provide an upper bound on the extra execution time that a task experiences due to contention in a multicore. And therefore, such methods are inappropriate for hard real-time systems.

Paolieri et al [82] propose a hardware platform that enforces an upper bound on the delay. Once this bound is determined, each access request of a hard real-time task to a shared resource takes exactly this amount of time. They introduce the WCET Computation Mode. Here, the hard real-time tasks execute in isolation, but the platform enforces the

upper bound on the delay for each access request, hence resulting in a safe upper bound on the WCET. This approach allows to analyze hard real-time tasks in isolation from each other, since the interference by other tasks is abstracted by the upper-bound on the delay. However, hardware for such an enforcement support is required, which is unavailable in many cases, in particular when using COTS systems.

2.3.2 Existing research on Cache Analysis

Although the higher capacity of the caches was designed to decrease the accesses to main memory and thus reduce the stall time of executing tasks, non-ownership of these shared cache spaces by cores can lead to unregulated cache evictions – cache lines belonging to tasks scheduled on one core may map to the same cache lines of tasks executing on another core, thereby evicting each others cache lines. This defeats the purpose of a larger cache as it leads to higher number of memory requests. Also, since the memory request patterns of tasks are arbitrary, determining the time at which the cache lines are evicted can be really difficult. These caches have been analyzed to some extent in the research community.

Yan and Zhang addressed the problem of computing the WCET for direct mapped, shared L2 instruction caches on multicores [83]. They compute the worst-case instruction access interferences between different threads based on the program control flow information of each thread and use integer linear programming to compute the maximum number of cache misses that a task could suffer. The assumptions made in the paper, that data caches are perfect (all requests to the cache are hits) and data references from different threads will not interfere with each other in the shared L2 cache are very strong. Since the work in the paper does not analyze data caches, it fundamentally limits the applicability of this method, considering the widespread use of data caches in multicores and their significant impact on the worst-case execution time. The work was later improved by discovering the timing order of the potential inter-core conflicts using cache conflict graphs [84].

Li et al. [85] proposed a method to estimate the worst case response time (WCRT) of concurrent programs running on multicores with shared L2 caches. Their work considered set-associative instruction caches which employ the LRU policy for replacement. They tighten their WCRT estimates by iteratively eliminating infeasible contentions on the shared cache. The contention elimination is enabled by checking whether a pair of tasks can arrive concurrently, given their timing properties, by considering the task dependencies (dependent tasks cannot co-execute) and by considering the task to core assignments. Their work was later extended in [73] by adding TDMA bus analysis technique to bound the memory access delay.

In summary, given the complexity of the problem, researchers have made assumptions which limit the applicability of their solution. They assume direct mapped caches or caches with low set associativity. They make the assumptions that data caches are perfect and thereby analyze instruction caches only or assuming that the underlying replacement policy

is LRU. Most of the works do not discuss whether the caches employ a write-back/write-through mechanisms, each of which greatly influences the time at which a request is served. The process of committing the pending buffered writes to memory in a write-back cache maybe deferred during a given tasks' lifetime, but the update may happen during the execution of the next task, and delaying its requests in the meanwhile. Such updates are done in a non-transparent manner, without the programmer's knowledge. If not factored in the eventual analysis, the resulting WCET estimates can be unsafe.

Researchers have also tried to avoid the problem of shared cache contention by employing software and hardware techniques of isolation, thereby circumventing the interference. We shall briefly visit these works in the upcoming subsection.

2.3.3 Avoiding cache interference by isolation techniques

An approach for multi-cores with shared instruction caches is proposed in [86] and is based on the combined use of cache locking and partitioning. Cache locking allows the user to load selected contents into the cache and subsequently prevents these contents from being replaced at runtime. Cache partitioning assigns a portion of the cache to each task and restricts cache replacement to each individual partition. The objective of such a joint use of locking and partitioning is to completely avoid intra-task and inter-task conflicts, which then do not need to be analyzed.

Cache partitioning techniques have also been proposed by Guan et al. [87]. Their method employs cache partitioning techniques such as page-coloring [88] combined with scheduling to isolate the cache spaces of hard real-time tasks running simultaneously to avoid the interference between them. Page coloring is a software technique that controls the mapping of physical memory pages to a processors' cache blocks. Memory pages that map to the same cache blocks are assigned the same color. With partitioning approaches, interferences caused by shared caches are avoided; on the other hand, partitioning comes at the cost of a smaller cache available per task/core. This in turn leads to more cache misses, more references to main memory thus increasing the traffic on the shared bus and subsequently the execution time.

Cache bypass techniques for instruction caches is proposed by Hardy et al. [89]. This approach is based on the fact that many blocks stored in the cache after a miss may not be accessed again before its eviction. Such blocks, named single-usage blocks contribute to cache pollution (a situation in which an executing computer program loads data into cache unnecessarily, thus causing other necessary data to be evicted from the cache into lower levels of the memory hierarchy, potentially all the way down to main memory, thus causing a performance hit). The authors propose a method for identifying such single-usage blocks and force the bypass of such blocks from the shared cache(s) thus tightening the WCET estimates. However, the method does not address data caches which heavily impact the WCET analysis. The proposed method also requires special support in hardware to identify instructions as non-cacheable and thus is inappropriate for COTS based systems.

2.3.4 Reflections on shared caches

As stated earlier, this work will consider multicore systems in which the caches are *not* shared. We believe that given the complexity of the caches present in modern day processors, it is extremely challenging to derive tight estimates. The literature survey carried out for shared cache analysis in Section 2.3.2 has been an important factor in the decision. Also, no analysis for shared caches has been verified on actual hardware. As seen earlier, methods of locking and partitioning have been researched and mature techniques are available to provide the required isolation desired by real time systems, which is another driver for adoption of non-shared caches. Our decision of using private caches is also guided by the certification requirements imposed by the industry that recommend partitioning for easier analyzability. Given these facts and norms, it is very unlikely that shared caches will be deployed in hard-real time systems. The state space of possible cache line assignments and evictions among (all possible) co-executing tasks on different cores sharing the same cache, is just too high to be analyzed safely at design time, for currently available caches with high set associativity employing non deterministic replacement algorithms like pseudo-LRU. We believe that partitioned or private caches are the way ahead for hard-real time systems and hence throughout our work, this assumption will hold.

2.4 Scope for further work

The research to-date has been crucial in setting up the building blocks towards the end goals of designing a robust, reliable industry acceptable solution. However we believe, there are enough avenues for improvement considering the current work in this area. We have listed some of these below:

- Firstly, there is the scope to go beyond TDMA buses and consider the issues of dealing with general work-conserving front-side buses. TDMA buses are real-time friendly but not work-conserving, leading to a large number of precious bus cycles being wasted when there are pending requests to be served. Hence this design is not currently preferred by performance driven commercial multicores, which are in contrast trying to bridge the gap between the processors and the bus speeds by increasing the pipeline stages in buses, employing split transactions to minimize response times amongst other features. This drives the need to carry out the analysis for a general work-conserving bus. The initial framework should be generic and then should be customizable later to suit other specific arbitration mechanisms.
- The memory request profiling presented by Schliecker et al. [80] can be improved. Their analysis is based on what is termed by the authors as the “minimum request distance” which means the minimum time between issuing two requests in a given code. Based on this minimum distance notion, they compute the maximum number of requests that can be generated in a time t . But such a simplistic assumption holds

for uniform request distribution but otherwise is agnostic to the arrival pattern of the requests. Clearly the bounds derived based on this metric are pessimistic and can be tightened.

- The method for computing per-core interference based analysis for non-static schedules is clearly missing in the existing works: A key step after analyzing the request pattern of an individual task is to be able to find the maximum number of requests, that the all the tasks on that core can generate in a given time t . While a method for computing such an interference for statically assigned task blocks is proposed in [76], such a method needs to be designed for non-static schedules. Such a general framework can then be tailored to suit different scheduling algorithms.
- There is scope for exploiting the request distribution of tasks to tighten the worst-case estimates. While earlier analysis have divided tasks into logical blocks and analyzed the resulting WCET, a finer grained analysis is possible by utilizing this request distribution to identify the gaps when co-executing tasks do not make memory requests. We believe this information can be leverage to tighten the analysis. Also, although the exact arrival instants of individual request cannot be known apriori, the knowledge of a coarser request distribution can also be vital in availing the idle slots on the bus.
- Most of the above works assume equal read and write memory access times. Asymmetric latencies are not dealt with. Existing approaches for contention analysis a fixed constant time for reads and writes, which may hold for systems in which the main memory is DRAM. Access times for reads and writes can vary highly for alternative memories like PCM (Phase Change memory) and Flash memory and then considering an equal upper bound on the access latencies may add up, leading to overestimation of the execution time.
- Existing work addresses the problem of deriving the upper bounds on bus contention to some extent, but the analysis is tightly coupled to a particular arbitration policy, such as TDM [90, 73, 74, 75, 76] or non-specified work-conserving arbiters [91, 80], and is not portable to the other policies employed in contemporary platforms. As a result, worst-case execution time estimation tools are limited to different point solutions for each system under analysis, complicating implementation and maintenance. This warrants the need for a unified framework which clearly demarcates between the arbiter dependent and independent phases and provides a common interface for analysis. We also work towards that aim in this thesis.

This chapter gave a brief insight into the timing analysis techniques, introducing the shared resources and enlisted the problems arising due to them in timing analysis. A summary of current research carried out in the area of shared resource contention was also

presented. This will help us towards formulating the steps to solve the problem, which is the main focus of the next chapter.

Chapter 3

Computing Per-Task and Per-Core Memory Request Profiles

*Possible is more a matter of attitude,
A matter of decision, to choose
Among the impossible possibilities,
When one sound opportunity
Becomes a possible solution.*

Dejan Stojanovic

3.1 Introduction

When tasks execute on a multicore system in conjunction with other tasks, there is a marked increase in their execution time in comparison to their execution time in isolation. This increase is mainly attributed to the fact that the co-executing tasks on different cores compete for access to the shared resources, like the shared memory bus. In this chapter, we develop the building blocks to estimate this increase in execution time, by computing the memory traffic (interference) generated by the other tasks. An important pre-requisite to the analysis is understanding the model and clearly enlisting the assumptions for which the proposed solutions hold, which is the focus of the upcoming subsection.

3.1.1 Design issues and assumptions

The underlying assumptions which will hold throughout the analysis for *multicores* are listed below:

A1. The interconnection network to memory is a bus: the rationale for this assumption is that although the general trend among chip makers is towards switched interconnection networks, the simple topology of the shared front side bus with a central arbiter makes it appealing to embedded system developers. Given that no mature solutions exist in

this design space, it forms the foundational steps before we investigate more complex bus topologies. We shall also explore the mesh interconnection network in Chapter 6.

A2. Non preemptive tasks: This assumption is made as a first step to avoid dealing with cache-related preemption delays and the effect of context switching overhead associated with preemptive scheduling.

A3. A constrained deadline sporadic task model: sporadic tasks have proven remarkably useful for the modeling of event-triggered real-time systems. Recall that in a sporadic task model, there is a pre-set minimum inter-release time between any two consecutive jobs.

A4. Partitioned scheduling (tasks have been assigned to processors before run-time and they do not migrate at run-time): With task migration, besides the delay of suspending the task and reloading the execution context on the other core, the private cache lines of the migrated task must be also re-fetched from memory over the bus. This extra time incurred by the migrated task in re-fetching its content and reloading the context constitute its *migration delay*. Since we want to focus on the problem of bus contention only, we do not allow tasks to migrate at run-time, thereby avoiding migration-related delay.

A5. Only one memory request can be handled at a time. Today, most of the commercial memory controllers implement complex and optimized features to improve the memory performance, such as multiple data rates or multiple channels. In such memory controllers, memory requests can be overlapped and multiple requests can then be served simultaneously. However, this assumption is made to simplify the analysis while still providing safe results.

A6. Each core has a private cache. The shared caches at all higher levels (L2 or L3) are disabled or partitioned. This assumption is made to focus on the problem of bus contention and is also driven by the certification requirements, like the ISO26262 [29] standard for the automotive domain and IEC 61508 [30] standard for programmable safety related devices. These standards typically favor isolation of components. Many cache partitioning and locking techniques have been proposed in literature which make this isolation possible. Processors like Freescale 8641D with only private caches are also available commercially in the market. Given the complexity of handling shared cache spaces in modern processors, we believe this assumption is not restrictive.

As described previously, other assumptions made in this work include write-through caches, absence of hardware prefetching mechanisms and the presence of a memory subsystem in which an upper bound on the time for a memory access can be determined. In addition, we assume that the core stalls during the data fetch or write operation to memory and assume a bus with an atomic transaction protocol.

3.1.2 Outline of the problem and the proposed solution

Program visualization Let us assume we have the multicore setup as in Figure 3.1. Tasks 1 and 2 are assigned to core 1, while tasks 3 and 4 are assigned to core 2. Let us

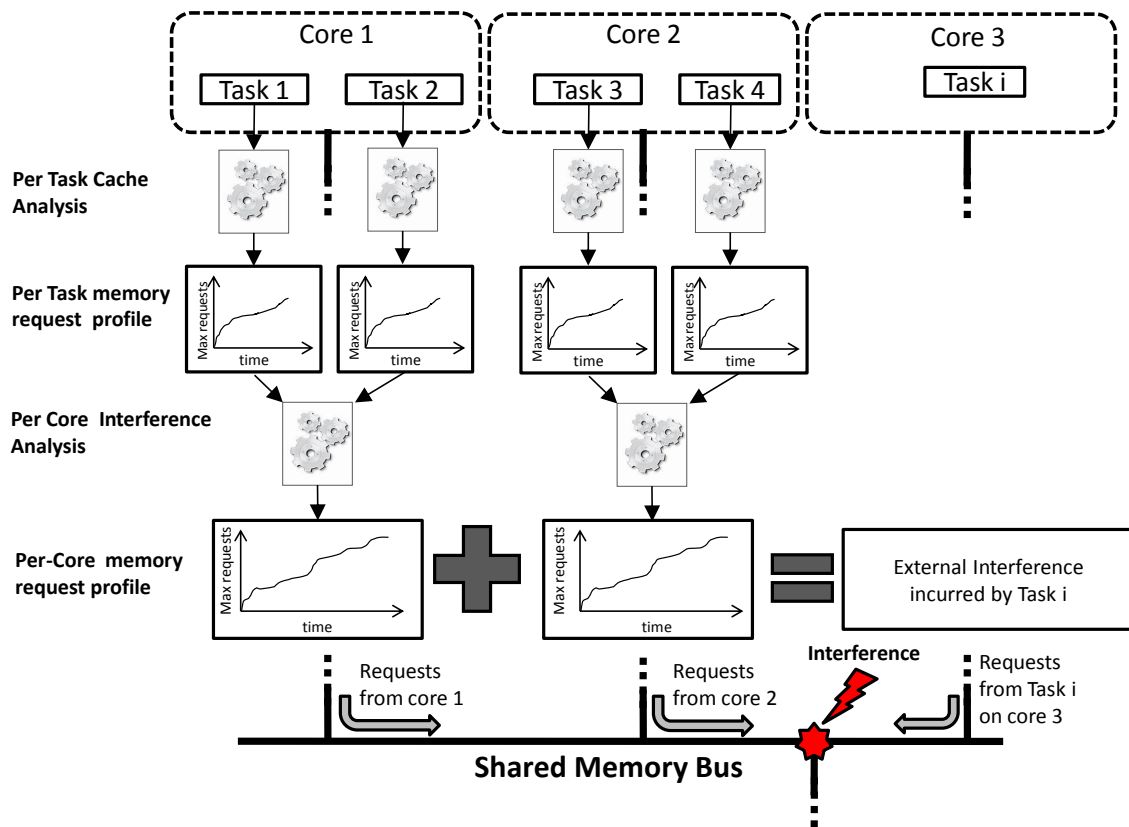


Figure 3.1: Demonstration of Contention on the memory bus. The gear boxes symbolize the methods to be employed.

assume we have to analyze task i executing on core 3. The execution time of task i is computed as the time for processing the data and the time for fetching/writing the data from/to the main memory. While computing this time is not overly complex in isolation, this computation is challenging if there is an “external interference” or extra delay due to contention on the off-chip resources like the shared bus and the shared memory. In this particular example, task i faces interference from the co-scheduled tasks executing on cores 1 and 2. We need to quantify this interference. In order to do so, it is necessary to model the memory access pattern or the traffic introduced on the shared bus from each core. Looking deeper into the cores, the traffic pattern of every task executing on that core must be modeled.

The analysis is performed in different steps, as illustrated in Figure 3.1 and summarized below:

- **Step 1: Per-Task Cache analysis:** In this step, a task is executed in isolation and the maximum and the minimum number of memory requests is captured during the span of its entire execution (these memory requests are the result of the last level cache misses). Cache analysis tools already exist as part of the tool-chain in timing analysis tools (static timing analysis and measurement based methods) and are leveraged in

the further analyses presented in this chapter. More detailed characterization of the memory request pattern of a task is obtained by sampling the task at different points in the code. As a first step, we model the bounds (lower and upper) on the number of requests generated by a task for a *single* execution. This step is explained in detail in Section 3.3.

- Step 2: *Per-Task Memory Profile Analysis*: Task memory profile analysis entails computing the maximum number of memory requests that can be generated by the task over *any given interval of time*. The input to this analysis is the model of the task characteristics obtained in Step 1 and given this, the task memory profile analysis tool computes the maximum number of requests the *task* will generate in any given time interval of length t . Note that unlike the per-task cache analysis tool, the task memory profile analysis tool takes into account *several jobs* that may have been released by the task in the given time interval of length t . This step is explained in detail in Section 3.4.
- Step 3: *Per-Core Memory Profile Analysis*: Since there can be *jobs of different tasks* executing on a given core, we then develop a per-core memory profile analysis tool. The input to this analysis is the set of *different* tasks assigned to the core under analysis, their respective arrival patterns and the task memory request profiles computed in Step 2. The tool then computes the maximum number of requests that the set of tasks assigned to the given *core* will generate in any given time interval of length t . This step is explained in detail in Section 3.5.
- Step 4: *External interference analysis* : Given a task under analysis assigned to a given core, we imply by *external* interference, the memory traffic generated by the tasks assigned to the *other cores*. These external requests compete with the requests of the analyzed task for the shared bus and thereby introduce a further delay in the execution time of the task.

The objective of this chapter is model the task characteristics with the help of existing cache analysis tools, and develop tools for task profile analysis and core profile analysis. It is important to note that these tools are independent of the bus arbitration mechanism and only deal with the amount of traffic reaching the shared bus from any core in a given time interval of length t . Hence they can be used to develop a generic framework for analyzing the WCET of the task which can address different arbitration mechanisms. We delve into the details of computing the increased delay due to contention, which is a function of the arbitration mechanisms employed by the bus, in the next chapter.

The rest of the chapter is organized as follows. The system model, task model and the scheduler specifications is described in Section 3.2. The cache profile of a task is modeled in Section 3.3, while the per-task memory profile analysis is detailed in Section 3.4. The need for a per-core analysis function is highlighted in Section 3.5 while the analysis to compute

the memory profile of a core is discussed in Section 3.6. The later part of the chapter deals with the properties of the per-core memory profile analysis in Section 3.7. The complexity of the per-core profile function is analyzed in Section 3.8. Next, we describe how this function can be adapted and used in different scenarios in Section 3.9 and finally evaluate it with experiments presented in Section 3.12.

3.2 System and Task Model

3.2.1 Platform Model

We shall introduce some notations here that will hold for the rest of the document. The platform is composed of a set of m cores denoted by $\pi_1, \pi_2, \dots, \pi_m$, and as stated, the cores do not share cache space. This model applies to systems in which each core has a private cache, or the shared cache if present, is disabled or partitioned. All the cores communicate over a shared bus in order to access the shared main memory. We borrow the terminology, Front-Side Bus from Intel to refer to the shared bus in this document.

We denote by TR, an upper bound on the time needed to perform a *bus transaction*. In general, a bus transaction is a complete sequence of bus actions required to perform a read (or write) operation. For example, during a read operation, TR includes the time for: the processor to drive the address onto the address lines, the memory controller to look up the address and fetch it from the memory and then drive the data in the data lines, and finally the time for the processor to read the data value from the data lines.

To focus on requests that are generated by cache misses only, we assume that any *hardware prefetching mechanism* is disabled in the processor. Earlier works in WCET analysis have overlooked mentioning this assumption but since most multi-core processors feature this, it *must* be highlighted. Turning off this mechanism reduces the unpredictability introduced by speculative prefetches, as such prefetches generate additional memory requests over the bus at arbitrary times (beyond programmer control): these extra requests consume bandwidth and contribute to the external interference. Finally, we consider that a core is stalled and performs no computation nor issue any new request, while it is waiting for the pending previous request to be served. This implies that there cannot be multiple outstanding requests from a given core at any time.

3.2.2 Task Model

The application is composed of a set of n tasks $\tau = \{\tau_1, \tau_2, \dots, \tau_n\}$. We assume a constrained-deadline sporadic task model in which each task τ_i is characterized by $\langle C_i, D_i, T_i \rangle$; a worst-case execution time C_i , a minimum inter-arrival time T_i and a deadline $D_i \leq T_i$, with the interpretation that, during the execution of the system, task τ_i releases a potentially infinite sequence of jobs such that two subsequent jobs from τ_i are released at least T_i time units apart. In order to meet its deadline, each job released by τ_i must execute

completely, for at most C_i time units within D_i time units from its release. We denote by R_i an upper-bound on the worst-case response time (WCRT) of task τ_i . The response time of a job denotes the time between its arrival and its completion and the WCRT of a task is the maximum amongst the response time of all the jobs released by the task. A method to compute the WCRT of tasks scheduled by non-preemptive, fixed-priority scheduling on uniprocessor systems has been proposed by researchers [92, 93].

Given a task τ_i , its memory request profile is modeled by the function $BR_i(t)$, that returns an upper bound on the number of bus requests that task τ_i can generate, when run in isolation, in a time interval of length t . We denote by $\pi(i)$, the set of tasks, excluding τ_i , that are assigned to the same core as τ_i . The notation $\bar{\pi}(i)$ will be used to denote the set of tasks *not* assigned to the same core as τ_i . Also, we denote by $lp(i)$ and $hp(i)$ the subset of tasks executed *on the same core* as τ_i and which have a lower and higher priority than τ_i , respectively.

3.2.3 Scheduler Specification

As noted, tasks are assigned to processors before run-time; i.e., we consider a partitioned scheme of task-to-core assignment in which tasks are not allowed to migrate from one core to another at run-time. As mentioned earlier, tasks run to completion and are not preempted. For the analysis, we will assume that each task assigned to a core is assigned a unique priority at design time. Note that the assumption of fixed priority scheduling has only been made for clarity of representation, but in principle the approach can be used with any fixed job priority algorithm which allows the computation of the WCRT R_i . To summarize, the proposed approach assumes a non-preemptive, fixed priority, partitioned model for the task set under analysis.

We make the following *non work-conserving* assumption: whenever a task τ_i completes in less time than indicated by its WCET C_i (say it completes in x time units on the core π_p), the scheduler idles the core π_p up to the theoretical WCET of the task, i.e., it idles π_p for the remaining $(C_i - x)$ time units. This assumption is made to ensure that the number of bus requests within a time window computed at design time, is not higher at run-time due to early completion of a task and the subsequent early execution of the next tasks. The effect of jitter which is inherent to any timing based design is not the focus of this work and thus will not be handled explicitly in the theory that follows.

3.3 Per-Task Cache Analysis

Given the complexity of the tasks' code, it may not be practically feasible to determine the exact time-instants at which tasks issue requests before run-time. However, there exist tools to compute the maximum number of requests that a task can issue in a given period of time, when the task runs in isolation. These tools are based on measurements [79, 91] or static analysis techniques. Measurement based methods use performance monitoring

counters [94] to monitor events like cache misses. The code of a task is instrumented at different points in the program and the minimum and maximum number of last-level cache misses (all of which then translate to bus/memory requests) at each instrumentation point are recorded after running the tasks a significant number of times over different inputs.

We model the memory requests over the bus (also called bus requests) issued by a task in isolation, as a result of the last-level cache misses, by these two functions.

- $ARH_i^j(t)$: returns an upper bound on the number of bus requests that a task τ_i may generate in an interval $[0, t]$ –which implies the time from the beginning of execution of the j^{th} execution path up to time t . Similarly,
- $ARL_i^j(t)$: returns a lower bound on the number of bus requests that a task τ_i may generate in an interval $[0, t]$ in the j^{th} execution path of task τ_i .

The execution time C_i^j of the j^{th} execution path of task τ_i is also recorded. We note that different executions of the same path may result in different number of bus requests owing to the underlying cache replacement policy; this is the reason why we distinguish between $ARH_i^j(t)$ and $ARL_i^j(t)$ for the same execution path j . We let $\text{paths}(\tau_i)$ denote the set of all the execution paths of task τ_i . By definition, $ARH_i^j(t)$ and $ARL_i^j(t)$ are non-decreasing functions for all i, j .

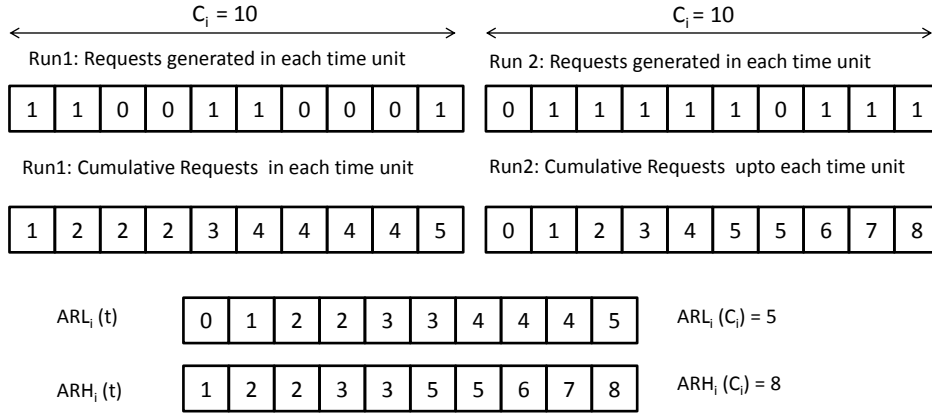


Figure 3.2: Illustration of the computation of ARH() and ARL() functions. The path index is dropped for brevity

We illustrate the computation of these bounds in Figure 3.2. Consider a task which executes for a maximum of 10 time units. Consider that we instrument the main memory requests at each time unit. In the figure, a “1” in a particular time unit represents that the task issues a memory request and a “0” implies the contrary. In this example, the memory requests obtained during two different runs for the same path j is captured. The cumulative number of requests upto each time unit has also been represented. In the first run, the task issues five memory requests until the end of its execution, while in the second run the task issues eight requests. For each time unit, the minimum and the maximum

requests issued correspond to the $ARL_i^j(t)$ and $ARH_i^j(t)$ values for the corresponding time units. We also denote by $NReq_i$, the maximum number of requests generated by task τ_i during its execution i.e., $NReq_i \stackrel{\text{def}}{=} ARH_i^j(C_i)$ for the path j that generates the maximum number of requests.

3.4 Per-Task Memory Profile Analysis

As seen above, methods exist to compute the number of requests over a *single execution-span* of the task. However, in order to model the task behaviour and to compute the traffic over a any given interval, we must be able to define a function $BR_i(t)$.

Definition 12. *The memory profile of a task is defined by the function $BR_i(t)$ that returns an upper bound on the number of bus requests that task τ_i can generate during any time interval of duration t , when run in isolation.*

To compute this function, we introduce the interval splitting technique.

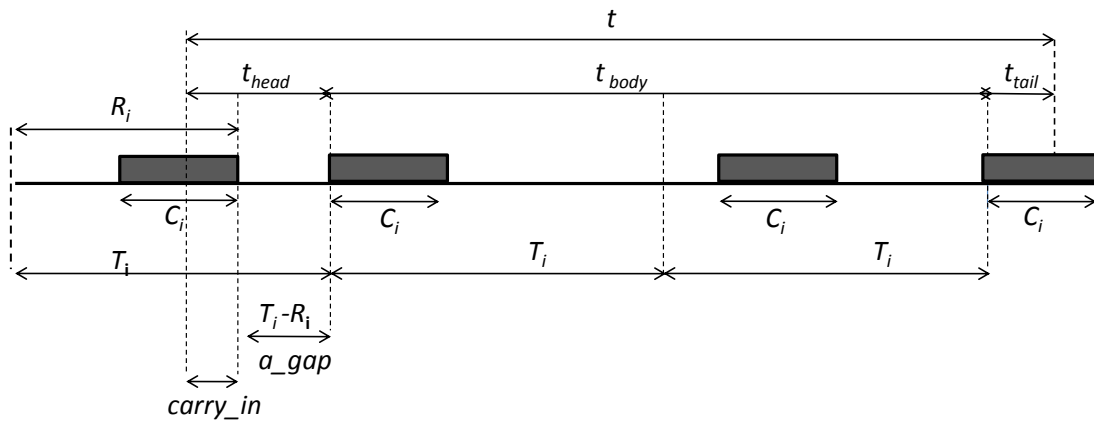


Figure 3.3: Calculation of $BR_i(t)$ for $t \geq C_i$

Interval splitting technique: Consider a time window of a given length t , for which we need to compute $BR_i(t)$ for task τ_i . To do so, we divide the time window t into three portions correspondingly: the *head* portion of length t_{head} , the *body* portion of length t_{body} , and the *tail* portion of length t_{tail} , such that $t_{\text{head}} + t_{\text{body}} + t_{\text{tail}} = t$ as shown in Figure 3.3.

The Head Portion: This portion consists of a *single job* that is released before the start of the time window but has its deadline in the time window, which means it may execute partially or completely within the window. Partial execution also includes the case when no portion of the job executes within the window. By definition, the head portion has a length of less than T_i . The head portion is in turn divided into two parts, namely, the *carry_in* and the *arrival gap* (a_gap). The carry-in portion represents the execution segment of the task which lies within the time window under consideration and it ranges from 0 to

C_i . On the other hand, the `a_gap` part represents the time between the completion of one job of τ_i and its next release and as shown in the figure has a length of $T_i - R_i$, where R_i as described earlier, is the response time of the job, and represents the time between the arrival of the job and its completion.

To summarize,

$$t_{\text{head}} \stackrel{\text{def}}{=} \begin{cases} \text{carry_in} + \text{a_gap} & \text{if } \text{carry_in} > 0 \\ 0 & \text{otherwise} \end{cases}$$

with $0 \leq \text{carry_in} \leq C_i$ and $\text{a_gap} = T_i - R_i$

The Body Portion: This portion consists of *job(s)* that are released within this time window and complete their entire execution within it. For a task τ_i , with minimum interarrival time T_i , the length of the body portion is given by can range from $0 \leq t_{\text{body}} \leq \left\lfloor \frac{t}{T_i} \right\rfloor \times T_i$.

The Tail Portion: This portion consists of a *single* job released within the given time window but has its deadline outside the window and hence may execute partially or completely within the time window. By definition, the tail portion has a length of less than T_i or $0 \leq t_{\text{tail}} \leq T_i$.

Having given an overview of the interval splitting technique, we next formulate a method (see Algorithm 1) which computes the maximum number of requests in an interval of time t , using the aforementioned concepts.

3.4.1 Algorithm to compute $BR_i(t)$

Algorithm 1 describes a method to compute the function $BR_i(t)$. The input to the algorithm is t , the duration for which the number of requests needs to be upper bounded, R_i , the response time of the task, C_i and T_i . When the task is run in isolation, we trivially set $R_i = C_i$. The algorithm computes the maximum number of requests by considering every feasible combination of t_{head} , t_{body} and t_{tail} .

Setting the length of each portion: The algorithm proceeds by initially fixing the `carry_in` part of the head portion which ranges from 0 to C_i and computes the arrival gap given by $T_i - R_i$. It then correspondingly calculates t_{body} portion as described in Equation 3.1. Finally the tail portion is assigned to the remaining portion of the time interval, as described in Equation 3.2. The assignment is also reflected in lines 3 to 16 of

Algorithm 1: ComputeBR()

```

input :  $R_i, C_i, T_i$  and time interval  $t$ 
output:  $BR_i(t)$ 

1 begin
2   total  $\leftarrow$  maxreq  $\leftarrow$  0 ;
3   for carry_in  $\leftarrow$  0 to min( $C_i, t$ ) do
4     if (carry_in == 0) then
5        $t_{\text{head}} \leftarrow 0$  ;
6        $t_{\text{body}} \leftarrow \lfloor \frac{t}{T_i} \rfloor \times T_i$ ;
7        $t_{\text{tail}} \leftarrow t - t_{\text{body}}$ ;
8     else
9       a_gap  $\leftarrow T_i - R_i$ ;
10       $t_{\text{head}} \leftarrow$  carry_in + a_gap;
11      if  $t_{\text{head}} > t$  then  $t_{\text{body}} \leftarrow t_{\text{tail}} \leftarrow 0$  ;
12      else
13         $t_{\text{body}} \leftarrow \lfloor \frac{t - t_{\text{head}}}{T_i} \rfloor \times T_i$ ;
14         $t_{\text{tail}} \leftarrow t - t_{\text{head}} - t_{\text{body}}$ ;
15      end
16    end
17    total  $\leftarrow f_i^H(\text{carry\_in}) + f_i^M(t_{\text{body}}) + f_i^T(t_{\text{tail}})$ ;
18    if total > maxreq then maxreq  $\leftarrow$  total
19  end
20  if  $t < C_i$  then
21    Compute maxreq1 as per Equation (3.6) ;
22    if maxreq1 > maxreq then maxreq  $\leftarrow$  maxreq1
23  end
24  return maxreq ;
25 end

```

the algorithm.

$$t_{\text{body}} \stackrel{\text{def}}{=} \max \left\{ 0, \left\lfloor \frac{(t - t_{\text{head}})}{T_i} \right\rfloor \right\} \times T_i \quad (3.1)$$

$$t_{\text{tail}} \stackrel{\text{def}}{=} \max \{ 0, t - t_{\text{head}} - t_{\text{body}} \} \quad (3.2)$$

Once the lengths of these portions are decided, the maximum number of requests that can be generated by the task in the corresponding portions is determined.

Computing the number of requests in each portion: The head portion: As said earlier, the head portion of τ_i consists of two parts: the carry_in and the a_gap. Since the task executes in the carry-in portion, it represents the portion of the *head* segment where requests are issued. On the other hand, the a_gap part represents the time between the completion of one job of τ_i and its next release; and therefore in the a_gap portion of the

head, no bus requests can be generated. An upper bound on the number of bus requests generated in the head portion is given therefore by:

$$f_i^{\text{head}}(t_{\text{head}}) \stackrel{\text{def}}{=} f_i^{\text{head}}(\text{carry_in}) \stackrel{\text{def}}{=} \max_{j \in \text{paths}(\tau_i)} \left\{ \text{ARH}_i^j(C_i^j) - \text{ARL}_i^j([C_i^j - \text{carry_in}]) \right\} \quad (3.3)$$

The body portion: In the body portion, there are *exactly* t_{body}/T_i complete executions of τ_i and the maximum number of request generated in the body portion is given by:

$$f_i^{\text{body}}(t_{\text{body}}) \stackrel{\text{def}}{=} \frac{t_{\text{body}}}{T_i} \times \max_{j \in \text{paths}(\tau_i)} \left\{ \text{ARH}_i^j(C_i^j) \right\} \quad (3.4)$$

The tail portion: Finally, the length of the tail part is less than T_i , implying either one partial or one complete execution. The number of bus requests generated in the tail part can be bounded from above by:

$$f_i^{\text{tail}}(t_{\text{tail}}) \stackrel{\text{def}}{=} \max_{j \in \text{paths}(\tau_i)} \left\{ \text{ARH}_i^j(\min\{t_{\text{tail}}, C_i^j\}) \right\} \quad (3.5)$$

For every combination of t_{head} , t_{body} and t_{tail} , the algorithm computes the number of requests in line 17. The maximum recorded value of the number of requests generated is updated as the algorithm proceeds and the final value is returned as $\text{BR}_i(t)$.

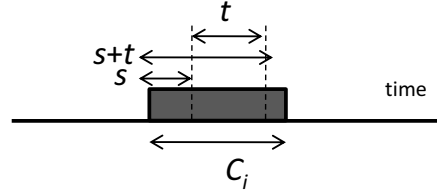


Figure 3.4: Calculation of $\text{BR}_i(t)$ for $t < C_i$

For the special case in which $t < C_i$ (Line 20), the maximum number of requests may be generated across two jobs (with only a `carry_in` and tail portion, and no body portion), or *in any arbitrary segment of the task*. In the latter case, we compute $\text{BR}_i(t)$ as per Equation 3.6, illustrated in Figure 3.4.

$$\text{BR}_i(t) = \max_{\substack{j \in \text{paths}(\tau_i) \\ 0 \leq s < (C_i - t)}} \left\{ \text{ARH}_i^j(\min\{s + t, C_i^j\}) - \text{ARL}_i^j(s) \right\} \quad (3.6)$$

3.4.2 Illustration of Computation of $\text{BR}_i(t)$

To illustrate the computation of the $\text{BR}_i(t)$ function, given the values of $\text{ARH}_i^j(t)$, $\text{ARL}_i^j(t)$, we consider a request pattern for task τ_i with a single execution path. We therefore drop the path index for readability in this example. The analyzed task τ_i has a C_i of 5 time units and T_i of 10 time units. The number of requests presented in Table 3.1 show the $\text{ARH}_i(t)$ and $\text{ARL}_i(t)$ values for the task during its execution i.e., $\forall t \in [1 \dots 5]$. For this

Time t	1	2	3	4	5
$ARL_i(t)$	1	3	5	7	12
$ARH_i(t)$	2	4	6	9	15

Table 3.1: ARL, ARH values for a single instance of a task

example, let us compute $BR_i(t)$ for a given value of $t = 24$, in isolation. We assume $R_i = C_i = 5$ time units and the value of a_gap therefore given by $T_i - R_i = 5$ units.

carry_in	$t_{head} = carry_in + a_gap$	t_{body}	t_{tail}	f_i^{head}	f_i^{body}	f_i^{tail}	sum
0	0	20	4	0	30	9	39
1	6	10	8	8	15	15	38
2	7	10	7	10	15	15	40
3	8	10	6	12	15	15	42
4	9	10	5	14	15	15	44
5	10	10	4	15	15	9	39

Table 3.2: Computation of $BR_i(t)$ for $t = 24$, $C_i = 5$, $T_i = 10$, $a_gap=5$

Table 3.2 illustrates the computation of the function $BR_i(t)$ for the given example with $t = 24$. We first fix the incoming $carry_in$ portion which ranges from 0 to C_i and the subsequent body and tail portions are determined accordingly as described in Equations 3.1 and 3.2. After enumerating all the feasible combinations of the head, body and tail portions of the task within the given time interval, we calculate the number of requests that each portion can generate using Equations 3.3, 3.4 and 3.5. The corresponding values are represented in columns f_i^{head} , f_i^{body} and f_i^{tail} respectively; in each row these values are summed up to obtain the total number of requests for the given combination. The maximum value obtained amongst all these combinations is then recorded as the final value of $BR_i(t)$. For the example, where $t=24$, the maximum number of requests are generated when the task executes with a partial head of 9 time units with $carry_in$ of 4 time units, executes one full execution in the body portion of 10 time units and a tail portion of 5 time units, as shown in the second last row, giving a maximum of 44 requests.

3.4.3 A brief analysis of the proposed method

Although it appears that the algorithm loops over all the values from 0 to C_i , in practice it is not feasible to compute the value of $ARH_i^j(t)$ or $ARL_i^j(t)$ for all execution paths and all values of t from 0 to C_i , as it is computationally expensive and hence the values must be computed at a coarser granularity. In practice, a limited number (say k) of sampling points are chosen from 0 to C_i and readings are recorded only at these k points. In such a method, whenever t is not equal to one of these k sampling points while reading $ARH_i(t)$ or $ARL_i(t)$, it is always important for these two functions to round-up the returned value to the next sampling point. This may result in an over-approximated number of requests for a given t , but the returned value will be safe. The algorithm is presented as such,

to separate the theoretical method which is generic, from the implementation which may depend on the hardware (e.g. the resolution of timers, which will decide the frequency of sampling).

The current method of exploring all paths is inevitable in static analysis, measurement-based or hybrid methods to ensure safe upper bounds. It can be optimized on an application-to-application basis, considering the input sets and eliminating paths which will not contribute to the maximum number of requests (for e.g. simple error reporting/recovery paths which return immediately or paths with certain conditional clauses). The proposed method can thus be applied after a path truncation phase and application of other optimization techniques which are not in the focus of this work. The proposed solution as such, is meant to serve as a generic method, irrespective of the application or the input set.

After analyzing the tasks to compute the per-task memory profile, we next proceed to model the upper bound on the memory traffic generated by a set of tasks executing on a given core.

3.5 Per-Core Memory Profile Analysis

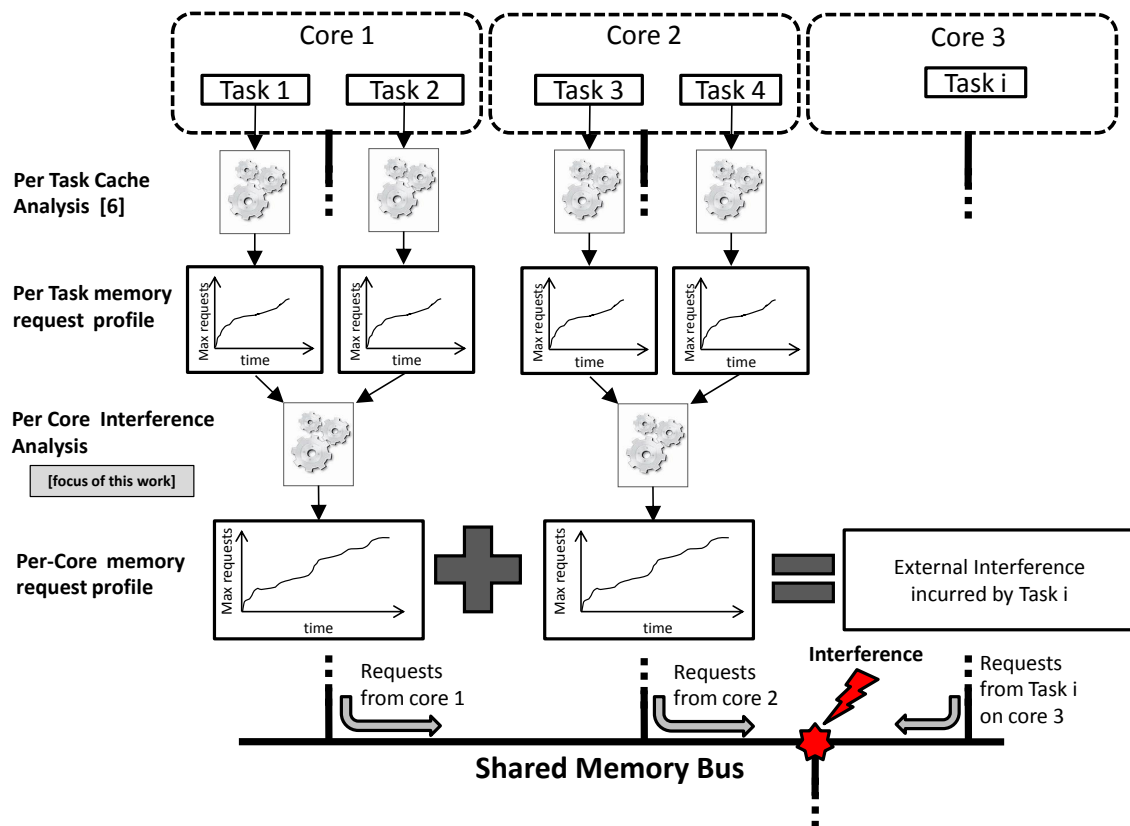


Figure 3.5: Need for a Per-Core Analysis Function

Definition 13. *The Per-Core Memory Profile of a task represents the maximum number of requests that can be generated by the set of tasks assigned to a given core π_p , in any time interval of length t and is given by the function $\text{PCR}_p(t)$, short for Per-Core-Request-Profiler.*

This section describes the role of this function and proposes a method to compute it.

3.5.1 Role of the PCR functions in the analysis cycle

Suppose that we have to compute the WCET of a task τ_i when it runs in conjunction with other tasks in a multicore system. As depicted in Figure 3.5 (which is repeated here to ease readability), let us consider a system with 4 cores (with core 4 being idle; hence not shown in the diagram). Tasks τ_1 and τ_2 are assigned to core π_1 , and tasks τ_3 and τ_4 are assigned to core π_2 . The analyzed task τ_i is assigned to Core 3.

To compute the WCET of task τ_i considering the contention on the shared bus, it is necessary to estimate the maximum interference (in terms of memory requests) that τ_i can incur during its execution. In this example, the interference can be attributed to the requests issued from tasks co-executing on cores 1 and 2. For each of these two cores, it is thus necessary to derive a function that computes an upper-bound on the number of requests that the cores may issue during the execution of τ_i , because every request issued by cores 1 and 2 may potentially compete for the bus with a request of τ_i , and thus contribute to the total interference incurred by τ_i .

A prerequisite to derive these two required functions $\text{PCR}_1()$ and $\text{PCR}_2()$ is the memory request profile of each task, assigned to these 2 cores. For a given task, the maximum number of requests that it can generate in a given time window can be obtained by the interval splitting technique described in the previous section. For each core π_1 and π_2 , the individual memory profile of each task assigned to it, along with other parameters like the task minimum inter-arrival times and their WCET in isolation are then fed into an analysis framework to derive the *per-core memory profile* i.e., the functions $\text{PCR}_1()$ and $\text{PCR}_2()$. The computed per-core memory profiles can be used to derive the total interference posed by cores π_1 and π_2 to the analyzed task τ_i assigned to core π_3 .

It must be noted that pessimistic estimates of the WCETs can lead to over-dimensioning the system resources. The WCET is a key input to the schedulability analysis; this analysis is carried out at design time to ensure that all tasks in the system will meet their deadlines during run-time. In the absence of tight WCET estimates, many tasks may be (wrongly) deemed unschedulable. The function $\text{PCR}_p(t)$ is thus a vital intermediate tool in the analysis cycle. The main focus of this section is compute such a function and show how it can be seamlessly integrated in the higher level analysis.

3.5.2 An basic additive method to compute the PCRFP functions

In the previous section we studied a method to model the memory profile of a task by the $BR_j(t)$ function which returns an upper bound on the number of bus requests that task τ_j can generate in time t . Let τ^p represent the set of tasks assigned to core π_p . Then a basic method to compute the total interference from all the tasks running on core π_p is inferred simply by adding up the functions $BR_j(t)$ of all the tasks τ_j assigned to that core π_p , as described in the following equation.

$$\text{PCRFP}_p(t) = \sum_{\forall \tau_j \in \pi_p} BR_j(t) \quad (3.7)$$

Before we present a better solution, we understand the role of PCRFP() and the demerits of this particular approach by applying it to determine the response time of a task.

3.5.2.1 General Response-Time Analysis

The research literature provides methods for computing the worst-case response-time of tasks scheduled by non-preemptive fixed-priority scheduling on uniprocessor system [92, 93]. For the task model considered in this paper, an equation for the response time can be derived from [95] by applying the following recursive equation:

$$\widehat{R}_i^{(k+1)} = C_i + B_i + \sum_{j \in \text{hp}(i)} \left\lceil \frac{\widehat{R}_i^k}{T_j} \right\rceil \times C_j \quad (3.8)$$

where B_i is the maximum blocking time imposed on task τ_i due to lower-priority tasks, i.e., $B_i \stackrel{\text{def}}{=} \max_{j \in \text{lp}(i)} \{C_j\}$. The WCRT R_i of the task τ_i is computed in an iterative manner, starting from $\widehat{R}_i^{(0)} = C_i + B_i$, and is given by the smallest value of \widehat{R}_i^k that satisfies Equation (3.8). The process terminates when either it reaches the first fixed-point value of the equation at which $\widehat{R}_i^{(k+1)} = \widehat{R}_i^{(k)}$, in which case the WCRT R_i is given by the value of $\widehat{R}_i^{(k+1)}$. Alternatively the computation terminates when $\widehat{R}_i^{(k+1)} > D_i$ with the implication that the deadline of task τ_i is missed.

3.5.2.2 Extended Response-Time analysis

The computation of the WCRT in the *multicore* scenario must consider the increased delay due to tasks executing on the same core and the additional delays due to contention on the FSB from tasks running on the other cores. We now introduce the extended response-time equation which, in addition to the original WCRT equation, also factors-in the contention

delay due to requests generated by the co-scheduled tasks on the other cores competing for the shared FSB. We assume that task τ_i is assigned to core π_p . Then,

$$\begin{aligned}
\widehat{R}_i^{(k+1)} &= C_i + B_i + \sum_{j \in \text{hp}(i)} \left\lceil \frac{\widehat{R}_i^k}{T_j} \right\rceil \times C_j + \sum_{\pi_q \neq \pi_p} \text{PCR}_p(\widehat{R}_i^k) \times \text{TR} \\
&= C_i + B_i + \sum_{j \in \text{hp}(i)} \left\lceil \frac{\widehat{R}_i^k}{T_j} \right\rceil \times C_j + \sum_{\pi_q \neq \pi_p} \sum_{\tau_j \in \pi_q} \text{BR}_j(\widehat{R}_i^k) \times \text{TR} \quad (3.9) \\
&= C_i + B_i + \sum_{j \in \text{hp}(i)} \left\lceil \frac{\widehat{R}_i^k}{T_j} \right\rceil \times C_j + \sum_{\tau_j \in \bar{\pi}(i)} \text{BR}_j(\widehat{R}_i^k) \times \text{TR}
\end{aligned}$$

Equation (3.9) encapsulates the effects of

1. the blocking by the lower priority tasks on the same core represented by the term B_i
2. the delay due to interference by higher priority tasks on the same core represented by the term $\sum_{j \in \text{hp}(i)} \left\lceil \frac{\widehat{R}_i^k}{T_j} \right\rceil \times C_j$ and
3. the delay caused by interference from tasks running on the other cores represented by the term $\sum_{\tau_j \in \bar{\pi}(i)} \text{BR}_j(\widehat{R}_i^k) \times \text{TR}$. Recall that $\bar{\pi}(i)$ denotes the set of tasks not assigned to the same core as τ_i .

The underlying rationale governing Equation 3.9 is that the traffic generated by the other cores will first impact and increase the execution time of the higher priority tasks (than τ_i) and assigned to the same core (as τ_i). This in turn will impact the WCRT of task τ_i . With the newly computed response time, more requests may be generated by the tasks running on the other cores. This iterative process continues till the value of \widehat{R}_i stabilizes (like the regular response time equation).

3.5.3 Analysis of the extended response time analysis

The third term introduced in Equation 3.9, i.e., $\sum_{\tau_j \in \bar{\pi}(i)} \text{BR}_j(\widehat{R}_i^k) \times \text{TR}$, to compute the interference from the other cores must be carefully scrutinized. The method presented above seems straight-forward but is overly pessimistic. The computation of $\text{PCR}_p()$ assumes that all the tasks assigned to cores $\bar{\pi}_i$ co-execute simultaneously with the analyzed task – an assumption which is too strong and may lead to conservative estimates as the number of cores and tasks increases. An obvious drawback of the method stems from the fact that unless the analyzed task has a very long execution time, *all* the tasks assigned to other cores may not co-execute with it during its execution span. Another drawback is that this analysis does *not* consider the memory profile of the analyzed task. The results will be same regardless of whether the analyzed task τ_i , generates very few requests or is highly memory intensive. The problem of computing tight bounds is thus non-trivial and

cannot make the above basic assumption to compute the total interference from other cores. Ernst et. al [80] also use a similar basic additive approach, acknowledging that finding the optimal solution to the problem is an instance of a bounded non-linear knapsack problem — which implies that finding the optimal solution must explore all possible combination of tasks executing within the interval of length t and select that specific combination of tasks that leads to the maximum number of requests. They also say that given its nature, the problem is NP-hard, without proposing a specific method to tackle it.

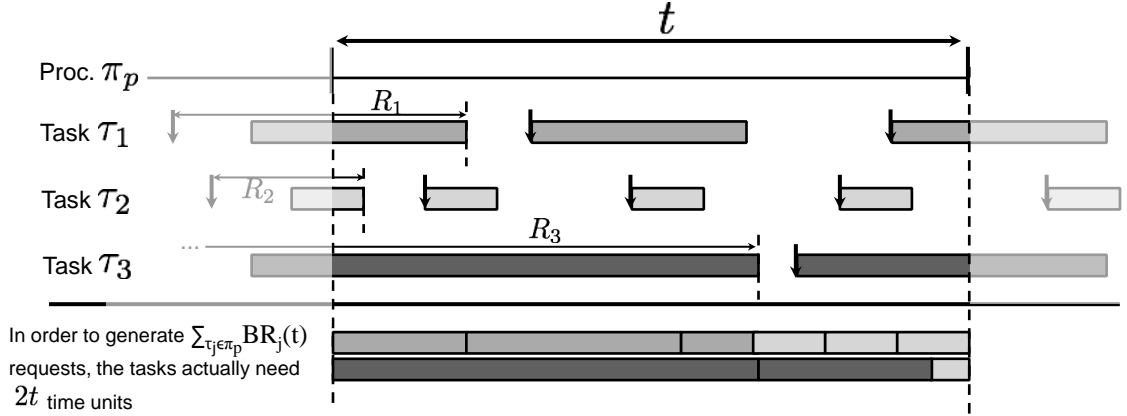


Figure 3.6: Illustration of the pessimism of the approaches in [91, 80].

Clearly, the basic additive method of computing the $\text{PCR}_p(t)$ function leads to an overestimation of the number of requests, as *all* the tasks assigned to π_p may not be scheduled in (or rather fit within) the time interval t . The effect of this overestimation is enhanced further as the number of tasks assigned to each core increases. Figure 3.6 illustrates the overestimation. For each of the three tasks τ_1 , τ_2 and τ_3 depicted in this figure, the methods proposed in the earlier section and by [80] identify the job-release pattern that entails the maximum number of requests within t time units, i.e., it is the pattern considered in the computation of $\text{BR}_j(t)$, $j = 1, 2, 3$. Then, $\text{PCR}_p(t)$ is computed by adding up $\text{BR}_1(t)$, $\text{BR}_2(t)$ and $\text{BR}_3(t)$, which clearly leads to an over-approximation as these three tasks *cannot execute simultaneously* on the same core and will execute in an interleaved manner depending on the scheduling algorithm on that core. The main drawback of the proposed basic method is that it does not place any constraints on the cumulative execution time of tasks executing within the time window under analysis. A method to address this is therefore warranted and is presented in the next section.

3.6 Computation of the Per-Core Request Profile

In this section, we propose an alternative technique to compute an upper bounds on the number of requests a core can generate in a given time window. Recall that the function $\text{PCR}_p(t)$ returns an upper bound on the number of requests that can be generated by tasks executing on a given core p in any time window of length t .

The schedule of the tasks on a core π_p within any time window of length t is split into three consecutive and non-overlapping portions: the “carry-in”, the “body”, and the “carry-out” (depicted in Figure 3.7). The key difference in the interval splitting technique employed earlier is that while the earlier method considered one or more jobs of the *same* task within an interval t , in the per-core analysis, jobs of *different tasks* assigned to that core may occupy the same window.

1. The “carry-in” portion starts at the beginning of the window and ends at the completion of the first job scheduled in that window. However, this portion is defined only if this first scheduled job starts its execution *outside* the window and completes *within* the window; otherwise, the length ℓ_{cin} of the carry-in is assumed to be zero. By definition, ℓ_{cin} is smaller than the maximum execution time of all tasks assigned to core π_p , i.e.,

$$\ell_{\text{cin}} < C_p^{\max} = \max_{\tau_i \in \pi_p} \{C_i\} \quad (3.10)$$

2. The “carry-out” portion begins at the start-of-execution of the last job scheduled in the window and extends to the end of the window. Analogous to the carry-in, this carry-out portion is defined only if this last scheduled job starts its execution *within* the window and completes *outside* the window; otherwise, its length ℓ_{cout} is zero. By definition, ℓ_{cout} is smaller than the maximum execution time of all tasks assigned to core π_p , i.e.,

$$\ell_{\text{cout}} < C_p^{\max} = \max_{\tau_i \in \pi_p} \{C_i\} \quad (3.11)$$

3. The “body” portion extends from the end of the carry-in (or from the beginning of the window if $\ell_{\text{cin}} = 0$) to the beginning of the carry-out (or to the end of the window if $\ell_{\text{cout}} = 0$). By construction, it contains all the jobs that execute entirely within the window and we have

$$0 \leq \ell_{\text{body}} \leq t \quad (3.12)$$

where ℓ_{body} denotes the length of the body.

The central idea underlying the computation of $PCR P_p(t)$ is to calculate separately, the maximum number of requests that can be generated in each of these portions (assuming all possible lengths for each one) and then computing the global maximum under the constraint that

$$\ell_{\text{cin}} + \ell_{\text{body}} + \ell_{\text{cout}} = t \quad (3.13)$$

As seen in Figure 3.7, depending on the parameters of the tasks and the length t of the window under scrutiny, the schedule that generates the maximum number of requests within t time units may contain jobs executing in all the three portions as depicted in Figure 3.7a, only a single carry-in portion ($\ell_{\text{body}} = \ell_{\text{cout}} = 0$), as in Figure 3.7b, or a single carry-out ($\ell_{\text{cout}} = \ell_{\text{body}} = 0$), as in Figure 3.7c. It may be also contained within a single task or across two tasks as seen in Figure 3.7d.

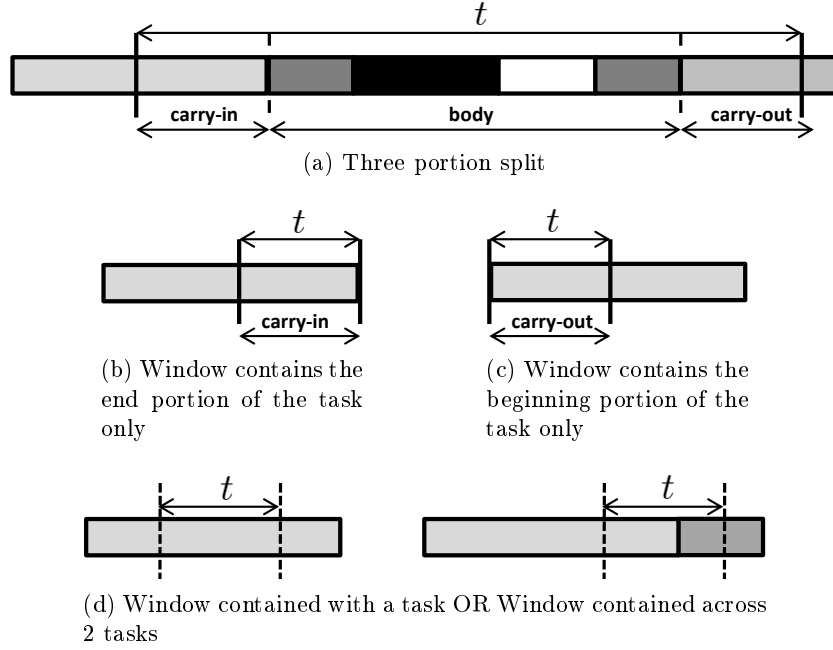


Figure 3.7: Illustration of interval splitting

The following subsections describe the methods of computing an upper bound on the number of request in the carry-in, carry-out, and the body portions and the technique to deal with the special case. We shall use the following notations: the functions $\text{inreq}_p(k)$, $\text{outreq}_p(k)$ and $\text{breq}_p(k)$ will record the upper bounds on the number of requests generated within $k \leq t$ time units on core π_p in the three portions, respectively.

3.6.1 Maximization of the number of requests in the carry-in and carry-out portions

As stated by Inequalities 3.10 and 3.11, the length of the carry-in and carry-out portions can range from 0 to C_p^{\max} , the maximum of the C_i 's of all the tasks assigned to core π_p . However, since the size t of the window under analysis *may* be less than C_p^{\max} , our method computes the values of $\text{inreq}_p(k)$ and $\text{outreq}_p(k)$ for all values of k in the range 0 to $\min(t, C_p^{\max})$ as:

$$\forall k \in [0, \min(t, C_p^{\max})] : \quad \text{inreq}_p(k) \leftarrow \max_{\tau_i \in \pi_p} \{\text{head}_i(k)\} \quad (3.14)$$

$$\text{outreq}_p(k) \leftarrow \max_{\tau_i \in \pi_p} \{\text{tail}_i(k)\} \quad (3.15)$$

The method $\text{head}_i(k)$ computes an upper bound on the number of requests that τ_i can generate in the *last* k time units of its execution. Analogously, $\text{tail}_i(k)$ is an upper bound on the number of requests that τ_i can generate in the *first* k time units of its execution.

3.6.2 Maximization of the number of requests in the body portion

As stated by Inequality 3.12, given a time window of size t the length of the body portion can vary from 0 to t . Hence, the value of $\text{breq}_p(k)$ is computed for all $k \in [0, t]$ by calling the $\text{TaskPack}(k)$ function that we outline in Algorithm 2. A description of this algorithm follows.

$$\forall k \in [0, t] : \text{breq}_p(k) \leftarrow \text{TaskPack}(p, k) \quad (3.16)$$

Recall that NReq_i denotes the maximum number of requests generated by task τ_i during its complete execution span. The algorithm “ $\text{TaskPack}(p, k)$ ” converts the problem of deriving an upper-bound on the number of requests that can be issued from a core π_p in a given time interval of length k , into an instance of a 0/1 knapsack problem formulated as follows [96]:

The 0/1 knapsack problem: Given a set of items, each with a corresponding weight and value, and a knapsack of capacity k , determine the items to be included in the knapsack so that the cumulative weight of the items in the knapsack is less than or equal to its maximum capacity k and the cumulative value is maximized.

The transformation of computing $\text{breq}_p(k)$ into an instance of the 0/1 knapsack problem is carried out as follows. As stated earlier, the body portion contains only *entire* executions of jobs from different tasks (and/or possibly from the same task). Moreover, irrespective of the scheduling algorithm employed, each task τ_i can release at most $\lceil k/T_i \rceil$ jobs within a time window of length k . Thus, there are $\sum_{\tau_i \in \pi_p} \lceil k/T_i \rceil$ jobs (i.e., items) on core π_p ; each job from task τ_i has a weight of C_i and a value of NReq_i and the objective is to determine which of these jobs (or items) to include in the time window (the knapsack) such that the total value is maximized, but subject to the constraint that the total weight is no greater than the given capacity k . In short, the problem is to pack the window of length t with the set of $\sum_{\tau_i \in \pi_p} \lceil k/T_i \rceil$ jobs such that the number of requests is maximized.

Algorithm Description The algorithm first transforms the problem into an instance of a 0/1 knapsack problem [96] by creating $n_i = \lceil k/T_i \rceil$ items $\langle C_i, \text{NReq}_i \rangle$ from each task τ_i (line 7). To maximize the number of requests, a natural candidate for selection is a job with the highest request density, i.e., the highest ratio NReq_i/C_i . Therefore, the algorithm fills the analogous knapsack of capacity ℓ_{body} by traversing the list of jobs (in descending order of NReq_i/C_i) and starts packing the knapsack by filling in upto n_i items from each τ_i ; each (included) job of τ_i consumes C_i units of the knapsack while contributing a weight of NReq_i . This is essentially a greedy approach: the algorithm packs jobs within the body window until the capacity of the knapsack (i.e., the size of the body window) is not exceeded (lines 9-15). Note that, since this method primarily aims at computing the maximum number of requests, and *not* at generating the exact schedule leading to it, placing tasks in the order τ_a, τ_b, τ_a leads to the same number of requests as in the schedule τ_a, τ_a, τ_b . As the items are packed, the algorithm accordingly updates the variable

Algorithm 2: TaskPack(p, ℓ_{body})

```

input :  $p$ : core index,  $\ell_{\text{body}}$ : length of the body portion
output: maxrequests
1 if ( $\ell_{\text{body}} \leq 0$ ) then return 0 ;
2 maxrequests  $\leftarrow$  0 ;
3 foreach  $\tau_i \in \pi_p$  do
4 |  $n_i \leftarrow \lceil \ell_{\text{body}}/T_i \rceil$ ;
5 end
6 capacity  $\leftarrow$   $\ell_{\text{body}}$  ;
7 list  $\leftarrow$  list containing  $n_i$  items  $\langle C_i, \text{NReq}_i \rangle$  for each task  $\tau_i \in \pi_p$ , sorted by
   non-increasing order of  $\text{NReq}_i/C_i$  ;
8 rem_cap  $\leftarrow$  capacity ;
   // Add requests of the complete tasks
9 while list  $\neq \phi$  and rem_cap  $>$  0 do
10 | if rem_cap  $-$  list.first(). $C_i \geq 0$  then
11 | | maxrequests  $\leftarrow$  maxrequests + list.first().NReq $_i$ ;
12 | | rem_cap = rem_cap  $-$  list.first(). $C_i$ ;
13 | else
14 | | break ;
15 | end
16 | list.delete first();
17 end
   // Add the fractional number of requests of the next task in the list
18 if list  $\neq \phi$  and rem_cap  $>$  0 then
19 | maxrequests  $\leftarrow$  maxrequests +  $\frac{\text{rem\_cap}}{\text{list.first().}C_i} \times \text{list.first().NReq}_i$ ;
20 end
21 return maxrequests ;

```

“maxrequests” (in line 11), which holds the maximum number of requests and the variable “rem_cap” (in line 12) which holds the currently unoccupied capacity of the knapsack.

When the last popped job cannot fit entirely in the remaining capacity, then the algorithm allows a fraction of this job to fit in the remaining capacity and updates the “maxrequests” variable by adding the corresponding number of requests, assuming that the requests are uniformly generated over the job’s execution (reflected in line 19). This fractional assignment transforms the problem into an instance of a *fractional* knapsack problem; it is a source of pessimism in our approach but it ensures safe upper bounds on the number of requests (as proven in the next section). It also violates our description of the body portion in which only complete executions are permitted and can lead to a final schedule containing two partial executions of jobs (one at the end of the body portion and one in the carry-out), but given that the objective is not to draw up the optimal schedule (which requires the knowledge of the scheduling algorithm), we believe that this is an acceptable solution.

3.6.3 Maximization of the number of requests over the entire time interval of length t

As seen earlier, Equations 3.14, 3.15 and 3.16 can be used to compute the maximum number of requests in the carry-in, carry-out, and the body portions over the relevant ranges for a given duration of time t . The final step consists in using Algorithm 3 that leverages these computed values to maximize the number of requests generated over the entire interval under analysis. To do so, it considers all possible combinations of lengths for the carry-in and carry-out portions (ℓ_{cin} and ℓ_{cout}) and assigns the remaining length to ℓ_{body} (line 8), such that $\ell_{\text{cin}} + \ell_{\text{cout}} + \ell_{\text{body}} = t$.

Algorithm 3: $\text{PCR}P_p(t)$

```

input :  $t$ : duration of the time interval;  $p$ : core index
output: maxrequests
1  $C_p^{\text{max}} \leftarrow \max_{\tau_i \in \pi_p} \{C_i\}$  ;
2 maxrequests  $\leftarrow 0$  ;
3 foreach  $\ell_{\text{cin}} \in [0, \min(t, C_p^{\text{max}})]$  do
4   | foreach  $\ell_{\text{cout}} \in [0, \min(t - \ell_{\text{cin}}, C_p^{\text{max}})]$  do
5     | // Assign the rest to the body portion
6     |  $\ell_{\text{body}} \leftarrow t - \ell_{\text{cin}} - \ell_{\text{cout}}$  ;
7     | total  $\leftarrow \text{inreq}_p(\ell_{\text{cin}}) + \text{bre}q_p(\ell_{\text{body}}) + \text{outreq}_p(\ell_{\text{cout}})$  ;
8     | if (maxrequests < total) then maxrequests  $\leftarrow$  total ;
9   | end
10  | end
11 // Special case:  $t <$  Execution time of the task
12 maxrq1  $\leftarrow 0$  ;
13 foreach ( $\tau_i \in \pi_p$ ) do
14   | if ( $t < C_i$ ) then maxrq1  $\leftarrow$  max(maxrq1, inscan( $i, t$ )) ;
15 end
16 return max(maxrq1, maxrequests) ;

```

Special case (lines 10–13). If the duration t of the time window is less than the execution time of a task, then this task could have started its execution before the beginning of the window and finishes its execution outside the window (as illustrated in Figure 3.7(d)). In such a case, the maximum number of requests may be found within the execution of a single task. The method $\text{inscan}(i, t)$ internally scans the task τ_i for the maximum number of requests and records the maximum in the variable maxrq1. The value returned by the algorithm is the higher of the two maximum values computed.

3.7 Correctness and properties of the $\text{PCR}P_p(t)$ function

Theorem 1. *Algorithm 3 provides a safe upper-bound on the number of requests that can be issued from a core π_p in a time interval of length t .*

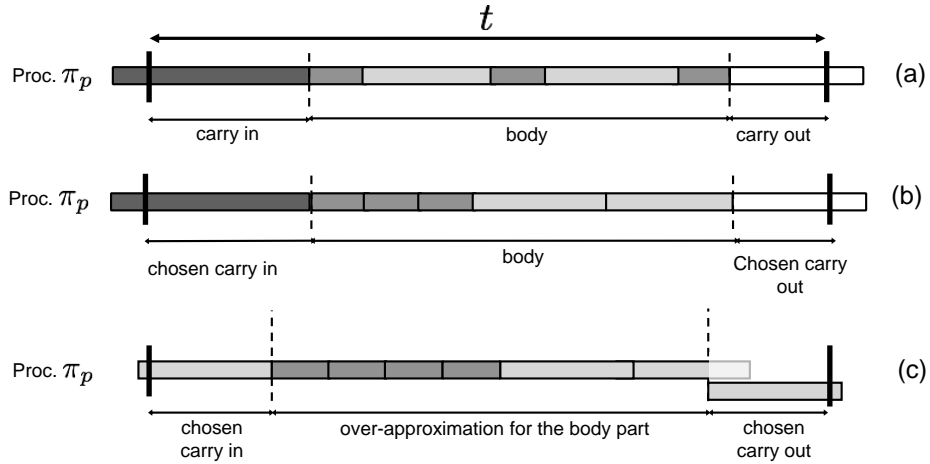


Figure 3.8: (a) The worst-case scheduling scenario (in terms of number of requests) that can occur at run-time in a time frame of length t . (b) A possible combination for which Algo. 3 returns the maximum number of requests (c) Another illustration of how Algo. 3 could pack the tasks within the body portion, and the final schedule it assumes.

Proof. Let $S^{\text{opt}}(t)$ denote the “optimal” schedule of the tasks that generates the maximum number of requests in a time window of length t . Consider that $S^{\text{opt}}(t)$ is the schedule depicted in Figure 3.8(a). We use different scales of gray to represent jobs from different tasks and we use the notations $\ell_{\text{cin}}^{\text{opt}}$, $\ell_{\text{body}}^{\text{opt}}$, and $\ell_{\text{cout}}^{\text{opt}}$ for the size of the carry-in, body, and carry-out portions in $S^{\text{opt}}(t)$, respectively. Since Algo. $\text{PCR}_p()$ considers all combinations of feasible lengths for the carry-in and carry-out portions, it eventually investigates the lengths corresponding to $S^{\text{opt}}(t)$, i.e., at some point we have $\ell_{\text{cin}} = \ell_{\text{cin}}^{\text{opt}}$ and $\ell_{\text{cout}} = \ell_{\text{cout}}^{\text{opt}}$ at lines 3 and 4. Consequently, Algo. $\text{PCR}_p()$ finds the same maximum number of requests as in $S^{\text{opt}}(t)$ for these two portions as depicted in Figure 3.8(b); the length of the body portion, ℓ_{body} , computed at line 5 also corresponds to the length $\ell_{\text{body}}^{\text{opt}}$ of the body in $S^{\text{opt}}(t)$.

In the body portion, we know that $S^{\text{opt}}(t)$ contains only entire (i.e., non partial) executions of jobs, which are arranged in the descending order of request densities. This firstly ensures that the algorithm captures the maximum requests that could be generated by the constituent tasks in the body portion. Additionally, we relax the requirement of containing only complete executions in the body portion to include a fractional job execution at the end of the portion. With this relaxation, the problem can be now expressed as an instance of a fractional bounded knapsack problem for which the greedy approach applied in Algorithm 2 is guaranteed to provide an upper-bound to the corresponding integer knapsack problem [97]. Therefore, the cumulative sum of the maximum requests corresponding to the three portions is guaranteed to provide an upper-bound on the number of requests in the given time interval of length t . \square

As a side note, it is worth noticing that the maximum number of requests returned by Algorithm $\text{PCR}_p()$ may not be the same as that computed while considering $\ell_{\text{cin}} = \ell_{\text{cin}}^{\text{opt}}$

and $\ell_{\text{cout}} = \ell_{\text{cout}}^{\text{opt}}$. The algorithm may find other combinations of portion lengths leading to infeasible schedules, which over-estimate the numbers of requests generated as opposed to an optimal schedule (as depicted in Figure 3.8c). This is due to two main reasons:

1. Firstly, it may be infeasible for a task which constitutes the carry-in portion in $S^{\text{opt}}(t)$ to have another job in the body portion of $S^{\text{opt}}(t)$, because of the constraint imposed by its minimum inter-arrival time. However, since Algo. PCRP() divides the problem into the sub-problems of finding the maximum number of requests in the carry-in, carry-out portions and the body portions which are solved independently. As a consequence, some constraints on feasible schedules may be violated in the algorithm. This may lead to a scenario in which a task has an extra job in the schedule constructed by PCRP() than in the optimal schedule, $S^{\text{opt}}(t)$ and therefore computing a higher number of requests than the optimal schedule.
2. The second over-approximation is attributed to the number of requests computed in the fractional assignment of the last packed task in the body portion, and the assumption that its requests are assumed to be uniformly distributed over its execution.

In short, the pessimism arises from a) the over-approximation made while computing the number of requests in the body and b) the fact that the maximum number of requests generated in each of the three portions is computed regardless of which tasks are scheduled in the other portions, hence allowing potentially more jobs of the same task to execute within the t time units.

The monotonicity property It is important to assess the monotonicity of the $\text{PCR}_p(t)$ function in order to apply it as an intermediate building block in the computation of higher level parameters like the worst-case execution time or the response time of a task, which in turn are key inputs for the schedulability analysis.

Property 1 (Monotonically Increasing). *Given core π_p and durations t_1 and t_2 , we have*

$$t_1 \leq t_2 \Leftrightarrow \text{PCR}_p(t_1) \leq \text{PCR}_p(t_2)$$

Proof. Let maxrequests_1 and maxrequests_2 be the maximum number of requests returned by $\text{PCR}_p(t_1)$ and $\text{PCR}_p(t_2)$ (computed as per Algo. 3), respectively. Let ℓ_1^{cin} and ℓ_1^{cout} be the lengths of the carry-in and carry-out portions in the solution returned by $\text{PCR}_p(t_1)$. Since all possible lengths for the carry-in and carry-out portions are considered by Algo. 3, the computation of $\text{PCR}_p(t_2)$ considers these lengths ℓ_1^{cin} and ℓ_1^{cout} as well. Therefore, two cases may arise:

1. maxrequests_2 is obtained for these lengths ℓ_1^{cin} and ℓ_1^{cout} of carry-in and carry-out, which results in a larger body portion than during the computation of maxrequests_1

(i.e., $t_2 - \ell_1^{\text{cin}} - \ell_1^{\text{cout}} \geq t_1 - \ell_1^{\text{cin}} - \ell_1^{\text{cout}}$) and thus a greater number of requests within the body as the set of jobs that can execute within $t_2 - \ell_1^{\text{cin}} - \ell_1^{\text{cout}} \supseteq$ the set of jobs that can execute within $t_1 - \ell_1^{\text{cin}} - \ell_1^{\text{cout}}$. Hence, $\text{maxrequests}_2 \geq \text{maxrequests}_1$.

2. maxrequests_2 is obtained for different lengths of carry-in and carry-out, which means that Algo. 3 found other lengths of carry-in and carry-out for which maxrequests_2 is even greater (hence $\text{maxrequests}_2 \geq \text{maxrequests}_1$ holds as well).

□

3.8 Optimization and Computational Complexity

3.8.1 Optimization by PreComputations

In the entire analysis cycle, the $\text{PCR}P()$ function is used as in intermediate function in the determination of key parameters like the WCET or the worst case response time of a task and is invoked a significant amount of times (with a large range of values for the input parameter t). An optimized implementation is therefore vital for an efficient and scalable algorithm. This optimization can be done by pre-computing the values of all the required parameters in Algorithm 3 upto the possible maximum ranges. As said earlier, given a window of length t , we need to compute an upper bound on the number of requests that a task τ_i assigned to core π_p . Then it will suffer external interference from the tasks executing on other cores $\pi_q \neq \pi_p$. Hence we have to compute $\text{PCR}P_q()$ for those cores to compute the external interference.

Pre-computation range for the carry_in and the carry_out portions: Given a window of length t , we need to compute an upper bound on the number of requests that a tasks assigned to core π_q can generate. In the carry_in and carry_out portion, a single task $\tau_j \in \pi_q$ may partially execute within the window and hence the length of the carry_in or the carry_out portion for τ_j has a range of $[0, C_j]$, as shown in Equations 3.10 and 3.11. Since any of the tasks assigned to core π_q may occupy this portion, the algorithm first computes C_q^{max} , the maximum of the C_j 's of all the assigned tasks (line 1). Then, for all values from 0 to C_j^{max} we precompute the values leading to the maximum number of requests in these portions. Next, we proceeds to compute the range of the body portion.

Pre-computation range for the body portions: Since the length of the three portions must add up to t , a natural range of the body portion is $[0, t]$. In order to compute the maximum range that t can take, let us consider the broader picture. Let us assume that we employ the function $\text{PCR}P()$ to compute the WCET of task τ_i assigned to core π_p . In order to do so, we maximize the cumulative interference posed to τ_i from tasks co-executing on the *other* cores by invoking the $\text{PCR}P_q(t)$ function (for all the interfering cores $\pi_q \neq \pi_p$). As a result of this external interference, the execution time of τ_i increases by a value, say δ . Meanwhile requests issued from other cores may still keep arriving in this increased execution time. To account for this increase, the function $\text{PCR}P_q()$ must now be invoked

Algorithm 4: PreComputeAndSort(q, τ_i)

input : q is the core index, τ_i is the analyzed task with deadline D_i

- 1 Sort tasks $\tau_j \in \pi_q$ by descending order of $NReq_j/C_j$;
- 2 $C_q^{\max} = \max_{\tau_j \in \pi_q} \{C_j\}$;
- 3 **foreach** $k \in [0, C_{\max}]$ **do**
- 4 $inreq_q(k) = \max_{\tau_j \in \pi_q} \{\text{tail}_j(k)\}$;
- 5 $outreq_q(k) = \max_{\tau_j \in \pi_q} \{\text{head}_j(k)\}$;
- 6 **end**
- 7 **foreach** $k \in [0, D_i]$ **do**
- 8 $breq_q(k) = \text{TaskPack}(q, k)$;
- 9 **end**

with the input parameter $t + \delta$. In order for τ_i to meet its deadline, its (increased) execution time should not exceed its deadline D_i : thus t must lie between 0 and D_i . To reiterate, this upper limit is chosen in the broader context of employing $\text{PCRPP}_p()$ as an intermediate step for schedulability analysis of task τ_i – testing whether task τ_i will meet its deadline when run in conjunction with other tasks.

Algorithm 4 summarizes the precomputation step. It pre-computes the maximum number of requests that can be generated within the three portions and records the maximum number of requests in the globally accessible $inreq$, $breq$ and $outreq$ arrays. This function should be invoked in the initialization phase of the analysis process prior to the invocation of $\text{PCRPP}_q(t)$. This algorithm also sorts the tasks assigned on each core on the basis of their request densities. This is a pre-requisite for Algorithm 2 (which finds an upper bound on the number of requests generated in the body portion).

3.8.2 Computational Complexity

Algorithm $\text{TaskPack}(p, t)$ has a worst-case computing complexity of $O(t)$, because in the worst-case scenario all the tasks have a WCET of 1. Algorithm $\text{PCRPP}()$ has a complexity of $O((C_p^{\max})^2)$. Assuming that the value of $\text{head}_i(k)$ and $\text{tail}_i(k)$ is given for all tasks τ_i and durations k , it can be seen that the complexity of Algorithm $\text{PreComputeAndSort}(\pi_p, \tau_j)$ is $O(n \log(n) + n \times C_p^{\max} + D_j \times t)$.

It is important to note that $\text{PCRPP}()$ is an intermediate functional tool in the computation of parameters like the WCET and is invoked a significant amount of times. Therefore, although it may seem trivial, the one time pre-computation step provided by Algorithm 4, facilitates an efficient design by avoiding obsolete re-computations of the values of $\text{PCRPP}()$ for the same inputs in successive invocations, thereby decreasing the cumulative analysis time.

3.9 Adaptations of PCRP() and Integration with existing work

Algorithm 3 derives a PCRP function for each core but considers a generic model wherein there is no specific scheduling algorithm and no specific bus arbitration mechanism (except that the bus is work-conserving). In this section we adapt the computation of this function to different settings.

3.9.1 PCRP() for synchronous periodic tasks and fixed task-level priority schedulers.

The problem of computing the PCRP functions is inherently simpler for a system in which tasks are periodic, non-preemptive and the scheduler enforces a fixed ordering of task execution (fixed task-level priority). Within a fixed task-level priority scheme [98], a unique priority is associated with each task and all jobs generated by a task have the priority associated with that task. In the case that task τ_1 has higher priority than task τ_2 , an activated job of τ_1 will have a higher priority over an activated job of τ_2 . An example of such a scheduling algorithm is the Rate Monotonic algorithm [99]. For this category of scheduling policies, it has been shown in [100] that the entire schedule eventually repeats (cyclic scheduling) every H units of time, where H is the period of the schedule.

Since the pattern of task arrivals is known for such a task model, it is not necessary to find the combination of tasks that leads to the maximum number of bus requests. Instead, we first draw up the entire schedule of the tasks from time 0 to time $H + t$, by considering that every job executes for its WCET. Note that we still make the non work-conserving assumption here, i.e., if tasks do not execute up to their WCET, the core must be idled up to the WCET. Since the arrival times of the tasks and their execution order is known in this task model, this schedule can be constructed at design time. Then, this schedule is scanned by sliding a time window of length t from time 0 to time $H + t$. The extra t time units beyond the period of the schedule must be considered, as the maximum number of bus requests may be generated across two schedule periods. As the interval is scanned, the maximum number of requests observed so far within the sliding window of length t is recorded and is finally returned by the $\text{PCRPP}_p(t)$ function.

3.9.2 PCRP() for fixed task-level priority schedulers and a priority-driven bus

In the context of bus arbitration policies, one of the challenges with currently existing COTS-based multicore systems is that the front-side bus does not recognize/respect task priorities. This is because the bus is generally designed with the aim of enhancing the average case performance and not tailored for real-time systems. This can lead to a case of priority inversion in which requests from higher priority tasks are delayed by requests

from lower priority tasks on the bus. Although the scheduler enforces these priorities while allocating the processing element (CPU) to tasks, these priorities are not passed over to the shared low-level hardware resources like the bus and the memory controllers, which have their own scheduling policies. In an interesting work [101], the authors have designed a priority driven bus in which *external* priorities assigned by the operating system are passed over to the underlying hardware upto the memory controller by tagging the request with its priority. We shall assume for this subsection, that the bus follows such an arbitration mechanism. Another design for a priority driven bus arbiter is proposed in [102].

Given that the scheduler on each core employs a fixed task-level priority algorithm and the bus arbiter follows the same policy (i.e., the requests are tagged with the priority information of the tasks they are issued from), tighter bounds can be derived. To that end, Algorithm 3 must be slightly adapted and an important pre-requisite to derive tighter bounds is that we must be able to assign relative priorities globally to all the tasks in the system.

Let us assume that the analyzed task τ_i has a priority $\lambda(i)$. To recall, the rationale behind the proposed algorithm in order to find the combination of tasks which leads to the maximum number of requests in a given interval of time t , we divide the time into three portions: the carry-in, the carry-out, and the body portions. For each of these portions we determine the job(s) which maximize(s) the number of requests.

1. For the carry-in portion: Pass the priority of the task to the `tail()` function as an additional parameter. Unlike the earlier case in which any task could be a part of the carry-in portion, this priority information is used to limit the selection to only those tasks with a priority $\geq \lambda(i)$.
2. For the carry-out portion: Pass the priority of the task to the `head()` function as an additional parameter. This priority information is used to narrow down the set of candidate tasks to only those tasks with a priority $\geq \lambda(i)$.
3. For the body portion: Here the knapsack needs to be filled in with the set of tasks with the highest request densities. This requires a change in the way the tasks are sorted. To capture the set of tasks which maximize the number of requests, the task are ordered in two steps. Note that this grouping implies that, for the analyzed task, the relative priority ordering among the tasks with a higher priority than itself is not relevant.
 - (a) Split the task set into two groups: Group 1 contains all the tasks with a higher priority than $\lambda(i)$. Group 2 contains the remaining tasks.
 - (b) Sort the tasks in Group 1 by decreasing order of their request densities NReq_i/C_i . The body portion is packed using only the tasks \in Group 1.

The steps above ensure that a request from the analyzed task can be blocked only by requests from higher priority tasks. The maximization phase and the rest of the logic remains unchanged for Algorithm 3.

3.9.3 PCRP() for systems with main memories with asymmetric read and write latencies

In the current state-of-the-art, the characterization of the memory request profile of tasks generally does not differentiate between read and write requests and implicitly assumes that the time to serve a read request is same as the time needed to serve a write. That is, it is assumed in the previously proposed analyses that each request is served in a fixed and constant time, irrespective of its type.

While this may be an acceptable assumption for DRAM-like memories for which read and write latencies are of same order of magnitude, it does not hold for other types of memory like Phase Change Memory (PCM) [103, 104, 105] or Flash memories, in which write requests have a substantially higher memory latency than a read request (about 10 times higher in PCM). For systems using such memories, the assumption of equal read and write latencies will lead to over-estimations of the timing parameters and the problem eventually cascades to the over-allocation of system resources at design times. Hence, the interference contributed by a read and a write transaction must be distinctly dealt with, considering their respective worst-case service time. While Algorithm 3 returns the maximum *number of requests* that can be generated in t time units, for systems with asymmetric read/write latencies the algorithm should be adjusted to output the maximum number of *time units* during which the processor will be stalling, waiting for the requests to be served.

In order to make this adjustment, we change each of the building blocks of the PCRP() Algorithm. First, the individual task profiling done by cache analysis (a pre-requisite to the PCRP() computation) must be modified to return the number of read and write requests in a given time window of length t (instead of simply returning the number of requests, without distinguishing between reads and writes). Task profiling is generally done by measurements or with the aid of static analysis tools. For example, in the case of experimentally profiling a task, many modern processors provide exclusive events (like `l2_store_misses` and `l2_load_misses`) which enable performance monitoring counters [94] to keep track of the number of reads and write misses. Hence, computing the PCRP() functions in this context is practically feasible.

Let us denote by T_{read} and T_{write} , an upper bound on the time to complete a read and a write transaction, respectively. Also, let $n_{\text{read}}(t)$ and $n_{\text{write}}(t)$ denote an upper bound on the number of read and write requests generated in a time window of length t , respectively.

1. For the carry-in portion: The task which returns the maximum delay in the carry-in portion must be selected. That is, Algorithm 3 must select the task for which the

delay computed by $n_{\text{read}}(\ell_{\text{cin}}) \times T_{\text{read}} + n_{\text{write}}(\ell_{\text{cin}}) \times T_{\text{write}}$ is maximized in its last ℓ_{cin} time units of execution.

2. For the carry-out portion: Analogously, Algorithm 3 must select the task for which the delay computed by $n_{\text{read}}(\ell_{\text{cout}}) \times T_{\text{read}} + n_{\text{write}}(\ell_{\text{cout}}) \times T_{\text{write}}$ is maximized in its *first* ℓ_{cout} time units of execution.
3. For the body portion: The knapsack must be filled in with the set of tasks with the highest request densities. Recall that in Algorithm 3 the request density of each task τ_i is defined as NReq_i/C_i . This quantity has to be redefined here as $(n_{\text{read}}(C_i) \times T_{\text{read}} + n_{\text{write}}(C_i) \times T_{\text{write}})/C_i$. The algorithm then proceeds as described in Algo. 3, by sorting the tasks in decreasing order of request density.

Although the main aim of the analysis is to design a unified framework using the PCR(\cdot) function, we showcase its applicability in computing the worst-case execution time for a given arbitration algorithm.

3.10 PCR case study: WCET analysis

In this analysis, we assume that the contention over the FSB is resolved based on a RR arbitration mechanism, in which all the cores are treated equally. The order in which the cores acquire the ownership of the bus is fixed a priori. When more than one core tries to access the bus, ties are resolved based on the fixed-ownership ordering. Given the WCET C_i of a task τ_i in isolation, here we compute the extra execution time that should be added to C_i to take into account the delay due to contention on the FSB. As mentioned earlier, TR denotes an upper-bound on the time to serve a memory request when a task runs in isolation and NReq_i denotes the maximum number of requests the task generates over its execution span.

3.10.1 Basic round robin equation

Given a RR bus arbitration mechanism, an upper-bound C'_i on the WCET of each task τ_i considering bus contention is given by

$$C'_i \stackrel{\text{def}}{=} C_i + \text{NReq}_i \times (m - 1) \times \text{TR} \quad (3.17)$$

Since the access to the shared FSB is granted using the RR protocol, each request generated by τ_i can be blocked by *at most* 1 request issued by the tasks running on each of the other $(m - 1)$ cores, hence creating an extra delay of *at most* $\text{NReq}_i \times (m - 1) \times \text{TR}$ time units.

Equation (3.17) implicitly assumes that the tasks running on each of the $(m - 1)$ interfering cores **will** generate NReq_i requests during the execution of task τ_i , which might not be true as tasks running on these cores may generate lesser number of requests. Hence

the above equation may lead to pessimistic bounds. We tackle this over-pessimism by providing a tighter upper-bound in the following subsection.

3.10.2 Improved Round Robin equation

Lemma 1. *Considering that a task τ_i is executing with contention on the FSB, an upper-bound C'_i on its execution time is given by the first solution (i.e., $C_i^k = C_i^{k-1}$) at which the following fixed-point iteration converges:*

$$C_i^k \stackrel{\text{def}}{=} C_i + \sum_{\pi_p \in \bar{\pi}(i)} \min(\text{NReq}_i, \text{PCR}_P(C_i^{k-1})) \times \text{TR} \quad (3.18)$$

with $C_i^0 \stackrel{\text{def}}{=} C_i$. The fixed point iteration terminates when $C_i^k = C_i^{k-1}$, at which, the value of C'_i is given by the corresponding C_i^k .

Proof. Equation (3.18) recursively computes a new value of C_i at each iteration $k \geq 1$, and incorporates the extra delay incurred by task τ_i due to the requests generated by the tasks running on the interfering cores, i.e., the cores $\pi_p \in \bar{\pi}(i)$. By definition, we know that τ_i generates at most NReq_i requests during its execution. For a RR bus arbitration algorithm, each of the interfering cores can delay every request issued by τ_i by at most 1 request and hence can delay the execution of τ_i by at most $\text{NReq}_i \times \text{TR}$ time units. Hence, at each iteration k , Equation (3.18) considers for each core $\pi_p \in \bar{\pi}(i)$ the minimum between

1. the number of requests that π_p might actually generate in the (currently computed) execution time of τ_i (i.e. $\text{PCR}_P(C_i^{k-1})$) and
2. the maximum number of requests that can be used by π_p to block τ_i 's execution (i.e., NReq_i).

□

In the next subsection, we discuss some properties of this improved RR equation.

3.10.3 Properties of the Improved RR equation

Lemma 2. *In Equation (3.18), for any iteration $k \geq 1$, the value of C_i^k monotonically increases, i.e $C_i^k \geq C_i^{k-1}$*

Proof. The proof is by induction. Initially, $C_i^0 = C_i$ and it can be inferred from Equation (3.18) that $C_i^1 \geq C_i^0$. The induction step consists in showing that, if $C_i^k \geq C_i^{k-1}$ then $C_i^{k+1} \geq C_i^k$. According to Equation (3.18), the expression $C_i^{k+1} \geq C_i^k$ can be rewritten as

$$\begin{aligned} & C_i + \sum_{\pi_p \in \bar{\pi}(i)} \min(\text{NReq}_i, \text{PCR}_P(C_i^k)) \times \text{TR} \\ \geq & C_i + \sum_{\pi_p \in \bar{\pi}(i)} \min(\text{NReq}_i, \text{PCR}_P(C_i^{k-1})) \times \text{TR} \end{aligned}$$

By subtracting/dividing the common terms from both sides we have:

$$\begin{aligned} \sum_{\pi_p \in \bar{\pi}(i)} \min(\text{NReq}_i, \text{PCR}_p(C_i^k)) &\geq \\ \sum_{\pi_p \in \bar{\pi}(i)} \min(\text{NReq}_i, \text{PCR}_p(C_i^{k-1})) &\end{aligned} \quad (3.19)$$

Given the monotonicity of the $\text{PCR}_p(t)$ function ($\forall t_1 \leq t_2 : \text{PCR}_p(t_1) \leq \text{PCR}_p(t_2)$), stated earlier in Property 1, for any π_p we have $\text{PCR}_p(C_i^k) \geq \text{PCR}_p(C_i^{k-1})$. Therefore, only three cases may arise:

1. $\text{NReq}_i \geq \text{PCR}_p(C_i^k) \geq \text{PCR}_p(C_i^{k-1})$
2. $\text{PCR}_p(C_i^k) \geq \text{NReq}_i \geq \text{PCR}_p(C_i^{k-1})$
3. $\text{PCR}_p(C_i^k) \geq \text{PCR}_p(C_i^{k-1}) \geq \text{NReq}_i$

and it can be easily shown for all of them that

$$\min(\text{NReq}_i, \text{PCR}_p(C_i^k)) \geq \min(\text{NReq}_i, \text{PCR}_p(C_i^{k-1}))$$

which provides Inequality (3.19) and thereby, establishes the proof. \square

Lemma 3. *Equation (3.18) always terminates in at most $(m - 1) \times \text{NReq}_i$ iterations and may provide a tighter upper-bound than Equation (3.17).*

Proof. The proof is a direct consequence of Lemma 2. The highest value of C_i^k is reached when for all the other cores, it holds that $\text{PCR}_p(C_i^k) \geq \text{NReq}_i$. In this case, Equation (3.18) becomes $C_i^k \stackrel{\text{def}}{=} C_i + \sum_{\pi_p \in \bar{\pi}(i)} \text{NReq}_i \times \text{TR}$ which corresponds to Equation (3.17). In order to maximize the number of iterations to reach this highest value of C_i^k , we have to consider that at each iteration k , there exists only one core $\pi_\ell \in \bar{\pi}(i)$ such that $\min(\text{NReq}_i, \text{PCR}_\ell(C_i^{k-1})) = \min(\text{NReq}_i, \text{PCR}_\ell(C_i^{k-2})) + 1$ and for all cores $\pi_p \in \bar{\pi}(i)$ with $p \neq \ell$, it is the case that $\min(\text{NReq}_i, \text{PCR}_p(C_i^{k-1})) = \min(\text{NReq}_i, \text{PCR}_p(C_i^{k-2}))$. In this scenario, we get $C_i^k = C_i^{k-1} + 1$ at each iteration k and it takes $(m - 1) \times \text{NReq}_i$ iterations to reach the highest value of C_i^k given above. Finally, if Equation (3.18) converges to a solution $C_i^k = C_i^{k-1}$ before this extreme value, then the resulting C'_i (where $C'_i = C_i^k$) provides a tighter upper-bound than the C'_i computed by Equation (3.17). \square

3.11 System wide Analysis

In this section, we describe the process of applying the method described earlier to *all* the tasks in the system. Consider an example system with 2 cores $\{\pi_1, \pi_2\}$ and 4 tasks $\{\tau_1, \tau_2, \tau_3, \tau_4\}$. Let tasks τ_1 and τ_2 be assigned to π_1 and tasks τ_3 and τ_4 be assigned to π_2 . We calculate the functions $\text{PCR}_1(t)$ and $\text{PCR}_2(t)$ using the method described in Section 3.5 (left box in Fig. 3.9). Tasks assigned to core π_1 are subject to interferences from tasks co-scheduled on π_2 and vice versa. Therefore, we compute C'_1 and C'_2 against $\text{PCR}_2(t)$

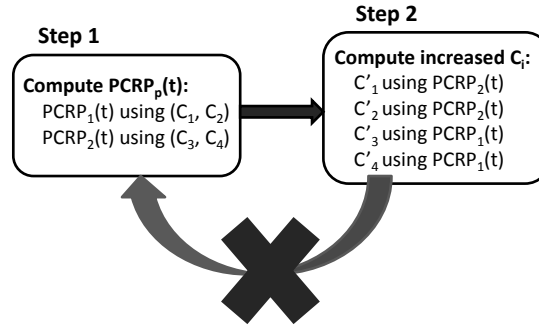


Figure 3.9: Our system-wide analysis is a non-cyclic process.

and C'_3 and C'_4 against $\text{PCRPP}_1(t)$, using the method introduced in Section 3.10 (right box in Fig. 3.9). At this point, it may seem that the functions $\text{PCRPP}_1(t)$ and $\text{PCRPP}_2(t)$ can be refined using as input, the newly computed C'_1, C'_2, C'_3 and C'_4 . If so, the process may re-iterate and a natural question is “when should the process stop iterating?”. We answer this question based on the following Lemma 4.

Lemma 4. *For every core p , the function $\text{PCRPP}_p(t)$ monotonically decreases as the WCET of the tasks running on core π_p is inflated due to the contention for the FSB.*

Proof. The proof is a consequence of the fact that incorporating the interference from other tasks into the WCET estimate of a given task τ_i does not increase the number of requests that τ_i can potentially generate in any time window of any length t . That is, the number of requests that are inherently generated by each task τ_j assigned to π_p does not increase as its WCET inflates. In the computation of $\text{PCRPP}_p(t)$, the impact of inflating the WCET of each task τ_i (without modifying its maximum number of requests NReq_i) is that the requests of their jobs are spaced further apart (resulting in a lower request density). Another consequence is that potentially lesser jobs of τ_i can execute within the body portion and lesser requests can potentially be generated within a given length of carry_in and carry_out portions Hence the lemma. \square

As proven in Lemma 4, re-iterating the process of computing $\text{PCRPP}_p(t)$ (for all cores π_p) and C'_i (for all tasks τ_i) alternately will decrease the value returned by the function $\text{PCRPP}_p(t)$ at each iteration, hence ultimately providing an unsafe upper-bound for the WCETs. As a result, our analysis is a one-step process, i.e., it is not cyclic. This also means that the given model facilitates the determination of the value of C'_i for every task τ_i at design-time itself.

3.12 Performance Comparison: Simulations

In this section, we will evaluate the performance of the analysis techniques developed for deriving the memory profile for a given task and for a given core against the approaches developed by contemporary researchers.

3.12.1 Comparison of the task profile computations with the state of the art

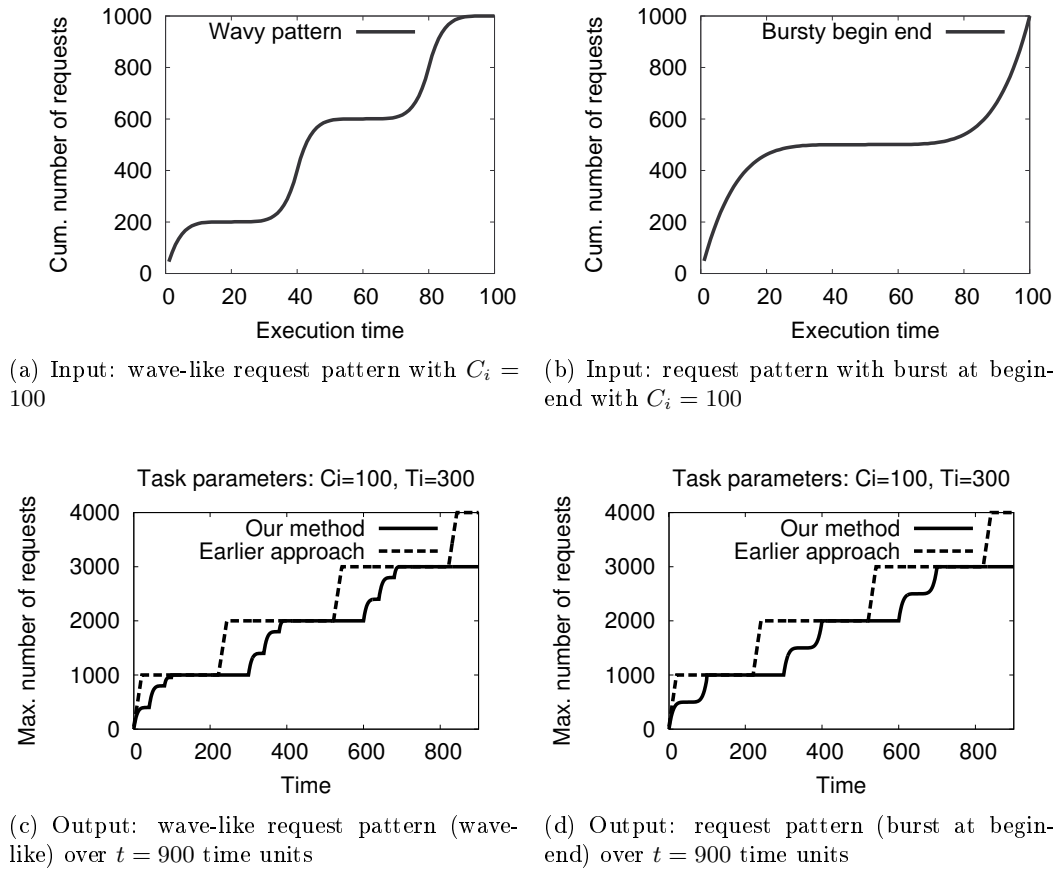


Figure 3.10: Comparison of the approaches

An arbitration agnostic method has been proposed by [80], [106] and hence warrants a comparison with our method, since the method may look similar in principle to the reader. The approach presented in [80] uses an event activation model to compute an upper bound on the time to access the shared resources in a given interval of time t . To compute the maximum number of requests for a single task instance, they assume that there is a known minimum time “d_{sr}” between two requests to a shared resource. They propose a simple lower bound to compute the minimum time that a task must execute, to generate n requests, given by $\delta^-(n) = (n - 1) \times \text{dsr}$. This is then extended, to compute the minimum time to make n requests by multiple jobs of the task. An inverse function $\eta^+(t)$, is used to derive the maximum number of requests in time t . The assumption of a minimum request distance is agnostic to the request pattern of the task and inherently implies a uniform distribution of requests and hence leads to an over-estimation of the maximum number of requests that a task can generate in a given interval of time t .

It is important to note that the method proposed here, uses a different technique

(compared to the method proposed in [80]) to compute the maximum number of requests for a task in a time interval t and hence the experiments presented here are used to highlight only that phase of the overall analysis.

The input to the analysis is a set of synthetic request patterns depicted in Figures 3.10a and 3.10b. These patterns are representative of applications having a (i) burst of requests at the beginning and end and (ii) wave like request distribution. In these graphs, $C_i = 100$, $T_i = 300$ and the maximum number of requests, $BR(C_i)$ in one task instance (referred to N_j^{\max} in their approach) is 1000. The experiments are run with $R_i = C_i$ as inputs to both algorithms. The maximum number of requests are computed for all values of t from 0 to 900 (i.e. $3 * T_i$ time units). Since our approach to compute $BR_i(t)$ takes into consideration, the request profile of a task and is sensitive to the request pattern, the bounds computed are tighter, as seen in Figures 3.10c and 3.10d.

As seen in the graphs, our method for determining the maximum number of requests first characterizes the task behavior and then derives the bounds. In contrast, the method proposed by Ernst et. al [80] (called the ‘‘Earlier approach’’ in Figures 3.10c and 3.10d), does not consider the request distribution and base their analysis on the minimum release time between two requests. As a result, their approach yields more pessimistic upper bounds on the number of requests that a task can generate. We compared the two approaches for other types of request patterns (like bursts at the beginning of the application, bursts at the end of the application, etc.) as well and found that our method outperforms their method. As expected, for tasks with uniform distribution of requests, both methods yield the same upper bounds. The graphs with other patterns are not presented here due to space limitations. Summarizing the discussion above, we believe that our approach dominates their approach in yielding tighter upper bounds on the number of requests in a given time interval.

3.12.2 Comparison of the per-core profile computations with the state of the art

The following benchmarks from the ChStone suite [107] were used for the comparison tests.

1. ADPCM decoder: Adaptive differential pulse code modulation decoder
2. GSM: Linear predictive coding analysis of global system for mobile communications
3. JPEG: JPEG image decompression
4. MOTION: Motion vector decoding of the MPEG-2
5. MIPS: Simplified MIPS processors
6. AES: Advanced encryption standard
7. BLOWFISH: Data encryption standard

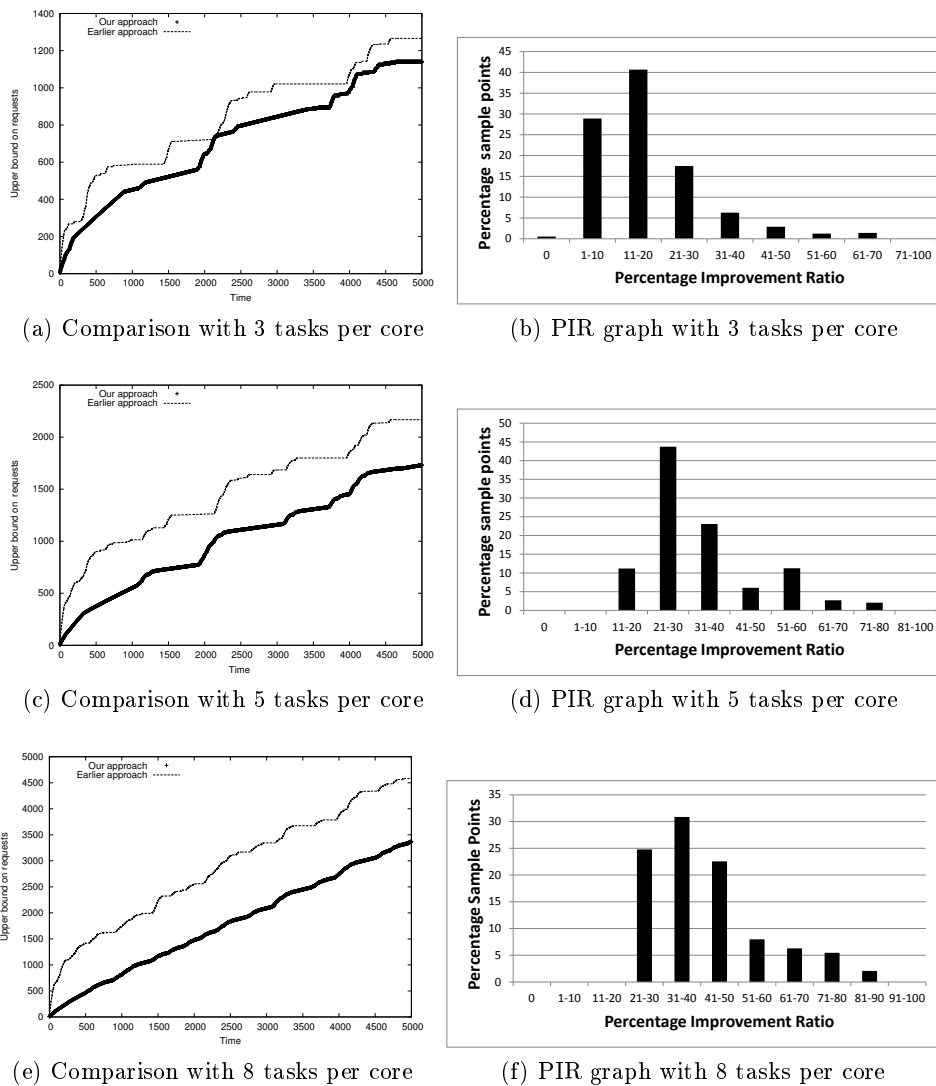


Figure 3.11: Comparison with the approach in [91]

8. SHA: Secure hash algorithm

The tests are used to highlight that as the number of tasks assigned to a core increases, the basic approach presented earlier in Section 3.5.2 starts producing very pessimistic results. Recall that the basic approach considers that *all* tasks on the interfering cores pose a delay to the analyzed task and adopts a basic additive approach to compute the per-core interference, while the improved approach finds the combination of tasks that may fit in the time interval and also generate the maximum number of requests.

To compare the approaches, we computed an upper bound on the number of requests generated on a given core by assuming 3 tasks, 5 tasks and 8 tasks on each core in the above tests. It can be clearly seen in Figures 3.11a, 3.11c and 3.11e that as the number of tasks assigned to a core increases, our improved method using the task packing algorithm produces tighter bounds on the number of requests. The graphs also serve to illustrate the monotonically increasing property of the PCR_P() function. The graphs show the values

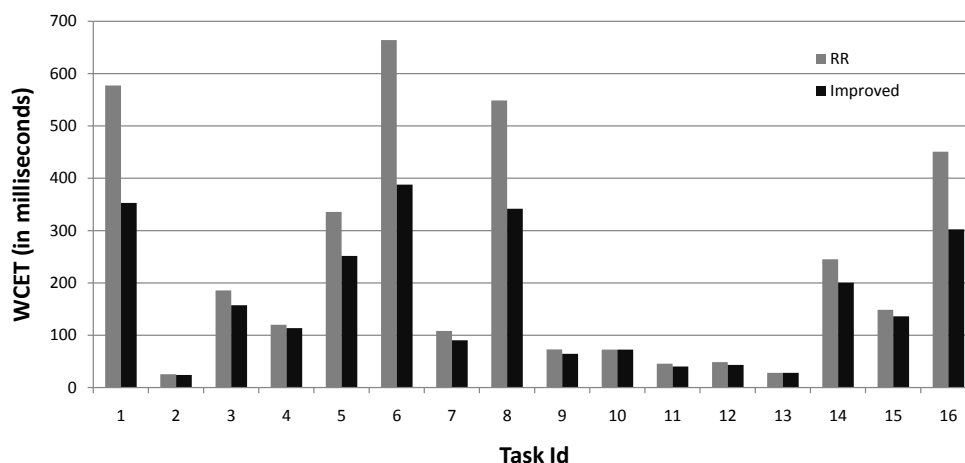


Figure 3.12: WCET comparison: improved approach vs. basic RR

for $\text{PCR}P()$ computed in the time range from 1 to 5000 units. To further quantify the performance of the tightness, we computed the percentage distribution of improvements in tightness for each of these three cases by deriving a metric which we term the Percentage Improvement Ratio (PIR). At each time point t let $\text{bpcrp}(t)$ denote the bounds computed by the $\text{PCR}P()$ function while bsoa denote the bounds computed by the state of the art. Then PIR for each point is given by $(\text{bsoa}() - \text{bpcrp}()) * 100 / (\text{bsoa}())$. Hence a PIR of 25% meant that the bound computed by our approach is 25% tighter than the bounds computed by the basic additive approach [80]. As seen in Figure 3.11b, 0.52% of the sampled points showed no improvements, while 40+% of the sampled points showed a PIR of 11-20%. At the higher end less than 2% of the samples showed a PIR increase of 61-70%. Interestingly, as seen in Figure 3.11f, in the case of 5 tasks being assigned on the core, 40+% samples showed an increase in the range 21-30% and at the higher end the percentage of samples having a 50-60% improvement also increased. This effect is more pronounced in Figure 3.11f as more samples shift towards a higher PIR. The observation is as expected, since as more tasks are added to the system, the possibility of all of them being co-scheduled with the analyzed task decreases and thus the pessimism of the computed bounds of the existing additive approaches increases. A simple case with 3, 5 and 8 tasks was enough to bring forth this drawback in the existing mechanisms.

Next we evaluate the performance of the $\text{PCR}P()$ function for a round robin arbiter.

3.12.3 Comparison: Basic Round Robin vs Improved Round Robin

The resulting WCET of a task (when in contention for the shared resources) is sensitive to the properties of the co-scheduled tasks (C_i , T_i , memory profile) besides core assignments and the scheduling algorithm. No direct co-relation between the increase in WCET and any individual parameter can be drawn without exhaustive tests. However, the aim here is to validate and compare our approach and hence we provide a “proof of concept” with a small set of tasks. We generated 16 random tasks with different memory profiles (with different

request densities) and assigned them to 4 different cores randomly. We used Algo. 3 to compute the PCR_P(\cdot) function in Eq. (3.18) to compute the WCET. As seen in Fig. 3.12, for all the tasks, our method performs equally or better (in most cases) against the basic RR arbitration. The tightness of the improved WCET varies from (0 to 41%). There is no improvement using our approach for task 2 and 13, which can be explained as follows: These tasks have a very low request density (given by $NReq_i/C_i$) of around 2 and a low execution time. Hence their WCET increases marginally due to the contention on the bus and there is little scope for improvement. For tasks 1, 5, 6, 8, 16 the request densities varied from 25 to 30 (high for this example). For such tasks, the impact of contention is high and the tightness varied from (25-41%). The rest of the tasks showed moderate improvements (5 to 18%) with the new approach.

While the above experiments were carried out by simulations with synthetic traces, it was important to know if the basic parameters can be computed on a real platform. The following section summarizes the results of the exercise.

3.13 A method to obtain the parameters experimentally

In *principle*, it is possible to use the substantial amount of work developed in the WCET analysis community [10] to provide suitable bounds on *ARH* and *ARL*. However, these approaches generally need an important amount of information about the hardware to provide accurate results. Since it is difficult to obtain suitably accurate documentation for COTS hardware, those techniques might provide highly pessimistic results and we focus on an alternative technique based on measurements, as this is still the de-facto standard in the analysis of safety critical systems. This alternative is also preferable when the underlying cache replacement policy is pseudo-LRU, because static/offline analysis methods generally lead to highly pessimistic results for such policies (and pseudo-LRU is usually employed in COTS-based hardware).

The approaches proposed above for task-analysis requires as an input, the parameters TR, an upper bound on the time to complete one bus transaction. It also needs the cache profile of a task modeled by the *ARH* and *ARL* values. This section details how these values can be obtained by measurement on the actual hardware. A bus transaction involves a sequence of sub-operations, and hence the value of TR is very hardware specific and cannot be obtained from manuals provided by vendors directly, and offline techniques cannot be used to compute them unless all details are provided. Thus it is necessary to obtain them by measurement.

The experiments were carried out on an IntelTMCore2 Quad Q8300 processor consisting of four cores placed on two dies on a single chip. Each die has two cores and each core has its own instruction and data cache (denoted as I\$ and D\$). However, the two cores on the same die share the L2 cache i.e., (i) Core-1 and Core-2 share a L2 cache on one die and (ii) Core-3 and Core-4 share a L2 cache on another die. All the 4 cores access the main

memory via a single shared bus. On one die, tasks were run only on Core-1, keeping Core-2 idle, thereby giving Core-1 access to the entire L2 cache available on that die. Analogously, on the other die tasks were run only on Core-3, keeping Core-4 idle, thereby giving Core-3 access to the entire L2 cache available on that die. Experiments were performed on the VxWorks 6.8 [108] real-time operating system. Other relevant details of the experimental setup are presented in Table 3.3.

System characteristics	
Processor model	Intel® Core2™ Quad Processor
CPU	Q8300 @ 2.50GHz
L1 cache	32 KB D-cache, 32KB I-cache, 8-way associative
L2 cache	2048 KB, unified, 8-way associative
FSB Specs	333 MHz, 1333 MTps, 10656 MBps
OS kernel	VxWorks 6.8

Table 3.3: Test System Description

3.13.1 Measurement Setup

The experiment set-up is described here.

1. Before each run of the experiments, the cache was invalidated, ensuring that the state of the cache was consistent across runs. The experiments were run with the same input, thereby forcing single execution paths.
2. To reduce the non determinism, hardware prefetching and adjacent cache line prefetching features were disabled in the processor. It is necessary to disable the prefetching feature (i) to isolate the bus contention problem and (ii) to have more determinism while taking the measurements, as prefetchers speculatively fetch data and add to the traffic on the bus and run in the background at arbitrary times, thus making the timing measurements inaccurate.
3. To avoid migration of the tasks across cores, tasks were pinned to the cores using the taskAffinity feature in VxWorks.
4. Another feature namely, “CPU Reservation” (in VxWorks terminology) that dedicates a core to a task was also used to ensure that the task to which the core is dedicated runs non-preemptively.
5. Since the memory is shared between several peripherals, the interference from these must be kept to a minimum. Hence the experiments were run with a basic console

device and a diskless system to avoid any DMA activity to influence measurement results. the arbitration overhead and contention in the memory controller unit is minimal in our setup.

Events were monitored at the micro-architectural level by writing to model-specific registers and reading Performance Monitoring Counters (PMCs) directly. PMCs are a set of special-purpose registers built into modern microprocessors to store the counts of hardware related activities, such as cache misses ([94], [109]).

3.13.2 Measurement of TR

TR is defined as an upper bound on the time to complete one bus transaction. To obtain this value experimentally, a task called the cache thrasher (CTC) was generated that constantly accessed the memory and generated an L2 cache miss on each access. We programmed this task by declaring an array twice the size of the cache and accessing each line of the cache sequentially, thereby causing an L2 miss for every access. Since the array size is twice the cache size, the task scans the entire cache twice in each run, hence evicting all the cache lines that were already fetched, prior to the next run. The number of bus requests, denoted by NBR, is obtained by monitoring the Bus_Requests_Mem event, for each run and the time taken for each run, denoted by TBR is recorded. The number of bus requests generated was verified against the expected number of bus requests (which is twice the number of cache lines) to validate the approach and was found to be consistent. The value of TR is thus computed for thousands of runs and the maximum is recorded over all the runs. Then the final TR is given by Equation (3.20).

$$TR = \max_{k=1..nr} (TBR_k / NBR_k) \quad (3.20)$$

where k denotes the run index, nr denotes the number of runs and TBR_k and NBR_k denote the corresponding values in that run. The value of TR from the experiments was 46.6 nano seconds.

3.13.3 Measurement of ARH and ARL

The ARH and the ARL values described earlier, represent an upper and lower bound on the number of bus requests generated by a task from the beginning of its execution up to time t . To measure these values for a given task, we chose some sampling points by dividing the execution time of the tasks into subintervals. We obtained the cumulative number of bus requests upto that point by interrupting the task and reading the performance monitoring counters at the required sampled point. We then re-ran the task and interrupted the task at the next sampling point. At each sampling point, the highest measured value was recorded as ARH and the lowest value was recorded as ARL, over multiple iterations. It is to be noted that unlike simulations, where it is assumed that a task will have fixed number

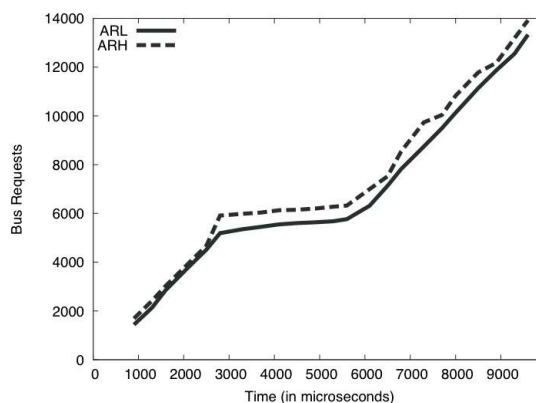


Figure 3.13: ARH, ARL Curve for the Search Benchmark

of memory accesses at a given time instance, this presents a more realistic approach, as it takes into account the variations in the number of requests issued due to the underlying cache replacement policy employed and makes this method very generic. We also recorded the exact time when the interrupt was issued and the time time at which the interrupt service routine was fired to increase the precision of our results. For the given system, the `Bus_Requests_Mem_This_Core_This_Agent` event was monitored to precisely measure the number of requests issued by the task. An example of the cache analysis profile, showing the ARH and ARL values at each sampling point for the Search Benchmark from the MiBench Suite [110] is presented in Figure 3.13. The graph for the search program shows a variability in the number of cache misses across runs during one complete execution. It can be seen that after a certain time, the number of bus requests reaches a plateau and then increases again. This decline in the slope to reach a plateau form, seen in the graph corresponds to the time when the task is not issuing any requests and this was achieved by the introduction of a task delay in the program (to demonstrate the variability in the request pattern which can be captured by PMCs).

3.14 Chapter Summary

In this chapter, we defined the system and task model under which the analysis holds and presented two primary tools, the per-task memory profiler and the per-core memory profiler that will be leveraged in the upcoming interference analysis aimed at determining the WCET of a task contending with other tasks for the shared bus. The primary focus was towards characterizing the memory usage pattern of a task and determining the interference it can incur from the co-executing tasks assigned to other cores. The methods developed employed an interval splitting technique to determine the maximum number of requests than can be issued in a given interval of time by a given core. It was shown through simulations that the proposed methods perform better than the existing approaches. Further,

the properties and the computational complexity of these methods was analyzed. An application of the Per-Core Request profiler was demonstrated with respect to the round robin arbitration algorithm. It is important to note that both these methods are independent of the bus arbitration mechanism and only deal with the amount of traffic reaching the shared bus from any core in a given interval of time t . The scheduling of the requests will next depend on the arbitration mechanism of the bus and will decide the delay incurred by each of the requests. The cumulative delay incurred by all the requests from a task along with its execution time in isolation will eventually lead us to the final WCET of the task in contention. In the next chapter, with the help of the tools developed here, an analysis of the delay due to contention on the memory bus will be computed.

Chapter 4

Unified Framework for Bus Contention Analysis in Multicores

*One ring to rule them all, one ring to find them,
One ring to bring them all and in the darkness
bind them.*

J. R. R. Tolkien, Lord of the Rings

The previous chapter laid the foundations for the upcoming analysis — we systematically developed a per-core memory request profiler (or the $\text{PCR}_p(t)$ function) to determine the amount of memory traffic that a core π_p can inject into the front side bus in a given interval of time t . Recall that the per-core memory request profiler models only the traffic injected into the bus, and as a result is agnostic of the underlying arbitration mechanism employed by the bus. As a next step in the analysis, we leverage the information provided by the per-core memory request profiler, together with the front side bus arbitration models, in order to achieve the objective of determining the increased execution time of the tasks due to contention on the shared bus. The main focus of this chapter is to design a framework that provides a common interface to different arbitration algorithms and apply this framework to compute an upper bound on the execution time of tasks when run in conjunction with other co-executing tasks.

The need for a unified framework stems from the fact that existing works address the problem of deriving an upper bound on the delay due to bus contention to some extent, but the analysis is tightly coupled to a particular arbitration policy, such as TDM [90, 73, 74, 75, 76] or non-specified work-conserving arbiters [91, 80], and do not provide a common mechanism to handle different arbitration mechanisms. As a result, worst-case execution time estimation tools are limited to different point solutions for each system under analysis, complicating implementation and maintenance. We address this problem by proposing a general framework for shared bus contention analysis that addresses a wide

range of arbitration policies in multi-core systems and can be implemented in worst-case execution time estimation tools.

The next section introduces the system model used in this chapter. First, we present the platform model, followed by a characterization of tasks and their corresponding memory profiles. We then explain the assumptions on the task scheduler, before arriving at the problem statement.

4.1 System and Task Modeling

We revisit the notations in this chapter to avoid re-referencing backwards in the documents.

4.1.1 Platform Model

The assumed multicore platform π contains m cores denoted by $\pi_1, \pi_2, \dots, \pi_m$. It is assumed that there is no cache memory shared between them or all levels of shared cache, if present, are disabled or partitioned. All the cores communicate with the memory through the same shared bus that we refer to as the shared front side bus (FSB). Contention between the cores is resolved by the arbitration policy in the front side bus, which depends on the considered platform. Fixed-priority arbitration are typically used in systems with diverse response time requirements, TDM in systems that require robust partitioning between applications, and round robin when a simple notion of fairness between applications executing on different cores is required.

4.1.2 Task Model

The workload is modeled by a set of sporadic and constrained-deadline tasks in which a task τ_i is characterized by three parameters: C_i , T_i , and $D_i \leq T_i$. The parameter C_i denotes an upper bound on the execution time of task τ_i when it executes uninterrupted in *isolation*, i.e., with no contention on the front side bus. T_i denotes the minimum interval arrival time between two consecutive activations of τ_i and D_i is the deadline of the task. The parameter C_i can be computed by well-known techniques in WCET analysis [10]. This work focuses on computing C'_i , which denotes an upper bound on the execution time when τ_i executes *with* contention on the front side bus, i.e., when the co-scheduled tasks are running on the other cores. Clearly, the value of C'_i is not an inherent property of τ_i but depends on the arbitration policy on the FSB and on the memory request pattern of the tasks executing concurrently on the other cores during its execution.

We also introduce a few new notations required for modeling the requests in the following analysis. To gain a deeper insight into the request distribution across the execution of a task, the task is divided into sampling regions and the maximum number of requests *within* each sampling region is recorded (either using static analysis techniques or measurement based techniques). It is important to note that the newer modeling of the sampling regions

is subtly different from modeling defined in the previous chapter: Earlier the cache profile of a single task was represented by two functions $\text{ARH}_i(t)$ and $\text{ARL}_i(t)$ denoting the maximum and minimum number of requests that task τ_i can generate in the time interval $[0, t]$ i.e., *from the beginning of the execution of the task to time t* , while in the newer analysis we consider the maximum number of requests that can be generated *within* each region. We formally model the sampling regions in the upcoming subsection.

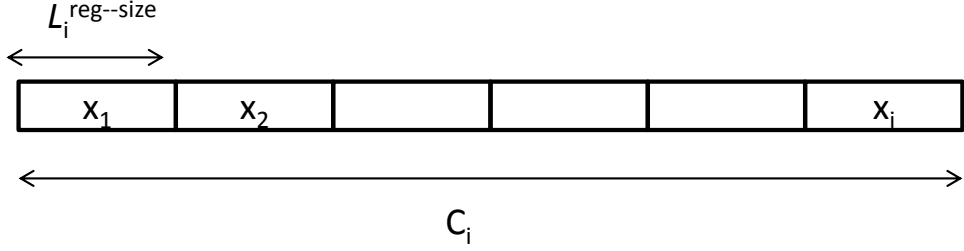


Figure 4.1: Illustration of sampling regions

4.1.3 Request and Region Modeling

First, the entire execution of each task τ_i is divided into $x_i = \frac{C_i}{L_i^{\text{reg-size}}}$ sequential logical sampling regions, where $L_i^{\text{reg-size}}$ is the length of each region. Figure 4.1 depicts this segmentation. It is not necessary for all the region lengths to be equal and the analysis will hold for regions with unequal sizes. For each task τ_i , the maximum number of memory requests issued *within* each region is recorded after running it a significant number of times over different inputs. This method returns a set $\mathbb{G}_i = \{\eta_{i,1}, \eta_{i,2}, \dots, \eta_{i,x_i}\}$, where each $\eta_{i,g}$ (where $g \in [1 \dots x_i]$) is an upper bound on the number of requests that task τ_i can generate *within* its g 'th logical region, as depicted in Figure 4.2. Note that $\sum_{g=1}^{x_i} \eta_{i,g}$ denotes the maximum number of requests that task τ_i can generate during the entire execution of one of its jobs and, for simplicity, we sometimes use the notation $\eta_{(i)}$ to denote this value, i.e., $\eta_{(i)} \stackrel{\text{def}}{=} \sum_{g=1}^{x_i} \eta_{i,g}$.

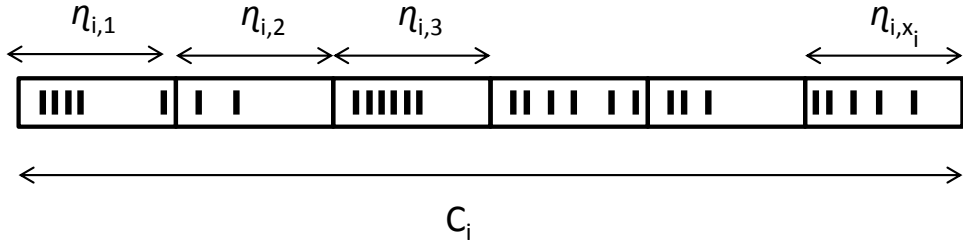


Figure 4.2: Illustration of task region profiling. Dark lines within regions symbolize memory requests

We next denote by $\mathbb{R}_i = \{\text{req}_{i,1}, \text{req}_{i,2}, \dots, \text{req}_{i,\eta_{(i)}}\}$, the set of all requests that τ_i can generate during its execution. Each request $\text{req}_{i,k}$ is modeled by the tuple $\langle \text{rel}_{i,k}, \text{srv}_{i,k} \rangle$, where $\text{rel}_{i,k}$ and $\text{srv}_{i,k}$ denote the release and service time of request $\text{req}_{i,k}$ during τ_i 's

execution, respectively. As mentioned above, the exact values of $\text{srv}_{i,k}$ and $\text{rel}_{i,k}$ cannot be determined at design time.

To summarize, for each task τ_i we define a region length $L_i^{\text{reg-size}}$ and compute the set $\mathbb{G}_i = \{\eta_{i,1}, \eta_{i,2}, \dots, \eta_{i,x_i}\}$. Then, the aim is to compute $\text{rel}_{i,k}$ and $\text{srv}_{i,k}$, $\forall \text{req}_{i,k} \in \mathbb{R}_i$, with the objective of maximizing the cumulative waiting time (also called cumulative delay) of all the requests, i.e. $\sum_{k=1}^{\eta(i)} (\text{srv}_{i,k} - \text{rel}_{i,k})$ is maximum.

4.1.4 Scheduler Specification

We consider a partitioned scheme of task assignment in which each task is assigned to a core at design time and is not allowed to migrate from its assigned core to another one at run time (fully partitioned non-migrative scheduling scheme). Recall that we denote by $\bar{\pi}(i)$, the set of $m - 1$ cores to which task τ_i is *not* assigned (called the “interfering cores” of task τ_i). Regarding the scheduling policy, we consider a non-preemptive scheduler and hence do not deal with cache-related and task-switching overheads. We make the non-work-conserving assumption as follows: whenever a task completes earlier than its WCET (say on its assigned CPU π_p), the scheduler idles the core π_p up to the theoretical WCET of the task. This assumption is made to ensure that the number of bus requests within a time window computed at design time, is not higher at run time due to early completion of a task and the subsequent early execution of the next tasks.

4.1.5 Problem Statement

The problem is stated as follows: Given: (i) a multi-core platform conforming to the model described in Section 4.1.1, (ii) a given task $\tau_i \in \tau$ and its WCET C_i *in isolation* as described in Section 4.1.2, and (iii) the region-profiles of all tasks as described in Section 4.1.3, the problem is to compute the WCET C'_i of τ_i when τ_i executes concurrently with other tasks. In essence, the problem is to find a tight upper bound on the *cumulative delays* incurred by all the requests of τ_i due to the contention for the front side bus.

We tackle this problem by proposing a general framework for bus contention analysis that addresses different arbitration policies in multi-core systems and can be implemented in worst-case execution time estimation tools. The three main contributions of this chapter are:

1. A model that captures the best-case and worst-case availability of the shared front side bus to a given task. This model can be applied to a range of arbitration policies in a streamlined manner, and we demonstrate its flexibility by applying it to two very different cases, being non-work-conserving TDM and work-conserving fixed-priority arbitration.
2. An algorithm that uses the proposed bus model and leverages the cache profiles to compute the maximum interference on the bus that a given task may incur.

3. A method to tighten the computed bounds and increase the efficiency and scalability of the algorithm by splitting the task into smaller sampling regions and leveraging their cache profiles.

We experimentally evaluate the proposed approach by applying it to a multi-core COTS system providing access to a DRAM via a shared bus. The flexibility of the framework is demonstrated by applying it to different arbiters on a set of applications from the WCET test suite [111]. We additionally evaluate the accuracy and the run-time of the analysis for different sample region sizes. Apart from the proof-of-concept by implementation, we also formally prove the key concepts upon which the algorithm is designed.

The rest of this chapter is organized as follows. An overview of our approach is provided in Section 4.2. The different steps of our approach are then discussed in detail, starting with the proposed bus availability model in Section 4.3. We then proceed by showing how to bound worst-case interference in Sections 4.4 and 4.5, respectively. This is followed by a method to improve the accuracy and increase the efficiency of the algorithm, in Section 4.6. We discuss the related work in Section 4.7. The approach is experimentally evaluated in Section 4.8 and the chapter is summarized in Section 4.9.

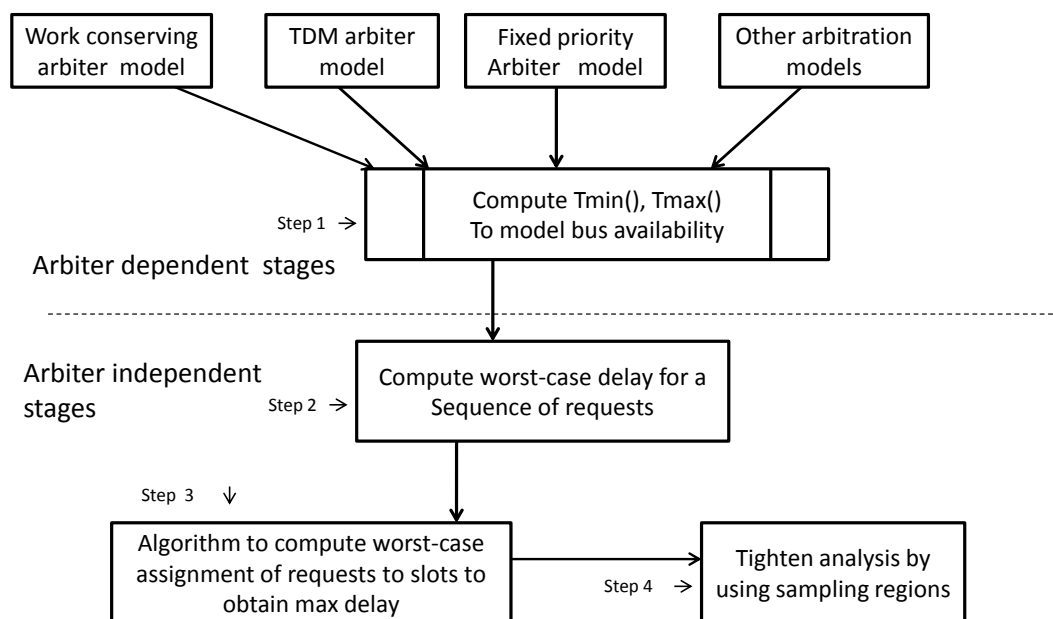


Figure 4.3: An overview of the unified framework

4.2 Overview of Approach

Figure 4.3 gives a high-level overview of the approach in arriving at a generalized framework. This section proposes a 4-step approach to solve the aforementioned problem. The details of each step are later explained in the following sections.

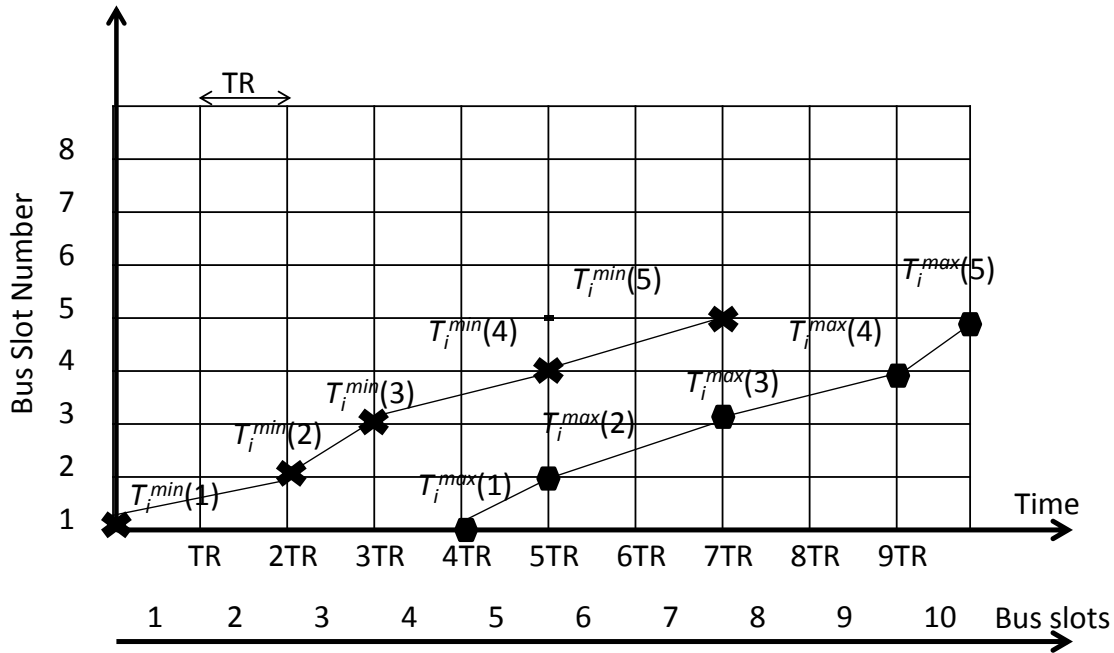


Figure 4.4: Illustration of $T_i^{\max}(j)$ and $T_i^{\min}(j)$

Step 1: Modeling the availability of the bus

In Section 4.3 we will first show how to model the availability of the bus to task τ_i using a general model $\mathbb{B}_i = \langle T_i^{\min}(), T_i^{\max}() \rangle$. It is key to note that in the entire analysis that follows, the bus controller grants access to the bus in units of bus slots, where each bus slot is of length TR and TR is defined as an upper bound on the time to serve a memory request. Given that several tasks contend for the same shared bus, a given task τ_i may not get access to the bus immediately on generating a request (owing to the contention from co-scheduled tasks from other cores). From now on, we will refer to the bus slots that are available to τ_i , as *the free bus slots* of τ_i .

Definition 14. The function $T_i^{\min}(j)$ represents the earliest time instant at which the bus can be available to τ_i for the j 'th time or in other words, the earliest availability of the j^{th} free bus slot of τ_i .

Definition 15. The function $T_i^{\max}(j)$ represents the latest time instant at which the bus can be available to τ_i for the j 'th time or in other words, the latest availability of the j^{th} free bus slot of τ_i .

The order in which these bus slots are granted to the tasks depend on the arbitration mechanism; as a consequence it follows that the two functions $T_i^{\min}(j)$ and $T_i^{\max}(j)$ also depend on the arbitration mechanism as depicted in Figure 4.3. As we shall see in the next section, for some arbitration policies like Time Division Multiplexing, the availability of the bus modeled by $T_i^{\min}(j)$ and $T_i^{\max}(j)$ is independent of the traffic generated by the

other cores, while for other arbitration mechanisms like priority based mechanisms, the interfering requests do influence the time at which the analyzed task can avail the bus.

Figure 4.4 illustrates the earliest and the latest times at which a given slot is available to task τ_i . As seen in the figure, the earliest time at which slot 1 may be available to task τ_i , $T_i^{\min}(1)$ is at time 0, meaning there are no pending requests or task τ_i is executing in isolation and there is no contention on the bus. However, as seen, $T_i^{\max}(1) = 5$ i.e., τ_i may at most have to wait for 4 slots before it can get a free bus slot and thus can only be served at the beginning of the fifth slot. Similarly, the availability for the subsequent slots is depicted in the figure. Note that this particular example is not representative of any particular arbitration mechanism.

Step 2: Compute maximum cumulative delay

Given the bus availability model $\mathbb{B}_i = \langle T_i^{\min}(), T_i^{\max}() \rangle$ of task τ_i , we propose a function to compute the *maximum cumulative* delay incurred by requests of τ_i due to contention on the shared bus. We introduce two concepts in this regard.

Definition 16. We define a *request-to-slot assignment* in the context of a single request by the notation $\sigma_i(k)$, which represents that the k 'th request generated by τ_i , i.e., $\text{req}_{i,k}$ is served in the $\sigma_i(k)$ 'th bus slot available to task τ_i .

Similarly, for a sequence of requests we define a mapping as follows.

Definition 17. We define a *request-set mapping* $\mathbb{M}_i = \{\sigma_i(1), \sigma_i(2), \dots, \sigma_i(\eta(i))\}$ to represent that $\forall k \in \mathbb{R}_i$: $\text{req}_{i,k}$ is assigned to $\sigma_i(k)$.

We further divide this step is divided in 2 phases

- Given the bus availability model $\mathbb{B}_i = \langle T_i^{\min}(), T_i^{\max}() \rangle$ of task τ_i , its request $\text{req}_{i,k}$ and a request-to-slot assignment $\sigma_i(k)$, we propose a mechanism to compute the maximum delay that request $\text{req}_{i,k}$ can incur. To do so, we compute the release time $\text{rel}_{i,k}$ and service time $\text{srv}_{i,k}$ with the objective of maximizing the waiting time (i.e., $\text{srv}_{i,k} - \text{rel}_{i,k}$) of $\text{req}_{i,k}$.
- In the second phase, given the bus availability model $\mathbb{B}_i = \langle T_i^{\min}(), T_i^{\max}() \rangle$ of task τ_i and a request-set mapping $\mathbb{M}_i = \{\sigma_i(1), \sigma_i(2), \dots, \sigma_i(\eta(i))\}$, we propose a mechanism to compute the maximum cumulative delay incurred by the set of corresponding requests. As in the previous phase, assuming a given request-set mapping \mathbb{M}_i , we find the release time and service time ($\text{rel}_{i,k}$ and $\text{srv}_{i,k}$), for all the corresponding requests with the objective of maximizing the cumulative delay of all these requests.

Determining the values of the release and service times given a request-set mapping is, however, complicated by the constraints imposed on these variables, such as:

1. Single outstanding request assumption – For all requests $\text{req}_{i,k}$, we have $\text{rel}_{i,k} > \text{srv}_{i,k-1}$ and
2. Slot availability constraint – A request $\text{req}_{i,k}$ will be served no later than the latest time instant at which its assigned free bus slot can be available or formally $\text{srv}_{i,k} \leq T_i^{\max}(\sigma_i(k))$.

The proposed mechanism to handle these constraints and find the cumulative delay is discussed in detail in Section 4.4. The focus of Step 2 is how to compute the maximum cumulative delay for a *given mapping* and the next step in the analysis ventures into proposing a technique to arrive at a mapping (among several mappings) for which the maximum cumulative delay is the largest among the maximum cumulative delays computed for all feasible mappings.

Step 3: Finding the worst-case request-set mapping

In this step, we propose an algorithm (in Section 4.5) to determine a request-set mapping \mathbb{M}_i for task τ_i that maximizes the cumulative delay of all its $\eta_{(i)}$ requests. To do so, our technique first computes an upper bound, UBslot_i , on the number of free bus slots that can possibly be used by task τ_i . This upper bound gives us a range $[1, \text{UBslot}_i]$ of free bus slots within which all the requests of the analyzed task τ_i will be served. Note that the number of slots, UBslot_i may be much greater than the number of requests to be served. In that case, a naive approach to maximize the cumulative delay incurred by the requests of τ_i is to apply a brute force approach, i.e. all the request-set mappings are explored and a maximum cumulative delay is computed for each of them by using the method proposed in Step 2; At the end, only the largest cumulative delay (amongst all the mappings) is returned. However, such a method does not scale and is computationally inefficient due to the exhaustive exploration of all the possible mappings. Therefore, we reduce the complexity of the problem by eliminating, at an early stage of the analysis, the request-set mappings that cannot possibly lead to the worst-case delays. This improvement substantially reduces the time-complexity of the proposed solution.

Step 4: Tightening the analysis using sampling regions

Having shown how to determine the worst request-set mapping in Step 3, and bounding the maximum cumulative delay for that mapping using the technique explained in Step 2, there is further scope of tightening the analysis by exploiting the information about the maximum number of requests in each of the constituent regions of the analyzed task. The region based analysis helps us to limit the range of the potential free bus slots for a set of requests. For example, if the k 'th request of τ_i is generated in the g 'th region, then it *cannot* be served in the j 'th free bus slot of τ_i if $T_i^{\max}(j) < L_i^{\text{reg-size}} \times (g - 1)$, where $L_i^{\text{reg-size}}$ is the size of the sampling interval. From these constraints, we define a range

$[\text{LBslot}_{i,g}, \text{UBslot}_{i,g}]$ for each region g , which represent the first and last free bus slots in which requests from region g can be served, respectively. These bounds are employed by the proposed algorithm to tighten the analysis by defining a request-set mapping for each individual region. The maximum delays incurred by the requests of each region are computed successively and the overall WCET is subsequently computed. This process is described in detail in Section 4.6.

4.3 Step 1: Modeling the Availability of the Bus

The front side bus is a shared resource, which means that any access to it by a given task may be deferred because of concurrent accesses from other tasks. To estimate the overall delay that can be incurred by a task due to the contention for the shared resource, a basic approach could be that we first derive an upper bound on the delay that a *single* access may incur. This upper bound is computed by constructing a worst-case scenario, in which every competing task gathers all its accesses to the resource within the shortest possible time window, thereby creating a burst of accesses all concentrated in time and occurring exactly when the access from the analyzed task occurs, thereby inducing the maximum delay for this access. Then, the overall delay that a *sequence* of accesses may suffer is computed by assuming that each access to the shared bus incurs this precomputed maximum delay. This assumption is clearly not valid, since the other tasks keep progressing in their execution, alternating between computation and memory fetch phases, and do not congest the front side bus at all times.

We propose an alternative approach which bases its computation on a new modeling framework. Instead of computing a worst-case scenario for a single access to the shared bus and then considering that scenario for each and every request of the analyzed task, we model the overall availability of the bus to the analyzed task. Then, as the next step we leverage this new model to derive an upper bound on the *cumulative* delay that a *sequence* of requests may incur.

Our model captures the best-case and worst-case availability of the shared bus. It is based on the arbiter and coarse-grained memory access information provided by the task cache profiles. Specifically, for a given task τ_i under analysis and any positive integer j , we compute two functions $T_i^{\min}(j)$ and $T_i^{\max}(j)$ that give the *earliest* and *latest* instants at which the bus can be available to τ_i for the j 'th time, i.e. the *earliest* and *latest* instants of the j 'th free bus slot of τ_i .

If τ_i is run in isolation, there are no competing requests for the bus, which implies that the bus is always available to τ_i and we have $T_i^{\min}(j) = T_i^{\max}(j) = j$. Otherwise, we will have $T_i^{\min}(j) < T_i^{\max}(j)$. These two functions form what we call the *bus availability model* $\mathbb{B}_i = \langle T_i^{\min}(), T_i^{\max}() \rangle$ of task τ_i . This model can be computed for any predictable resource and a wide range of arbitration policies. Next, we demonstrate the computation of this bus

model for two distinct cases: a non-work-conserving TDM arbiter and a work-conserving fixed-priority arbiter.

4.3.1 Bus Availability Model: Non-Work-Conserving TDM Arbitration

A TDM arbiter works by periodically repeating a schedule, or frame, with fixed size, f . Each core π_p is allocated a number of slots ϕ_p in the frame at design time, such that $\sum_{\pi_p} \phi_p \leq f$. There are different policies for distributing the slots allocated to a core within the TDM frame, but here we consider the case where slots are assigned contiguously for simplicity. An example of a TDM frame, a contiguous allocation, and some of the associated terminology is illustrated in Figure 4.5.

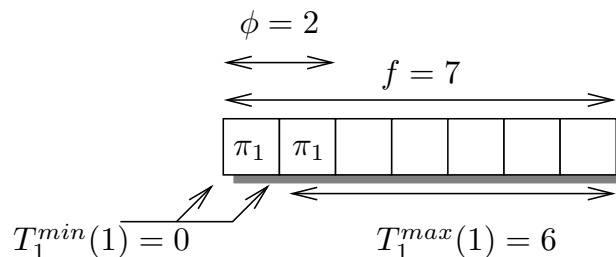


Figure 4.5: TDM frame with 7 slots using a contiguous slot allocation per core.

We consider a non-work-conserving instance of the TDM arbiter, which means that requests from a core are only scheduled during bus slots allocated to that core. Empty slots or slots allocated to other cores without pending requests are hence not utilized. This type of policy makes the timing behavior of memory requests of tasks scheduled on different cores completely independent. As a result, only the configuration of the arbiter has to be considered when determining $T^{\min}()$ and $T^{\max}()$. For non-work-conserving TDM arbitration with a contiguous slot allocation, $T^{\min}()$ and $T^{\max}()$, for task τ_i assigned to core π_p are derived according to Equations (4.1) and (4.2), respectively.

$$T_i^{\min}(j) = \left(\left\lfloor \frac{j-1}{\phi_p} \right\rfloor \times f + ((j-1) \bmod \phi_p) \right) \times \text{TR} \quad (4.1)$$

$$T_i^{\max}(j) = T_i^{\min}(j) + (f - \phi_p + 1) \times \text{TR} \quad (4.2)$$

The first term in the computation of $T^{\min}()$ in Equation (4.1) corresponds to the minimum required number of full iterations of the TDM frame to serve j requests and the second term corresponds to the remaining number of required slots after these iterations. The computation of $T^{\max}()$ is similar, except that it adds an additional $f - \phi_p + 1$ slots to account for releases with maximum misalignment with respect to the set of contiguous slots allocated to the core in the TDM frame. Note that these equations also cover non-work-conserving round-robin arbitration, which is a special case of TDM where f equals the number of cores sharing the bus, m , and $\forall \tau_i \phi_p = 1$. Work-conserving versions of

both these arbitration policies can be derived by additionally considering the task cache profiles, although this is omitted for brevity. Figure 4.5 graphically illustrates the arrival times and waiting times corresponding to $T_1^{\min}(1)$ and $T_1^{\max}(1)$. As seen in the figure, the $T_1^{\min}(1) = 0$, is achieved for a request that arrives just at the beginning of any of the two slots allocated to its corresponding core and $T_1^{\max}(1) = 6$ for a request arriving just after the last slot allocated to its core has been left idle. For this particular arbitration policy, the best-case and worst-case arrival with respect to the TDM frame is the same for any value of j , although this does not hold in general.

4.3.2 Bus Availability Model: Work-Conserving Fixed-Priority Arbitration

In the context of bus arbitration policies, one of the challenges with currently existing COTS-based multi-core systems is that the front-side bus does not recognize/respect task priorities. This is because the bus is generally designed with the aim of enhancing the average-case performance and is not tailored for real-time systems. This can lead to a scenario similar to priority inversion in which requests from higher priority tasks are delayed by requests from lower-priority tasks on the bus. Although the scheduler enforces these priorities while allocating the processing element (CPU) to tasks, these priorities are not passed over to the shared hardware resources like the bus and the memory controllers, which have their own scheduling policies. This problem has been addressed in research by enabling priorities in priority-driven arbiters to be software programmable directly [112] or indirectly by tagging each request with its priority [101]. We assume in this section that the bus is designed according to any of these strategies. Based on this, we design a bus-availability model for a fixed-priority arbiter.

4.3.2.1 Introducing functions $\text{PCR}_q^{\min}(t)$ and $\text{PCR}_q^{\max}(t)$

Assume that the analyzed task τ_i is scheduled on core π_p . In spite of the uncertainty of the arrival patterns of the requests, it is important to determine a lower and upper bound on the cumulative number of requests that tasks of a higher priority than the analyzed task τ_i and scheduled on cores $\pi_q \neq \pi_p$ may inject into the bus. These bounds are denoted by the $\text{PCR}_q^{\min}(i, t)$ and $\text{PCR}_q^{\max}(i, t)$ functions. Such bounds can be computed as described in the previous chapter.

4.3.2.2 Computation of $T_i^{\min}(j)$ and $T_i^{\max}(j)$

The $T_i^{\min}(j)$ and $T_i^{\max}(j)$ curves represent the earliest and the latest time at which a j^{th} free bus slot is available to requests of task τ_i assigned to core π_p . When run in isolation, in the absence of any competing requests for the bus, the bus is always available to τ_i and the $T_i^{\min}(j)$ and $T_i^{\max}(j)$ curves merge. Then, the number of interfering requests issued from core $\pi_q \neq \pi_p$, can vary between $\text{PCR}_q^{\min}(i, t)$ and $\text{PCR}_q^{\max}(i, t)$ in a time interval

of duration t . With this information, we derive the corresponding earliest and the latest times at which free slots are available to the analyzed task τ_i assigned to core π_p . As stated earlier, TR is an upper bound on the time to access the memory over the shared front side bus and each bus slot is of duration TR. Then, we compute $T_i^{\min}(j)$ and $T_i^{\max}(j)$ as:

$$T_i^{\min}(j) = \min_{t \geq 0} \{t | t - (\sum_{\pi_q \neq \pi_p} \text{PCR}P_q^{\min}(i, t) \times \text{TR}) = j \times \text{TR}\} \quad (4.3)$$

$$T_i^{\max}(j) = \min_{t \geq 0} \{t | t - (\sum_{\pi_q \neq \pi_p} \text{PCR}P_q^{\max}(i, t) \times \text{TR}) = j \times \text{TR}\} \quad (4.4)$$

From the perspective of the analyzed task τ_i executing on core π_p , the bus can be viewed as resource with two alternating phases: a busy phase, in which it serves the requests from the other cores and an idle phase which task τ_i may avail. Equation (4.4) can be interpreted as follows: Scan the timeline to identify the earliest time instant at which the (continuous stream of) requests from the other cores ($\neq \pi_p$) have been served and j free slots have been detected. When the j^{th} slot is free, the time t will exceed the time for servicing the request (given by the summation term $(\sum_{\pi_q \neq \pi_p} \text{PCR}P_q^{\max}(i, t) \times \text{TR}))$ by $j \times \text{TR}$.

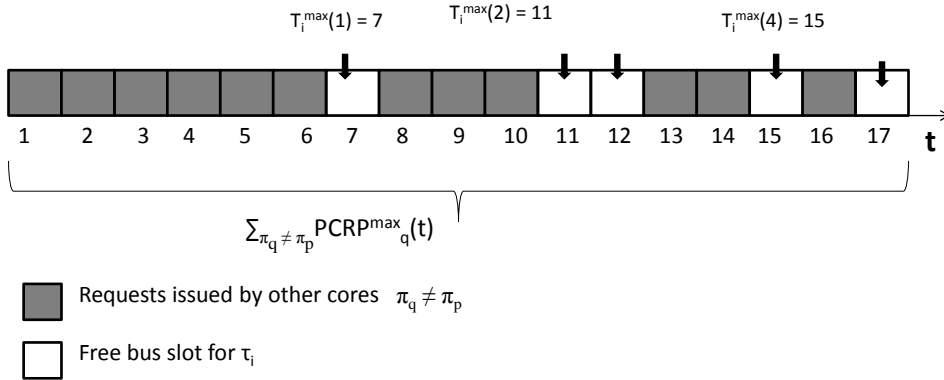


Figure 4.6: Illustration of computation of $T_i^{\max}(j)$. Time is expressed in units of TR. Task τ_i is assigned to core π_p .

Example 1. We illustrate the method of computing $T_i^{\max}(j)$ with the example illustrated in Figure 4.6. The figure represents the cumulative number of requests $\sum_{\pi_q \neq \pi_p} \text{PCR}P_q^{\max}(i, t)$ issued by the other other cores in a period of time t . To clarify $\sum_{\pi_q \neq \pi_p} \text{PCR}P_q(1) = 1$, $\sum_{\pi_q \neq \pi_p} \text{PCR}P_q(8) = 7$, $\sum_{\pi_q \neq \pi_p} \text{PCR}P_q(13) = 10$ and so on. Let us compute $T_i^{\max}(4)$ in this case. The latest time at which the fourth free bus slot is available to task τ_i is the first instance, when the time t exceeds the total number of requests issued by the other cores in time t by 4. This happens in the example at time 15 where the cumulative requests at time 15 is 11. And hence $T_i^{\max}(4) = 15$.

As seen in this section, the $T_i^{\min}(j)$ and $T_i^{\max}(j)$ functions are arbitration dependent and can be computed for different arbiters (TDM, round-robin, fixed-priority and FIFO

(omitted here)). They serve as an input to the next blocks of the proposed framework that compute the increased execution time based on the model. In contrast, the methods described in the following sections are independent of the arbitration mechanism.

4.4 Step 2: Find the maximum cumulative delay for a given request-set mapping

In this section, we first describe a method to compute the maximum waiting time, given a single request, a free bus slot assignment to that request and the bus availability model. The same rationale is then extended to compute the cumulative waiting time for a sequence of requests of a given task in conformance to certain constraints. For a given request-to-slot assignment, the key idea to maximize the waiting time of that request is to release it as early as possible and delay its servicing to the latest possible time. In other words, for the given free bus slot $\sigma_i(k)$ we need to determine a *lower* bound on the release time of request $\text{req}_{i,k}$, an *upper* bound on its service time of a request for the given slot and then compute the resulting maximum waiting time. A set of lemmas are provided below as foundations to this central theme.

Property 2. *By construction, $T_i^{\max}(1)$ is the longest waiting time for one request before it can be assigned a free bus slot.*

In order to compute $T_i^{\max}(1)$, the maximum traffic that all the potentially competing tasks can generate in order to fully occupy the system bus is computed (recall the task packing algorithm). For non-fair bus arbitration schemes, this means that the first request of the analyzed task may be served after all pending requests from other tasks. The subsequent requests of the analyzed task may incur an equal or lesser waiting time than that incurred by the first request. In this respect, $T_i^{\max}(1)$ represents the longest waiting time for a given request.

4.4.1 Maximum delay for a single request-to-slot assignment

We now proceed in Lemmas 1 and 2 by lower bounding the release time of a request and upper bounding the service time to enable the computation of its maximum delay.

Lemma 1 (A lower bound on the release time of a request). *For any task $\tau_i \in \tau$ and for all $k > 1$, let $\text{req}_{i,k-1}$ and $\text{req}_{i,k}$ be two consecutive requests generated by τ_i . For a given request-to-slot assignment $\sigma_i(k-1)$ and $\sigma_i(k)$, if request $\text{req}_{i,k-1}$ has been served at time $\text{srv}_{i,k-1}$ in the $\sigma_i(k-1)$ 'th free bus slot then it holds that*

$$\text{rel}_{i,k} \geq \max(T_i^{\min}(\sigma_i(k) - 1) + 1, \text{srv}_{i,k-1} + (\sigma_i(k) - \sigma_i(k-1)) * \text{TR}) \quad (4.5)$$

Proof. The lemma is based on two simple observations:

1. The earliest time of releasing a request is in the scenario when it is released *immediately* after the earliest time instant at which the bus can be free for the $(\sigma_i(k) - 1)$ 'th time. Otherwise the request would have been served in the previous available free slot, $(\sigma_i(k) - 1)$. Formally, $\text{rel}_{i,k} \geq T_i^{\min}(\sigma_i(k) - 1) + 1$, and more importantly,
2. A request can only be released after the previous request is served i.e. $\text{rel}_{i,k} \geq \text{srv}_{i,k-1}$.

In addition, for it to be served in slot $\sigma_i(k)$, all the intermediate slots between the slot occupied by the previous request must be occupied and not available to τ_i . This gets us to the term $\text{rel}_{i,k} \geq \text{srv}_{i,k-1} + (\sigma_i(k) - \sigma_i(k-1)) * \text{TR}$. In order to satisfy both conditions, the maximum of the resulting values is considered. \square

Lemma 2 (An upper bound on the service time of a request). *For any task $\tau_i \in \tau$ and for all $k > 1$, if request $\text{req}_{i,k}$ is served at time $\text{srv}_{i,k}$ in the $\sigma_i(k)$ 'th free bus slot then it holds that*

$$\text{srv}_{i,k} \leq \min(T_i^{\max}(\sigma_i(k)), \text{rel}_{i,k} + T_i^{\max}(1)) \quad (4.6)$$

Proof. The latest time at which a request $\text{req}_{i,k}$ assigned to slot $\sigma_i(k)$ is served is $T_i^{\max}(\sigma_i(k))$ (by definition). Since $T_i^{\max}(1)$ denotes the maximum delay that a request may suffer, the value of $\text{srv}_{i,k}$ should not be greater than $\text{rel}_{i,k} + T_i^{\max}(1)$. Equation (4.6) upholds these two conditions by considering the minimum of the respective values. \square

The maximum delay for servicing the given request k in slot $\sigma_i(k)$ is then given by $\text{srv}_{i,k} - \text{rel}_{i,k}$.

4.5 Step 3: Finding the worst-case assignment

4.5.1 Maximum cumulative delay for a request-set mapping

In the previous section, we established a method to compute an upper bound on the delay of a single request and a given slot assignment for that request. Now, we extend this result to maximize the cumulative delay of a *sequence* of requests, given a request-set mapping $\mathbb{M}_i = \{\sigma_i(1), \dots, \sigma_i(\eta_{(i)})\}$. To maximize the cumulative delay for the mapping \mathbb{M}_i , we compute the individual maximum delay for each request by applying the lemmas described in Section 4.4.1. Since the release time (and thus the delay) of a given request $\text{req}_{i,k}$ is dependent on the service time $\text{srv}_{i,k-1}$ of the previous one (see Equation (4.5)), we start by computing the maximum delay of the first request $\text{req}_{i,1}$ and iterate up to request $\text{req}_{i,\eta_{(i)}}$. We show in Lemma 3 that this iterative process leads to a worst-case delay.

Lemma 3 (Worst-case cumulative delay). *Let $\mathbb{M}_i = \{\sigma_i(1), \dots, \sigma_i(\eta_{(i)})\}$ refer to a request-set mapping for the $\eta_{(i)}$ requests of task τ_i . Let $D_i(k)$ be the maximum cumulative delay for the first k requests $\{\text{req}_{i,1}, \text{req}_{i,2}, \dots, \text{req}_{i,k}\}$, given this mapping \mathbb{M}_i and $\Delta_k = (\sigma_i(k) -$*

$\sigma_i(k-1)) * \text{TR}$. Then the delay, $D_i(\eta(i)) = \sum_{k=1}^{\eta(i)} \text{srv}_{i,k} - \text{rel}_{i,k}$ of all these requests is maximized for:

$$\text{rel}_{i,k} = \begin{cases} T_i^{\min}(\sigma_i(k) - 1) + 1 & \text{if } k = 1 \\ \max(T_i^{\min}(\sigma_i(k) - 1) + 1, \text{srv}_{i,k-1} + \Delta_k) & \text{otherwise} \end{cases} \quad (4.7)$$

$$\text{srv}_{i,k} = \min(T_i^{\max}(\sigma_i(k)), \text{rel}_{i,k} + T_i^{\max}(1)) \quad (4.8)$$

Proof. We prove the lemma by induction. First, we show in the basic step that the claim is true considering only the first request $\text{req}_{i,1}$ and its slot assignment $\sigma_i(1)$. That is, we show that the release and service times given by Equations 4.7 and 4.8 result in a maximum cumulative delay $D_i(1) = \text{srv}_{i,1} - \text{rel}_{i,1}$. Then, in the inductive step, we show that if the claim is true considering the set of the first k requests, $k \geq 1$ (induction hypothesis), then the property holds for the first $(k+1)$ requests as well. In other words, assuming that Equations 4.7 and 4.8 assign a release and service time to the k first requests that result in a maximum cumulative delay $D_i(k)$, then the same equations provide a maximum cumulative delay $D_i(k+1)$ when applied to the first $(k+1)$ requests. Both the basic and inductive steps are proven by showing that any other choice of release and service time, for any of the requests in the considered set of requests, results in a lower cumulative delay. In order to ease the reading of the proof, we shall make use of Figure 4.7 which depicts different cases, as well as the notations used in the proof.

Basic step. By considering only the first request $\text{req}_{i,1}$, it is easy to see that any release time $\text{rel}_{i,1}$ different from that given by Equation 4.7 leads to $\text{rel}_{i,1} > T_i^{\min}(\sigma_i(1) - 1) + 1$. This follows from the fact that having $\text{rel}_{i,1} < T_i^{\min}(\sigma_i(1) - 1) + 1$ is not possible, as shown in Lemma 1. Besides, choosing any other release time $\text{rel}_{i,1} > T_i^{\min}(\sigma_i(1) - 1) + 1$ would have as sole impact, a decrease in the difference $(\text{srv}_{i,1} - \text{rel}_{i,1})$, and subsequently a lower delay $D_i(1)$ incurred by request $\text{req}_{i,1}$. In short, since $T_i^{\min}(\sigma_i(1) - 1) + 1$ is a lower bound on the release time of request $\text{req}_{i,1}$ (from Lemma 1), choosing $\text{rel}_{i,1} = T_i^{\min}(\sigma_i(1) - 1) + 1$ is the best choice to guarantee a maximum delay for the first request. Similarly, since $\min(T_i^{\max}(\sigma_i(k)), \text{rel}_{i,k} + T_i^{\max}(k))$ was shown to be an upper bound on the service time of request $\text{req}_{i,k}$, $\forall k$ (see Lemma 2), it is easy to see that the choice of $\text{srv}_{i,1}$ by Equation (4.8) also guarantees a maximum delay for this first request.

In conclusion, we showed that $D_i(1) = \text{srv}_{i,1} - \text{rel}_{i,1}$ is maximum when $\text{rel}_{i,1}$ and $\text{srv}_{i,1}$ are given by the equations of Lemma 3.

Inductive step. Assuming that Equations 4.7 and 4.8 define a release and a service time for the first k requests of τ_i such that their cumulative delay $D_i(k)$ is maximized, we will show that defining $\text{rel}_{i,k+1}$ and $\text{srv}_{i,k+1}$ using the equations of Lemma 3 maximizes $D_i(k+1)$. By applying the same reasoning as in the basic step, it is evident that choosing

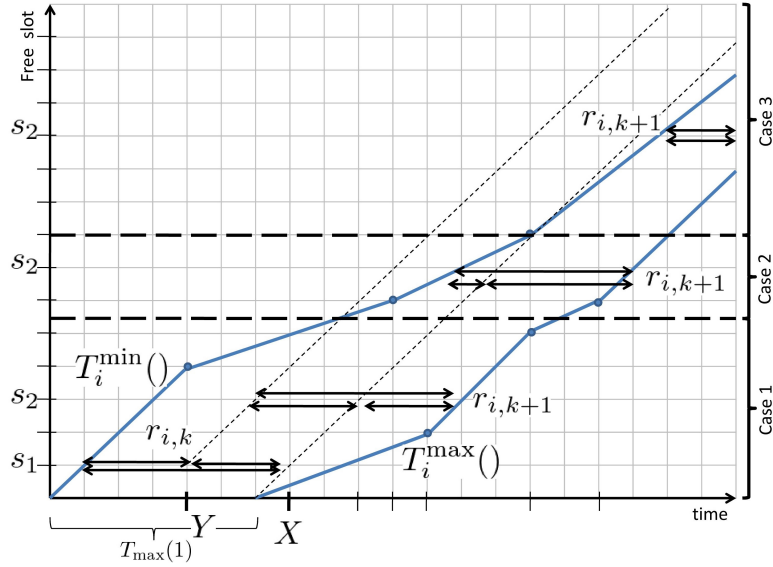


Figure 4.7: Illustration of the three cases 1, 2 and 3 of Lemma 3.

any other value of $rel_{i,k+1}$ greater than its lower bound (given in Lemma 1 and Eq. (4.7)) and/or any other service time $srv_{i,k+1}$ lower than its upper bound (given in Lemma 2 and Equation (4.8)) induces a lower delay for request $req_{i,k+1}$, and thus a lower cumulative delay $D_i(k+1)$.

However, it may be noted from the release-time equation (Eq. 4.7) that the choice of service time $srv_{i,k}$ of the previous request $req_{i,k}$ influences the lower bound on $rel_{i,k+1}$, and subsequently an upper bound on $srv_{i,k+1}$ (see Equation (4.8)). One should therefore investigate the following question: although choosing $srv_{i,k} = \min(T_i^{\max}(\sigma_i(k)), rel_{i,k} + T_i^{\max}(1))$ guarantees a maximum cumulative delay $D_i(k)$ for the first k requests (from the induction hypothesis), doing so might define a range of possible values for $rel_{i,k+1}$ that discards those leading to a maximum cumulative delay $D_i(k+1)$. The remainder of this proof consists in showing that any value of $srv_{i,k}$ different from that given by Equation (4.8) results in a lower cumulative delay $D_i(k+1)$.

To figure out how $srv_{i,k}$ affects the range of possible values for $rel_{i,k+1}$ and $srv_{i,k+1}$, let us consider different values X and Y for $srv_{i,k}$, where $X = \min(T_i^{\max}(\sigma_i(k)), rel_{i,k} + T_i^{\max}(1))$ (as given by Expression (4.8)) and Y is any positive number $< X$. An example of X and Y is depicted in Figure 4.7 (note that in this example, we have $X = rel_{i,k} + T_i^{\max}(1)$). We show in the following that $D_i(k+1)$ is always maximum for $srv_{i,k} = X$.

We first introduce two notations for compaction and readability: Δ_{k+1} and Q_1 . Let $\Delta_{k+1} = (\sigma_i(k+1) - \sigma_i(k)) * TR$ and $Q_1 = T_i^{\min}(\sigma_i(k+1) - 1) + 1$. We know from Lemma 1, $rel_{i,k+1} \geq \max(T_i^{\min}(\sigma_i(k+1) - 1) + 1, srv_{i,k} + \Delta_{k+1})$ and thus three cases may arise depending the bus-slot assignment $\sigma_i(k+1)$ of request $req_{i,k+1}$:

1. $Q_1 \leq Y + \Delta_{k+1} < X + \Delta_{k+1}$

$$2. Y + \Delta_{k+1} < Q_1 \leq X + \Delta_{k+1}$$

$$3. Y + \Delta_{k+1} \leq X + \Delta_{k+1} \leq Q_1$$

Case 1. $Q_1 \leq Y + \Delta_{k+1} < X + \Delta_{k+1}$

In this case, choosing $\text{srv}_{i,k} = Y$ leads to $\text{rel}_{i,k+1} \geq Y + \Delta_{k+1}$ (from Lemma 1). By setting $\text{rel}_{i,k+1}$ to $Y + \Delta_{k+1}$, we get

$$\begin{aligned} D_i(k+1) &= \sum_{\ell=1}^{k+1} (\text{srv}_{i,\ell} - \text{rel}_{i,\ell}) \\ &= \sum_{\ell=1}^{k-1} (\text{srv}_{i,\ell} - \text{rel}_{i,\ell}) + (\text{srv}_{i,k} - \text{rel}_{i,k}) + (\text{srv}_{i,k+1} - \text{rel}_{i,k+1}) \\ &= \sum_{\ell=1}^{k-1} (\text{srv}_{i,\ell} - \text{rel}_{i,\ell}) + Y - \text{rel}_{i,k} + \text{srv}_{i,k+1} - (Y + \Delta_{k+1}) \\ &= \sum_{\ell=1}^{k-1} (\text{srv}_{i,\ell} - \text{rel}_{i,\ell}) + \text{srv}_{i,k+1} - \text{rel}_{i,k} - \Delta_{k+1} \end{aligned} \quad (4.9)$$

On the other hand, choosing $\text{srv}_{i,k} = X$ leads to $\text{rel}_{i,k+1} \geq X + \Delta_k$ (from Lemma 1). If we choose $\text{rel}_{i,k+1} = X + \Delta_{k+1}$ (i.e., the earliest possible release time) then applying the same reasoning as above leads to the same equality, i.e.,

$$D_i(k+1) = \sum_{\ell=1}^{k-1} (\text{srv}_{i,\ell} - \text{rel}_{i,\ell}) + \text{srv}_{i,k+1} - \text{rel}_{i,k} - \Delta_{k+1} \quad (4.10)$$

Since (4.9) = (4.10), we can claim that choosing $\text{srv}_{i,k} = X$ leads to a worst-case cumulative delay $D_i(k+1)$.

Case 2. $Y + \Delta_{k+1} < Q_1 \leq X + \Delta_{k+1}$

In this case, choosing $\text{srv}_{i,k} = Y$ leads to $\text{rel}_{i,k+1} \geq T^{\min}(\sigma_i(k+1) - 1)$ (from Lemma 1). Let $\text{rel}_{i,k+1} = T_i^{\min}(\sigma_i(k+1) - 1)$ (i.e., the earliest possible release time-instant), from a reasoning similar to that above it holds that

$$\begin{aligned} D_i(k+1) &= \sum_{\ell=1}^{k+1} (\text{srv}_{i,\ell} - \text{rel}_{i,\ell}) \\ &= \sum_{\ell=1}^{k-1} (\text{srv}_{i,\ell} - \text{rel}_{i,\ell}) + Y - \text{rel}_{i,k} + \text{srv}_{i,k+1} - Q_1 \\ &< \sum_{\ell=1}^{k-1} (\text{srv}_{i,\ell} - \text{rel}_{i,\ell}) + Y - \text{rel}_{i,k} + \text{srv}_{i,k+1} - (Y + \Delta_{k+1}) \\ &< \sum_{\ell=1}^{k-1} (\text{srv}_{i,\ell} - \text{rel}_{i,\ell}) - \text{rel}_{i,k} + \text{srv}_{i,k+1} - \Delta_{k+1} \end{aligned} \quad (4.11)$$

On the other hand, choosing $\text{srv}_{i,k} = X$ leads to $\text{rel}_{i,k+1} \geq X + \Delta_{k+1}$ (from Lemma 1). If $\text{rel}_{i,k+1} = X + \Delta_{k+1}$, then the cumulative delay $D_i(k+1)$ of requests $\text{req}_1, \text{req}_2, \dots, \text{req}_{k+1}$ is given by

$$\begin{aligned}
D_i(k+1) &= \sum_{\ell=1}^{k+1} (\text{srv}_{i,\ell} - \text{rel}_{i,\ell}) \\
&= \sum_{\ell=1}^{k-1} (\text{srv}_{i,\ell} - \text{rel}_{i,\ell}) + X - \text{rel}_{i,k} + \text{srv}_{i,k+1} - Q_1 \\
&\geq \sum_{\ell=1}^{k-1} (\text{srv}_{i,\ell} - \text{rel}_{i,\ell}) + X - \text{rel}_{i,k} + \text{srv}_{i,k+1} - (X + \Delta_{k+1}) \\
&\geq \sum_{\ell=1}^{k-1} (\text{srv}_{i,\ell} - \text{rel}_{i,\ell}) + X - \text{rel}_{i,k} + \text{srv}_{i,k+1} - \Delta_{k+1}
\end{aligned} \tag{4.12}$$

Since (4.12) > (4.11), we can conclude that the cumulative delay is higher for $\text{srv}_{i,k} = X$.

Case 3. $Y + \Delta_{k+1} \leq X + \Delta_{k+1} \leq Q_1$

In this case, choosing either $\text{srv}_{i,k} = Y$ or $\text{srv}_{i,k} = X$ leads to $\text{rel}_{i,k+1} \geq T_i^{\min}(\text{srv}_{i,k+1} - 1)$ (from Lemma 1). Therefore, the range of possible values for $\text{rel}_{i,k+1}$ is not affected by the choice of $\text{srv}_{i,k}$ and the maximum cumulative delay is obviously obtained for $\text{srv}_{i,k} = X$.

□

With Lemma 3, we established that the maximum cumulative delay of a request-set mapping can be computing in an iterative manner. Next, we formulate a method to *select* such a mapping amongst the available candidate mappings. While an obvious brute-force is available, it is computationally expensive and hence the next section proposes a more efficient method.

4.5.2 Algorithm foundations

This section proposes a method to find the request-set mapping among a set of mappings that maximizes the cumulative delay. In order to eliminate unfeasible mappings that will *provably* not contribute to the global maximum, we present two important observations, which eventually forms the basis of the proposed algorithm.

Observation 1. *Let us assume a sequence of k requests $\{\text{req}_{i,1}, \text{req}_{i,2}, \dots, \text{req}_{i,k}\}$ from task τ_i , and a given request-set mapping $\mathbb{M}_i = \{\sigma_i(1), \sigma_i(2), \dots, \sigma_i(k)\}$ for these requests. Let us denote by $D_i(k)$ the maximum cumulative delay for these k requests (computed using Lemma 3). Now, suppose that we extend the sequence with an extra request with index $(k+1)$ assigned to slot h , i.e. $\sigma_i(k+1) = h$ such that $h > \sigma_i(k)$. The maximum cumulative delay $D_i(k+1)$ for the $k+1$ requests can be obtained by simply adding to $D_i(k)$*

the maximum delay for that last request $\text{req}_{i,k+1}$. This maximum delay can be obtained using Lemma 3 by assuming only the service time of the k^{th} request that was obtained during the computation of $D_i(k)$.

Observation 2. *If a sequence of $(k + 1)$ requests are served within a range $[1, h]$ of free bus slots, then the maximum cumulative delay for these $(k + 1)$ requests is the maximum between the largest delay computed by assuming*

- C1. the $(k + 1)$ requests are all served within the range $[1, h]$ of free bus slots, and*
- C2. the first k requests are served within the range slot $[1, h - 1]$ and request $(k + 1)$ is served in slot h .*

Based on these observations, we construct a method to compute $D_i(k)$ from $D_i(k - 1)$, $\forall k$, which ultimately yields $D_i(\eta_{(i)})$. The method is shown in Algorithm 5 and an explanation of its operation is given below. Note that this algorithm is “safe-by-construction” as it computes $D_i(\eta_{(i)})$ by investigating all possible assignments of these $\eta_{(i)}$ requests to free bus slots (only those assignments that are proven unfeasible are discarded).

4.5.3 Algorithm Description

The request-set mappings are captured in a two-dimensional array with $\eta_{(i)}$ rows and UBslot_i columns. The input to the algorithm is the number of requests of the analyzed task τ_i , and an upper bound on the available slots, UBslot_i in which the $\eta_{(i)}$ requests may be served. Note that the variables k and j are used to refer to requests and slots, respectively. Each cell $c(k, j)$ of this array holds a list of tuples $e_{k,j} = \langle D_i(k), \sigma_i(k), \text{srv}_{i,k} \rangle$, where each tuple $e_{k,j}$ in that list reflects a feasible assignment of the first k requests to k free bus slots within the range $[1, j]$. The members of this tuple denote:

- the maximum delay $D_i(k)$ that can be obtained with the corresponding assignment,
- the free bus slot in which the k^{th} request has been served to reach that maximum delay $D_i(k)$, i.e. $\sigma_i(k) \in [k, j]$, and
- the corresponding time $\text{srv}_{i,k}$ at which that k^{th} request has been served in that slot.

The algorithm proceeds in a row-wise manner, by assigning the first request $\text{req}_{i,1}$ to all feasible slots and computing the cumulative delays and then proceeding to analyze the second request (next row of the array) and so on. For the first request and first slot, the algorithm computes *the* worst-case delay when the first request is assigned to the first free bus slot (Lines 7, 9, 10, and 11). To do so, it uses Lemma 3 and adds the corresponding tuple $e_{1,1}$ to the list of cell $c(1,1)$, in this case $e_{1,1} = \langle T_i^{\max}(1), 1, T_i^{\max}(1) \rangle$. The list contains only this tuple.

For $k = 1$ and $j > 1$, the algorithm computes *all* the maximum delays by considering every assignment of the first request, $\text{req}_{i,1}$, to free bus slots $\leq j$. First, the list of the

Algorithm 5: MaxRegDelay($\eta_{(i)}$, UBslot $_i$)

```

input :  $\eta_{(i)}$  : number of requests, UBslot $_i$ : last available slot
output:  $D_i(\eta_{(i)})$ : maximum cumulative delay incurred by  $\tau_i$ .
1 Create a 2D array of  $\eta_{(i)}$  rows and UBslot $_i$  columns, where each cell  $c(k, j)$  at row  $k$ 
  and column  $j$  is a list of tuples  $e_{k,j}$  as explained in the description. ;
2 Set every cell of this array to an empty list ;
3 for  $k \leftarrow 1$  to  $\eta_{(i)}$  do
4   for  $j \leftarrow k$  to UBslot $_i - (\eta_{(i)} - k)$  do
5     if  $k = 1$  then
6       if  $j > 1$  then  $c(k, j) \leftarrow c(k, j - 1)$ ;
7        $rel_{i,k} \leftarrow T_i^{\min}(j - 1) + 1$ ;
8       // we assume  $T_i^{\min}(0) = 0$ 
9       if  $rel_{i,k} < C_i$  then
10         $srv_{i,k} \leftarrow \min(T_i^{\max}(j), rel_{i,k} + T_i^{\max}(1))$ ;
11         $D_i(k) \leftarrow srv_{i,k} - rel_{i,k}$  ;
12         $c(k, j).add(\langle D_i(k), j, srv_{i,k} \rangle)$ ;
13      end
14    else
15       $c(k, j) \leftarrow c(k, j - 1)$ ;
16      //  $c(k, j - 1) = \phi$  if  $j = k$ 
17      foreach  $e_{k-1,j-1} \in c(k - 1, j - 1)$  do
18        //  $e_{k-1,j-1} = \langle D_i(k - 1), \sigma_i(k - 1), srv_{i,k-1} \rangle$ 
19         $rel_{i,k} \leftarrow \max(T_i^{\min}(j - 1) + 1, srv_{i,k-1} + (j - \sigma_i(k - 1)) \times TR)$ ;
20        if  $rel_{i,k} < C_i + D_i(k - 1)$  then
21           $srv_{i,k} \leftarrow \min(T_i^{\max}(j), rel_{i,k} + T_i^{\max}(1))$ ;
22           $D_i(k) \leftarrow D_i(k - 1) + srv_{i,k} - rel_{i,k}$  ;
23           $c(k, j).add(\langle D_i(k), j, srv_{i,k} \rangle)$ ;
24        end
25      end
26    end
27  end
28 end
29 return  $\max_{e_{\eta_{(i)}}, UBslot_i \in c(\eta_{(i)}, UBslot_i)} D_i(\eta_{(i)})$  ;

```

current cell $c(1, j)$ is initialized to the list of the previous cell $c(1, j - 1)$ (Line 6), thereby carrying on all the possible worst-case delays that were obtained when this first request was assigned to a previous free bus slot $< j$. Then, the algorithm addresses the case where the first request is assigned to the j 'th bus slot: it makes use of the equations of Lemma 3 to compute $rel_{i,1}$ and $srv_{i,1}$ and appends the corresponding tuple $e_{1,j}$ to the list of cell $c(1, j)$ (lines 7, 9, 10, and 11).

Any two requests belonging to task of length C_i cannot have their release times separated by more than the time C_i . The addition of the "if-statement" at Line 8 filters out a considerable number of unfeasible slot assignments for request $req_{i,1}$, as this condition is violated when j gets larger. It ensures that any partial solution in which the first re-

quest is released after the task has run for C_i time units is immediately discarded, thereby pruning the search space by eliminating all solutions that start with this first erroneous request-to-slot assignment $\sigma_i(1) > C_i$ as soon as they are detected.

When $k > 1$ and $j \geq k$, the algorithm computes *all* worst-case delays that can be obtained when the first k requests of τ_i can be assigned to any free bus slots within $[k, j]$. On Line 14, the algorithm initializes the list of cell $c(k, j)$ to the list of results obtained for the cell $c(k, j - 1)$. Informally, this reflects case C1 above, which states that the worst-case cumulative delay of the first k requests may be found in the set of maximum delays obtained when these k requests are *all* served *before* the j 'th free bus slot. Then on Line 15, the algorithm inspects every maximum delay that has been obtained assuming that the first $k - 1$ requests were served *before* the j 'th free bus slot. For each of these delays $D_i(k - 1)$, assuming that the k 'th request is now served in the j 'th free bus slot, lines 16 and 18 compute the release and service time of that request $\text{req}_{i,k}$ using the equations of Lemma 3, by referring to the corresponding request-to-slot assignment $\sigma_i(k - 1)$ of the $(k - 1)$ 'th request, as well as its service time $\text{srv}_{i,k-1}$ in this free bus slot $\sigma_i(k - 1)$. This reflects case C2 presented above, as it gives a corresponding maximum delay $D_i(k)$ for the first k requests assuming that request $\text{req}_{i,k}$ is assigned to the j^{th} free slot and the previous $k - 1$ requests are served in the earlier bus slots. The filter at Line 17 is similar to the one at Line 8 to filter out a host of infeasible solutions. Here we consider the maximum delay $D_i(k - 1)$ that τ_i may have incurred due to interference with the first $(k - 1)$ requests.

Note that k spans from 1 to $\eta_{(i)}$, while j takes all values within $[k, \text{UBslot}_i - (\eta_{(i)} - k)]$. The reason for limiting the range of j is because the k 'th request of τ_i cannot possibly be served in a free bus slot $\leq k$ (leading to a lower bound $j \geq k$) and the next $(\eta_{(i)} - k)$ requests following $\text{req}_{i,k}$ require at least $(\eta_{(i)} - k)$ slots in order to be served (leading to the upper bound $j \leq \text{UBslot}_i - (\eta_{(i)} - k)$).

4.5.4 Elimination of unfeasible request-set mappings

Given a set of possible request-set mappings, the following lemma provably determines the mappings that cannot possibly lead to the global worst-case delay. By discarding them at an early stage, they are not propagated as the analysis progresses, restricting the number of assignments that must be handled. The purpose of pruning the solution tree in each iteration is to increase the efficiency of the algorithm and improve its scalability with respect to the number of requests and potential free slots.

Lemma 4. *Let $\mathbb{M}_i = \{\sigma_i(1), \dots, \sigma_i(k)\}$ refer to a request-set mapping for the first k requests of task τ_i . Let $D_i(k)$ be the maximum cumulative delay for these k requests considering this assignment \mathbb{M}_i , and let $\text{srv}_{i,k}$ be the absolute time at which the k 'th request is served in a scenario leading to this delay $D_i(k)$. Similarly, let $\mathbb{M}'_i = \{\sigma'_i(1), \dots, \sigma'_i(k)\}$ denote another request-set mapping for the first k requests of task τ_i . Let $D'_i(k)$ be the maximum cumulative delay considering this mapping \mathbb{M}'_i , and let $\text{srv}'_{i,k}$ be the absolute*

time at which the k 'th request is served in a scenario leading to this delay $D'_i(k)$. If it holds that

$$\sigma_i(k) \leq \sigma'_i(k) \quad (4.13)$$

$$\text{and } D_i(k) \leq D'_i(k) \quad (4.14)$$

$$\text{and } \text{srv}_{i,k} + (\sigma'_i(k) - \sigma_i(k)) \times \text{TR} \geq \text{srv}'_{i,k} \quad (4.15)$$

then for all $h > \sigma'_i(k)$, assigning an extra request $\text{req}_{i,k+1}$ to the h 'th free bus slot in both mappings \mathbb{M}_i and \mathbb{M}'_i , i.e., $\sigma_i(k+1) = \sigma'_i(k+1) = h$, leads to

$$\sigma_i(k+1) = \sigma'_i(k+1) \quad (4.16)$$

$$\text{and } D_i(k+1) \leq D'_i(k+1) \quad (4.17)$$

$$\text{and } \text{srv}_{i,k+1} + (\sigma'_i(k+1) - \sigma_i(k+1)) \times \text{TR} \geq \text{srv}'_{i,k+1} \quad (4.18)$$

The vital inference from the above observations is that the maximum cumulative delay for the first $(k+1)$ requests of τ_i is higher, and the service time of the $(k+1)$ 'th request smaller, by using the mapping \mathbb{M}'_i for the first k requests (instead of the mapping \mathbb{M}_i). Note that since Conditions (4.16), (4.17), and (4.18) are the same as (4.13), (4.14), and (4.15), the lemma continues to hold for all the subsequent requests $> k+1$.

Proof. From the claim itself, Equation (4.16) trivially holds (we stated this equality only for completeness, in order to show that the situation after assigning the $(k+1)$ 'th request is same as the situation before assigning it). Let us start the proof by introducing some notations for readability:

$$C_1 = T_i^{\min}(h-1) + 1 \text{ and } C_2 = T_i^{\max}(h)$$

$$\text{and } \Delta_k = (h - \sigma_i(k)) \times \text{TR} \text{ and } \Delta'_k = (h - \sigma'_i(k)) \times \text{TR}$$

According to these notations and from the equations of Lemma 3, the four quantities $\text{srv}_{i,k+1}$, $\text{rel}_{i,k+1}$, $\text{srv}'_{i,k+1}$, and $\text{rel}'_{i,k+1}$ can be re-written as

$$\text{rel}_{i,k+1} = \max(C_1, \text{srv}_{i,k} + \Delta_k) \quad (4.19)$$

$$\text{srv}_{i,k+1} = \min(C_2, \text{rel}_{i,k+1} + T_i^{\max}(1)) \quad (4.20)$$

$$\text{rel}'_{i,k+1} = \max(C_1, \text{srv}'_{i,k} + \Delta'_k) \quad (4.21)$$

$$\text{srv}'_{i,k+1} = \min(C_2, \text{rel}'_{i,k+1} + T_i^{\max}(1)) \quad (4.22)$$

According to (4.15), we have

$$\text{srv}'_{i,k} - \sigma'_i(k) \leq \text{srv}_{i,k} - \sigma_i(k)$$

and thus

$$\text{srv}'_{i,k} + h - \sigma'_i(k) \leq \text{srv}_{i,k} + h - \sigma_i(k)$$

which gives

$$\text{srv}'_{i,k} + \Delta'_k \leq \text{srv}_{i,k} + \Delta_k \quad (4.23)$$

Therefore, regarding Inequalities (4.17) and (4.18), we have three cases to investigate.

- Case 1: $\text{srv}'_{i,k} + \Delta'_k \leq \text{srv}_{i,k} + \Delta_k \leq C_1$.
- Case 2: $\text{srv}'_{i,k} + \Delta'_k \leq C_1 \leq \text{srv}_{i,k} + \Delta_k$.
- Case 3: $C_1 \leq \text{srv}'_{i,k} + \Delta'_k \leq \text{srv}_{i,k} + \Delta_k$.

Case 1: $\text{srv}'_{i,k} + \Delta'_k \leq \text{srv}_{i,k} + \Delta_k \leq C_1$.

In this case, we have from (4.19) and (4.21), $\text{rel}_{i,k+1} = \text{rel}'_{i,k+1} = C_1$ and from (4.20) and (4.22), $\text{srv}_{i,k+1} = \text{srv}'_{i,k+1}$, which satisfies (4.18) since $\sigma_i(k+1) = \sigma'_i(k+1) = h$.

Since $\text{rel}_{i,k+1} = \text{rel}'_{i,k+1}$ and $\text{srv}_{i,k+1} = \text{srv}'_{i,k+1}$, using $D_i(k) \leq D'_i(k)$ from (4.14), we get

$$D_i(k) + \text{srv}_{i,k+1} - \text{rel}_{i,k+1} \leq D'_i(k) + \text{srv}'_{i,k+1} - \text{rel}'_{i,k+1}$$

and then,

$$D_i(k+1) \leq D'_i(k+1)$$

which satisfies (4.17).

Case 2: $\text{srv}'_{i,k} + \Delta'_k \leq C_1 \leq \text{srv}_{i,k} + \Delta_k$.

In this case, we get from (4.19) and (4.21),

$$\text{rel}_{i,k+1} = \text{srv}_{i,k} + \Delta_k \geq \text{rel}'_{i,k+1} = C_1 \quad (4.24)$$

Next, we need to handle the relation between the service times $\text{srv}_{i,k+1}$ and $\text{srv}'_{i,k+1}$ and we have to explore three sub-cases.

- Case 2.1: $\text{rel}'_{i,k+1} + T_i^{\max}(1) \leq \text{rel}_{i,k+1} + T_i^{\max}(1) \leq C_2$.
- Case 2.2: $\text{rel}'_{i,k+1} + T_i^{\max}(1) \leq C_2 \leq \text{rel}_{i,k+1} + T_i^{\max}(1)$.
- Case 2.3: $C_2 \leq \text{rel}'_{i,k+1} + T_i^{\max}(1) \leq \text{rel}_{i,k+1} + T_i^{\max}(1)$.

Case 2.1: $\text{rel}'_{i,k+1} + T_i^{\max}(1) \leq \text{rel}_{i,k+1} + T_i^{\max}(1) \leq C_2$.

From (4.20) and (4.22) we get

$$\text{srv}_{i,k+1} = \text{rel}_{i,k+1} + T_i^{\max}(1) \quad (4.25)$$

$$\text{srv}'_{i,k+1} = \text{rel}'_{i,k+1} + T_i^{\max}(1) \quad (4.26)$$

From (4.24), (4.25) and (4.26), it immediately follows that $\text{srv}_{i,k+1} \geq \text{srv}'_{i,k+1}$, which satisfies (4.18) since $\sigma_i(k+1) = \sigma'_i(k+1) = h$. Also from (4.25) and (4.26), it holds that $\text{srv}_{i,k+1} - \text{rel}_{i,k+1} = T_i^{\max}(1) = \text{srv}'_{i,k+1} - \text{rel}'_{i,k+1}$. Using $D_i(k) \leq D'_i(k)$ from (4.14), we get

$$D_i(k) + T_i^{\max}(1) \leq D'_i(k) + T_i^{\max}(1)$$

and then

$$D_i(k) + \text{srv}_{i,k+1} - \text{rel}_{i,k+1} \leq D'_i(k) + \text{srv}'_{i,k+1} - \text{rel}'_{i,k+1}$$

This implies

$$D_i(k+1) \leq D'_i(k+1)$$

which satisfies (4.17).

Case 2.2: $\text{rel}'_{i,k+1} + T_i^{\max}(1) \leq C_2 \leq \text{rel}_{i,k+1} + T_i^{\max}(1)$.

From (4.20) and (4.22), we get $\text{srv}_{i,k+1} = C_2$ and $\text{srv}'_{i,k+1} = \text{rel}'_{i,k+1} + T_i^{\max}(1)$. We thus get $\text{srv}_{i,k+1} \geq \text{srv}'_{i,k+1}$, which satisfies (4.18) since $\sigma_i(k+1) = \sigma'_i(k+1) = h$. Then, if Inequality (4.17) is *not* satisfied we must have:

$$D_i(k+1) > D'_i(k+1)$$

and thus,

$$D_i(k) + \text{srv}_{i,k+1} - \text{rel}_{i,k+1} > D'_i(k) + \text{srv}'_{i,k+1} - \text{rel}'_{i,k+1}$$

By replacing $\text{srv}_{i,k+1}$ and $\text{srv}'_{i,k+1}$ with their values, we get

$$D_i(k) + C_2 - \text{rel}_{i,k+1} > D'_i(k) + T_i^{\max}(1)$$

and then,

$$D_i(k) > D'_i(k) + T_i^{\max}(1) - (C_2 - \text{rel}_{i,k+1})$$

and since from the case $C_2 - \text{rel}_{i,k+1} \leq T_i^{\max}(1)$, it holds from the above inequality that

$$D_i(k) > D'_i(k)$$

which contradicts (4.14). This contradiction implies that Equation 4.17 is satisfied.

Case 2.3: $C_2 \leq \text{rel}'_{i,k+1} + T_i^{\max}(1) \leq \text{rel}_{i,k+1} + T_i^{\max}(1)$.

From (4.20) and (4.22), we get $\text{srv}_{i,k+1} = \text{srv}'_{i,k+1} = C_2$ and it immediately follows that $\text{srv}_{i,k+1} \geq \text{srv}'_{i,k+1}$, which satisfies (4.18) since $\sigma_i(k+1) = \sigma'_i(k+1) = h$. Then, if Inequality (4.17) is *not* satisfied we must have:

$$D_i(k+1) > D'_i(k+1)$$

and thus,

$$D_i(k) + \text{srv}_{i,k+1} - \text{rel}_{i,k+1} > D'_i(k) + \text{srv}'_{i,k+1} - \text{rel}'_{i,k+1}$$

By replacing $\text{srv}_{i,k+1}$ and $\text{srv}'_{i,k+1}$ with their values, we get

$$D_i(k) + C_2 - \text{rel}_{i,k+1} > D'_i(k) + C_2 - \text{rel}'_{i,k+1}$$

and then,

$$D_i(k) > D'_i(k) + \text{rel}_{i,k+1} - \text{rel}'_{i,k+1}$$

From Equation 4.24, we have $\text{rel}_{i,k+1} \geq \text{rel}'_{i,k+1}$ and it holds from the above inequality that

$$D_i(k) > D'_i(k)$$

which contradicts (4.14). This contradiction implies that Equation 4.17 is satisfied.

Case 3: $C_1 \leq \text{srv}'_{i,k} + \Delta'_k \leq \text{srv}_{i,k} + \Delta_k$. In this case, we get from (4.19) and (4.21), $\text{rel}_{i,k+1} = \text{srv}_{i,k} + \Delta_k$ and $\text{rel}'_{i,k+1} = \text{srv}'_{i,k} + \Delta'_k$ and thus, according to (4.23), it holds that

$$\text{rel}'_{i,k+1} \leq \text{rel}_{i,k+1} \quad (4.27)$$

Again, we need to handle the relation between the service times $\text{srv}_{i,k+1}$ and $\text{srv}'_{i,k+1}$ and we have three sub-cases to explore.

- Case 3.1: $\text{rel}'_{i,k+1} + T_i^{\max}(1) \leq \text{rel}_{i,k+1} + T_i^{\max}(1) \leq C_2$.
- Case 3.2: $\text{rel}'_{i,k+1} + T_i^{\max}(1) \leq C_2 \leq \text{rel}_{i,k+1} + T_i^{\max}(1)$.
- Case 3.3: $C_2 \leq \text{rel}'_{i,k+1} + T_i^{\max}(1) \leq \text{rel}_{i,k+1} + T_i^{\max}(1)$.

Case 3.1: $\text{rel}'_{i,k+1} + T_i^{\max}(1) \leq \text{rel}_{i,k+1} + T_i^{\max}(1) \leq C_2$.

From (4.20) and (4.22), we get

$$\text{srv}_{i,k+1} = \text{rel}_{i,k+1} + T_i^{\max}(1) \quad (4.28)$$

$$\text{srv}'_{i,k+1} = \text{rel}'_{i,k+1} + T_i^{\max}(1) \quad (4.29)$$

From (4.27), (4.28) and (4.29), it immediately follows that $\text{srv}_{i,k+1} \geq \text{srv}'_{i,k+1}$, which satisfies (4.18) since $\sigma_i(k+1) = \sigma'_i(k+1) = h$. Also from (4.28) and (4.29), it holds that $\text{srv}_{i,k+1} - \text{rel}_{i,k+1} = T_i^{\max}(1) = \text{srv}'_{i,k+1} - \text{rel}'_{i,k+1}$. Similar to Case 2.1, using $D_i(k) \leq D'_i(k)$ from (4.14), we get

$$D_i(k) + T_i^{\max}(1) \leq D'_i(k) + T_i^{\max}(1)$$

and then

$$D_i(k) + \text{srv}_{i,k+1} - \text{rel}_{i,k+1} \leq D'_i(k) + \text{srv}'_{i,k+1} - \text{rel}'_{i,k+1}$$

This implies

$$D_i(k+1) \leq D'_i(k+1)$$

which satisfies (4.17).

Case 3.2: $\text{rel}'_{i,k+1} + T_i^{\max}(1) \leq C_2 \leq \text{rel}_{i,k+1} + T_i^{\max}(1)$.

From (4.20) and (4.22) we get $\text{srv}_{i,k+1} = C_2$ and $\text{srv}'_{i,k+1} = \text{rel}'_{i,k+1} + T_i^{\max}(1)$. We thus get $\text{srv}_{i,k+1} \geq \text{srv}'_{i,k+1}$, which satisfies (4.18) since $\sigma_i(k+1) = \sigma'_i(k+1) = h$. Then, if Inequality (4.17) is *not* satisfied we must have:

$$D_i(k+1) > D'_i(k+1)$$

and thus,

$$D_i(k) + \text{srv}_{i,k+1} - \text{rel}_{i,k+1} > D'_i(k) + \text{srv}'_{i,k+1} - \text{rel}'_{i,k+1}$$

By replacing $\text{srv}_{i,k+1}$ and $\text{srv}'_{i,k+1}$ for their values, we get

$$D_i(k) + C_2 - \text{rel}_{i,k+1} > D'_i(k) + T_i^{\max}(1)$$

and then,

$$D_i(k) > D'_i(k) + T_i^{\max}(1) - (C_2 - \text{rel}_{i,k+1})$$

and since from the case $C_2 - \text{rel}_{i,k+1} \leq T_i^{\max}(1)$, it holds from the above inequality that

$$D_i(k) > D'_i(k)$$

which contradicts (4.14). This contradiction implies that Equation 4.17 is satisfied.

Case 3.3: $C_2 \leq \text{rel}'_{i,k+1} + T_i^{\max}(1) \leq \text{rel}_{i,k+1} + T_i^{\max}(1)$.

From (4.20) and (4.22), we get $\text{srv}_{i,k+1} = \text{srv}'_{i,k+1} = C_2$ and it immediately follows that $\text{srv}_{i,k+1} \geq \text{srv}'_{i,k+1}$, which satisfies (4.18) since $\sigma_i(k+1) = \sigma'_i(k+1) = h$. Then, if Inequality (4.17) is *not* satisfied we must have:

$$D_i(k+1) > D'_i(k+1)$$

and thus,

$$D_i(k) + \text{srv}_{i,k+1} - \text{rel}_{i,k+1} > D'_i(k) + \text{srv}'_{i,k+1} - \text{rel}'_{i,k+1}$$

By replacing $\text{srv}_{i,k+1}$ and $\text{srv}'_{i,k+1}$ for their values, we get

$$D_i(k) + C_2 - \text{rel}_{i,k+1} > D'_i(k) + C_2 - \text{rel}'_{i,k+1}$$

and then,

$$D_i(k) > D'_i(k) + \text{rel}_{i,k+1} - \text{rel}'_{i,k+1}$$

From Equation (4.27), we have $\text{rel}_{i,k+1} \geq \text{rel}'_{i,k+1}$ and therefore it holds from the above inequality that

$$D_i(k) > D'_i(k)$$

which contradicts (4.14). This contradiction implies that Equation 4.17 is satisfied. \square

In order to leverage the result of Lemma 4, we can add a function `ListReduce(c(k, j))` at the end of the first inner loop, i.e., “for $j \leftarrow k$ to $\text{UBslot}_i - (\eta_{(i)} - k)$ ” in Algo. 5. This function makes sure that \nexists two distinct tuples $e_{k,j}^1$ and $e_{k,j}^2$ in the list of $c(k, j)$ such that

$$\begin{aligned} \sigma_i(k)^1 &\leq \sigma_i(k)^2 \\ D_i(k)^1 &\leq D_i(k)^2 \\ \text{srv}_{i,k}^1 + (\sigma_i(k)^2 - \sigma_i(k)^1) &\geq \text{srv}_{i,k}^2 \end{aligned}$$

Each time such a pair of tuples is found, only the tuple $e_{k,j}^2$ is kept and the tuple $e_{k,j}^1$ is discarded. This is a key addition to the algorithm that *significantly* reduces the number of tuples in $c(k, j)$. We later return to experimentally evaluate the benefits of this elimination in Section 4.8.

4.6 Step 4: Region-Wise Analysis

As seen in Section 4.1.3, we can obtain more information on the distribution of requests by dividing the execution of each task into a sequence of sampling regions. For each region, we can derive a lower and upper bound on the number of requests that can be issued by the task within that region. However Algorithm 5 did not leverage this region-specific information and used only a coarser grain information about the number of requests in the *entire task*, represented by $\eta_{(i)}$. In other words, Algorithm 5 views the input task τ_i as a single region that can issue up to $\eta_{(i)}$ requests. As a consequence, the resulting analysis may lead to a pessimistic upper bound as illustrated in the following example.

Example 2. *As a simple example, consider that a task issues 10 requests and there are 500 potential free slots, such that slots numbered [491 to 500] contribute to the 10 highest delays. Then a single-region based approach will assign all the 10 requests to slots [491 to 500]. Next, assume we break the task into 2 regions and find that there are 7 requests in Region 1 and 3 requests in Region 2. Likewise, we also compute that the first 300 slots are feasibly available for region 1 and the next 200 slots are available for Region 2. It can be seen that the previous mapping will lead to conservative estimates. The resulting analysis can be made tighter with this information of request distributions and slot availability, since with this information, the algorithm will assign the 7 requests to the slots (with the 7 highest delays) from these 300 slots and the 3 requests to 3 slots from 491 to 500.*

Although the exact intervals of the arrivals of these requests are difficult to discern, if it is possible to divide the task into regions and derive an upper bound on the number of

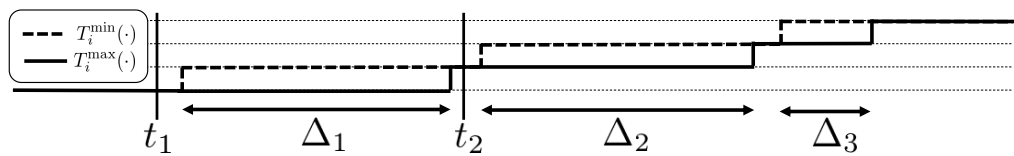


Figure 4.8: Notations used in proof of Lemma 5

requests that can be generated in each region, then likewise we can find an upper bound on the range of slots that can be potentially available to the requests of a given region. In the absence of such demarcations, requests may be assigned to unfeasible slots, leading to pessimistic outcomes.

Thus, the advantage of region-based analysis is two-fold: Firstly, they decrease the computation time by limiting the number of possible candidate slots that must be explored and secondly, they lead to tighter analysis by discarding a considerable amount of infeasible mappings. We proceed by elaborating on the theoretical foundations of region-based analysis, followed by a detailed description of the algorithm.

4.6.1 Theoretical Foundation

When a task is divided into regions and runs in conjunction with other tasks, the time at which each of its regions starts executing depends on the delays incurred by the requests issued in its previous regions. The following lemmas express the relation that exist between the starting time of a region and the maximum delay that it can incur. These properties allow for a fine-tuned WCET analysis in which the distribution of requests across regions is exploited to obtain region-accurate estimates.

Lemma 5. *Consider two execution scenarios of a task τ_i of region g . In the first scenario, region g starts executing at time t_1 , whereas in the second scenario region g starts executing at time t_2 and $t_1 < t_2$. It may happen that the maximum delay that region g can possibly incur in Scenario 1 is higher than the delay incurred in Scenario 2.*

Proof. We prove the claim by using a simple example. Let us consider the functions $T_i^{\min}(\cdot)$ and $T_i^{\max}(\cdot)$ depicted in Figure 4.8 and assume that $\eta_{i,g} = 2$. By starting at time t_2 the maximum delay that region g can incur is given by $\Delta_2 + \Delta_3$ while it can be seen that, by starting at time t_1 , the maximum delay is $\Delta_1 + \Delta_2 > \Delta_2 + \Delta_3$. \square

Lemma 6. *Although Lemma 5 holds and the delay incurred by beginning the execution at time t_1 may be greater than the delay incurred at time t_2 ($> t_1$), the finishing time of region g can never be higher if the task begins to executes at time t_1 . Informally, the extra delay that region g may incur in Scenario 1 by starting earlier does not make up for the difference of starting time between the two scenarios.*

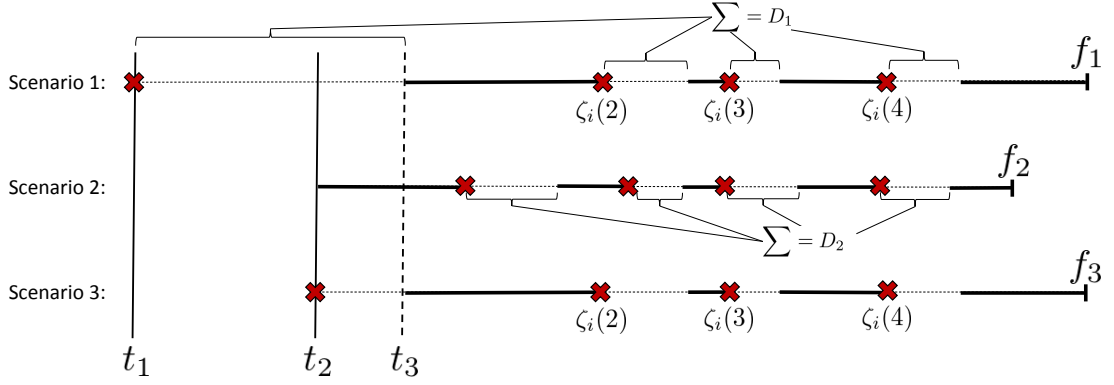


Figure 4.9: Notations used in proof of Lemma 6

Proof. The proof is obtained by contradiction. Let us denote by f_1 and f_2 the finishing time of region g in Scenario 1 and 2, respectively. By contradiction, assume that $f_1 > f_2$. Figure 4.9 illustrates these two scenarios: an “X” represents the release of a request, a continuous line represents the execution of the region, and a dashed line is an interval of time during which the task stalls, waiting for a request to be served. It is assumed in this illustration that region g generates a maximum of $\eta_{i,g} = 4$ requests.

Let D_1 and D_2 denote the *maximum delay* that region g can incur in Scenarios 1 and 2, respectively. There are two cases: if $D_1 \leq D_2$, we have $f_1 = t_1 + L_i^{\text{reg-size}} + D_1$ and $f_2 = t_2 + L_i^{\text{reg-size}} + D_2$ and since $t_1 < t_2$, it holds that $f_1 < f_2$, which contradicts our assumption. Otherwise, if $D_1 > D_2$, suppose that region g incurs the maximum delay of $(t_2 - t_1)$ during the time-interval $[t_1, t_2]$, with a single request generated upon beginning its execution. The delay incurred by this single request can even extend until time $t_3 > t_2$, as depicted in Scenario 1 of Figure 4.9. This scenario can easily be shown to be a worst case (with respect to the finishing time), as it generates the maximum delay with the fewest requests, thereby delaying the actual workload of $L_i^{\text{reg-size}}$ units of execution as much as possible.

Now, let us denote by $\{\sigma_i(2), \dots, \sigma_i(\eta_{i,g})\}$ the request-set mapping of the $(\eta_{i,g} - 1)$ last requests of region g in Scenario 1 (note that, unlike what is depicted on Figure 4.9, the mapping of these requests may be the same as in Scenario 2). We can create a third scenario, in which region g starts its execution at time t_2 (as in Scenario 2) and such that the first request is released upon beginning its execution, thereby incurring the same delay between $[t_2, t_3]$ as in Scenario 1, and all the subsequent requests follow the same free-bus-slot assignment as in Scenario 1, thereby incurring again the same delay as in Scenario 1. In this new Scenario 3, it thus holds that region g starts at time t_2 and finishes at time $f_3 = t_2 + D_3 = f_1 > f_2 = t_2 + D_2$, which contradicts our initial assumption defining D_2 as the maximum delay that region g can incur when starting at time t_2 . \square

To summarize, an important inference from Lemma 6 is that the WCET of a task (considering contention) can be determined by computing the worst-case finishing time f_1

of its first region, and then iterating over the subsequent regions, assuming for each region g , a starting time of f_{g-1} . The WCET of the entire task is then given by the worst-case finishing time of its last region.

4.6.2 Description of the Algorithm for Region-Based Analysis

Algorithm 6: ComputeTaskWCET($\tau_i, T_i^{\min}(\cdot), T_i^{\max}(\cdot)$)

input : $\tau_i, T_i^{\min}(\cdot), T_i^{\max}(\cdot)$
output: WCET of τ_i (considering contention)

- 1 $w_i = \frac{C_i}{L_i^{\text{reg-size}}}; C'_i \leftarrow 0;$
- 2 **for** region g in task τ_i from 1 to w_i **do**
- 3 $\eta_{i,g} \leftarrow$ No of requests in region g ;
- 4 UBTime $_{i,g} \leftarrow f_{i,g-1} + L_i^{\text{reg-size}} + \eta_{i,g} * T_i^{\max}(1);$
 // with $f_{i,0} = 0$
- 5 LBslot $_{i,g} \leftarrow \min_{x>0} \{x \mid T_i^{\max}(g) \geq f_{i,g-1}\};$
- 6 UBslot $_{i,g} \leftarrow \min_{x>0} \{x \mid T_i^{\min}(g) \geq \text{UBTime}_{i,g}\};$
- 7 $\delta_{i,g} = \text{MaxRegDelay}(\eta_{i,g}, \text{LBslot}_{i,g}, \text{UBslot}_{i,g});$
- 8 $f_{i,g} = f_{i,g-1} + L_i^{\text{reg-size}} + \delta_{i,g};$
- 9 **end**
- 10 **return** $f_{i,w_i};$

With Algorithm 6, we propose an arbiter-independent method to determine the worst-case cumulative delay. It is basically an extension of Algorithm 5 and augments it with region-based information. Since the inputs to this algorithm are the $T_i^{\min}(\cdot), T_i^{\max}(\cdot)$ functions and the details of the analyzed task, any arbiter for which these values can be determined can leverage this algorithm.

The algorithm commences by computing the number w_i of regions (Line 1) and then considers each region g successively (Line 2). Next, given the number $\eta_{i,g}$ of requests in the analyzed region g , it finds a *coarse* upper bound on its increased execution time UBTime $_{i,g}$ assuming that each request in region g may incur a delay of $T_i^{\max}(1)$. Then, it computes the range of the free bus slots that the requests of region g may occupy (Lines 5-6), assuming on Line 5 a starting time of $f_{i,g-1}$.

To compute the worst-case delay of each region, the algorithm invokes a slightly modified version of Algorithm 5 in which (i) j now spans from $g + \text{LBslot}_{i,g}$ to $\text{UBslot}_{i,g} - (\eta_{i,g} - g)$ on Line 4, (ii) the 2D array contains $\text{UBslot}_{i,g} - \text{LBslot}_{i,g}$ columns, (iii) all the references to a cell $c(k, j)$ are replaced with a reference to cell $c(k, j - \text{LBslot}_{i,g})$, and (iv) references to C_i are substituted for references to $L_i^{\text{reg-size}}$. Note that a task modeled as a single region is a special case in which $\text{LBslot}_{i,1} = 1$, the region size $L_i^{\text{reg-size}}$ is C_i , and the maximum number of requests is $\eta_{(i)}$. The delay of the currently analyzed region $\delta_{i,g}$

is computed on Line 7 and is then accounted for in the worst-case finishing time $f_{i,g}$ computed on Line 8. The process is repeated for all the regions and the finishing time of the last region gives the increased WCET of the task.

4.7 Related Work

Bus contention analysis has received considerable attention in recent years and these efforts can be classified into two classes: 1) approaches that modify the hardware or the software of the system to enable or improve analysis, and 2) approaches that analyze a given system. We proceed by discussing each of these in turn.

On the hardware side, a number of memory controllers have been designed specifically for real-time systems and proposed together with corresponding analyses that bound the WCRT of memory requests [57, 59, 58, 113, 114]. These analyses benefit from full knowledge of the internals of the memory controller, such as page policies, transaction scheduler and the DRAM command scheduler, and exploit this information to produce tight bounds. On the software side, servers with memory budgets, built into the operating system, have been proposed to limit the memory interference [115, 116] from tasks executing on other cores, enabling it to be bounded based on enforcement rather than characterization. Our work contrasts to these efforts in the sense that it targets COTS platforms and considers both the software and hardware to be given.

Several approaches have been proposed for bus contention analysis in given COTS platforms. Similarly to our work, most analyses consider multi-core systems with a bus providing access to a shared memory with a single port [80, 106, 79, 91, 117]. However, these works are quite different with respect to the considered task models and scheduling policies for both the tasks themselves and their memory requests. Applications are typically modeled as independent periodic/sporadic task sets or acyclic task graphs [90, 73], and the scheduling is often based on fixed-priorities [91, 106], while tasks in task graphs are *statically scheduled* using techniques that respect precedence constraints, e.g. list scheduling. The approaches support different task preemption models, ranging from fully preemptive [80, 106] to non-preemptive [91, 117, 90, 73], and with limited-preemption at the granularity of TDM time slots as a compromise in between [79].

A problem with most of the previously mentioned analysis approaches is that they only support a single bus arbiter, such as any work-conserving arbiter [91, 80], fixed-priority arbitration, round robin [117], TDM [90, 73, 74, 75, 76] or first-come first-served. This does not address the diversity of memory arbiters in COTS platforms, making them point solutions exclusive to a single platform rather than a reusable framework that applies more generally. This problem is partially mitigated by the analysis in [79] that supports three of these arbitration mechanisms in a single unified framework, although this work is limited to systems where periodic tasks are modeled as sets of superblocks and scheduled using TDM. In contrast, our work is more general as it applies to any sporadic constrained-deadline

tasks under any non-preemptive task scheduler. To conclude, this work presents a scalable framework for bus contention analysis that is more general than previous work for COTS-based non-preemptive real-time systems with respect to supported task schedulers and memory arbiters.

4.8 Experimental Results

This section experimentally evaluates the proposed framework by simulating a multi-core system running real application traces. First, the experimental setup is explained, followed by an experiment that demonstrates the generality of our approach by executing the applications with three different arbiters and evaluating the accuracy and run-time of the proposed analysis. Lastly, we experiment with different region sizes and show how finer-grained task region-profiles improve accuracy and increase the efficiency of the analysis.

4.8.1 Experimental Setup

The hardware platform in our experiments is based on the SimpleScalar 3.0 processor simulator [118] with separate data and instruction caches, each with a size of 16 KB. The L2 cache is a private unified 128 KB cache with 128 B cache lines and an associativity of 4. The processor core is assumed to run at a frequency of 1.6 GHz. The memory device corresponds to a 64-bit DDR3-1600 DIMM [119] running at a frequency of 800 MHz, meaning that one memory cycle equals two processor cycles. The memory access time $TR = 80$ processor cycles for a request of 128 B, corresponding to an in-order DRAM scheduler with limited pipelining of requests. This setup is similar to contemporary COTS-platforms, such as Freescale P4080. The experiments consider a platform instance with 4 cores, each core running an application from the WCET test suite [111] as a single independent task. For each application in the benchmark, memory-trace files were generated by running it on the experimental platform. The traces were finally post-processed according to the sampling regions used in the experiments to compute the region-profiles of the task. Similar experiments were also carried out for the ChStone [107] benchmarks.

4.8.2 Application to Different Arbitration Mechanisms

The objective of this experiment is to demonstrate the generality of our approach by applying it to three commonly used arbiters, being fixed-priority, an unspecified work-conserving arbiter, and TDM, respectively. For each task, we determine the interference from other tasks and compute the increase in WCET for each of the three arbiters using a region size of 2000 cycles. We also examine the run-time of the proposed analysis for the different arbiters. To get a representative sample of applications for the WCET benchmark, we chose the two most memory-intensive (*minmax* and *lcdnum*) and the two least memory-intensive (*lms* and *adpcm*) applications. The results of the experiment are shown in Figure 4.10,

where tasks are arranged in descending order of priorities (*minmax* has the highest priority) for the case of fixed-priority arbitration. As expected, the task with the highest priority experiences minimal interference (an increase factor of 1x) from the other tasks. We observe a counter-intuitive effect in that *lcdnum* (priority 2) experiences a larger increase in WCET than the lower priority tasks. This is because *lcdnum* is more memory intensive than the lower priority tasks, and each of its requests is vulnerable to external interference from *minmax* which is again a memory intensive task.

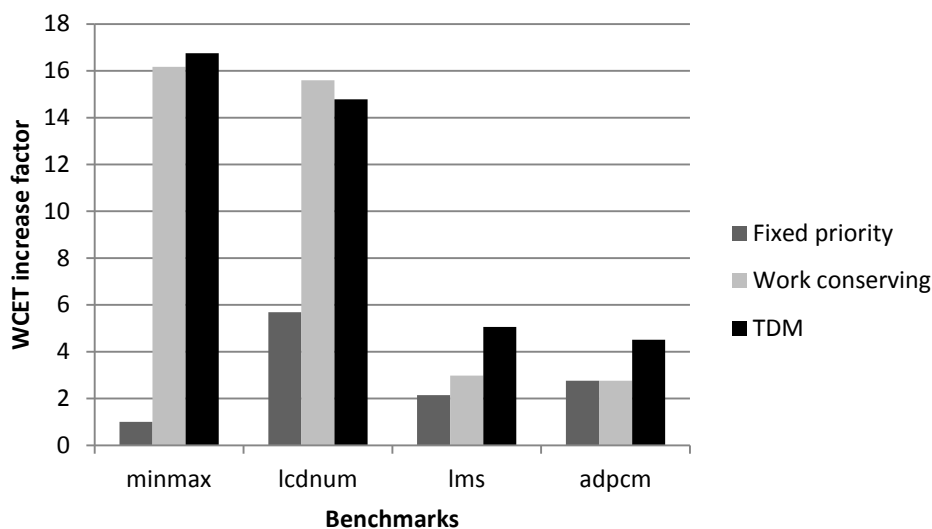


Figure 4.10: Increase in WCET for different arbitration mechanisms.

For the work-conserving arbiter, the requests of a given task may be blocked by all requests from all concurrently executing tasks. Such a mechanism hence leads to a very pessimistic WCET as seen in the figure. Note that this arbitration mechanism is equivalent to fixed-priority arbitration where every task is assumed to have the lowest priority. This can be seen in Figure 4.10, where the lowest priority task, *adpcm*, has the same WCET with fixed-priority arbitration and the unspecified work-conserving arbiter.

Unlike the previous two arbiters, TDM is neither priority-based, nor work conserving. Here, it is configured with a frame size of 4 and each core is allocated one slot. This basic fair configuration statically ensures periodic access to the memory, but its non-work conserving nature leads to poor performance, as allocated slots may be left unused despite pending requests from other tasks. Since this arbiter statically offers equal shares of the memory bandwidth, we see a direct relation between the memory intensity of a task and the increase in WCET.

Considering the run-time of the analysis, fixed-priority arbitration took 12 minutes to complete for all tasks. The tasks with higher priorities complete faster than the slower ones, since they are less impacted by interference, resulting in fewer request-set mappings. This is reflected in the analysis of the unspecified work-conserving arbiter, where all tasks can suffer interference from all other tasks, increasing the analysis time to approximately

35 minutes. In contrast, the TDM arbiter is non-work-conserving and thereby completely independent of other tasks, enabling the computation of $T_i^{\min}(\cdot)$ and $T_i^{\max}(\cdot)$ in constant time. Furthermore, small TDM frame sizes provide relatively few possible request-set mappings, reducing the total analysis time to less than 5 minutes. While running the analysis, we further-more instrumented the algorithm to evaluate the benefits of the optimization proposed in Section 4.5 (List reduction). The result of this evaluation showed that the hit-ratio ranged from 20-40% (with an average of 30%), which considerably reduces the run-time for cases where the number of candidate slots is very high.

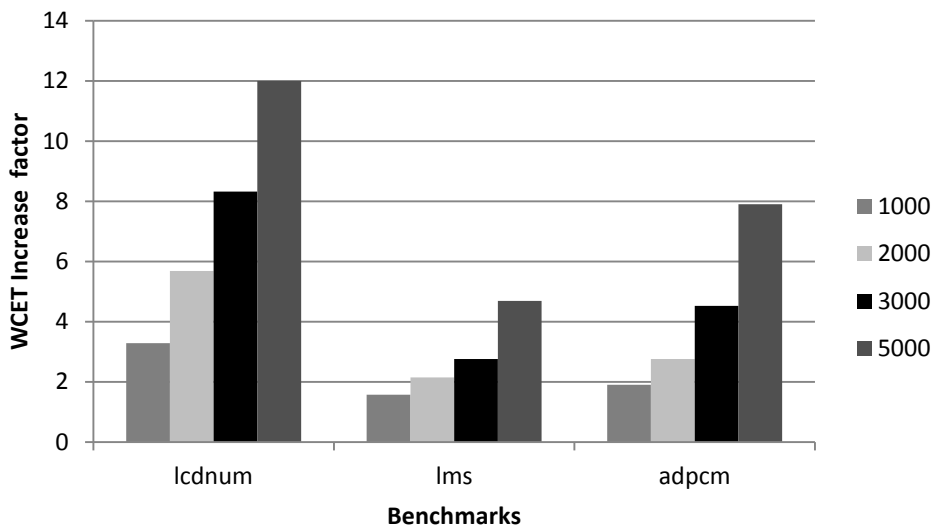


Figure 4.11: Increase in WCET for different region sizes (in cycles).

4.8.3 Impact of Region Size

We conclude by experimentally evaluating the impact of the region size. To this end, we reran the previous experiments with the fixed-priority arbiter using both smaller and larger region sizes. Four different sizes are used: 1000, 2000, 3000 and 5000 cycles, respectively, where larger region sizes imply fewer regions and coarser-grained cache profiles for each region. The results of the experiment are shown in Figure 4.11. Note that the highest priority task, *minmax*, is not shown in the figure, as it suffers the same negligible interference across all region sizes. For the other tasks, the results confirm the intuition that smaller regions result in tighter WCET, since finer-grained task region profiles eliminate a lot of uncertainty. In terms of run-time of the analysis, the results reflect that smaller region sizes imply fewer candidate slots, reducing run-time. To quantify this claim, the total analysis time was 4, 12, 34 and 125 minutes for region sizes of 1k, 2k, 3k and 5k cycles, respectively.

4.9 Conclusion

In this chapter we developed a framework to compute the worst-case execution time of a task which can work for different arbitration mechanisms. By using the tools for task and core profiling developed in the previous chapter, we proposed a method to model the availability of the bus to a given task and leveraged this model further to compute the increased delay that the task incurs when co-scheduled with other tasks contending on the bus. The proposed algorithm presented a general interface into which different arbiters can be seamlessly plugged to compute the resulting WCET. We also demonstrated the applicability of our framework for two different arbiters: a non-work-conserving TDM arbiter and work-conserving fixed-priority arbiter. In the next chapter, we will explore another component — the memory controller and look into its inner workings.

Chapter 5

Bus Contention Analysis of Phase Change Memory based Multicores

If the facts don't fit the theory, change the facts.

Albert Einstein

5.1 Introduction to Phase Change Memory

A key development in the embedded systems arena is the adoption of the multicore technology as their core processing platform. Another research trend now in memory technology is to find a single memory for both temporary storage and permanent storage in personal computers as well as embedded systems. The goal is the unification of memory, to avoid having a separate SRAM, DRAM and flash. An interesting viable option is the possibility of adopting Phase Change Memory (PCM) as main memory for embedded systems [120, 26, 104, 121, 103]. Phase change memory (PCM) is an emerging non-volatile solid-state memory technology employing materials that change states or phases. These materials are among the most ubiquitous materials in information storage, as they are already mass-deployed in rewritable optical discs such as CDs and DVDs. PCM leverages the significant change in electrical resistivity when the material changes between its two states i.e the amorphous and crystalline phases. The material has high electrical resistivity in its amorphous state and low resistivity in its crystalline state — corresponding to the 1 and 0 states of binary data.

PCM has been positioned to complement or replace existing volatile memories like Dynamic Random Access Memory (DRAM) as the main memory and as a potential alternative to FLASH memory. PCM is more power efficient than DRAM because it is non-volatile and therefore unlike DRAM does not need periodic refreshes. The experts from Ovonyx [26] state that:

“PCM can displace a significant amount of DRAM in both mobile and PC/server applications. PCM today already offers a cell size smaller than DRAM and with PCM’s inherent enhanced scalability over DRAM, the cost advantage of PCM will increase with time. As more volatile DRAM is displaced by non-volatile PCM, significant power savings will be realized, providing extended battery life in mobile applications and significantly reduced power consumption in PC and server applications. Initially, PCM will not be targeted as a direct replacement for all DRAM, but rather to displace a large percentage of DRAM in applications that don’t require the infinite DRAM cycle endurance and can benefit the most from the dramatically reduced power consumption of PCM.”

Challenges in adoption: In spite of the aforementioned benefits, its adoption for real-time embedded systems is not without its own challenges: its read latency is acceptable but the write latency is very high. While DRAM read and write latencies are in the range of 20-50ns, PCM read latency is of the order of 50ns while the write latency is of the order of 0.5–1 μ s [122]. With such high latencies, from the real-time context, many tasks on systems with PCM-based memory (without any modifications) may miss their deadlines or incur unacceptable delays in their execution times [101]. To address this issue, researchers have proposed PCM memory controller scheduling policies and designs that overcome these challenges, facilitating its adoption in real-time systems [104, 101]. From the architecture side, increasing the cache sizes can also mitigate the penalties associated with the high write latencies. Researchers have also envisioned and architected a multi-tiered vertical memory hierarchy which consists of the on-chip caches, an off-chip DRAM memory and then a PCM main memory as the last memory level. Another problem of PCM is its limited endurance (up to 10^8 writes), which can be mitigated with a large dedicated on-chip cache (SRAM or embedded DRAM) that can absorb most of the write misses – PCM-only memories then become feasible with the advantage of energy efficiency and density.

Our work focuses on developing a mechanism to aid the timing analysis of real-time embedded systems hosted on multicores systems with PCM as the main memory.

5.1.1 Problem overview and contributions

To ensure at design time that *real-time* embedded applications deliver the required functionality within pre-set time limits, bounds on key parameters like the worst-case execution time (WCET) must be established. In this chapter, we build upon the state-of-the-art methods that compute these WCET estimates, and address the problem of extending such upper bounds *considering the contention for the PCM memory controller and the asymmetric read and write latencies*. We assume a multicore system with private caches and a *PCM-based main memory* system.

Main contributions The currently existing analysis techniques to compute the delay due to contention on the shared memory do not consider the request handling mechanisms

within the memory controller and treat it as a black box. A fixed latency for servicing read and write memory requests is typically assumed in the analysis, which is appropriate for DRAM based memory systems. However, given the substantial difference in the time to service a read and write request, the above assumptions may lead to unsafe or pessimistic estimates. A new memory scheduling policy proposed by contemporary researchers Zhou et.al [101] considering PCM's read/write timing asymmetries reduces the number of deadline misses and makes it practical to deploy real-time applications. This work builds on the work of Zhou et.al and provides the timing analysis for PCM main memories in multicore systems.

1. We believe that this is the *first* work to derive the increased WCET of a task considering asymmetric-latency based systems and the memory request scheduling policy within the realm of real-time systems. Although this particular analysis focuses on PCM, it could be used for other memory technologies with asymmetric read and write latencies like Spin Transfer Torque (STT) memories.
2. In this work, we propose a method to model the arrival and servicing of the requests in the PCM memory controller considering the memory scheduling policy.
3. We leverage the model to compute the increased WCET of a task considering the contention on the bus and the memory controller. Our method exploits the memory request profile of the analyzed tasks in order to tighten the WCET.
4. The analysis is then validated by running our proposed method on benchmarks from MediaBench [123]. A set of experiments have been performed to highlight the impact of other parameters like the nature of co-scheduled tasks and the task priorities on the WCET.

The rest of the chapter is organized as follows: Section 5.2 discusses the related work in the area of timing analysis and PCM. The system model is described in Section 5.3. An initial basic approach is proposed in Section 5.4, followed by Section 5.5 which describes our new method. This method is validated and the results are presented in Section 5.6. The chapter finally concludes in Section 5.7.

5.2 Related Work

5.2.1 Earlier work on PCM

PCM has been proposed as a promising candidate for energy-efficient main memory systems. Lee et al. [124] propose area-neutral buffer organizations and partial write techniques to mitigate the negative impacts of PCM's long latencies, high energy and limited endurance. Qureshi et al. [125] propose a hybrid architecture that uses a DRAM cache to filter accesses to PCM. The hybrid architecture has the latency benefits of DRAM and the

capacity and scalability advantages of PCM. Ferreira et al. [126] study page partitioning in the DRAM cache to reduce the amount of data written back to PCM. Zhou et al. [127] propose PCM as a direct replacement for DRAM in main memory without buffer organization. Zhang et al. [128] present a hybrid PCM/DRAM memory architecture that uses a small DRAM as write buffer. OS-level paging scheme is applied to improve PCM write performance and lifetime.

Researchers have also proposed techniques for mitigating the impact of undesirable PCM characteristics. As mentioned above, buffer organizations [126, 124, 125, 128] are effective to hide the impacts of slow PCM writes (compared to DRAM). Techniques like write cancellation and write pausing [129] have also been proposed to improve the performance of PCM reads by delaying the extremely slow write operations.

PCM controller modifications to make it real-time friendly Given the high delays for servicing write requests, many tasks executing on a system with the basic PCM memory system can experience deadline misses. To overcome this issue, Zhou et.al [101] proposed three main features to be integrated into the PCM memory controller, which resulted in substantially reducing the number of tasks that missed their deadlines.

1. Ability to attach external priorities to each memory request, together with the type of the request (read or write) and its arrival time. Priorities are assigned to requests based on the task properties, using algorithms like EDF and RMA.
2. Critical read boosting, which prioritizes critical reads over non-critical prefetch reads.
3. Preference of Reads over Writes. The rationale is that since writes can be buffered and the latency due to a write operation is very high, reads must be prioritized over writes to reduce the waiting time for read responses.

However, their work did not focus on the timing analysis of their proposed model which is the main theme of this chapter. Furthermore, the analysis in this chapter is different from earlier proposed approaches for multicore systems as it takes into account the memory scheduling policy, exploits the memory profiling information of the analyzed task and deals with asymmetric read and write times, which was not considered in these previous works.

5.3 Model of computation

Figure 5.1 depicts the system model with m processor cores $(\pi_1, \pi_2, \dots, \pi_m)$, each of which has one or several levels of large private cache. The main difference from the previous work (assumed earlier in the analysis for multicores) is that DRAM is replaced by PCM main memory in this model. All the cores are connected to the memory controller by a single *shared bus*, which we refer to as the Front-Side Bus (FSB). All the traffic between the cores and the memory controller is transmitted over the FSB and memory requests are scheduled by the PCM controller.

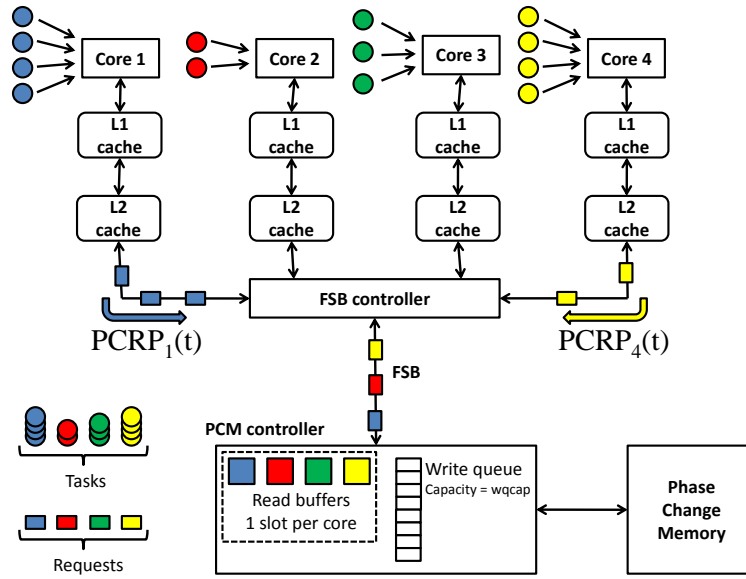


Figure 5.1: Platform model

As in the earlier analysis, the workload is modeled as a set $\tau = \{\tau_1, \tau_2, \dots, \tau_n\}$ of n tasks, each of which is characterized by three timing parameters: C_i , T_i and $D_i \leq T_i$. Each task τ_i generates a (potentially infinite) sequence of jobs released at least T_i time units apart (T_i is referred to as the period or minimum inter-arrival time) and each such job has to execute for *at most* C_i time units within D_i time units from its release. The parameter D_i is called the “deadline” of the task and the parameter C_i denotes an *upper bound* on its execution time when it executes uninterrupted and in *isolation*, i.e., with no contention on any of the shared low-level hardware resources. C_i is called the “worst-case execution time” (WCET) of τ_i and can be computed by well-known WCET analysis techniques [10].

Besides the three computation parameters, each task is also characterized by its *worst-case memory request profile* that can be computed using the task memory request profiling tool presented in Chapter 3. The memory request profile of a task indicates the maximum number of read and write requests that it can generate in any time interval of a given length t . Given the task memory request profiles, the task-to-core assignment, and the timing parameters of the tasks, the per-core memory profile can be computed. This “Per Core Request Profiler”, denoted by $PCRP_j(t)$ as described earlier in Chapter 3, computes the maximum number of requests that can be issued from tasks executing on core π_j in any time interval of length t .

As in the previous analysis in Chapter 3 and Chapter 4, we consider a partitioned scheme of task assignment and a non-work conserving scheduler on the core. The non-work conserving assumption implies that whenever a task τ_i completes in less time than indicated by its WCET C_i (say it completes in x time units on the core π_p), the scheduler idles the core π_p up to the theoretical WCET of the task, i.e., it idles π_p for the remaining $(C_i - x)$ time units. This assumption is made to ensure that the number of bus requests

within a time window computed at design time, is not higher at run-time due to early completion of a task and the subsequent early execution of the next tasks.

5.3.1 Request scheduling in the FSB controller

Generally in a real-time system, tasks are prioritized and scheduled accordingly on the processing element (cores) so that they all meet their deadlines. While the task scheduler respects these priorities and gives preferential access to the core to tasks with a high priority, in a multicore system with shared main memory, a task may still miss its deadline due to memory contentions if the shared bus and the memory controller do not enforce this prioritization. Therefore, we adopt *globally unique external priorities* to manage memory requests of tasks scheduled on different cores [101]; each memory request inherits the priority of the task issuing it, ensuring that requests from higher-priority tasks arrive earlier at the PCM controller. These request priorities are assigned externally by the user or operating system (in accordance with either the scheduling algorithms or some other heuristics) and must be passed to the memory subsystem.

In this work we assume that a request inherits the priority of the tasks it is issued from. The FSB controller uses these priorities to schedule the pending requests so that requests from high priority tasks are served earlier than the lower priority requests. Note that in this work, we assume that every request inherits the priority of the task issuing it. The scheduler mechanism employed by the PCM controller however, is more complicated (as described later). To preserve the priority ordering of the requests on their path from the cores to the memory, when requests from co-executing tasks arrive concurrently at the FSB controller, the arbitration unit at the FSB reorders them on the basis of their priorities. This priority-based mechanism at the bus level ensures that requests from tasks with higher priority have precedence over those from the lower priority tasks and arrive earlier at the PCM controller. The bus is thus priority-driven and is work-conserving: if there is any pending request to be served, the bus cannot be idle.

5.3.2 Request scheduling in the PCM controller

Constraints on the read requests: We assume that there cannot be multiple outstanding *read* requests from any core, i.e., a core cannot issue a new read request before receiving a response to its previous request. Thus, a core is stalled on issuing a read request until it receives the required response (data).

Handling the write requests: Since the write latency is much higher than the read latency, non-preemptive writes can considerably increase the task response times. This means that the core is stalled, the executing task incurs long delays and the core is under-utilized. To reduce these delays and associated core stalls, the PCM controller provides a write queue of finite length to buffer the write requests. Since the execution of a task can proceed without waiting for a write operation to be completed, it translates to lesser

stall cycles for the core thereby leading to faster execution of the tasks. The following key points describe the working of the PCM controller.

1. As long as the write buffer is not full, the PCM controller schedules the pending read requests — Read over write prioritization.
2. In the unlikely case that a read request is issued to an memory address pending in a write queue buffer, the controller responds with the data in the write buffer.
3. When the write queue is full, all the pending requests (reads and writes) are sorted in decreasing order of priority in their respective queues, with the highest priority read/request being positioned at the front of the corresponding read/write queue and the controller starts serving the reads and writes based on their respective priorities until the write queue is non-full again.
4. The PCM controller then switches back to prioritizing reads over writes.
5. Since the memory controller is work conserving, the write requests are also served when there are no pending read requests issued by any of the tasks.

Having described the system model, we next formally define the problem to be addressed in this work.

5.3.3 Problem Definition

For each task $\tau_i \in \tau$, given its *WCET* C_i and *memory profile in isolation*, compute the *increase* in the *WCET* C'_i when it runs *in conjunction with other tasks* deployed on a multi-core system with a shared PCM (conforming to the model described above). The problem consists of finding a tight upper-bound on the cumulative delay that memory requests may incur in the FSB and PCM controllers. Let N_i^{read} (N_i^{write}) denote the maximum number of read (write, resp.) requests generated by task τ_i during its execution time C_i and $w_{i,k}^{\text{rd}}$ ($w_{i,k}^{\text{wr}}$) denote the waiting time for the k^{th} read (write, resp.) request of τ_i . The objective is to find a tight upper bound on C'_i .

$$C'_i = C_i + \sum_{p=1..N_i^{\text{read}}} w_{i,p}^{\text{rd}} + \sum_{q=1..N_i^{\text{write}}} w_{i,q}^{\text{wr}} \quad (5.1)$$

5.4 An Initial Approach to the Problem

A basic approach to derive C'_i is to compute an upper bound on the delay that a single request can incur and then assign the same delay to each request. That is, if \bar{w} denotes the maximum delay for a single request and N_i denotes the maximum number of requests issued by task τ_i , the resulting *WCET* can be upper-bounded as follows.

$$C'_i = C_i + N_i \times \bar{w} \quad (5.2)$$

The above method clearly leads to an overly pessimistic estimation of the increased WCET, C'_i , because it assumes that all the requests of τ_i are subjected to the same (bursty phase of) external task interference from other tasks (which is the worst-case scenario for a single request). It is very unlikely that this assumption is valid since the other tasks will keep progressing in their execution (alternating between computation and memory fetch phases) and will not keep on congesting the memory system at all times. However, this concept of assuming the worst-case scenario for a given parameter and applying it to all other instances is *widely* used in the area of timing analysis. For example, the WCET or the worst-case response time of a task are typically computed by considering the worst-case scenario for a *single* job, and all the jobs are then assigned the same values in the subsequent schedulability analysis. The next section proposes an alternative method which will lead to tighter estimates.

5.5 An Upper Bound on the external interference

5.5.1 Busy and Idle periods

Let τ_i denote the task under analysis and $\text{hp}(i)$ denote the set of all the tasks of higher priority than τ_i . Also, recall that $\bar{\pi}_i$ represents the set of all the cores, excluding the one on which task τ_i is assigned.

During the execution of τ_i , higher priority tasks running on the other cores (in $\bar{\pi}_i$) may generate requests that interfere with the requests issued by τ_i . With respect to the analyzed task τ_i we define the term *busy period* as follows:

Definition 18. *The contiguous span of time during which requests from higher priority tasks are being served by the memory controller will be referred to as a “busy period”*

Since tasks have alternating phases of computation and memory fetches, there are some “gaps” during which the tasks co-executing with τ_i may *not* be issuing requests (or they issue only requests of lower priority) and the memory controller can thus schedule requests from the analyzed task τ_i or lower priority tasks (if there are no requests from τ_i at those instants).

Definition 19. *The contiguous span of time during which the memory controller is not serving requests from higher priority tasks and may therefore serve the requests of lower priority tasks or the requests of the analyzed task τ_i is referred to as an “idle period”.*

Note that these concepts of the busy and idle periods are defined in the context of the *analyzed task* τ_i . An extended timeline can thus be visualized, which models the schedule of the requests in the controller, consisting of alternating busy and idle periods. The proposed method achieves the objective of computing the increased WCET in two main phases:

1. It determines all the busy and idle periods over an extended duration $[0, D_i]$ where D_i is the deadline of the analyzed task τ_i .
2. It then schedules the requests of the analyzed task τ_i in such a way that its overall execution time is maximized. Towards that goal, we take into account the information on the busy periods to maximize the waiting time of the requests.

5.5.2 Phase 1: Determination of the busy and idle periods

Notation	Meaning
wqcap	the capacity of the write queue
wqlen	the number of slots currently used in the write queue
inRd	the number of incoming (high priority) read requests
inWr	the number of incoming (high priority) write requests
k and curtime	the iteration index and the current time
BP^k	the current time after the k^{th} iteration
StartBusy(w)	store the time at which the w^{th} busy period starts
EndBusy(w)	store the time at which the w^{th} busy period ends
StartIdle(w)	store the time at which the w^{th} idle period starts
EndIdle(w)	store the time at which the w^{th} idle period ends
LengthBusy(w)	the length of the w^{th} busy period
LengthIdle(w)	the length of the w^{th} idle period
TR	upper bounds on the time to serve a read request by the PCM memory module
TW	upper bounds on the time to serve a write request by the PCM memory module

Table 5.1: Notations used in the automata

5.5.2.1 Overview and notations

The rationale behind the proposed approach is to compute the busy and idle periods by analyzing the working of the PCM controller, considering that the maximum number of requests from the cores in $\bar{\pi}_i$ are generated. The analysis is carried out for a pre-set time interval: from task release to deadline (i.e., during D_i time units). The computation of the alternating sequence of busy and idle periods is performed by using two automata: the busy and idle automata.

1. In the busy automaton, the algorithm iterates as long as interfering higher-priority requests can be generated, with the aim of maximizing the length of the computed busy period.
2. When no further higher priority requests can be generated by the cores in $\bar{\pi}_i$, the algorithm switches to the idle automaton wherein it keeps increasing the idle period duration until there is a new incoming higher-priority request issued by tasks executing on the other cores, and then switches back to the busy automaton.
3. Termination condition: The algorithm terminates when the deadline is exceeded either in the busy or the idle automaton. While the deadline of the task marks the

end of the analysis interval in the proposed approach, other parameters like a specific threshold on the number of busy periods may be used to limit this interval.

Before modeling the working of the PCM controller to capture the worst-case scenario (in terms of sequence of busy and idle periods), a pre-requisite is to capture the *maximum* number of requests that can be issued from the interfering cores (i.e., the cores in $\bar{\pi}_i$) in any given time interval. We leverage the function $\text{PCRPR}_p(t)$ defined in Chapter 3 to compute the required interference from tasks of higher priority and compute the lengths of the busy and idle periods. The notations used are shown in Table 5.1.

Since the function $\text{PCRPR}_q(t)$ did not differentiate between read and write requests, we introduce two new functions: $\text{PCRPR}_q(i, t)$ and $\text{PCRPW}_q(i, t)$ that denote an upper bound on the number of reads and write requests of *higher priority* (than the requests of task τ_i) generated by core π_q in a time interval of length t . Then, for the analyzed task τ_i we denote by $\text{NHR}(i, t)$ ($\text{NHW}(i, t)$, resp.) an upper bound on the *cumulative* number of read (write, resp.) requests issued from tasks in $\text{hp}(i)$ executing on the other cores (in $\bar{\pi}_i$) in a time interval of length t .

$$\text{NHR}(i, t) = \sum_{q \in \bar{\pi}_i} \text{PCRPR}_q(i, t) \quad (5.3)$$

$$\text{NHW}(i, t) = \sum_{q \in \bar{\pi}_i} \text{PCRPW}_q(i, t) \quad (5.4)$$

For brevity, we will *drop the task index i* in the automata and denote the functions as $\text{NHR}(t)$ and $\text{NHW}(t)$.

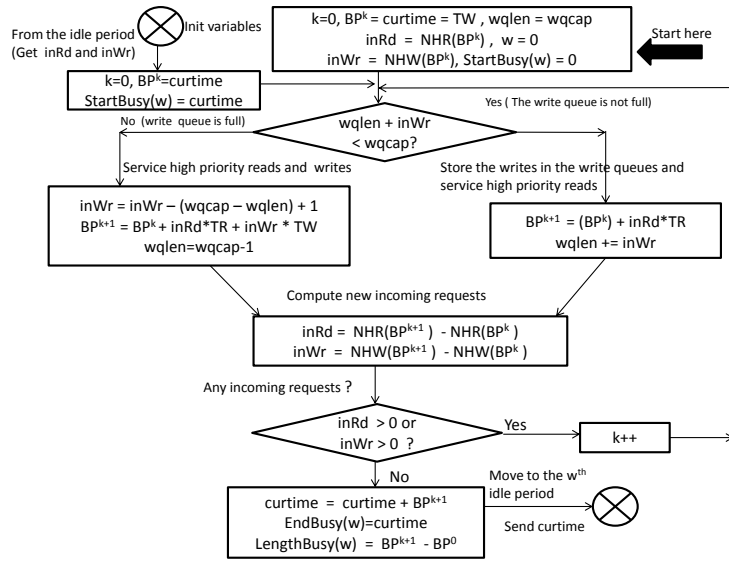


Figure 5.2: The busy period automata

5.5.2.2 The busy period automaton

The flowchart in Figure 5.2 models the working of the PCM controller when read and/or write requests are generated by the higher priority tasks running on the cores in $\bar{\pi}_i$. Note that the termination condition is not shown explicitly, but whenever the variable *curtime* exceeds the deadline, the automation is exited.

To create the scenario leading to the maximum duration of the busy period, the algorithm begins with the initial condition that the write queue is full, reflected by $wqlen = wqcap$, and that a write request is currently being served (hence $BP^0 = TW$). Before each iteration in the main loop, the algorithm checks if there is any new incoming read or write requests from the higher priority tasks. The incoming write requests may cause the write queue to overflow.

The PCM controller decides which request to schedule based on the current write queue occupancy. Note that the status of the write queue (Full or Non-Full) is decided taking into account the current occupancy of the write queue *and* the number of incoming write requests. Two cases may arise:

Case 1. If the write queue is *not* full, the algorithm takes the right branch of the flowchart. Since the incoming writes can be buffered in the queue (reflected by “ $wqlen += inWr$ ”), the controller serves only the *read* requests. The delay $inRd \times TR$ is thus added to the total busy period length.

Case 2. If the write queue is or will be full, at least one new incoming write request cannot be buffered and the cores issuing them are stalled (the algorithm takes the left branch). The controller then starts serving *read and write* requests in priority order *until the write queue is non-full again* (in other words, the controller does not have to serve *all* the pending write requests). In the worst-case scenario, it has to serve all the pending read requests plus enough write requests (including new incoming requests) so that the write queue is no longer full.

Example 3. Assume that the capacity of the write queue is 6, 4 slots are currently occupied and there are 2 incoming read requests and 5 incoming write requests. In the worst case, the controller has to serve the 2 incoming reads but only $inWr - (wqcap - wqlen) + 1 = (5 - (6 - 4) + 1) = 4$ writes, after which 5 slots will be occupied in the write queue and thus there will be one vacant slot (i.e., the queue is non-full again).

The variables $wqlen$ and $inWr$ are correspondingly updated to reflect the execution of this procedure and the delay ($inRd \times TR + inWr \times TW$), computed with the reduced value of $inWr$, is added to the total busy period length. When there are no more read nor write requests issued between BP^k and BP^{k+1} from higher priority tasks in $hp(i)$ running on cores in $\bar{\pi}_i$, the process terminates and the controller is free to serve requests of other lower priority tasks (including those of τ_i). The length of the current (i.e., the w^{th}) busy period is given by $LengthBusy(w) = BP^k - BP^0$. The variable *curtime* is updated by a delay of $LengthBusy(w)$ and the algorithm moves to the idle automaton.

Example 4. A given busy period is computed by an iterative process. The process initially starts with the notion that the controller is busy serving a write request which needs TW units to be completed. Hence, the initial value, BP^0 , is set to TW . In the interval $[0, TW]$, assume that there are 3 new incoming read requests from the higher priority tasks. The memory serves these 3 requests and the length of the busy period is increased to $BP^1 = TW + 3TR$. While serving these 3 requests, assume that there are 2 incoming high priority requests, a write and a read requests. If the write queue is not full, then the write request is buffered and hence the write does not contribute to the delay; the controller serves the pending read and the busy period is now $BP^2 = TW + 4TR$. If the write queue is full, one of the buffered write requests must be served to prevent the core issuing the incoming write from being stalled. In that case, one of the write requests plus the incoming read request are served and $BP^2 = TW + 4TR + TW$. The write request that was pending is now buffered in the write queue and the algorithm checks for new incoming requests in the time interval $[BP^1, BP^2]$. If no new requests were issued in that time interval, it marks the end of the busy period. Otherwise, the algorithm keeps on iterating through the main loop until no more higher priority request is generated (or until the current time exceeds the deadline).

Note: It can be shown that the length of the first busy period is the maximum waiting time that a single request can incur. For the initial approach described earlier in Equation 5.2, the resulting WCET can be computed by setting the term \bar{w} to the maximum delay (= length of the first busy period). By construction, the first busy period is the longest because the analysis starts with an initial configuration to maximize the waiting time of any given request (the write queue is full and a write is being processed). Also, to compute the worst-case interference to the analyzed task, the functions $NHR()$ and the $NHW()$ consider that co-executing (interfering) tasks from other cores are generating the maximum number of requests.

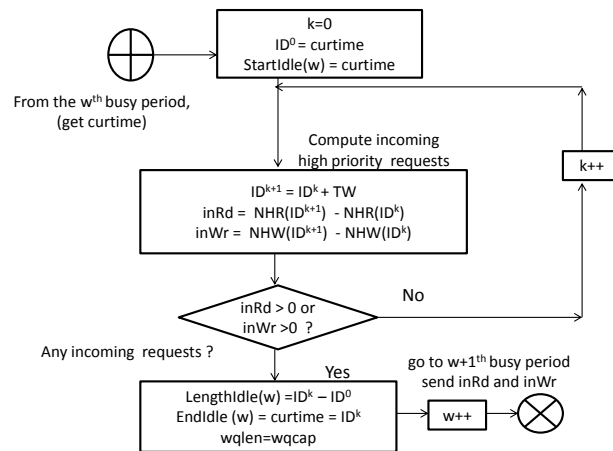


Figure 5.3: The idle period automata

5.5.2.3 The idle period Automaton

The idle period marks the phase in which there are no new requests from the higher priority tasks in $hp(i)$ running on the cores in $\bar{\pi}_i$. The requests generated by the analyzed task τ_i , if issued, may be served by the memory controller. Note that requests from low-priority tasks can also be serviced, but the algorithm we are describing is considering only requests from τ_i . Figure 5.3 depicts the flow through the automation. Note that the termination condition is not shown explicitly, but whenever the variable ID^k exceeds the deadline, the automation is exited.

The algorithm determines the length of the idle period by starting from the end of the last busy period; this time-instant is recorded in $curtime$. The iteration index k is initialized to 0 and ID^0 is set to $curtime$. The central idea of identifying an idle period is to poll at regular time instants if there are new requests being issued by the higher priority tasks. If there are no new requests, then the algorithm increases the idle period duration by the poll interval and continues looping in the idle automaton. If there are new incoming requests, the algorithm switches back to the busy automaton. Note that at the beginning, we assume that a write request was issued by a lower priority task in order to initiate the loop.

An important design issue is determining the ideal poll interval. A very small poll interval will allow us to capture the idle periods in small steps, leading to a longer analysis time if there are no higher priority requests issued during a long time, whereas a large poll interval will capture the arrival of new requests faster, but as a consequence overlooks (precious) idle gaps between two distant polling points. We assume a polling step of TW in the analysis, (assuming a hypothetical write request to be issued) as seen in Figure 5.3.

There can be two cases depending on the arrival of requests between two polling instants.

1. No new requests are issued: The algorithm increases the length of the idle period ($ID^{k+1} = ID^k + TW$) and proceeds to the next iteration.
2. New requests are issued: This marks the end of the idle period. The algorithm updates the current time to ID^k , computes the duration of the idle period and switches back to the busy period automaton.

5.5.3 Phase 2: Using the pre-computed busy and idle periods of the analyzed task to compute its increased WCET

5.5.3.1 Modeling Sampling Regions

This section focuses on computing a tight upper-bound for the cumulative waiting times of all the requests generated by a given task τ_i by considering the busy periods computed in Phase 1. The waiting time for a given request is maximized if it is issued just before

the longest (feasible) busy period (the request is issued but the bus has just started serving a contiguous stream of requests of higher priority). The cumulative waiting time is maximized by adding up the maximum waiting times of each requests (delays incurred due to the busy periods) which in turn results in an upper bound of the worst-case execution time of τ_i . To compute the increase in WCET, we start by modeling the memory request profile of the analyzed task τ_i *in isolation*. The memory profiling is done by dividing τ_i into logical *sampling regions* and determining the maximum number of requests issued in each of these regions. The number of memory requests generated in each region can be determined by static cache analysis [10] or by measurements by instrumenting the L2 cache misses [79] (using performance monitoring counters [94]).

For this analysis, we assume that the analyzed task τ_i is sampled in intervals of length lenregion and has NSR_i such sampling regions. That is, the worst-case execution time C_i of τ_i is split into NSR_i regions, each of length lenregion : $\text{NSR}_i \times \text{lenregion} = C_i$. We can also generalize it to different regions of unequal length lenregion_j where $\{j \in 1 \dots \text{NSR}_i\}$, but will keep it simple at this stage. We denote by $N_{i,j}^{\text{read}}$ and $N_{i,j}^{\text{write}}$ the maximum number of read and write requests (respectively) that can be generated in the j^{th} sampling region of task τ_i denoted by $SR_{i,j}$, where $1 \leq j \leq \text{NSR}_i$.

5.5.3.2 Description of Algorithm CompConDelay()

During the sampling of τ_i , the WCET of each region is determined by considering a finite service time of TR time units for the read request but a zero waiting time for the write requests. That is, the memory traces obtained at design time assume that the write queue is never full and all the write requests are thus buffered in the queue as soon as they are generated. This implies that the time for servicing every read request is accounted for in the original WCET C_i (and thus in the per-region WCET (lenregion) as well), whereas the time for servicing the write requests must be taken into consideration in the analysis. To this end, line 2 of Algorithm 7 adds the following to lenregion :

1. $N_{i,j}^{\text{write}} \times \text{TW}$, since the time for servicing write requests is not factored in the original WCET.
2. $(N_{i,j}^{\text{write}} + N_{i,j}^{\text{read}}) \times \text{TW}$, because every request of τ_i may be generated just after the PCM controller starts serving a lower-priority write request. Since the PCM serves requests in a non-preemptive manner, every request of τ_i can potentially be subjected to an extra delay of TW time units.

For each sampling region of τ_i , lines 4 and 5 compute the interval of time $[t_j^{\text{start}}, t_j^{\text{end}}]$ during which the j^{th} region executes (in the worst-case scenario): the j^{th} region starts after the $(j-1)^{\text{th}}$ region completes (assuming $t_0^{\text{end}} = 0$) and ends $\text{wcet}_{i,j}$ time units later. During this time interval, each request of τ_i will be assigned the maximum possible delay. The requests of a given region are considered in sequence (line 7).

Algorithm 7: CompConDelay(τ_i)

```

input :  $\tau_i$ : the task under analysis
output:  $C'_i$ : The increased WCET
/* Compute required time for a region considering its write requests
   and blocking write requests from lower priority tasks */
1 for  $j \leftarrow 1$  to  $NSR_i$  do
2   |  $wcet_{i,j} \leftarrow \text{lenregion} + N_{i,j}^{\text{write}} \times \text{TW} + (N_{i,j}^{\text{write}} + N_{i,j}^{\text{read}}) \times \text{TW};$ 
3 end
4 for  $j \leftarrow 1$  to  $NSR_i$  do
   | // Compute extended region boundaries
5   |  $t_j^{\text{start}} \leftarrow t_{j-1}^{\text{end}};$ 
6   |  $t_j^{\text{end}} \leftarrow t_j^{\text{start}} + wcet_{i,j};$ 
7   | for  $k \leftarrow 1$  to  $(N_{i,j}^{\text{read}} + N_{i,j}^{\text{write}})$  do
   |   | // Compute candidate set of busy periods that may delay requests
   |   |   in region  $j$ 
8   |   |  $B \leftarrow \{x \text{ such that either of the 2 conditions is met}\}$ 
   |   | // Case 1: Choose the busy period(s) that lie(s) or starts
   |   |   within the extended region boundaries
9   |   | 1.  $t_j^{\text{start}} \leq \text{StartBusy}(x) \leq t_j^{\text{end}}$  or ;
   |   | // Case 2: Choose the busy period which encloses the extended
   |   |   region boundaries
10  |   | 2.  $\text{StartBusy}(x) < t_j^{\text{start}} \wedge \text{EndBusy}(x) > t_j^{\text{start}};$ 
   |   | // Remove the marked busy periods that were used to delay
   |   |   previous requests
11  |   |  $B \leftarrow B \setminus \bigcup_{x=1}^{k-1} \{\text{markb}_x^{\text{max}}\};$ 
   |   | // Find max. delay among the candidates
12  |   |  $b_k \leftarrow \underset{w \in B}{\text{argmax}}\{\text{LengthBusy}(w)\};$ 
   |   | // current region is extended due to extra delay
13  |   |  $t_j^{\text{end}} \leftarrow t_j^{\text{end}} + \text{LengthBusy}(b_k);$ 
   |   | // Mark the busy period contributing to the delay of request  $k$ 
14  |   |  $\text{markb}_k^{\text{max}} = b_k;$ 
15  |   | end
16  |   | return  $t_{NSR_i}^{\text{end}};$ 
17 end

```

For each request k , the algorithm first creates a candidate set of busy periods, denoted by set B which can potentially delay it. Specifically, this set B contains all the busy periods that start within $[t_j^{\text{start}}, t_j^{\text{end}}]$ (condition 1), plus the busy period (if any) that overlaps the time-instant t_j^{start} (condition 2). Then, the algorithm eliminates $(k - 1)$ members from set B , that were already used to delay the previous $(k - 1)$ requests of τ_i in the current region j (line 11).

To maximize the waiting time for the given request, the algorithm determines (at line 12) which of these busy periods in set B is the longest and assigns the corresponding

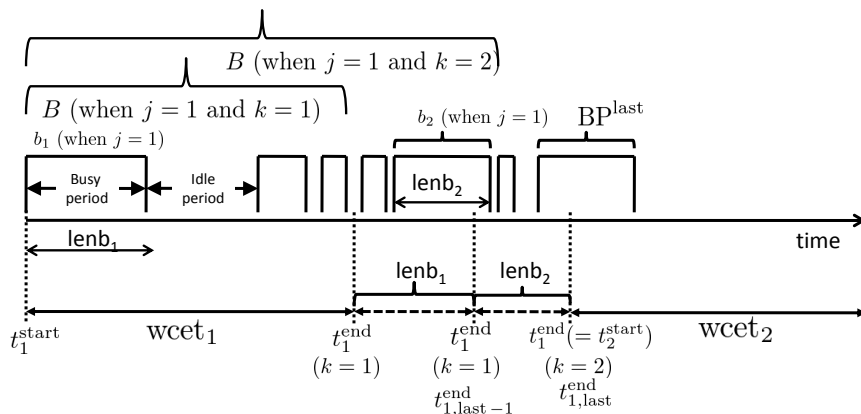


Figure 5.4: Visualization of the variables used in Algorithm 7. The task index is dropped in the wcet notation and only the region index j is retained

delay (assumed to be zero if B is empty) to the current request k . As the request is delayed, the length of the region is extended, which is reflected by the increase of t_j^{end} at line 13. Finally, the increased WCET C'_i of τ_i corresponds to the end of last region, NSR_i and is captured in the variable $t_{NSR_i}^{end}$, which is returned at the end of the entire analysis.

Note that the increased WCET (C'_i) being less than the deadline D_i does not automatically imply that τ_i is schedulable (i.e., will meet its deadline when scheduled with other tasks). All the tasks parameters (including their increased WCET) have to be further provided as an input into a schedulability analysis tool, which will assess the system schedulability by also considering the on-core interference. The focus of this work is to compute the increased WCET; the schedulability analysis should be carried out using existing approaches.

5.5.4 Proof of safety of Algorithm CompConDelay()

Next we provide a proof that our method indeed computes an upper bound, as desired, on the execution time of a task including the delays due to accesses to PCM.

Lemma 7. *The value of C'_i returned by Algorithm 7 is a safe upper-bound on the execution time of τ_i , considering the contention on the shared memory.*

Proof. The proof is obtained step-by-step, by examining the properties of all the time-instants t_j^{end} computed by the algorithm. Recall that j indexes the region being examined and k is used to index the request.

For the first region ($j=1$), the value of t_1^{end} computed at line 6 is an upper-bound on the completion time of the first region of τ_i , assuming that none of the requests generated by this region is blocked by higher-priority requests (see Figure 5.4). When $j=1$ and $k=1$, it can be seen that the value of t_1^{end} (re-computed at line 13) is an upper-bound on the completion time of this first request since it considers the maximum blocking for that request. Therefore, during the second iteration in the inner loop (i.e., when $k=2$), the

set B computed at line 8 is guaranteed to contain the maximum number of busy periods that can potentially be used to block a second request. This implies in turn that the value of t_1^{end} computed for the third time at line 13 (during this second iteration when $k = 2$) is an upper-bound on the completion time of the first region, assuming that two requests are blocked by higher-priority requests. The same reasoning can be applied for every subsequent request until the $(N_1^{\text{read}} + N_1^{\text{write}})^{\text{th}}$ request and thus, t_1^{end} is guaranteed to eventually provide an upper-bound on the completion time of the first region when all its requests can be blocked by higher-priority requests.

Note that during the last iteration (when $j = 1$ and $k = N_1^{\text{read}} + N_1^{\text{write}}$), t_1^{end} is increased for the last time at line 13. Let $t_{1,\text{last}-1}^{\text{end}}$ and $t_{1,\text{last}}^{\text{end}}$ denote the values of t_1^{end} before and after this last increase. To visualize this, let us assume in Figure 5.4 that the first region can generate only two requests. By construction of the algorithm, none of the busy periods starting within $[t_{1,\text{last}-1}^{\text{end}}, t_{1,\text{last}}^{\text{end}}]$ can be used to block any request generated in this first region (since there are no more requests from the first region to block). Among those busy periods, some may have their starting *and ending times* within this interval $[t_{1,\text{last}-1}^{\text{end}}, t_{1,\text{last}}^{\text{end}}]$ while *at most* one busy period may start within $[t_{1,\text{last}-1}^{\text{end}}, t_{1,\text{last}}^{\text{end}}]$ and end after $t_{1,\text{last}}^{\text{end}}$. Let us denote by BP^{last} this last busy period that overlaps $t_{1,\text{last}}^{\text{end}}$.

Regarding the busy periods that start *and end* within $[t_{1,\text{last}-1}^{\text{end}}, t_{1,\text{last}}^{\text{end}}]$, it is not interesting (in order to maximize the WCET) to assume that the first region finishes earlier than their starting times (i.e., at time $t_{1,\text{last}-1}^{\text{end}}$) so that requests from the second region can “use” these busy periods to increase the overall delay. Assuming so would imply that:

1. after $t_{1,\text{last}}^{\text{end}}$ time units of execution, τ_i is already progressing in its second region (while it could still be executing its first region without this assumption) and,
2. it uses some requests from the second region to take advantage of these busy periods (and these requests could be used later to further increase the overall delay).

However, in order to maximize the cumulative delay, it might be interesting to consider the busy period BP^{last} to block a request of the second region (this will be taken care of during the next iteration of the outer loop). To explore the second region, when $j=2$ (Line 4), the algorithm first computes the interval of time $[t_1^{\text{end}}, t_1^{\text{end}} + \text{wcet}_2]$, where the value of t_2^{end} is an upper-bound on the completion time of the second region, assuming that all the requests of the first region have incurred the maximum possible delay but none of the requests of the second region have been blocked by higher-priority requests. Then, the set B is computed (Line 8) and it can be seen that the busy period BP^{last} is included in that set, thanks to the second condition. By using the same reasoning as above, we can infer that after the $(N_2^{\text{read}} + N_2^{\text{write}})^{\text{th}}$ iteration in the inner loop (lines 7–16), t_2^{end} is an upper-bound on the completion time of the second region of τ_i . Following this reasoning, we can see that ultimately $t_{\text{NSR}_i}^{\text{end}}$ is an upper-bound on the execution time of τ_i . ■

5.6 Summary of the evaluations

The focus of the work is to compute the *increased interference due to the co-executing tasks and not obtaining the WCET or capturing the worst case memory profiling i.e., maximum number of cache misses for a given application*. The input is the worst case number of L2 cache misses and WCET obtained by running MediaBench benchmarks on Simics, which is a popular simulator for multi-core architectures [130]. The worst-case memory trace contains, for each memory request by the CPU, the time stamp, the type of request (read vs. write) and the physical address of the memory reference. The Simics configuration used to generate the traces has processors each speed of 1GHz x86 each with a L1 and a L2 cache. The L1 I-cache and D-cache are 4-way, 16KBytes with a cache line size of 64 bytes. The L2 is an 8-way, 512 KBytes unified instruction and data cache with a cache line size of 64 bytes. To re-iterate the inputs to the proposed method are

1. The WCET of the task in isolation, tasks assigned unique external priorities
2. An upper bound on the number of memory requests in each sampling region
3. The length of sampling region (20 ms)
4. Number of cores = 4
5. TR = 50ns and TW (500 ns)
6. Write queue buffer length (=32 here).

The benchmarks for this work were chosen from the MediaBench Test Suite [123]. MediaBench consists of a number of popular embedded applications for communications and multimedia. The suite includes codecs (encoders and decoders) for audio and video processing and programs for encryption, image compression and decompression. Each of these programs have different memory access behaviors and therefore serve as a good representative test suite [131]. Unless stated otherwise, unique external priorities are assigned based on the periods of the tasks as in the Rate Monotonic Algorithm [99]. Lower numbers indicate higher priority.

Demonstrating the idle and busy period schedule: Figure 5.5 is used to demonstrate the available of idle slots considering tasks of 3 different priorities (Priority 4, Priority 6 and Priority 7). The number of slots is restricted to 50 in this figure for clarity. As seen in the Figure, the Y axis represents the idle slots available to the tasks. There are 2 main observations from the graph.

1. The first busy period is the longest of all the busy periods in the schedule irrespective of task priorities. To ensure maximum interference, the analysis assumes that the co-executing higher priority tasks generate the highest possible number of memory

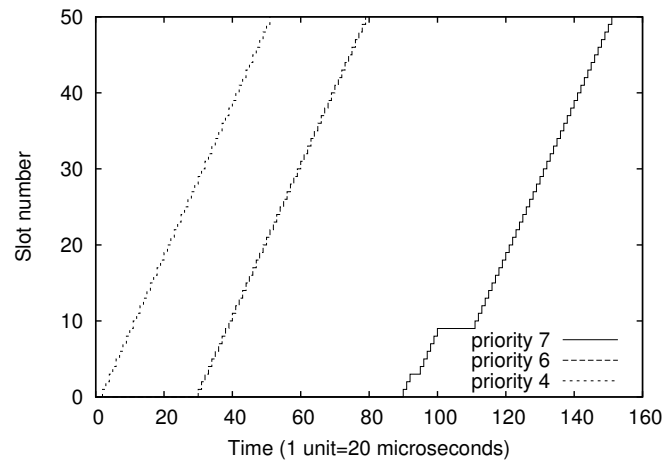


Figure 5.5: Slot Availability for tasks with different priorities

requests, while the analyzed task begins executing, in order to stall its progress. As seen in Figure 5.5, the first idle slot is available at the time 89 to the task with priority 7.

- Tasks with lower priority *may* have to wait longer to receive an idle slot, because they are prone to greater interference. Thus, to avail 50 idle slots, task with priority 7 (lowest priority) needs around 150 time units, while it is around 80 time units for a task with priority 6.

Comparison with the naive approach: Figure 5.6 illustrates the tightness of our proposed approach over the naive approach from Section 5.4. With the naive approach,

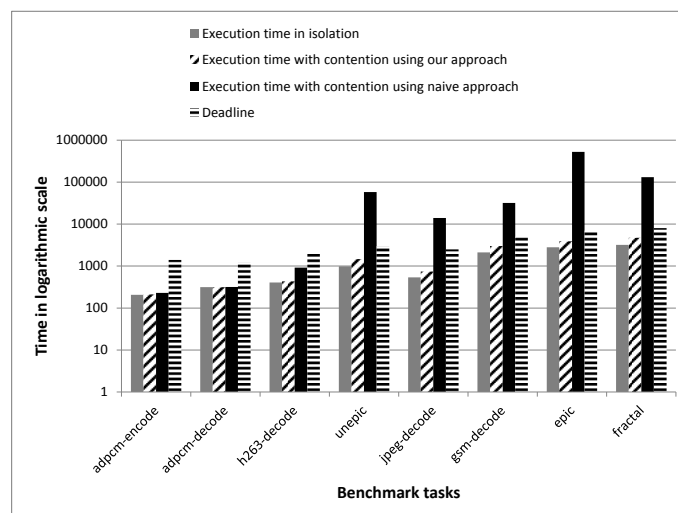


Figure 5.6: Comparison with the naive approach (Note: Y-axis is in log scale and 1 unit corresponds to 20 microseconds)

the WCET of many tasks exceeds the deadlines (in this case the tasks unepic, jpeg-decode,

gsm decode, epic and fractal). Epic and unepic are highly memory intensive tasks and thus issue a lot of memory requests and applying the naive approach to these tasks significantly increases their resulting execution times.

Correlation between Task Priorities and the Increase in the WCET: A counterintuitive result is that the impact of external interference from other cores cannot be directly co-related to their priorities, even with priority enforcements. While it generally holds that for the highest priority tasks, the external interference is smaller, this is not the case amongst all lower priority tasks (see Table 5.2). A task of lower priority might incur a lesser interference on its overall execution time than a task with a relatively higher priority. We denote the type of task with respect to their memory profiles: **Light**, **Moderate**, **Heavy**, and **Very Heavy** in the following tables. In this example in Table 5.2 it can be seen that task with priority 4, *unepic* which is highly memory intensive incurs a higher performance degradation than lower priority tasks. It faces interference from tasks with priorities 1 and 3, i.e, *adpcm-decode* which is a light task and *h263-decode* a heavy task. Since the analyzed task is memory intensive, as per the analysis, it incurs an delay for each request that it issues. In the same vein, it may also be noticed in the particular results that the *light* tasks incur relatively lesser interference than heavier tasks, irrespective of their priorities.

Benchmark	Priority	CoreID	%WCET increase	%Blocking	Type
adpcm-decode	1	1	1.17%	35.00%	L
adpcm-encode	2	0	1.90 %	21.47%	L
h263-decode	3	2	15.42%	17.53%	H
unepic	4	0	92.41%	11.05%	VH
jpeg-decode	5	3	34.03%	2.38%	M
gsm-decode	6	1	18.68%	0.43%	L
epic	7	2	60.12 %	1.30%	H
fractal	8	3	18.90 %	0.28%	L

Table 5.2: Contribution of blocking

Components of the Increase in WCET: As per the Algorithm CompConDelay, the increase in WCET can be attributed to 3 main components (i) the additional time for each write (ii) external blocking delay by lower priority non-preemptive writes (iii) external interference from higher priority tasks. In Table 5.2 we show, for each task, the blocking component as a percentage of the increased execution time, the other parameters and the memory-type of the task. It can be seen that the blocking delays contribute to a large percentage of increase in the WCET for the higher priority tasks. The impact on the lower priority tasks is smaller, especially for less memory intensive tasks.

Benchmark	Priority	%WCET increase	Memory Profile
adpcm-decode	1	1.17%	Light
adpcm-encode	2	1.90 %	Light
h263-decode	3	15.42%	Heavy
unepic	4	92.41%	Very heavy
gsm-decode	6	16.27%	Light
epic	7	52.13 %	Heavy
fractal	8	18.90 %	Light

Table 5.3: Removing a Moderate profile task of priority 5

Impact of removing a task As a proof of concept to ensure that priorities are respected and to study the effect of core assignments, the same tests were carried out by removing a task with priority 5 (jpeg-decode). In this case as expected, the higher priority tasks (1...4) did not see any changes while the tasks with lower priority than 5, with priorities 6 and 7 suffered lesser external interference. This is visible by comparing the respective values between Table 5.2 and Table 5.3. Also it may be observed, the task with priority 8 did not suffer any variation in the external interference, and this is because it was assigned to the same core as the task with priority 5.

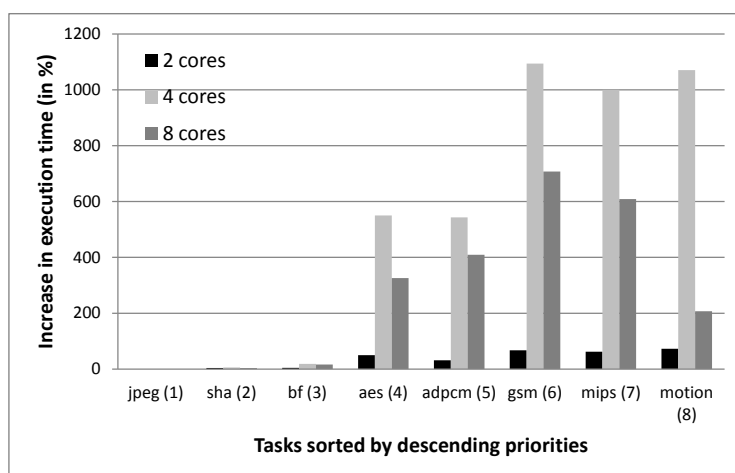


Figure 5.7: Tasks spread across 2, 4 and 8 cores

Impact of varying the number of cores: It has been observed that while the tasks with higher priorities are impacted marginally by scaling/increasing the number of cores, low priority tasks which are memory intensive are significantly impacted because of the increased external interference. Moreover, the average performance degradation per task increases as the number of cores accessing the same shared memory bus increases (and explains why the single FSB model does not scale and other inter-communication designs are warranted). In this example task set, the increase is 26%, 30% and 33% for 2, 4 and 8 cores, respectively.

1. **Impact of task mix:** As a proof of concept to ensure that priorities are respected and to study the effect of core assignments, the analysis with a reference task set was carried out by removing a task with a medium level priority. As expected, the higher priority tasks did not see any changes while the tasks with lower priority suffered less external interference.
2. **Impact of task assignments based on request densities:** To improve responsiveness, a possible intuitive scheduling algorithm is to prioritize tasks based on their memory request densities (more requests, higher priority, so that they finish earlier). With this set of experiments, we demonstrated that this strategy will lead to the performance degradation for most of the tasks. The effect is worse when highly memory intensive tasks with higher priorities arrive more frequently.

Our experiments show that the increase in execution time for tasks is a complex function of the task profiles (memory or computation intensive), the task assignments to cores, the priority enforcement mechanisms, and the temporal characteristics (the execution time and the period of tasks).

5.7 Chapter Summary

In this chapter, we delved deeper into the memory controller and modelled its scheduling. To ensure safe upper bounds, the impact of shared low-level resources on the timing behavior of tasks deployed on multicores must be taken into account while carrying out the timing analysis. In this chapter, we presented a method to compute the increase in the worst-case execution time of a task considering the contention on the shared Phase Change Memory. Our proposed method takes into consideration the different read and write latencies of the PCM controller, the priorities of the tasks, the request scheduling of the controller, and the interference arising from the co-executing tasks. Based on the request scheduling policy, the proposed method first determines the available slots in which the analyzed task can send its requests. The requests of the analyzed task are then assigned to the available slots such that its worst-case execution time is maximized. Our results using embedded benchmarks shows that there is a modest (for most real-time systems) increase in the worst-case computation time of a task, in comparison when the task is run in isolation; surprisingly, we noticed that the lower priority tasks do not always have a higher increase in execution time. Comparisons against a basic approach shows that the proposed method provides tighter upper bounds.

Chapter 6

NoC Contention Analysis of Many Core Systems

For over a decade prophets have voiced the contention that the organization of a single computer has reached its limits and that truly significant advances can be made only by interconnection of a multiplicity of computers.

Gene Amdahl in 1967

6.1 Introduction to many-core systems

The current trend in the chip manufacturing industry is towards the integration of previously isolated functionalities into a single-chip. Following this trend, the usage of multi-cores has become ubiquitous, not only for general-purpose systems but also in the embedded computing segment. Besides the increasing processing demand, advancements in the semiconductor arena have fostered in the “many-core” systems era and we are now witnessing the emergence of chips enclosing upto hundreds of cores. With the increase in the number of cores, the currently popular bus structure implementation prevents efficient scalability beyond eight cores in multicore processors where every memory request has to go through a central arbitration unit creating a critical bottleneck. To overcome this limitation, many-core designers developed a mesh-based tile architecture in which each building block called a tile consists of a processing core, a private cache plus a switch. This technology eliminates the single bus (bottleneck) by placing a communications switch on each processor core and arranging them in a grid fashion on the chip. This creates an efficient 2-dimensional traffic system for packets. Each tile in the grid is connected to its (up to 4) neighboring tiles located in the cardinal directions, thereby forming a 2D-mesh (c.f. right plot of Figure 6.1). The NoC serves as a communication channel among the cores

and between the cores and other off-chip subsystems, e.g. the main memory. Such many-core systems offer evident enhanced computational capabilities compared to the former (traditional) multi-core platforms. The Tile-Gx72 with 72 cores from Tileria [21], Kalray with 256 cores [22], Epiphany with 64 cores from Adapteva, Intel Xeon co-processor [23] with 60 cores and the 48-core Single-Chip-Cloud computer [24] are just some examples of many-core architectures. These systems like Kalray’s MPPA (Multi-Purpose Processor Array) have been optimized to address the demand of high performance, low power embedded systems and are therefore these architectures must be analyzed. In this document we focus on the structure and terminology of the Tile64 platform, but our analysis extends to other platforms which fits the assumed system model.

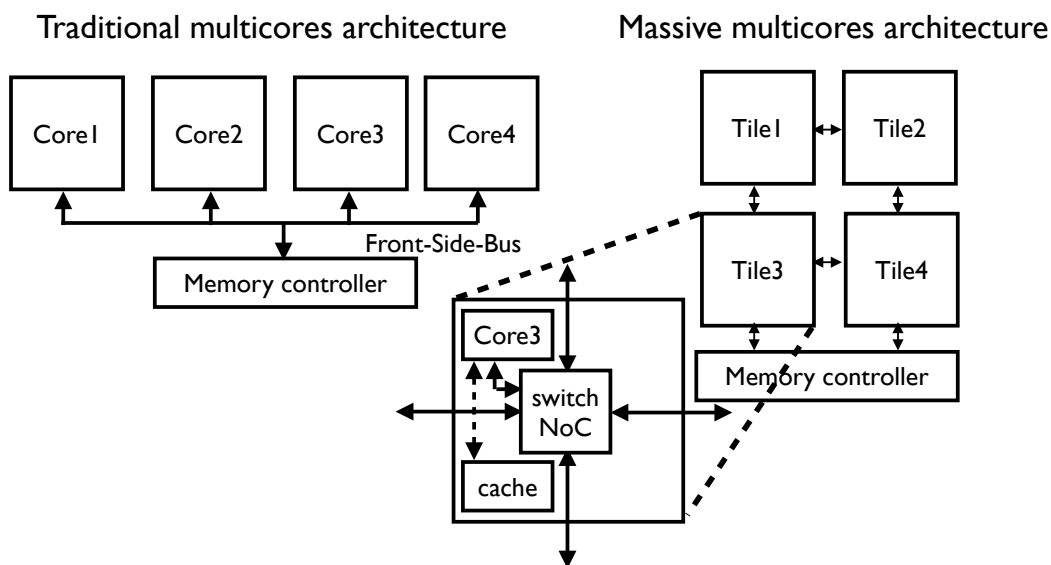


Figure 6.1: Multi-core vs. many-core systems

6.1.1 Motivation: Real-time applications and many-core systems

Although many-core systems offer various opportunities in terms of performance and computing capabilities, they do pose many challenges for the deployment of real-time systems, which must fulfill specific timing requirements at run time – It is therefore essential to identify, at design time, the parameters that have an impact on the execution time of the tasks deployed on these systems and the upper bounds on the other key parameters. It is also vital to *derive an upper bound on the execution time of these applications at design time itself* before these applications can be deployed — but this is non-trivial, for the reasons stated below.

In a scenario involving data transfers (amongst cores or from cores to memory), the execution time of a task running on a given core increases as the core stalls waiting for the data to be transferred over the underlying network. This waiting time can lead to a substantial increase in the execution time when the traffic on the network and thus

the contention for the network resources increases. Additionally, depending on their respective behavior, tasks running on different cores may release packets over the network independently and asynchronously. All the packets are transmitted over the same underlying interconnection network and share the available network resources like links and finite sized buffers (which prohibit the constant influx of packets after reaching a given limit). Thus the time to transmit a packet depends on the current load of the network, which is in turn determined by the number of packets generated by the tasks executing on the other cores. Other factors like the routing mechanism employed also impacts the traversal times as it influences the path taken by the packets to reach their destination –this in-turn decides whether they would directly or indirectly block the analyzed packet by contending for the same resources. The contention for the shared network thus leads to a substantial increase in the resulting traversal time of the analyzed packet. Additionally, tasks on different cores can release packets at arbitrary times on the shared communication infrastructure and these exact release time-instants are not known beforehand. To summarize, the number of parameters contributing to the unpredictability combined with the large number of cores poses a challenging problem to designers aiming to determine an upper bound on the traversal time of a (message/memory/IO) packet. In this work, we aim to compute such an upper bound which we refer to as the worst-case traversal time (WCTT) for a NoC based many-core system employing a wormhole switching technique [132].

The focus of this chapter is to determine an upper bound on the *traversal time* of a packet when it is transmitted over the NoC infrastructure. Towards this aim, we first identify and explore some limitations in the existing recursive-calculus based approaches to compute the worst-case traversal time (WCTT) of a packet. Then, we extend the existing model by integrating the characteristics of the tasks that generate the packets. For this extended model, we propose an algorithm called “Branch and Prune” (BP). Our proposed method provides safe and tighter estimates than the existing recursive-calculus based approaches. Finally, we introduce a more general approach - “Branch, Prune and Collapse” (BPC) which offers a configurable parameter that provides a flexible trade-off between the computational complexity and the tightness of the computed estimate. The recursive-calculus methods and BP present two special cases of BPC when the trade-off parameter is set to 1 or ∞ , respectively. Through simulations, we analyze this trade-off, reason about the implications of certain choices and also provide some case studies to observe the impact of task parameters on the WCTT estimates.

6.2 Related Work

A significant amount of research has been carried out on exploring the impact of the interconnect networks in systems employing wormhole switching [133]. In the works of [134] and [132], the respective authors elaborated on the estimation of end-to-end delays for wormhole switching networks, but with the primary focus on the determination of the

average latencies using queuing theory techniques. As mentioned earlier, in real-time systems, estimation of the worst case latencies rather than average case latencies is vital. Hence the earlier approaches do not suffice to perform a real-time analysis.

To ensure predictability and derive an upper bounds on the communication delay, some researchers have used mechanisms which require special hardware support to the NoC as in [135], priority mechanisms [136], time-triggered systems [137] and time division multiple access (TDMA) [138]. All these approaches assume that the basic NoC is designed to support predictability, but as seen in a survey of NoCs [139], existing commercial of the shelf (COTS) based NoC architectures are more suited to provide best effort service and hence to model the existing systems, a software-based analysis is warranted.

The existing works which address the issues of the worst-case end-to-end communication latencies in standard NoC-based many-cores can be broadly categorized into two groups: approaches applying network calculus and approaches applying Recursive calculus (RC). We borrowed the terminology RC from a previous approach [140].

Network Calculus (NC) based methods: In general queuing networks, network calculus [141] provides an elegant way to express and deal with the timing properties of traffic flows. Based on the powerful abstraction of arrival curves for traffic flows and service curves for network elements like routers and servers, it facilitates the computation of the worst-case delay and backlog bounds. For wormhole switching based networks, flow control is based on feedback received from the next router (downstream router). Determining the service curve of a given router independently (without the knowledge of the service curve of the next router involved in the transfer) is not straightforward by the basic abstractions provided by network calculus theory (which is designed to deal with forward networks) since there is a cyclic dependency between the service curves of the routers involved in the transfer.

To overcome this, Qian et.al [142] have modeled the flow control mechanism in the switch itself as another service curve. But in another related work by Ferrandiz et. al [143] clearly showed with an illustrative example the flaws of the design. The authors [143] consider a space wire network topology and introduced a special network element called the “wormhole section” to describe the wormhole routing with the network-calculus terminology. This element envelopes a set of routers lying in the shared path between an analyzed flow and the blocking flow(s): the analyzed and the blocking flows enter the first router and exit through the last router of the wormhole section, with no additional blocking flows either entering or leaving from any other link within the wormhole section. The analysis treats this section as a single element, with the arrival and service curves computed as a function of the individual curves of the flows contained within the section. Finally, an end-to-end service curve is derived by combining the service curves of all the wormhole sections in the path of the analyzed flow. In the presence of diverse traffic (with intersecting blocking flows with short shared paths), the direct application of this method

on the NoC-based many-core platform would force a wormhole section fragmentation, i.e. every router would be treated as an individual element, which renders the purpose of the wormhole section obsolete, and the results pessimistic.

Recursive Calculus (RC) based methods: The methods centered around this paradigm compute the end-to-end delays by recursively analyzing the contention at each router in the path of the analyzed flow. As a common denominator in these approaches is the rationale that flows inject packets at the maximum rate to saturate the network. The initial assumption of these approaches is that all the intermediate buffers in the switches between the source and the destination are filled to their capacity [140]. The method thus ensures capturing the worst-case scenario.

The works of Lee et. al [144], Rehmati et. al [145] and Ferrandiz et. al [146] have been noteworthy in this area. Initially, Lee et. al [144] proposed a model for real-time communication in wormhole networks based on the use of real-time wormhole channels. This was improved by Rehmati et. al [145] by computing real-time bounds for high bandwidth traffic in which they assume that all intermediate buffers are full, and for low latency regulated traffic, the concept of lumping flows is combined with the method of Ferrandiz et.al [146]. Lu et.al [147] proposed a contention tree based approach focused on feasibility analysis for a set of periodic messages with pre-assigned priorities, which were used to resolve arbitration conflicts in the switch. Their model does not classically fall into the recursive calculus based methods but it introduced the concept of contention trees (to capture direct and indirect blockings) which are analyzed in a recursive manner and thus conceptually fits in this category (and not in the NC based approaches).

In the approach proposed by Ferrandiz et.al [146], which is conceptually similar to the method of Rehmati et.al [145], an upper-bound on the traversal delay is computed, but with the assumption that the packets can be injected into the network continuously and therefore the computed WCTT is not tight.

The key advantage of these methods is that they compute the WCTT with low time complexity, but the main limitation is that they do not leverage the input arrival patterns and hence lead to over-approximations of the WCTT. Hence a method which provides tighter WCTTs in acceptable times is warranted.

Positioning our approach: In a very recent work by Ferrandiz et. al [140], the authors compare their newly proposed NC method against their previous RC method considering different parameters. In our approach we combine the best of both methodologies - an ability to exploit the simplicity and intuition behind RC methods without losing the input traffic characterization provided by NC methods. We first identify the key sources of pessimism in RC methods and introduce methods to characterize the traffic patterns. We then formulate a “Branch and Prune” algorithm which leverages these input characteristics in order to eliminate packets which cannot arrive at run-time owing to task constraints and

thus derive tighter bounds than the existing methods. We also propose a more general approach called “Branch, Prune and Collapse” which through a controllable parameter, offers the designer a trade-off between the tightness of the bound and computational complexity. By performing the simulations, we validate and verify the performance of our algorithm in comparison with the RC-based approach presented by Ferrandiz et. al [146] and observe that our approach dominates this method by yielding at least as tight as and in most cases tighter WCTT estimates than the related work. We investigate the influence of the trade-off parameter on the derived bounds.

The rest of the chapter is organized as follows: Section 6.3 describes the basic system model followed by the input characterization in Section 6.4. A brief description of the approach presented by Ferrandiz et.al [146] is described in Section 6.5. We introduce the basis of our method in Section 6.6. We propose the Branch and Prune algorithm in Section 6.7 followed by its variant in Section 6.8. The evaluations of the approaches are presented in Section 6.9. We finally summarize the work in Section 6.10.

6.3 System Model

6.3.1 Platform and Application Model

Platform model As previously noted, without loss of generality we drive our discussion in the context of tile-based platforms from Tilera. As seen in Figure 6.2, the tile-based architecture uses a 2D-mesh network to interconnect the processors and serves as the transport channel for off-chip memory access, I/O, interrupts, and other communication.

As illustrated in Figure 6.1, each tile comprises a general purpose processing engine (core), a cross-bar switch and a private cache. The platform is thus structured as a grid of $m \times n$ tiles, where “m” and “n” are the dimensions of the grid and r off-chip subsystems (e.g. memory controllers).

Another variation is the Intel SCC with the specification below:

Example 5. *The IA core on the SCC is based on the P54C core. The 48 cores are placed in a tile formation with 2 cores per tile and are connected by a $6 * 4$ 2D mesh fabric. Each of the P54C is a simple in-order processor having 2 level caches with on core L1 (16KB data, 16KB instruction) and unified 256KB L2. Each caches level are private to a given core so that there is no concurrent access to the cache between cores [148].*

Our model conforms to the above architecture, but by assuming a single tile per core to simplify the discussion. The off-chip subsystems are connected to some of the tiles on the periphery of the grid. Inter-tile communication is achieved by routing packets via the embedded switches. Note that the terms router and switch are used interchangeably in the rest of the chapter.

Each tile contains a switch engine. The switch engine connects to neighboring tiles and I/Os (including the on-chip memory controllers) via the intra-tile network. The tiles

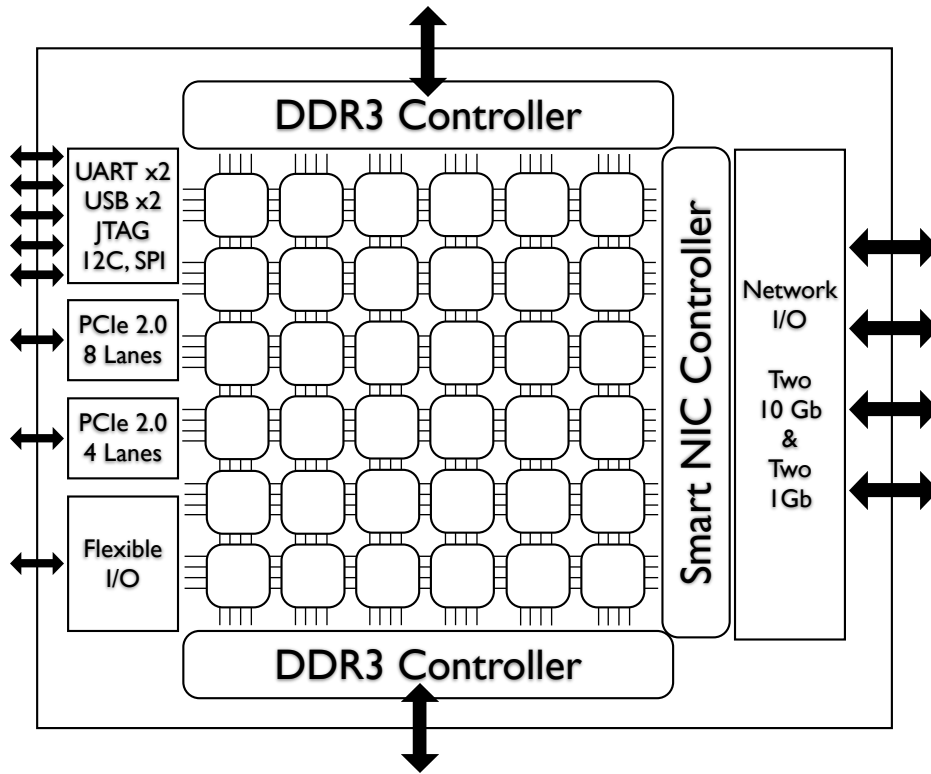


Figure 6.2: Tiler architecture. (Diagram taken from [21])

are laid out in a two dimensional grid, thus the switch engine connects to the neighbors to the north, south, east, and west. The switch engine connects directly to I/O devices if a tile is adjacent to an I/O device. Generally, the switch that is embedded in each tile is part of several networks. Independent networks are typically used to handle different types of traffic to minimize the interference and maximize the performance. For example, the TILEProTM and TILE64TM family of chips employ distinct networks to transmit traffic related to memory, caches, I/O and inter-tile communication between applications. Since a packet can travel (and interfere with other packets) only over one of the networks, the analysis of the WCTT of a given packet can be carried out by considering each network individually. Hence, the analysis presented in this chapter considers only the relevant inter-tile communication network.

The entire platform can thus be modeled by a directed graph $\mathcal{G}(\mathcal{N}, \mathcal{L})$, where

- $\mathcal{N} = \{n_1, n_2, \dots, n_{2m*n+r}\}$ is the set of $2m * n + r$ nodes comprising $m * n$ switches, $m*n$ cores and the r off-chip subsystems (caches are considered part of the processing cores) and
- \mathcal{L} is the set of directed (physical) links that interconnect the switches to the cores, to other switches or to the off-chip subsystems.

For a given link $l \in \mathcal{L}$, we denote by $lsrc(l)$ and $ldest(l)$ the source and destination node of the directed link, respectively. A bi-directional link is modeled by using two links in opposite directions and all the links have the same capacity denoted by C . We assume that the links support full-duplex transmission with the interpretation that request and response packets can be simultaneously sent across a tile and will not contend amongst each other for the link. Our model is applicable to any generic platform which can be modeled as a graph and hence is not restricted to the Tile64 platform.

Application Model As a first step, we assume that there is a 1:1 mapping between applications (called tasks hereafter) and cores; each task τ_i is non-preemptive, statically assigned to a dedicated core and does not migrate during its execution. We also assume that the cores do not support hyperthreading. The assumption of a single task is made to focus on the network latency delays, while efficiently abstracting away the problems of on-core interferences and dealing with the processor scheduling policies.

We assume a 1:1 task-to-core mapping

6.3.2 Switching and Routing Mechanism

Data is transmitted over the network, embedded in “packets”. A packet comprises a header containing the destination address and a payload, which contains the actual data to be transmitted.

6.3.2.1 Switching Mechanism

The switching technique defines how connections are established in the network. Ideally, connections between network resources are established or “switched in” only for as long as they are actually needed and exactly at the point that they are ready and needed to be used. This allows for efficient use of the available network bandwidth by the contending traffic flows while minimizing the latency of transmission of data.

Connections at each hop along the topological path that are allowed by the routing algorithm and granted by the arbitration algorithm can be established in three basic ways: prior to packet arrival using *circuit switching*, upon receipt of the entire packet using *store-and-forward packet switching*, or upon receipt of only portions of the packet with unit size no smaller than that of the packet header using *cut-through packet switching*.

In this work we consider a form of cut-through switching called the buffered wormhole switching mechanism. Every packet sent over the network is split into smaller irreducible units called flits (Flow control digITS). The packet is divided into the header flit, body flits and the tail flit. The header flit is the first flit of each packet which stores the destination address and arbitrates for a given output port at a switch. Each flit size is no smaller than the header flit. Specifically, when a packet is granted access to an output

port, it locks down that output port until its last flit has successfully traversed the switch. Since the subsequent (data) flits do not store any information about the destination, they always follow the same path as the header flit. When the output port is unavailable, the subsequent flits remain buffered in finite (and typically small) sized buffers in the router, until the output port is freed. In order to ensure fairness in the arbitration, we assume that the switches implement round-robin arbitration as in [149]. We denote by d_{sw} , the time needed for arbitration and subsequently grant access to the output port to one of the pending packet. The value of d_{sw} is typically less than 25 μs for the Tiler platform [149].

We assume a *worm-hole switching mechanism* for connection establishment

6.3.2.2 Routing Mechanism

Routing algorithms can be categorized into two main classes: Deterministic routing algorithms and non-deterministic routing algorithms. Given the source and destination nodes, a deterministic routing algorithm decides on a single unique route – this implies that route determination is possible at design time itself. Alternately, an algorithm for adaptive routing dynamically decides the route while the packet is in progression and bases its decision on the network conditions. It can thus deal with the problem of congestion by dynamically redirecting packets towards a lesser congested route. Clearly, the trade off is between complexity versus the performance. Deterministic routing algorithms are simple to design but may not perform optimally. In contrast, adaptive algorithms have a better performance in choosing paths of low congestion, may produce shorter paths but as a downside are relatively complex to implement and hard to analyze.

An example of deterministic routing is *dimension ordered routing* in which a packet is sent along first dimension until destination co-ordinate in that dimension is reached. The packet is then turned and routed in the next dimension till the destination co-ordinate is reached. The model in this work considers an XY/YX dimension routed algorithm. In XY routing, packets always travel in the X direction first and then in the Y-direction. A key principle of dimension ordered routed algorithms is that they only allow a single turn in the entire path. As a result, when packets are routed in conformance to this mechanism, certain potential turns that form a cycle are prohibited and hence *deadlocks* are avoided.

The XY/YX routing algorithm is by design deadlock and livelock free [150] and is employed by many-core architectures like the Tile64 [149]. However, in general, our model can adapt to any static routing algorithm as long as it is *deadlock free*. While adaptive routing schemes are more efficient than the static ones, they are difficult to analyze at design time and hence are not considered here. In the analysis that follows, as a first step, we assume that every physical link implements only a single virtual channel hence allowing only a single packet at every input port of a router.

We assume a NoC routed using *deterministic, deadlock-free routing algorithm*

6.3.3 Communication and traffic modeling

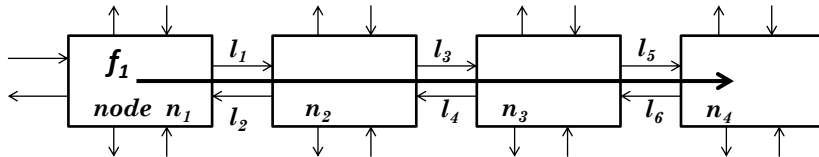


Figure 6.3: Example to illustrate the notations:

6.3.3.1 The basic flow model

The network traffic between two tasks or between a task and an off-chip subsystem is modeled by a *flow*. Each flow f is characterized by an origin and a destination node, denoted by $\text{fsrcnode}(f)$ and $\text{fdestnode}(f)$ (respectively) and a maximum packet size denoted by $\text{maxsize}(f)$. In order to reach its destination, every packet of a flow f is routed throughout the network over a pre-defined static *path* defined by an ordered list of *links* and denoted by $\text{path}(f)$. The number of hops traversed by the packets of f along this path is given by $\text{nbhops}(f)$. Also, we denote by $\text{first}(f)$ the first link of $\text{path}(f)$ and we use the notations $\text{prev}(f, l)$ and $\text{next}(f, l)$ to refer to the links directly *before* and *after* the link l in $\text{path}(f)$, respectively. We denote by $\text{lsrc}(l)$ and $\text{ldest}(l)$ the source and destination node of the directed link l . Finally, \mathcal{F} denotes the set of all the flows in the system.

Example 6. Consider Figure 6.3. In this example, $\text{fsrcnode}(f_1) = n_1$ and $\text{fdestnode}(f_1) = n_4$ with $\text{path}(f_1) = \{l_1, l_3, l_5\}$. The number of hops is given by $\text{nbhops}(f_1) = 3$. Next, for flow f_1 at link l_3 , $\text{prev}(f_1, l_3) = l_1$ while $\text{next}(f_1, l_3) = l_5$. Finally, the source and destination of link l_5 is represented as $\text{lsrc}(l_5) = n_3$ and $\text{ldest}(l_5) = n_4$.

6.3.3.2 Our extended model

We augment the simple model given above by distinguishing between two types of packet-release profiles, namely *regulated* (Reg) and *unregulated* (UnReg) flows.

Definition 20. A *regulated flow* models a sporadic communication between two nodes, with the interpretation that a packet of a regulated flow f can be released after a specific minimum duration after receiving the acknowledgement of the previous packet of the same flow from the destination node. This minimum time duration is referred to as the *minimum non-sending time* of the regulated flow f and is denoted by $\text{MinNonSend}(f)$.

The term non-sending is used to express the time span in which there is an application introduced delay. In practice, $\text{MinNonSend}(f)$ represents the application-specific delay (on

the core) before another packet can be generated: it may be an explicitly defined waiting phase or time spent for processing. A stream of video frames which must be transferred to an off-chip graphic controller is an example of a regulated flow.

Definition 21. *An unregulated flow, models an aperiodic communication between two nodes: the source node can release a packet at any instant in time after the receipt of its previous packet has been acknowledged, i.e., for all unregulated flows f , $\text{MinNonSend}(f)$ is null.*

Data transfers between a task and the system memory at arbitrary times due to random cache misses serves as an example of unregulated flows. It is important to re-iterate that our model inherently assumes “blocking” communication: any packet of a given flow can be generated only after the receipt of the acknowledgement of the previous packet.

6.4 Input Traffic Characterization Functions

In this section, we introduce two functions associated with each flow, namely the *minimum inter-release time* function and the *maximum packet release* function.

6.4.1 The minimum Inter-Release Time Function

Definition 22. *The Minimum Inter-Release Time function $\text{MinInterRel}(f)$ of a flow f is the minimum time gap between two consecutive packets released by f .*

Specifically, if p_1 and p_2 are two consecutive packets generated by flow f , then $\text{MinInterRel}(f)$ is the sum of (i) the minimum time needed to deliver *and acknowledge* p_1 — sometimes referred to as the round-trip time of p_1 — and (ii) the application-specific minimum delay that must elapse before the release of p_2 , i.e., $\text{MinNonSend}(f)$. We then compute $\text{MinInterRel}(f)$ as:

$$\text{MinInterRel}(f) = \text{MinDest}(f) + \text{MinDest}(ack) + \text{MinNonSend}(f) \quad (6.1)$$

where $\text{MinDest}(f)$ is the minimum time taken by a packet of f to travel from its source $\text{fsrnode}(f)$ to its destination $\text{fdstnode}(f)$. Note that $\text{MinInterRel}(f)$ differs from $\text{MinNonSend}(f)$ as it also includes the minimum time needed to send a packet of flow f and receive its corresponding acknowledgement. As a direct consequence of the need for acknowledging a packet, the following property holds.

Property 3. *No two packets of the same flow f can reach a given router separated by a time gap of less than $\text{MinInterRel}(f)$ time units.*

Note that these parameters are computed in isolation (i.e. without any contention from the other flows). Since the objective is to determine the WCTT of a given packet (say p), we must be able to capture the worst-case scenario in which the blocking flows can

cause maximum interference to any packet of the analyzed flow. We must therefore have a parameter which represents a *lower-bound* on the inter-release time of all these blocking flows and so a lower-bound on $\text{MinDest}(f)$ for all flows $f \in \mathcal{F}$. We shall use the following result.

Definition 23. *For the wormhole routing technique, the minimum time-to-destination $\text{MinDest}(f)$, for any given flow $f \in \mathcal{F}$, is given by*

$$\text{MinDest}(f) = \text{nhops}(f) \times (d_{\text{sw}} + d_{\text{across}}) + \frac{\text{minpsize}(f)}{C} \quad (6.2)$$

where d_{across} is the time for a flit to be read from an input buffer, traverse the crossbar (the switch) and reach the storage at the input of a neighboring switch.

The above equation can be interpreted as follows. The term $\text{nhops}(f)$ denotes the number of hops that the first (header) flit of the packet of f traverses while travelling from its source to destination. While traversing the network, the first flit locks down all the output ports on its path and at each intermediate switch, it incurs an arbitration delay of d_{sw} and a time of d_{across} to traverse the crossbar. In our model, d_{across} also accounts for the maximum time it takes to transfer flow-control tokens between the routers. Once this first flit reaches the destination, all the traversed output ports from its source to its destination have been locked down and the entire packet of size $\text{minpsize}(f)$ can travel over the network of capacity C , which requires $\text{minpsize}(f)/C$ time units. Hereafter, Equation (6.2) will be used as the value of $\text{MinDest}(f)$.

6.4.2 The Maximum Packet-Release Function

Definition 24. *The Maximum Packet Release Function $\text{MaxPcktRel}(f, t)$ of a flow f provides an upper-bound on the number of packets that f can generate in a time interval of length t .*

This function is computed considering that the task (initiating the flow) is run in isolation, i.e., without any contention from other packets on the network and hence can be determined at design time. Methods to compute an upper bound on the number of requests issued by a task in a given time interval have been proposed by [91], [80] and [79].

For *regulated* flows, the maximum packet release function can be expressed based on the minimum inter-release time of the given flow as in Equation (6.3), since their minimum non-sending time is clearly defined and integrated into their minimum inter-release time.

$$\text{MaxPcktRel}(f, t) = \left\lceil \frac{t}{\text{MinInterRel}(f)} \right\rceil \quad (6.3)$$

However, for *unregulated* flows, computing $\text{MaxPcktRel}()$ with the same approach may lead to an over-estimated number of packets, especially for large values of t . To overcome this pessimism in the computation, we can apply the method proposed in [91]. Although

the exact time-instants at which unregulated flows generate packets are not known, these methods calculate this parameter by instrumenting the task code at different sampling points when the task executes in isolation and uses this information to derive an upper bound on the maximum number of packets it can generate in any time interval of duration t . Note that the $\text{MaxPcktRel}(f, t)$ function roughly corresponds to the arrival curve abstraction used in network calculus theory.

6.5 Conceptual description of existing RC based methods

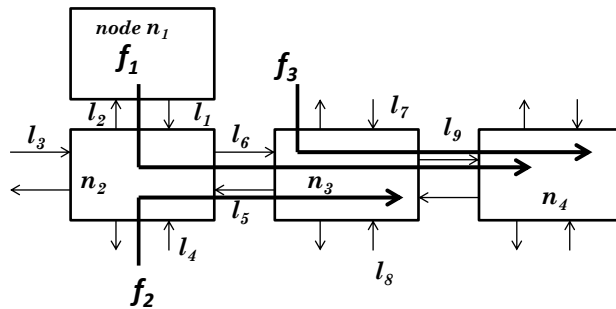


Figure 6.4: Example to illustrate the approach in [146]

To understand the concepts behind the recursive calculus based method, we present an algorithm to compute an upper bound on the traversal time of a packet of flow f from its source to the destination node. This will represent the approach proposed by Ferrandiz et. al [146] and is conceptually similar to that of Rehmati et.al [145].

Let us consider the part of Figure 6.4. There are four nodes n_1, n_2, n_3, n_4 and three flows: f_1, f_2 and f_3 . All the flows terminate at the core n_4 . Flow f_1 originates in n_1 and the source nodes of f_2 and f_3 are not specified in this example.

Let us compute the WCTT of flow f_1 for which $\text{fsrcnode}(f) = n_1$, $\text{fdestnode}(f) = n_4$ with $\text{path}(f) = \{l_1, l_6, l_9\}$ denoting the links that it traverses from the source to the destination. The process commences by invoking the function $d(f_1, l_1)$ (Algorithm 8). Since link l_1 is the first link in the path of flow f_1 , it could be blocked only if other flows generated by its source (core n_1) have to transit first. This particular case has been handled in earlier methods but in contrast to their approach, we assume that the core stalls while waiting for a given packet transmission to be completed before initiating a new transmission. Therefore, under this assumption, a flow f issued from one core can never be blocked by another flow issued from the same core and the first flit of the packet is directly transferred to the (top) input port of the switch n_2 . Thus, the algorithm directly calls the function $d(f_1, l_6)$ at line 1. At this stage, the flow f_1 traverses via link l_1 and next passes through l_6 via node n_2 .

The set of potential blocking links comprises those previously unexplored links for which the destination matches with the current destination of the analyzed link. Accordingly at

Algorithm 8: $d(f, l)$

```

input : a flow  $f$ , a link  $l$ 
output: WCTT of  $f$ , starting from link  $l$ , to the destination.
// there cannot be any contention on the first link.
1 if  $l = \text{first}(f)$  then return  $d(f, \text{next}(f, l))$  ;
/* Header flit reaches end of path and the entire packet transits */
2 if  $l = \text{null}$  then return  $\frac{\text{maxpsize}(f)}{C}$  ;
/* Determine the set of links excluding  $\text{prev}(f, l)$  and whose destination
node is  $\text{lsrc}$  */
3  $\text{BL} \leftarrow \{l_{\text{in}} \in \mathcal{L} \mid l_{\text{in}} \neq \text{prev}(f, l) \wedge \text{ldest}(l_{\text{in}}) = \text{lsrc}(l)\}$ ;
4 foreach  $l_{\text{in}} \in \text{BL}$  do
| /* Determine the set of flows  $f_{\text{in}}$  that use link  $l_{\text{in}}$  and have  $l$  as the
| next link */
5 |  $U_{l_{\text{in}}} \leftarrow \{f_{\text{in}} \in F \mid l_{\text{in}} \in \text{path}(f_{\text{in}}) \wedge \text{next}(f_{\text{in}}, l_{\text{in}}) = l\}$ ;
6 end
7  $\text{delay} \leftarrow \sum_{l_{\text{in}} \in \text{BL}} \max_{f_{\text{in}} \in U_{l_{\text{in}}}} \{d_{\text{sw}} + d_{\text{across}} + d(f_{\text{in}}, \text{next}(f_{\text{in}}, l))\}$ ;
8 return  $\text{delay} + d_{\text{sw}} + d_{\text{across}} + d(f, \text{next}(f, l))$  ;

```

line 3, the algorithm computes the set of links, BL, connected to the other input ports of n_2 (i.e., the links excluding l_1). Here, $\text{BL} = \{l_3, l_4, l_5\}$.

Then, for each of the links $l_{\text{in}} \in \text{BL}$, the algorithm determines the set $U_{l_{\text{in}}}$ of blocking flows which pass consecutively through the next link in the path of the analyzed flow i.e., l_6 . Here $U_{l_4} = \{f_2\}$ and the other sets (U_{l_3}, U_{l_5}) do not have flows matching the criterion stated above and are therefore empty. Note that exactly one blocking flow of each set $U_{l_{\text{in}}}$ may block f_1 since the switch follows a round-robin arbitration mechanism. Therefore, to maximize the delay, for each link l_{in} in BL, the algorithm explores all the flows f_{in} in $U_{l_{\text{in}}}$ by recursively invoking $d(f_{\text{in}}, \text{next}(f_{\text{in}}, l))$ and then chooses the flow which maximizes the delay in line 7. It then computes the cumulative delay by summing up the maximum delays obtained for each $l_{\text{in}} \in \text{BL}$. After the blocking flows are allowed to progress at the current link, the flow being analyzed, f_1 can progress to its next link. At line 8, the algorithm returns the cumulative delay computed in line 7 plus the time for the flow f_1 to traverse through n_2 (i.e., d_{sw}), plus the delay suffered by f_1 in the next hop, i.e., $d(f_1, \text{next}(f_1, l_6)) = d(f_1, l_9)$. Notice that at line 2, if $l = \text{null}$, then it implies that the flow f has reached its destination. In this case, the packet of f is fully transmitted, which requires, in the worst-case, $\frac{\text{maxpsize}(f)}{C}$ time units.

6.6 Proposed method for tighter WCTT

In order to compute a tighter WCTT, we first explore the sources of pessimism in the previous approach and then describe the methods to deal with it.

6.6.1 Sources of Pessimism

Although the computation presented in the previous section is correct and terminates within a reasonable computation time (as shown by [146]), we identified two main sources of pessimism. In order to highlight this pessimism, we constructed a computation tree as shown in Figure 6.5 based on Algorithm 8. In this tree, each recursive call to the function $d(f, l)$, with $l \neq \text{null}$, is a (non-leaf) node of the tree and each call to $d(f, \text{null})$ is a leaf node. Algorithm 8 traverses this computation tree in a *pre-ordered depth-first* manner: first the root node is visited and then each of the children are visited, from the left to the right.

As seen in Figure 6.5, the order in which the leaf nodes of the computational tree are reached reflects the following scenario. The flow f_1 is delayed because f_2 goes first through l_6 (step ①). f_2 is then blocked by f_3 at node n_3 . Once f_3 has reached the core n_4 , its whole packet is transferred to n_4 , hence adding $\text{maxsize}(f_3)/C$ to the delay (step ②, the first “leaf”). Then f_2 flows and reaches the core n_4 (step ③), followed by f_1 which passes through n_2 but gets blocked by another flow of f_3 in n_3 . This second flow of f_3 passes first (step ④) and finally f_1 can progress to its destination (step ⑤).

As a conclusion, the scenario considered by the computation of $d(f_1, l_1)$ assumes that f_3 blocks the flow f_1 twice before it finally reaches the core n_4 . These multiple blockings may not be possible for several reasons and can lead to an overestimation of the WCTT. In the next subsection we explore these reasons which we refer to as the “sources of pessimism” and propose methods to overcome them.

6.6.2 Network-level Pessimism

The basic premise behind earlier approaches was the assumption that every flow injects traffic continuously into the network, thereby assuming that for all flows, the packets do not expect any response and have no temporal constraints on their generation. In practice, the application initiating a flow may dictate that two consecutive packets cannot be generated separated by less than a minimum time gap (given by the $\text{MinInterRel}()$ functions). As

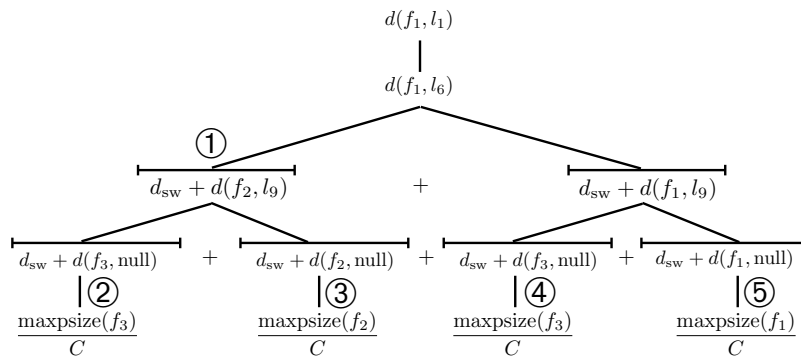


Figure 6.5: Computation tree of $d(f_1, l_1)$.

seen in the previous section, this minimum time gap cannot be null as it includes the round-trip communication delay incurred due to the underlying network. In a large setup, on ignoring these “minimum round-trip time” constraints, the delay incurred as a result of these non-feasible contentions can cascade and increase in magnitude as the flow path unrolls, ultimately leading to highly pessimistic WCTT estimates.

In the example of Figure 6.4, it is seen that flow f_3 blocks f_1 twice: once indirectly by blocking f_2 and once directly in step ④. However, because of its round-trip time constraint it may not be possible for flow f_3 to release a second packet by the time flow f_1 transits through node n_3 . Thus by taking into account this constraint, the analysis of the delay incurred by f_1 can be less pessimistic.

In order to tackle this source of pessimism, we introduce the notion of “current time” during the computation. The current time is initialized to 0 at the beginning of the analysis and it is then increased by $d_{sw} + d_{across}$ every time a flow traverses a router and by $\text{minpsize}(f_x)/C$ whenever a flow f_x reaches its destination. During the computation, whenever a flow f_x traverses a router n_k , the current time (denoted by t) is recorded and used as a time-stamp for this traversal, i.e., a time-stamp is attached to the pair $\langle f_x, n_k \rangle$. Then, in the time interval $[t, t + \text{MinInterRel}(f_x)]$, our proposed analysis will not recognize flow f_x as a potentially blocking flow in router n_k as it is not possible for f_x to have another packet at an input port of n_k in that interval of time in accordance with Property 3.

6.6.3 Task-level Pessimism

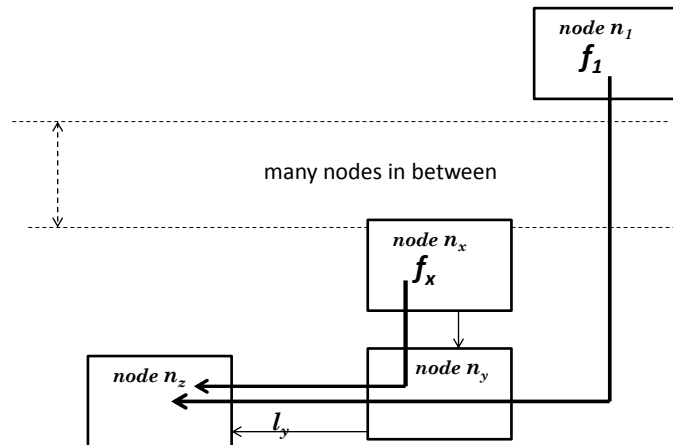


Figure 6.6: Example to illustrate task level pessimism

Intuitively, it may happen that many occurrences of a same flow f_x have to be considered by Algorithm 8 and none of them violates its $\text{MinInterRel}(f_x)$ constraint, i.e., at every router on f_x 's path, every occurrence of f_x is separated in time from the previous one by at least $\text{MinInterRel}(f_x)$ time units.

A manifestation of this situation can be seen in the example of Figure 6.6. Let us assume that the destination of the (dashed) flow f_1 is n_z , and that n_z is distantly located

from n_1 (in terms of number of hops). In addition, consider a flow f_x from the core n_x to n_z . When computing the WCTT of f_1 , chances are high that Algorithm 8 invokes the function $d(f_x, l_y)$ a significant number of times since it blocks all the flows directed to n_z . As stated above, in such a case the flow f_x may never violate the constraint imposed by $\text{MinInterRel}(f_x)$, as the distance between n_x and n_z is short, but at a given current time t during the analysis it may be the case that the task which initiates f_x is not able to generate that many packets in the time interval $[0, t]$. As a result, Algorithm 8 may return overly pessimistic WCTT estimates as it does not take into account the packet-release profile specific to each task.

This work proposes to tackle this source of pessimism by extending the solution for tackling the network-level pessimism. Instead of recording and maintaining a time-stamp only for the *last* occurrence of every flow f_x in every router n_k , we propose to save a time-stamp for *every* occurrence of all the flows in every router that they traverse. That is, for each pair of flow-router $\langle f_x, n_r \rangle$, we maintain the number of occurrences and the corresponding list of time-stamps reflecting all the time-instants at which f_x has traversed n_k during the computation. Let us assume t_0 is the time-stamp of the first occurrence of f_x in n_k . Then, at any current time t during the analysis, the flow f_x is deemed infeasible (and hence cannot potentially block the analyzed flow another time) if the number of recorded occurrences of f_x in router n_k exceeds $\text{MaxPcktRel}(f_x, t - t_0)$, which as described earlier, returns an upper bound on the number of packets generated by flow f_x in the specified time interval $(t - t_0)$.

6.7 The Branch and Prune Algorithm

This section introduces our “Branch and Prune” (BP) algorithm for calculating the WCTT of a packet released by a flow. While the basic principle of Algorithm 8, which consists of recursively tracking the progression of all flows throughout the network remains the same, our method differs from this algorithm in two aspects:

1. It considers the extended flow model presented in Section 6.3.3.2, in which the input traffic of the flows are characterized with specific functions and
2. It incorporates the ideas described in Section 6.6 to reduce the task- and network-level pessimism.

6.7.1 Overview of the Branch and Prune Algorithm

The basic principles of flow progression remain the same as in Algorithm 8. At each link l in the path of the analyzed flow f , we first determine the set of all flows that can potentially block f by accessing l first. Then, we enumerate all possible interfering scenarios for that link and we analyze each of them recursively. An interfering scenario is defined here as a flow sequence, i.e., an order of passage of the blocking flows over the considered link.

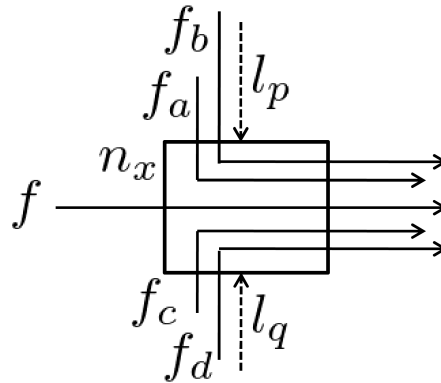


Figure 6.7: A simple example.

One of the main differences with Algorithm 8 is that we first branch-out, thereby enumerating all possible blocking flow sequences, then we validate if the flows in the sequence can arrive, given their task constraints and thereby prune the infeasible flows in each sequence. We compute and record the traversal times of these pruned sequences. Since the tests for constraint compliance are applied early-on in the computation, the resulting search space is greatly reduced. This is especially true for loaded networks wherein the impact of indirect contention of certain flows can cause the search space to grow exponentially. It can be seen that pruning an infeasible flow is equivalent to pruning the entire subtree of flows which would have blocked it later on (and would otherwise have to be explored by the algorithm, thereby increasing the search space).

6.7.2 Concepts behind the algorithm

The main steps of our approach are described here with a simple example, illustrated in Figure 6.7. Let us assume that f is the analyzed flow which traverses on its k th hop through the router n_x along its path to the destination. This implies that interfering flows of an earlier hop may have been already analyzed for their delay in node n_x .

6.7.2.1 Blocking Links and Flows

At every router in the path of f , we first determine the set of blocking links — those links which terminate at the same node as the analyzed link. In the given example, assuming that the analyzed link has router n_x as its destination, the set BL of blocking links at router n_x is given by $\text{BL} = \{l_p, l_q\}$. Then, for each blocking link l_{in} , we compute the associated set $U_{l_{in}}$ of blocking flows that can potentially block f in this router n_x . Here, $U_{l_p} = \{f_a, f_b\}$ and $U_{l_q} = \{f_c, f_d\}$.

At this stage, we still assume that all these blocking flows have a packet to transmit and are allowed to transmit it *before* the flow f progresses.

6.7.2.2 List of Interfering Scenarios

During the computation, the progress of all flows is ensured by the round-robin arbitration policy applied at each intermediate router, which implies that at most one packet from each of the blocking flows can block the analyzed flow f . At this phase, we are interested in finding the sequence of flows progression over the network that will delay f for as long as possible. To tighten the WCTT estimate by overcoming the limitations (sources of pessimism) presented earlier, at each router in the path of the analyzed flow we first enumerate all the possible flow sequences (called “interfering scenarios” hereafter) that might block it. Specifically, we denote by LIS the list of all possible “Local Interfering Scenarios” at the current router, assuming that the currently analyzed flow f is the last one allowed to progress. That is, at router n_x for example, LIS contains $\{f_a, f_c, f\}$, $\{f_a, f_d, f\}$, $\{f_b, f_c, f\}$, $\{f_b, f_d, f\}$, $\{f_c, f_a, f\}$, $\{f_c, f_b, f\}$, $\{f_d, f_a, f\}$, $\{f_d, f_b, f\}$, $\{f_a, f\}$, $\{f_b, f\}$, $\{f_c, f\}$, $\{f_d, f\}$, and $\{f\}$.

As a consequence of the pruning mechanism, there can be duplicate scenarios. These duplicates, when present, are eliminated by the algorithm. All the remaining scenarios are then investigated in order to eliminate any possible timing anomalies and ensure the safety of the algorithm. The necessity comes from the fact that any of the scenarios at a given router cannot be implicitly discarded, as the local maximum at a given router may not translate into the global maximum. For example, in the above LIS, we cannot ignore the scenarios $\{f_a, f\}$ – intuitively we may conclude that among scenarios $S1 = \{f_c, f_a, f\}$ and $S2 = \{f_a, f\}$, the scenario $S1$ is more likely to contribute to the WCTT, but it may not be so. In fact, $S2 = \{f_a, f\}$ may in the future progression, allow for flows contributing to a large interference to be included in the final WCTT while scenario $S1$ may prohibit it thus leading to a timing anomaly and also leading to an unsafe WCTT.

We traverse this LIS and investigate each interfering scenario individually. When considering $\{f_a, f_c, f\}$ for example, we first compute (recursively) the WCTT of f_a , then the WCTT of f_c and finally we allow f to progress to the next router on its path. However, before computing the WCTT of f_a (and the same holds for f_c later), we reduce the pessimism of the computation by applying the two optimization mechanisms that determine whether f_a is “feasible”. Being infeasible implies that it is impossible for a given flow to release a packet at the given time, considering that it either released a packet too close in time relative to its previous packet (thereby accounting for the network-level pessimism) or it has already exceeded the upper bound on the number of packets it could possibly generate from the beginning of the computation (task-level pessimism). If the flow f_a is declared *infeasible* then it is removed from the currently considered interfering scenario $\{f_a, f_c, f\}$ and the algorithm moves on with the next flow f_c of that scenario. As a side note, it can be observed that removing f_a from that scenario $\{f_a, f_c, f\}$ yields the scenario $\{f_c, f\}$ and thus, the equivalent scenario $\{f_c, f\}$ listed in LIS will not have to be investigated again later on. Thereby, removing flows from a scenario is equivalent to pruning the resulting

scenario from LIS, which considerably improves the time-complexity of this technique (as well as the accuracy of the WCTT estimates) as discarding a single flow from a scenario automatically cuts off a whole subtree from the computation tree.

6.7.2.3 Need for ordering

Since our approach considers the input flow characteristics, the order in which flows progress cannot be ignored as it can lead to different results.

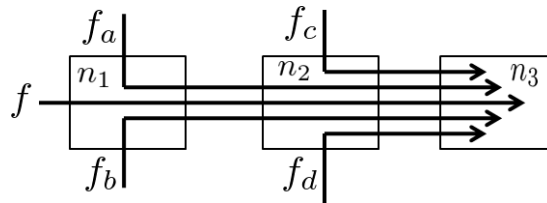


Figure 6.8: Illustration to understand the need for ordering

We illustrate this with an example given in Figure 6.8. Consider two possible scenarios: $S_1 = \{f_c, f_d, f_b, f_d, f_c, f_a, f_c, f_d, f\}$ and $S_2 = \{f_c, f_d, f_b, f_c, f_d, f_a, f_c, f_d, f\}$. These two scenarios only differ in the order in which f_c and f_d block f_a . However, notice that in S_1 the first and the second appearance of f_d are distanced only by f_b , while the second and the third appearance of f_c are distanced only by f_a . Conversely, in S_2 , any two appearances of the same flow are distanced by at least two other flows. Depending on flow characteristics, in some cases the entire S_2 might be feasible, while S_1 would require the pruning of some appearances of f_c and/or f_d . Thus, considering only S_1 in the analysis may result in unsafe worst-case estimates, and in order to capture the worst-case it is necessary to investigate all possible flow orderings at every traversed router.

Indeed, at a given router n_x along f 's path, the list of interfering scenarios can be computed as explained above but identifying which blocking flows are *infeasible* within each of these scenarios requires the knowledge of which flows have already progressed (and in which order) in the previously traversed routers, before f reaches n_x . Without this knowledge, our pruning mechanisms would not be able to determine whether a flow listed in an interfering scenario is feasible or not. This leads to the concept of “context” which is key in our algorithm.

6.7.2.4 Notion of a “context”

Formally, a context is a snapshot of all the information characterizing a unique sequence of flow progressions throughout the network before a given flow f reaches a given router n_x , including

1. the order in which the flows have progressed over the network so far,

2. all the past occurrences and the associated timestamps of all these flows in this flow sequence and
3. the delay incurred by f before it reaches n_x

At a given router n_x , for a given flow f and context ctx , which (informally speaking) reflects the history of what happened in the network before that flow f reached n_x , we explained above that every feasible blocking flow of every interfering scenario of LIS in n_x will be allowed to progress from n_x to its destination *before* the analyzed flow f . Therefore, it can be seen that the progression of each of these blocking flows towards their destination may in-turn generate a multitude of new contexts (more exactly, the progression of each blocking flow will make the current context ctx evolve in an unique way). Subsequently, all these new contexts derived from ctx are investigated when f eventually progresses to the next router on its path. At the end, the WCTT of f will be found by looking at all the flow sequences (i.e., the contexts) in which f finally reaches its destination.

Algorithm 9: getMaxDelay(Flow f , Link l)

input : a flow f , a link l
output: WCTT of flow f , starting from link l , to the destination.
1 StudiedFlow $\leftarrow f$, $\text{ctx.scenario} \leftarrow \text{“ ”}$, $\text{ctx.delay} \leftarrow 0$;
2 $\text{ctxSet} \leftarrow \text{getContexts}(f, l, \text{ctx})$;
3 $\text{maxdelay} \leftarrow \max_{\forall \text{ctx} \in \text{ctxSet}} \text{ctx.delay}$;
4 **return** maxdelay ;

6.7.3 Detailed Explanation of the Algorithm GetContexts()

Initially, the algorithm is invoked by Algorithm 9 with the following inputs: the flow f to be analyzed, the first link l on its path and an initial “context”. The initial context contains an empty flow sequence, a delay of zero, and past occurrences set to null. On arriving at a router, the algorithm (line 10) computes the set of blocking links BL (as explained earlier) and the corresponding blocking flows (lines 11-13) incident on each of the links in BL . Based on this information, the set LIS of *Local Interfering Scenarios* is computed (line 14) as follows: LIS contains all permutations of flow sequences in which (i) there is exactly zero or one flow from each set $U_{l_{in}}$ and (ii) the analyzed flow f is appended to each of these permutations.

Once the set LIS is computed, the algorithm investigates each of them. Let us revisit the example in Figure 6.8. For each scenario in LIS, (line 16), e.g, $\{f_a, f_c, f\}$, the list SCList will ultimately contain all the generated contexts arising from the execution of this scenario. The investigation starts with the first flow, here f_a (line 18), and considers every current context curCtx (line 19) that results in f reaching the link l . Remember that, (because our extended model considers flows with some timing constraints on their packet generation) the interfering scenarios that can occur for a flow f in a router n_x depend on

Algorithm 10: getContexts(Flow f , Link l , Context curCtx)

```

input : a flow  $f$ , a link  $l$ , a context curCtx
output: A set of contexts, each constituting a scenario string and its delay
1 if  $l = \text{null}$  then
2   | curCtx.delay +=  $\frac{\text{maxsize}(f)}{C}$  ;
3   | curCtx.scenario.Append( $f$ ) ;
4   | return curCtx;
5 end
6 if  $l = \text{first}(f)$  then
7   | curCtx.delay +=  $d_{\text{sw}} + d_{\text{across}}$  ;
8   | return getContexts( $f, \text{next}(f, l), \text{curCtx}$ ) ;
9 end
10 BL  $\leftarrow \{l_{\text{in}} \in \mathcal{L} \mid l_{\text{in}} \neq \text{prev}(f, l) \wedge \text{ldest}(l_{\text{in}}) = \text{lsrc}(l)\}$  ;
11 foreach  $l_{\text{in}} \in \text{BL}$  do
12   | // Find the set of blocking flows on link  $l_{\text{in}}$ 
13   |  $U_{l_{\text{in}}} \leftarrow \{f_{\text{in}} \in F \mid \text{next}(f_{\text{in}}, l_{\text{in}}) = l\}$  ;
14 end
15 LIS  $\leftarrow$  Set of local interfering scenarios based on  $U_{l_{\text{in}}}$  ;
16 GCList  $\leftarrow \{\emptyset\}$  ;
17 foreach scenario  $S_i \in \text{LIS}$  do
18   | SCList  $\leftarrow \{\text{curCtx}\}$ ;
19   | foreach flow  $f_j \in S_i$  do
20     | foreach context  $\text{ctx}_k \in \text{SCList}$  do
21       | SCList.pop( $\text{ctx}_k$ ) ;
22       | if isMITRCompliant( $f_j, \text{ctx}_k.\text{LogTbl}, \text{ctx}_k.\text{delay}$ ) then
23         | if isMPRFCompliant( $f_j, \text{ctx}_k.\text{LogTbl}, \text{ctx}_k.\text{delay}$ ) then
24           |  $\text{ctx}_k.\text{delay} += d_{\text{sw}} + d_{\text{across}}$  ;
25           | FCList $_k \leftarrow$  getContexts( $f_j, \text{next}(f_j, l), \text{ctx}_k$ );
26         | end
27       | end
28     | SCList  $\leftarrow \cup_{\forall k} \text{FCList}_k$ ;
29   | end
30   | GCList  $\leftarrow \text{GCList} \cup \text{SCList}$  ;
31 end
32 return GCList;

```

Algorithm 11: isMPRFCompliant(fid, flowLogTbl, curTime)

```

1 numGen  $\leftarrow$  flowLogTbl [fid]. numOccurrences ;
2 firstArrival  $\leftarrow$  timeStampArray[1] ;
3 timeDuration  $\leftarrow$  curTime - firstArrival ;
4 numMax  $\leftarrow$  MaxPcktRel( $fid, \text{timeDuration}$ );
5 if (numMax < numGen) then return FALSE ;
6 return TRUE;

```

Algorithm 12: isMITRCompliant(fid,flowLogTbl,curTime)

```

1 if (FirstOccurence(fid,flowLogTbl))|(curTime ≥ fid.NextfeasibleArrival) then
    // For the corresponding entry in the table
2   Increment numOccurrences ;
3   Append curTime to the timeStampArray ;
4   Reset NextfeasibleArrival to curTime + MinInterRel(f) ;
5   return TRUE ;
6 end
7 return FALSE ;

```

the order in which the previous flows progressed through the network before f reaches n_x . Hence, whenever a flow f reaches a router n_x , all possible contexts have to be investigated in order to determine all the future scenarios that could arise at router n_x .

First, lines 21 and 22 check whether f_a can legally block the analyzed flow f considering the time of its last arrival in the considered context (here, $curCtx$). If f_a can arrive and passes the round trip time test (line 21) as described in Algorithm 12, the task characteristics of the flow are checked. Specifically, line 22 checks if the task originating f_a can indeed generate that many packets in the time specified by calling the function defined in Algorithm 11. If both checks of lines 21 and 22 succeed, then f_a is allowed to progress in line 24, after updating the current context delay parameter (line 23). Ultimately, the passage of f_a returns a set of contexts (line 24), when flow f_a reaches its destination (which is reflected when its last link is null (lines 1-5)).

All these returned contexts end with flow f_a reaching its destination and each one corresponds to a different scenario in the subsequent routers along the path of f_a . All these resulting contexts are added to the scenario list $SCList$ (line 28) *as they must all be considered (line 17) while analyzing the next flow f_c of the current scenario*. When all the flows of the currently considered interfering scenario have been considered, all the contexts resulting from this scenario are added to the global list $GCList$ (line 30). That list is finally returned (line 32), as it contains all the possible flow sequence progressions in the routers traversed by f after progressing through the link l , starting with the context $curCtx$. The list $GCList$ that is ultimately returned (to Algorithm 9) at the end of the analysis, contains all possible scenarios in which f can reach its destination, with the corresponding delays. Finally, Algorithm 9 selects the scenario with the highest delay to return an upper-bound on the traversal time of the analyzed flow f .

6.8 A more efficient algorithm: Branch, Prune and Collapse

6.8.1 Description

The recursive calculus based method proposed by [146] scales well at the cost of providing a very pessimistic WCTT. In contrast, the proposed branch and prune (BP) algorithm

returns a very tight WCTT at the cost of a high time complexity and memory usage. The reason for the improved computational efficiency in the method by [146] is that it does not carry any history of the previous flows and only retains the maximum delay incurred at each router. From the two extreme approaches it may be inferred that a hybrid solution exists which can drop some history of the contexts (only) periodically while retaining the maximum delay seen so far as the analysis progresses. Such an approach is explored in this section.

As seen earlier, the identification of infeasible scenarios in BP was possible due to the explicit book-keeping of contexts of *all* investigated scenarios. The “Branch, Prune and Collapse” (BPC) algorithm presented (conceptually) in this section is motivated by the observation that, while the complexity of the BP algorithm is indeed exponential, for most flows, the number of scenarios to be considered is manageable (as seen in the experiments of Section 6.9). To handle the corner cases (in terms of time complexity) we propose as a trade-off, a more general BPC algorithm with a tunable parameter that we term “Scenario Information Retention Limit” (SIRL). The SIRL acts as a threshold on the number of scenarios whose contexts are retained.

In the BP algorithm, all the investigated scenarios and their contexts are back propagated and the algorithm proceeds by first pruning these investigated scenarios and then combining them with the local scenarios and then allowing the next feasible flow to progress. As a deviant version of this algorithm, which is hereafter referred to as BPC, *when the number of investigated scenarios reaches a pre-set limit of SIRL*, a dummy scenario with a unique dummy flow-id is created. The context of this scenario populates (i) the delay field to the maximum of the delays of the investigated scenarios and (ii) the other fields, relating to the history information i.e the past occurrences, timestamps, etc to NULL (or zero, as appropriate) – This marks the “collapse” phase of the BPC algorithm in which a set of investigated scenarios is “collapsed” into a new single dummy scenario with zero history information and a conservative delay estimate. As opposed to the branch and prune algorithm, only this dummy scenario is back propagated to the higher nodes and the algorithm gets back in to the branch and prune phase until the number of investigated scenarios again exceeds SIRL, thereby triggering another collapse phase.

The necessity to create a new dummy scenario Note, that at any *intermediate* stage of analysis, if the number of scenarios under investigation reaches the pre-set threshold i.e., the SIRL, a single scenario that will *provably* lead to the WCTT cannot be detected. That is, during the collapse phase, from the set of the constituent collapsed scenarios, a specific single scenario (containing a tightly coupled local maximum delay, flow sequences and other history information) cannot be specifically carried forward. This is due to the fact that in the later analysis stages such a scenario with the local maximum might be subject to pruning because of its flow history and thereby not contribute to the global maximum delay. Inorder to prevent this, we drop the history information (thereby reducing the chances of

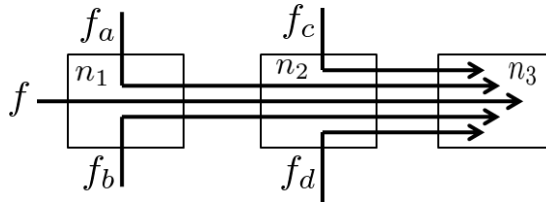


Figure 6.9: Example for “Branch, Prune and Collapse”

further optimization due to the loss of history retained in the collapsed scenarios) while only retaining the local maximum delay in a totally new dummy scenario. To summarize, the BPC method thereby creates a dummy scenario which inherits the delay of the local maximum, but drops the history of the flows constituting that scenario (context).

6.8.2 An example to illustrate the BPC method

We illustrate the working of the BPC method with the example of the flow-set presented in Figure 6.9 (repeated here for readability) – let us analyze flow f which traverses through routers n_1 and n_2 to finally reach its destination n_3 . As observed in Figure 6.9, flows f_c and f_d can potentially block flow f thrice: twice indirectly by blocking the passage of f_a and f_b at n_2 (f_a and f_b block f directly at node n_1), and finally directly at n_2 during f 's passage. Thus, f_c and f_d are promising candidates for pruning (lines 21 and 22 of Algorithm 10). Additionally, let us assume that $\text{SIRL} = 5$. At node n_1 , BPC constructs the LIS as $\text{LIS}(f, n_1) = \langle \{f_a, f_b, f\}, \{f_b, f_a, f\}, \{f_a, f\}, \{f_b, f\}, \{f\} \rangle$ and it starts exploring the first scenario $\{f_a, f_b, f\}$. At this time, the list SCList is reset to the current context (at line 17 of Algorithm 10). Note, that the list SCList will ultimately contain all generated contexts arising from the execution of this scenario $\{f_a, f_b, f\}$, before being appended to the global list of contexts GCList at line 30. Firstly, a recursive call is performed to node n_2 with f_a being the analyzed flow. This will result in a new LIS constructed at node n_2 as $\text{LIS}(f_a, n_2) = \langle \{f_c, f_d, f_a\}, \{f_d, f_c, f_a\}, \{f_c, f_a\}, \{f_d, f_a\}, \{f_a\} \rangle$. Similarly, LIS is generated for the flow f_b at n_2 , resulting with $\text{LIS}(f_b, n_2) = \langle \{f_c, f_d, f_b\}, \{f_d, f_c, f_b\}, \{f_c, f_b\}, \{f_d, f_b\}, \{f_b\} \rangle$.

These scenarios are back-propagated to the node n_1 , and should be combined before f progresses to n_2 itself. As both LIS sets contain 5 elements, the combined set of scenarios may contain 25 scenarios (5 contexts from f_a combined with 5 from f_b). It is obvious that for extremely complex flows, this back-propagation may produce a large number of scenarios, resulting in a combinatorial explosion, which is the drawback of the BP method. Given that $\text{SIRL} = 5$ in this example, the collapsing requirement is met. Those 25 scenarios are collapsed into a single one containing the dummy flow f_X and its delay is set to maximum delay amongst the collapsed scenarios. When f finally progresses to n_2 and encounters the blocking flows f_c and f_d , the algorithm checks the history in its sequence $\{f_X, f\}$ and since there is no prior information regarding f_c and f_d , the analysis

considers that these two flows are arriving for the first time and thus allows them to pass and interfere. The resulting scenarios would be $\{f_X, f_c, f_d, f\}$, $\{f_X, f_d, f_c, f\}$, $\{f_X, f_c, f\}$, $\{f_X, f_d, f\}$ and $\{f_X, f\}$. In contrast, BP would have retained the information regarding all scenarios, thus prohibiting the second interference caused by f_c and f_d , but at the expense of investigating $25 \times 5 = 125$ scenarios.

This example clearly brings forth two main principles:

1. The loss of past information can reduce the chances of pruning infeasible scenarios.
2. The number of scenarios to be explored significantly decreases with the decrease in the SIRL parameter – and more specifically in loaded networks in which the context of large scenarios have to be back-propagated to higher level nodes and combined to evolve the final scenarios.

Conceptually, a SIRL set to ∞ implies $BPC = BP$ while at the other end, a SIRL set to 1 tends towards obtaining the WCTT using the method proposed by Ferrandiz et. al [146], where no information about the past occurrence of any flow is retained. This approach is provided to the designer to handle the comparably small number of cases in which the BP algorithm may be inefficient. To formally validate the flexibility this offers, it will be seen in the experiment sections how lower SIRL will compute bounds tending towards those computed by Ferrandiz et. al [146], while with higher SIRLs we will have tighter WCTTs computed by BP. With this parameter, the system designer has the flexibility to trade-off computation time vs. pessimism in the computed WCTT.

6.8.3 Proof of Safety of “Branch, Prune and Collapse” (BPC) algorithm

In this section, we explain why the BPC method, by discarding some history information upon reaching the SIRL threshold, may output more pessimistic WCTT estimates compared to BP, but will under no circumstance lead to an unsafe WCTT estimate.

Let us denote by wcs the scenario (flow sequence) leading to the WCTT at run time which is *by definition a feasible scenario*. In order to prove that BPC is safe, we must prove that the BPC method does not eliminate this scenario wcs from the set of investigated scenarios – the method should never return a WCTT which is lower than that corresponding to the traversal time of wcs .

Firstly, it should be noted that, if we disable the two pruning mechanisms at lines 21 and 22 of Algorithm 10 and if SIRL is set to ∞ , then our BPC algorithm boils down to an exhaustive enumeration of all possible scenarios at each router, and thus considers all possible blocking scenarios in the context of the analyzed flow (brute-force approach which is inherently safe). The pruning mechanisms of lines 21 and 22 use the precedence and time stamp information to identify some infeasible flow sequences and reduce the list of scenarios that need to be explored and facilitates the objective of obtaining tighter WCTTs. By definition, wcs is a feasible flow sequence and therefore, it will not be eliminated by these pruning techniques.

Given the loss of history information, the BPC method is unable to identify as many infeasible scenarios as the BP method. These infeasible scenarios (flow sequences) have flows that actually cannot occur at run time due to the task properties and hence add to extra-delays and bloat up the traversal time. Eventually, the set of scenarios explored will consider the set of feasible scenarios which includes wcs but will also include some infeasible scenarios, which are not identified due to loss of previous history and precedence information. Finally, on taking the maximum traversal time of all the scenarios, the method will return a value which is higher than or equal to the WCTT corresponding to wcs – hence the method is safe.

To summarize, BP investigates all feasible (including the wcs) and infeasible scenarios and prunes *some infeasible scenarios* by retaining the history information, and thereby is safe. BPC investigates all feasible and infeasible scenarios and since it loses some history information, it is capable of pruning only a *subset of the infeasible scenarios* that could be pruned by BP and as a consequence is still safe but more pessimistic.

6.8.4 Proof of termination of Algorithm GetContexts (Algo. 10)

The system is modeled as a graph $\mathcal{G}(\mathcal{N}, \mathcal{L})$ with finite sets of nodes and bi-directional links and a set \mathcal{F} of flows. Let \mathcal{S} be the set of pairs $\langle f, \ell \rangle$, with $f \in \mathcal{F}$ and $\ell \in \mathcal{L}$, such that $\langle f, \ell \rangle \in \mathcal{S}$ if and only if $\ell \in \text{path}(f)$. Since $|\mathcal{L}|$ and $|\mathcal{F}|$ are finite, it holds that $|\mathcal{S}|$ is finite as well. A progress of a flow f from a link ℓ to a subsequent link ℓ' on its path is equivalent to the progress from the pair $\langle f, \ell \rangle$ to the pair $\langle f, \ell' \rangle$. If a flow f' blocks flow f on the link ℓ , it corresponds to the progress from the pair $\langle f, \ell \rangle$ to the pair $\langle f', \ell \rangle \in \mathcal{S}$. For a given flow f and a current link ℓ , the algorithm progresses in a forward manner to the next link $\text{next}(f, \ell)$ in the path of the flow f by invoking the function `getContexts()` at lines 8 and 24. Starting from any pair $\langle f, \ell \rangle \in \mathcal{S}$ (i.e. with f and ℓ as input), our algorithm investigates all the pairs, i.e. set of inputs, $\langle f', \text{next}(f', \ell) \rangle$ with $f' \neq f$ as a consequence of the round-robin arbitration policy. Then, the algorithm repeats the same (in a recursive manner) for each of these pairs $\langle f', \text{next}(f', \ell) \rangle$ and, as a consequence of the deadlock-free property of XY routing, we know that the initial pair $\langle f, \ell \rangle$ will never be re-visited. Additionally, since all the explored contexts are popped in line 20, the queue of pending scenarios is emptied and the algorithm eventually terminates.

6.9 Simulations and Results

We conducted several experiments with the dual objectives of comparing our method with the approach in [146] and studying the impact of varying different parameters on the WCTT of analyzed tasks. The simulation parameters have been summarized in the following table:

Network Size	8*8 mesh
Routing and switching mechanism	XY Routing, round robin arbitration
Router switching delay and transfer delay	1ns and 3ns (in-line with SCC [24])
Packet size and channel capacity	512 bytes, 1 Gbps
Platform details	Intel dual-core & Java (Max heap-size:4GB)

6.9.1 Comparison of BPC with the Approach of Ferrandiz et. al [146]

As the improvements cannot be quantified in the general sense, since they are highly flow-set specific, we performed experiments on a wide range of different flow-sets in order to understand the trends and the ranges of improvement achieved by employing the proposed approach.

Test 1: Network with moderate number of flows: We generated 200 random flow-sets, each having 64 flows. The flows originate from each tile but terminate at a random destination. The minimum inter-arrival time is a randomly generated parameter, varying between 5 to 20 microseconds. We computed the upper-bounds on the WCTT of each flow using both the approaches and compared the results. For our approach, we selected a $SIRL = 10000$.

In order to quantify the range of improvements, we computed a metric which we refer to as the “Percentage Improvement Ratio” (PIR) given by $(d_U - d_O^{10000}) * 100/d_U$, where d_U denotes the upper-bound on WCTT returned by the approach in [146] which we also refer to as *unoptimized WCTT*, and d_O^{10000} is the value returned by our algorithm for $SIRL = 10000$, which we call *optimized WCTT*. Therefore a $PIR = 25\%$ implies that our approach provided 25% lower (i.e. tighter) WCTT upper-bound.

Figure 6.10a summarizes our findings. We observed that for 31.84% of the flows, the bounds computed by both methods are equal, that is $d_O^{10000} = d_U$ and $PIR = 0\%$. We have also demonstrated the percentage of flows and the improvement they achieved, in order to provide a deeper insight into the performance of our algorithm. As evident from Figure 6.10a, 1.29% of the flows had a PIR in the range (1 – 10%), 13.22% in the range (11 – 20%) and so on. At the high end of the PIR scale, 3.55% of the analyzed flows returned 71 – 100% tighter WCTT bounds.

The WCTT* parameter: If the computation terminates with the number of investigated scenarios not exceeding $SIRL$ (implying that no collapses occur during the entire flow analysis), the method returns a value of the traversal time as would be computed by BP – we denote this result by $WCTT^*$. In other words, all possible scenarios were analyzed and the one inducing the highest worst-case delay was recognized. Conversely, in cases when collapses occur, the returned WCTT presents only an *upper-bound* on the worst-case delay, without any additional details on how tight that bound is. When viewed from that perspective, the approach in [146] presents a special case of the proposed approach

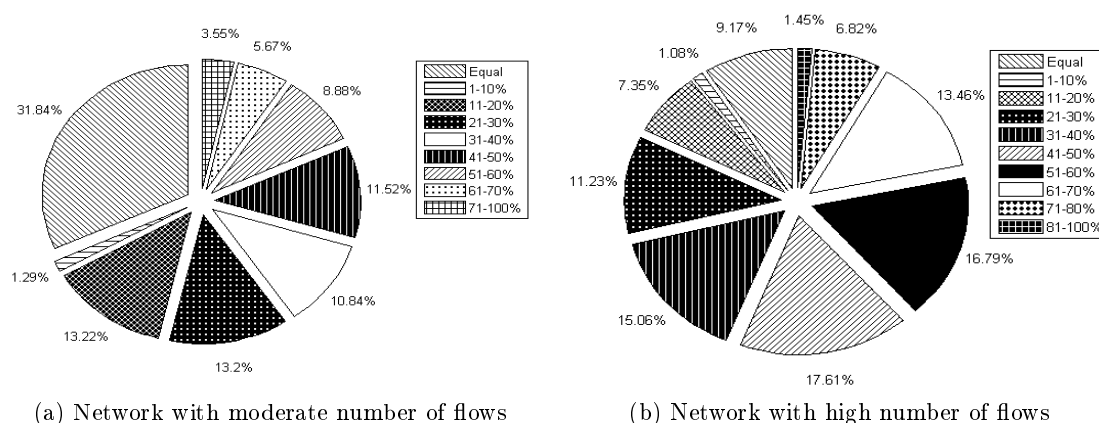


Figure 6.10: Distribution of WCTT improvement on the flows. The legends represent improvement ranges.

where $SIRL = 1$. Therefore, [146] returns $WCTT^*$ only when the number of investigated scenarios is equal to “1”.

In the 31.84% of the flows for which both methods returned equal values of WCTT, for $3/4^{th}$ of them, (23.96% of all the flows), the recursive-calculus method was able to capture $WCTT^*$, inferring that these scenarios were simple and triggered the investigation of only one scenario. Therefore, in these cases there was no further scope for improvement. For the rest of the 68.16% flows ($100 - 31.84\%$), our algorithm returned tighter estimates. Based on the experiments, we can say that our algorithm performed equally well or dominated the method proposed by [146]. Also, for the selected SIRL value, the proposed approach managed to capture $WCTT^*$ in 92.13% of the cases, inferring that any additional increase in SIRL would not provide significantly tighter WCTT bounds, but would require exponentially greater amount of time.

The offline analysis completed within 24 hours, averaging a little bit more than 7 minutes per flow-set (each with 64 flows). The most complex flow-set took around an hour for completion, suggesting that the execution times may vary drastically when applied to flow-sets with identical characteristics but different flow routes, sometimes even by a high order of magnitude due to increase in the indirect contentions.

Test 2: Network with high number of flows: The main purpose of this test was to check the efficiency of our algorithm when applied to a network with higher number of flows. In this test, we again generated 200 random flow-sets, 128 flows each, with *two flows originating from each tile* and terminating at a random destination. The minimum inter-arrival time is randomly generated parameter varying between 25 and 250 microseconds. For all flows, the values of d_U and d_O^{10000} were computed and compared. The simulation completed in 5 days, averaging 36 minutes per flow-set, where the most complex consumed

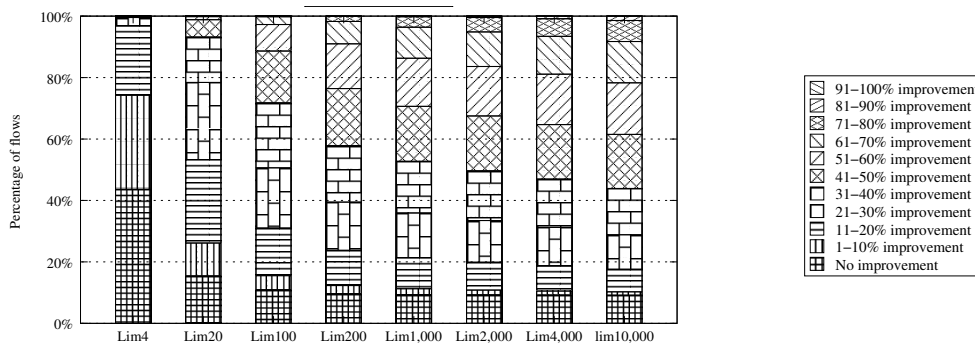


Figure 6.11: Our proposed approach with varying SIRL vs. method by [146]. The “Lim” on the x axis denotes the threshold limit (SIRL) followed by the value

around 3 hours, demonstrating that our approach is scalable and applicable to practical scenarios involving hundreds of concurrent flows.

As in the previous test-set, the PIR metric is used here to quantitatively express the improvements of the proposed method over the recursive calculus method by Ferrandiz et. al [146] and the results are reflected in Figure 6.10b. We observed that for 9.17% of the flows, no improvements were made (PIR = 0%). For most of the flows without improvement (8.11% among the 9.17% flows) the approach by Ferrandiz et. al [146] managed to capture WCTT*, with the same conclusion that for these simple, one-scenario cases no improvements were possible. For the rest, i.e. 90.73% of the analyzed flows, it holds that $d_O^{10000} < d_U$, that is the upper-bound on the worst-case of the analyzed flows was tighter with our approach and the distribution is reflected in Figure 6.10b. It is interesting to see that more than 13% of the flows showed an improvement of 61 – 70%, while more than 8% of the flows show an improvement greater than 70%. Due to more complex traffic patterns resulting from increased amount of traffic, our approach with SIRL = 10000 recognized WCTT* for 41.71% of the flows, which is significantly smaller when compared with the same of moderately loaded network. This suggests that the improvements can be achieved by increasing SIRL, but at the expense of additional computational complexity and memory consumption. Although the proposed approach takes a longer computation time, it clearly dominates the recursive calculus method in terms of obtaining tighter results. The selection of SIRL creates a trade-off between the computation time and the accuracy of the analysis.

Test 3: Impact of SIRL on WCTT estimates: The objective of this set of experiment is to understand the impact of varying SIRL on the computed WCTT. The general intuition is that retaining more information about the scenarios provides more opportunities for eliminating invalid scenarios and therefore leads to tighter estimates. To validate this idea, we implemented our algorithm and executed it, by providing a different value of SIRL for each run and compared them against the results obtained by the approach in [146]. The

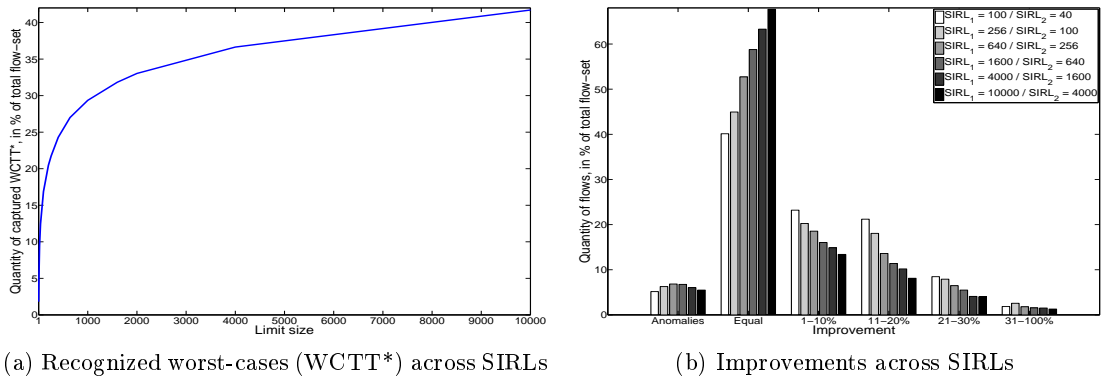


Figure 6.12: Inter-SIRL ratios

results have been demonstrated in Figure 6.11 and like the previous experiments use the PIR metric for performance.

We observed that as the SIRL increases, the percentage of flows which show no improvements over the values computed by [146] decreases. Thus, with an $\text{SIRL} = 4$, the WCTT computed for 43.6% flows exhibit no improvements, while with $\text{SIRL} = 2000$ only 9.29% of the flows show no improvements while the rest have tighter WCTTs. Note the marked shift in the distribution of improvements towards higher increased PIRs as the SIRLs increase. This is in accordance with the algorithm rationale that the retention of information about past flows in the scenarios can provide opportunities for tightening the WCTT. But as seen in the shift from 4000 to 10000, the PIR improvements do not differ much, as the opportunities for cutting down infeasible scenarios are exhausted. It can be then also inferred that choosing limits beyond a given SIRL will only burden the system memory of retaining information about those scenarios which may not lead to the WCTT. So a judicious decision must be taken by the system designer considering the tightness of results required and the time in which the tests must be performed.

Test 4: Inter-SIRL ratios: In the previous experiment, we compared the results of our approach with different SIRL values against the approach of [146]. In order to get a deeper insight into the impact of the SIRL parameter, we compared the results of our approach with different SIRL values against each other and plotted the results in Figure 6.12. The results coincide with the intuition, suggesting that greater values of SIRL improve the chances of capturing WCTT*, i.e. no collapses during the calculation occur (Figure 6.12a). This claim is confirmed with a logarithmic growth in the number of non-collapsed scenarios across SIRLs.

Figure 6.12b shows that the relative improvements across SIRLs diminish as SIRL increases. The legend represents the 2 settings of SIRL values under comparison for the same flowsets. So the first bars correspond to the improvement when $\text{SIRL} = 100$ and $\text{SIRL} = 40$ are compared. Similarly the second bars in the graph corresponds to the

improvement when $SIRL = 256$ and $SIRL = 100$ are compared. The X axis corresponds to the percentage of improvement across bands, with *equal* meaning no improvement across bands. Similarly, the Y axis reflects the percentage of the flows in the flow set for which the corresponding improvements were observed.

As seen in the figure, our method with $SIRL = 100$ shows improvement against the same method with $SIRL = 40$ in 60% of the cases (the first bar in the “equal” heading depicts that 40% flows did not benefit from increasing the $SIRL$ value meaning there is improvement in the rest of the cases, except for the anomalies), while the improvement is reported only in 30% of the cases when comparing results of $SIRL = 10000$ and $SIRL = 4000$. Thus, the number of scenarios with no improvement increases with $SIRL$. Conversely, the number of scenarios with improvements decreases with $SIRL$ across all improvement ranges, suggesting that it may not be essential to perform the analysis with very high values of $SIRL$ beyond a certain value. The benefits of analyzing with higher $SIRL$ diminish as $SIRL$ increases (especially for scenarios comprising of single-occurring flows for which no further scope of improvement is possible).

As already stated, the value of the $SIRL$ influences the frequency of scenario collapses. However, one interesting observation is the fact that higher $SIRL$ does not necessarily always lead to a tighter WCTT upper-bound. We explain this with a following example. Consider the flow f in the example depicted by Figure 6.9. Let us assume that f_c and f_d are potential candidates for pruning. Now, assume that greater $SIRL$ performs a collapse between occurrences of f_a and f_b . As the history information is lost, the flows f_c and f_d will contribute to the delays of both the flows, f_a and f_b . On the other hand, a smaller $SIRL$ might trigger a collapse before (and after) the appearance of both f_a and f_b . In this case, it may successfully prune one appearance of f_c and f_d , thereby resulting in the situation (which we refer to an “anomaly”) where a smaller value of $SIRL$ returns a tighter WCTT estimate. As is visible from the results, the number of anomalies never exceeds more than 8% in all the considered cases.

6.9.2 Trade off between the approaches

: The above study also brings a very important result. If the network is not loaded and the number of blockings experienced by a flow (inclusive of direct and indirect blockings) is low then the earlier recursive approaches as in [146] should be used as they will compute the same WCTT as computed by the proposed approach in shorter time. But for a more loaded network and for applications in which tighter WCTT estimates are required, the branch and prune method proposed here can be employed.

We believe that in order to harness the capacity of the many-core system efficiently, most cores will be assigned tasks. This will lead to an increased contention on the network as a result of the direct or indirect blockings and therefore for such a setup our method is highly preferable. Although the use of the approach in [146] will lead to safe WCTT

estimates, it is overly pessimistic and therefore will lead to over-dimensioning of resources and lower system utilization.

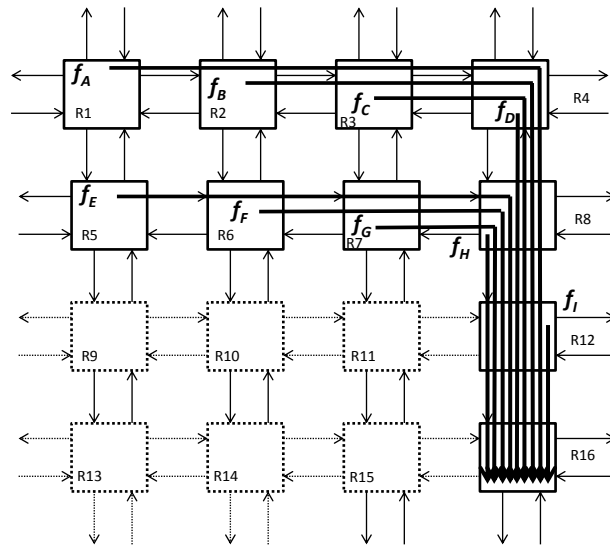


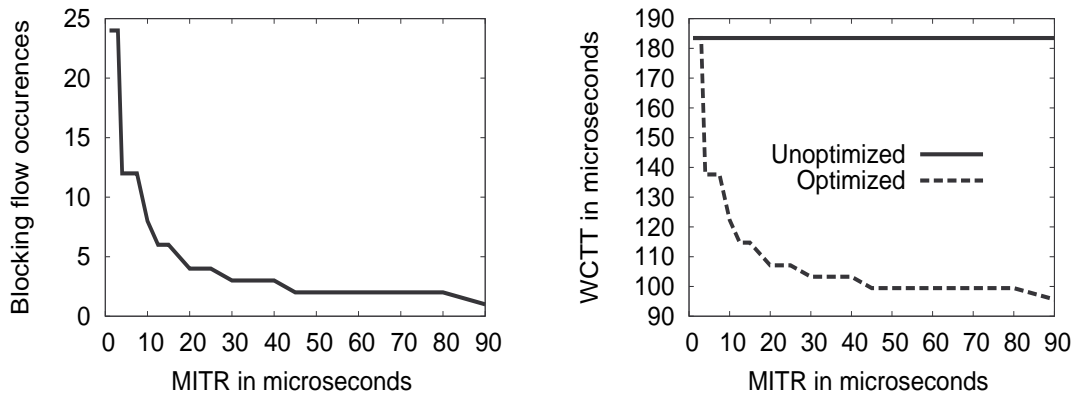
Figure 6.13: Example Flow Set in a portion of the grid

6.9.3 Case Study with a specific flow-set

Figure 6.13 shows one of the flow-sets analyzed over a 4*4 grid that we shall use to demonstrate some interesting properties. Additional details like the core and cache engine were omitted to make the figure simpler. In the rest of the document, we drop the prefix f and directly refer to the flow by its alphabetical name. In this flow set, we analyzed the flow A which originates in router R1 and terminates at the core associated with router R16. B, C, D, E, F, G, H and I are the other flows which also terminate at node R16. In this example, in the worst-case scenario, every flow can be potentially blocked by flow I (originating at R12) which is closest to the destination, then by flow H and so on. To provide a fair comparison with the approach in [146], we consider that every flow is by nature unregulated and non-blocking. By non-blocking we mean that the flow next packet can be sent without waiting for the acknowledgement of the previous packet. By applying the approach in [146] or using our approach without any optimizations, one of the scenarios which resulted in the WCTT for flow A was:

$\{IHIEIDIHIEICIHIEIDIHIEIBIHIEIDIHIEICIHIEIDIHIEIA\}$. This scenario is a manifestation of the “task-level” and “network level” pessimism and exemplifies the case of an over-estimated WCTT when infeasible blockings are not curtailed. Flows I and H are positioned in a manner which enables them to frequently block the other flows. This scenario also presents a useful example for exploring the delay on the WCTT of flow A if the task-profiles and task parameters of the blocking flows are varied.

6.9.4 Impact of Varying Packet Arrival Rates



(a) No. of blockings by flow I vs. its $\text{MinInterRel}(I)$ (b) WCTT of flow A vs. Packet Arrival rate of flow I

Figure 6.14: WCTT of flow A decreases with increase in MIA time of flow I

The flows originating closer to the destination of the analyzed flow A in Figure 6.13 have a higher tendency to block it (flow A) directly and indirectly (by blocking the other flows which are also in the path). To verify this, we tuned the $\text{MinInterRel}()$ (MITR in the figure) of flow I , increased it steadily and carried out the experiment, while keeping the nature of the other parameters constant. Figure 6.14a shows that as $\text{MinInterRel}(I)$ increases, the number of times it can block the other flows is invalidated and thus the WCTT of flow A decreases as expected as seen in Figure 6.14b. In contrast, since the approach in [146] does not take into account the task characteristics, it allows these invalid blockings to progress and as a result, irrespective of the change in the flow parameters, the computed WCTT remains constant (see solid line in Figure 6.14b).

6.9.5 Impact of Varying Task Patterns

The WCTT of a packet of a given flow is also affected by the packet release profiles of the other flows. To study this effect, we conducted the following tests in which we analyzed the WCTT of flow A (in Figure 6.13) by changing the packet profiles of the blocking flows. In addition to the unregulated non-blocking profile assumed for all the flows in [146], we defined three packet profiles S1, S2 and S3 (where S stands for Sparse) by generating synthetic pattern arrivals and computing the $\text{MaxPcktRel}(f, t)$ for each of these profiles using the method proposed in [91]. Figure 6.15 depicts the profiles, in which the X-axis represents the time-line (in nanoseconds) and the Y-axis shows an upper bound on the number of packets that can be generated in time t . The default profile, shown in Figure 6.15b, models the unregulated non-blocking profile. Figure 6.16 summarizes the results of different tests carried by varying the parameters of the blocking flows. The Y-axis represents the computed values of the WCTT of flow A . The X-axis contains the test name and

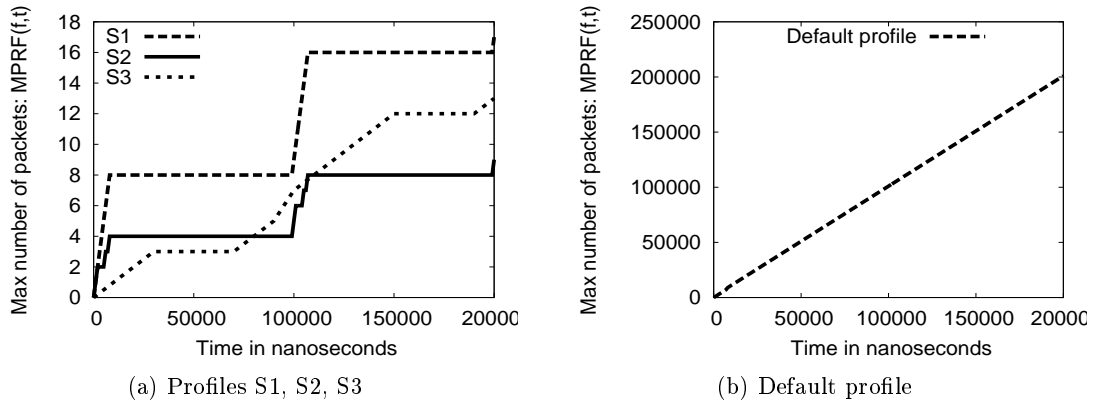


Figure 6.15: MaxPcktRel() function applied to different profiles

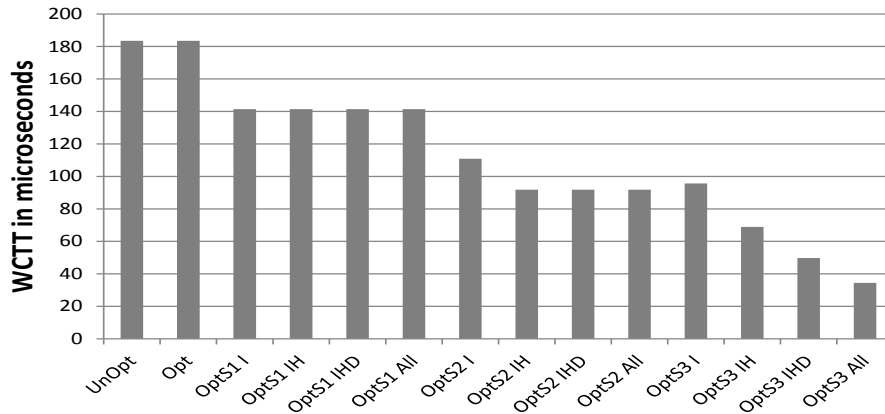


Figure 6.16: WCTT of Flow A by varying the flow profiles of the blocking flows

should be read as $\langle approach \rangle \langle profile \rangle \langle flows \rangle$, where $approach \in \{Unopt, Opt\}$ refers to the approach in [146] and our approach, respectively. All unmentioned flows by default have the profile presented in Figure 6.15b. So OptS2IH refers to a test case with our approach, the flows I and H have profile S2 and the other flows have the default profile.

As previously noted, the WCTT estimated by the Unopt method remained constant. Both the approaches computed the same WCTT for flow A for the default task profile. However, when we assigned the flows different profiles, *Opt* outperformed *Unopt* in all the tests. This test case was designed to emphasize the importance of reducing the “task pessimism” described earlier. When applying the S1 profile to flow *I*, the WCTT of flow A reduced, since many occurrences of flow *I* were not feasible and were eliminated by the tests in our approach. We then applied the profile S1 to flows *H* and *D*, but this did not further impact the WCTT of flow A since they did not intercept flow A more than the admissible number of times. The effects of applying profile S1 can be observed in the WCTT values corresponding to tests OptS1I, OptS1IH, OptS1IHD and OptS1All in Figure 6.16. The S2 profile, by nature limits the generation of packets further and additionally reduced the number of blockings of flows *I* and *H*. The profile S3 which is an extremely sparse packet

profile, caused a major impact by drastically reducing the number of blockings and the resulting WCTT decreased further. The effects of applying profile S3 can be observed in the WCTT values corresponding to tests OptS3I, OptS3IH, OptS3IHD and OptS3All in Figure 6.16.

6.9.6 Comparison with Related work

The proposed approach considers the impact due to direct and indirect blockings as in [147]. Unlike the works proposed by [135], [136], [137] or [138], it does not need any hardware support for predictability, which is commonly not present in existing platforms. Conversely our approach can be applied to a wider range of commercially available platforms. Furthermore, the proposed approach does not incur the delay of flushing out the preempted flits as done by pre-emption based techniques [151]. We make no assumptions on the state of the buffers as in Rehmati et.al [145] and do not restrict the model to flows generating periodically arriving packets only. Due to the $\text{MaxPktRel}(f, t)$ function, even flows which generate packets randomly can be captured and thus our analysis is not restricted to affine-arrival curves as in [142]. Through experiments we have demonstrated that our approach computes tighter bounds when compared with the approach of [146], which assumes a model that is closely related to ours. Additionally, the idea of retaining the history information of flows to prune further infeasible flows lends novelty to our approach and the concept of having SIRL as a tunable parameter makes the approach flexible.

6.10 Conclusions

In this chapter, we highlighted the problem of contention in a NoC as used in many-core architectures. We proposed a solution to compute the worst-case traversal time of a packet for such NoCs. This solution uses a branch and prune approach (BP) which improves on the work presented in [146] by leveraging the task characteristics and thereby provides tighter estimates on the computed WCTT. In order to tackle the complexity issues of BP in corner cases, we extended it to a branch, prune and collapse method (BPC), which via a configurable parameter provides a trade off between the computation time/memory usage and the WCTT tightness. A large set of experiments demonstrate the performance of the proposed algorithms in comparison with the approach of [146]. In particular, our work dominates their approach by yielding tighter WCTT estimates at the cost of extra computation time, the effects of which can be mitigated by the optimized version i.e. BPC. BPC on one hand limits the computational complexity, while on the other hand still provides the benefits of tighter WCTT bounds. Future work will focus on identifying the hot-spots in the network where a concentrated analysis effort promises substantial tightening of the results by our method. This work can be extended to identify safe criteria for dropping scenarios which provably do not contribute to the WCTT, or abstracting those, which do not promise substantial improvements in the results.

Chapter 7

Thesis Summary, Reflections and Future Work

*Once you have traveled, the voyage never ends,
but is played out over and over again in the
quietest chambers. The mind can never break off
from the journey.*

Pat Conroy

Real-time embedded system designers in many arenas are constantly facing competitive pressure to provide more application features and improve performance capabilities. As a result, it has become critical to master the ability to scale solutions and add features within embedded form factors without dramatically affecting energy variables such as power consumption and thermal output. Multicore systems have addressed these challenges by offering higher computing performance, reduced chip count and lower costs, with reduced power consumption. But multicore systems have yet to be certified and validated for their predictability, which features as an uncompromisable requirement for real-time systems. The major challenge has been the presence of shared hardware resources like the memory bus which poses a major hurdle to the timing analyzability of these systems. The aim of this thesis was to formulate new solutions and design methodologies which are clearly

required to analyze the impact of these shared resources. In this chapter we will summarize the work done and present the open areas of this research.

7.1 Summary of the work

7.1.1 Analysis of the impact of the shared bus in multicores

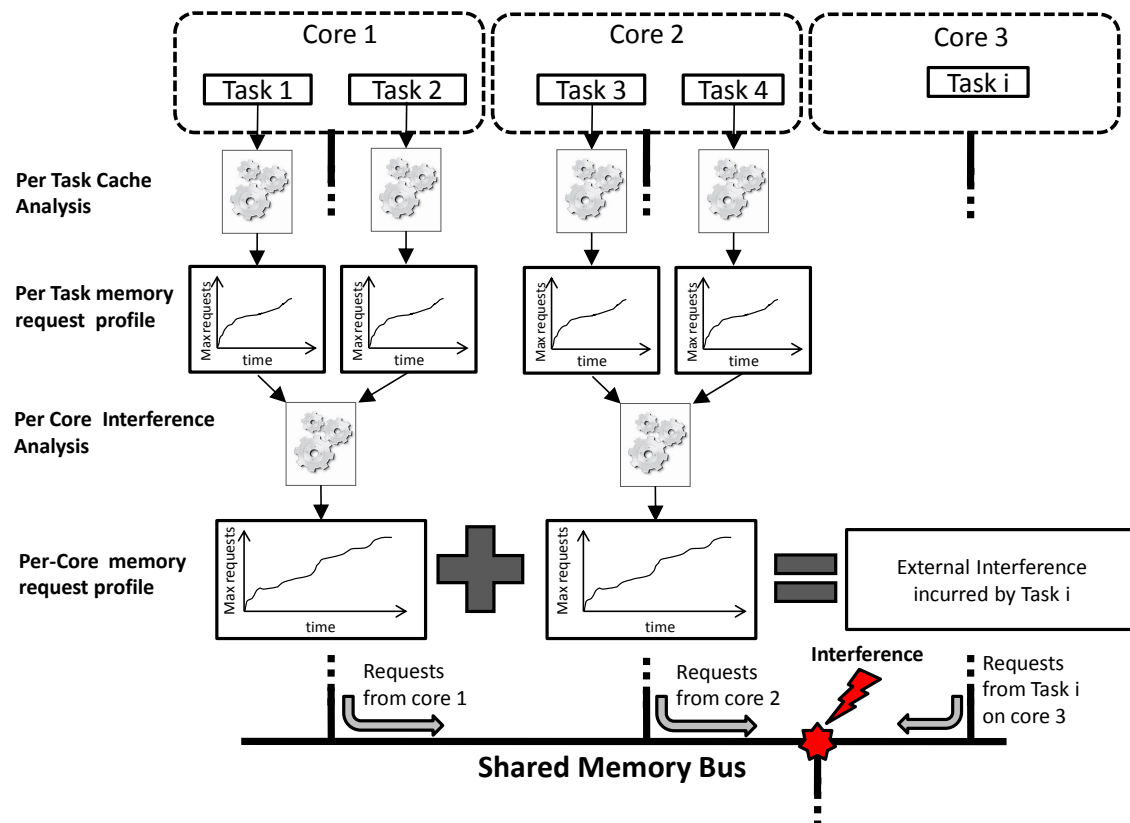


Figure 7.1: Different stages in the analysis

In this work, we followed a bottom up approach in computing the increased execution time that a task may incur, when contending for the shared bus. On the basis of the cache analysis of the tasks, we proposed two algorithms for deriving the *per-task memory request profile* and *per-core memory request profile* as illustrated in Figure 7.1 and discussed

in Chapter 3. Both the methods employed an interval splitting technique to reduce the search space (of job arrivals) that had to be investigated to arrive at the combination that can generate the maximum number of requests in a given time interval. It has been demonstrated that the bounds obtained for per-task profiles and per-core profiles are tighter than the existing state of the art. Also we believe that the problem of deriving the per-core interference has been dealt with in an elegant manner by using the interval splitting technique and transforming it to a knapsack problem, which is a novel solution to this approach.

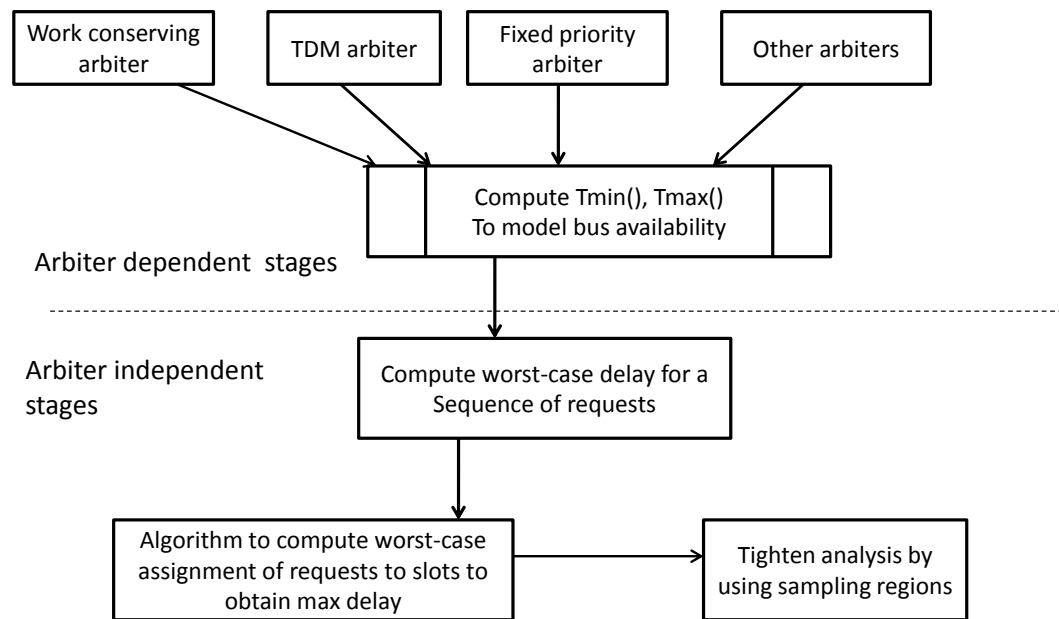


Figure 7.2: Stages of development of the unified framework

The tools developed in the earlier part of the work were critical in the development of a unified framework for analysis which we described in Chapter 4. They were instrumental in modeling the availability of the bus to a given task, given different arbitration models. The different stages of developing such a framework are described in Figure 7.2. The bus availability model facilitated the identification of potential free slots on the bus which the analyzed task could utilize. Considering that the exact arrival pattern of requests cannot be determined at design time, an algorithm was proposed to perform a request to free bus

slot mapping with the aim of maximizing the execution time of the analyzed task, due to the delay incurred on the shared bus. It was further shown that bounds can be tightened by dividing the task into sampling regions and analyzing the delay incurred in each of the regions. The highlight of the method was that it provided a general interface into which different arbiters can be seamlessly plugged to compute the resulting WCET of the tasks. We also demonstrated the applicability of our framework for two different arbiters: a non-work-conserving TDM arbiter and work-conserving fixed-priority arbiter.

7.1.2 Analysis of PCM based multi-core systems

In Chapter 5, we explored a multicore system in which Phase Change Memory (PCM) forms the main memory. As described earlier, what makes it different from the popular DRAM in terms of analysis is the wide difference in the time for completion of read and write operations. For such a system, researchers have proposed memory controller scheduling mechanisms to minimize core stall times, especially in the case of a time consuming write operation. Given such a controller and request scheduling mechanism, a method to compute the increase in the worst-case execution time of a task considering the contention on this shared memory was presented. The proposed method takes into consideration the different read and write latencies of the PCM controller, the priorities of the tasks, the request scheduling of the controller, and the interference arising from the co-executing tasks. The analysis was carried out in two main phases. In the first phase, the busy and the idle periods of the bus with respect to the analyzed task were determined. In the second phase, the requests were scheduled in the available idle periods of the bus, with the objective to maximize the overall execution time of the analyzed task. This work is important since it is the first analysis in this field, since previous works did not consider modeling the memory controller scheduling and assumed a constant access time for read and write accesses.

7.1.3 Analyzing the contention delay of a packet in many-core systems

Given that the shared bus architecture does not scale beyond a limited number of cores, “many-core” systems based on the NoC architecture have emerged. Chapter 6 highlights the problems of employing these systems for real-time applications and proposes a method to compute an upper bound on the traversal time of a packet when routed over the network

(on the chip) to its destination. The drawbacks of the existing approaches were highlighted first and then were overcome by modeling the flow characteristics (like the minimum inter-release time between packets) in the network and leveraging these vital characteristics to derive tighter estimates. We proposed two main algorithms: the Branch and Prune (BP) algorithm and the Branch, Prune and Collapse (BPC) algorithm. The BP algorithm provides a tight estimate by enumeration and early pruning of infeasible scenarios, but can be computationally intensive for a heavily loaded network. To tackle this problem, we propose the BPC algorithm that provides a tradeoff between complexity and tightness by providing a configurable parameter to the system designer. Both these approaches were validated by a set of experiments against the state of the art techniques and were shown to provide tighter bounds.

7.2 Limitations of current work and future directions

7.2.1 Support for preemptive tasks

The current analysis is done under the assumption that tasks cannot be preempted and will run to completion. But this rules out an important category of real-time applications in which tasks must be preemptible, and hence an analysis for such tasks is important. Consider a multicore system in which every core has its private cache. In such a scenario, a task which preempts a currently executing task may evict its cache lines. When the preempted task resumes, it may have to re-fetch the evicted cache lines from memory and thereby will incur an additional delay which is called Cache Related Preemption Delay (CRPD). Methods to compute this delay have been explored for uniprocessors and must be integrated in the current analysis.

This problem of computing the WCET, with such a model, is exacerbated in multicores, considering that re-fetching the (analyzed) preempted tasks' evicted caches increases the traffic on the bus and increases the interference. Hence, the analysis gets complex as we have a set of preemptible tasks on all cores and as a consequence computing the external interference on the shared bus will need to factor in all possible combinations of tasks and preemptions which is prohibitively expensive. To reduce the complexity of the analysis, a

feasible approach called the limited-preemption model can be employed, in which preemptions are allowed only at specifically marked points during a task execution. Such a model provides for tighter bounds, besides reducing the complexity.

7.2.2 Timing Analysis of many core systems.

The many-core area offers a range of unexplored problems. In the work that we presented, we assumed the presence of a single virtual channel. Some systems also allow the creation of multiple channels by having multiple buffers at the input ports of each router. In a scenario in which the flits of a packet are blocked due to congestion ahead, some other packet may transmit their flits and save it into the alternative buffers. Some book-keeping regarding which channels belong to each packet must be maintained, but the performance of these systems is better since it facilitates higher network utilization.

Another interesting feature in many-core systems like Tiler is that they offer the possibility of clustering cores and restricting traffic across cores using hardwalls. These capabilities can be leveraged to group tasks of different criticalities in various clusters and reserve resources in a manner to satisfy their quality of service requirements.

Many core systems generally have a non-uniform memory access model in which the memory controllers are placed on the periphery of the grid. Cores which are closer to the controllers incur a lower latency in memory access. Analyzing the traversal time of a packet between the core and the memory, given such a topology has its own challenges. In the same vein, mapping tasks to cores to ensure that all packets are delivered to the destination within pre-set deadlines is another interesting area of exploration.

7.2.3 DRAM and PCM hierarchy

The analysis carried out in this thesis is the first step in the analysis of memory systems with asymmetric read and write latencies and had a strong assumption that considered PCM as the main memory. But a more practical off-chip hierarchy is when PCM complements DRAM as the main memory. When data is not found in the cache, the DRAM is first consulted and then the PCM memory is consulted. This analysis will have its own challenges and will have to consider the scheduling of requests at the DRAM memory controller and the PCM memory controller.

7.2.4 WCET analysis in identical and heterogeneous multicores

Identical multicores which have the same ISA (instruction set architecture) but with asymmetric cores w.r.t performance, comprising of both simple and complex cores, have recently been proposed to cater to the quality of service requirements of different tasks. The processors in an asymmetric multi-core architecture share the same ISA but their micro-architectures (pipeline and caches) are very different. For example, ARM has recently announced big.LITTLE processing for mobile platforms where high-performance, out-of-order (bigger) Cortex A-15 cores with a 15-stage pipeline are integrated with energy-efficient, in-order (smaller) Cortex A-7 cores, armed with a 8 stage pipeline in the same chip. The execution time will correspondingly be different, depending on the processors on which the task is assigned. Additionally if the cores share the same hardware resources, then the delay due to contention has to be factored in the overall execution time of the task. The same is true for heterogeneous multicores in which the cores are specifically designed to handle special functions and therefore differ in their ISA as well as clock speeds –Examples of such systems are the GPGPU's from NVidia and OMAP processors from Texas Instruments. Analyzing the execution time of tasks in such systems is another unexplored area.

7.2.5 WCET and parallelization

The parallelization of software poses a number of difficulties, particularly when deriving its WCET for an application. A fundamental difference when software is executed in parallel is the need for the communication between different cores, either to exchange data to be processed and to perform synchronization to ensure that the final results are consistent. Even an operation as straightforward as writing a value into a shared variable and then reading it back involves some communication if the components reading and writing are executed on different cores. These effects must be factored in the eventual analysis.

7.2.6 End Notes

Although intelligent software based techniques can alleviate the existing challenges in employing multicores for real-time systems, it will take an equal effort from the industry to help build more predictable systems as well. Additionally, it holds for all system designers, that the true benefits of multicores can be leveraged only by studying their architecture

and understanding the causes of average-case performance degradation, and then designing applications accordingly to efficiently harness the inherent parallelism. Real-time system designers in particular, need to be able to analyze the worst-case degradation that an application may suffer in the context of their temporal behaviour. The results from the work done so far has been a strong motivator to strive towards the ultimate aim of contributing towards building a stronger timing analysis tool and this thesis has been an endeavor towards that aim.

Bibliography

- [1] T. D. Morton, *Embedded Microcontrollers*. Prentice Hall Publishers, 2001.
- [2] J. Hale, “Smarter sensor processing for UAS payloads.”
<http://mil-embedded.com/articles/smarter-sensor-processing-uas-payloads/>.
- [3] P. Koopman, “Embedded system design issues (the rest of the story),” in *Proceedings of the 1996 International Conference on Computer Design, VLSI in Computers and Processors*, ICCD '96, pp. 310–, IEEE Computer Society, 1996.
- [4] S. Baruah and J. Goossens, *Scheduling Real-time Tasks: Algorithms and Complexity*, 2003.
- [5] D. Isovich and G. Fohler, “Efficient scheduling of sporadic, aperiodic, and periodic tasks with complex constraints,” in *Real-Time Systems Symposium, 2000. Proceedings. The 21st IEEE*, pp. 207 –216, 2000.
- [6] R. Mall, *Real-Time Systems: Theory and Practice*. Pearson Power, 2007.
- [7] S. K. Baruah, “The non-preemptive scheduling of periodic tasks upon multiprocessors,” *Real-Time Syst.*, vol. 32, pp. 9–20, Feb. 2006.
- [8] B. Akesson, A. Molnos, A. Hansson, J. Ambrose Angelo, and K. Goossens, “Composability and predictability for independent application development, verification, and execution,” in *Multiprocessor System-on-Chip: Hardware Design and Tool Integration* (M. Hübner and J. Becker, eds.), pp. 25–56, Springer Verlag, November 2010.

- [9] C. Berg, J. Engblom, and R. Wilhelm, "Requirements for and design of a processor with predictable timing," in *Perspectives Workshop: Design of Systems with Predictable Behaviour, 16.-19. November 2003, volume 03471 of Dagstuhl Seminar Proceedings. IBFI, Schloss Dagstuhl*, 2004.
- [10] R. Wilhelm, J. Engblom, A. Ermedahl, N. Holsti, S. Thesing, D. Whalley, G. Bernat, C. Ferdinand, R. Heckmann, T. Mitra, F. Mueller, I. Puaut, P. Puschner, J. Staschulat, and P. Stenström, "The worst-case execution-time problem – overview of methods and survey of tools," *ACM Trans. Embed. Comput. Syst.*, vol. 7, pp. 36:1–36:53, 2008.
- [11] H. Kopetz, "An integrated architecture for dependable embedded systems," in *Proceedings of the 23rd IEEE International Symposium on Reliable Distributed Systems, SRDS '04*, pp. 160–161, IEEE Computer Society, 2004.
- [12] S. Chakraborty, M. Lukasiewicz, C. Buckl, S. Fahmy, N. Chang, S. Park, Y. Kim, P. Leteinturier, and H. Adlkofer, "Embedded systems and software challenges in electric vehicles," in *Design, Automation Test in Europe Conference Exhibition (DATE), 2012*, pp. 424–429, 2012.
- [13] J. Ramsey, "Integrated Modular Avionics: Less is More," 2007.
http://www.aviationtoday.com/av/commercial/Integrated-Modular-Avionics-Less-is-More_8420.html#.UoUIAI9IUak.
- [14] V. Tran, D.-B. Liu, and B. Hummel, "Component-based systems development: challenges and lessons learned," in *Software Technology and Engineering Practice, 1997. Proceedings., Eighth IEEE International Workshop on [incorporating Computer Aided Software Engineering]*, pp. 452–462, jul 1997.
- [15] S. Keckler, O. Olukotun, and H. Hofstee, *Multicore Processors and Systems. Integrated Circuits and Systems*, Springer London, Limited, 2009.
- [16] R. I. Davis and A. Burns, "A survey of hard real-time scheduling for multiprocessor systems," *ACM Comput. Surv.*, vol. 43, pp. 35:1–35:44, Oct. 2011.

- [17] L. Seiler, D. Carmean, E. Sprangle, T. Forsyth, M. Abrash, P. Dubey, S. Junkins, A. Lake, J. Sugerman, R. Cavin, R. Espasa, E. Grochowski, T. Juan, and P. Hanrahan, "Larrabee: a many-core x86 architecture for visual computing," *ACM Trans. Graph.*, vol. 27, pp. 18:1–18:15, Aug. 2008.
- [18] Techopedia, "Multicore," 2006.
[//http://www.techopedia.com/definition/5305/multicore](http://www.techopedia.com/definition/5305/multicore).
- [19] Intel Corporation, *Intel 4 Series Chipset Family Datasheet, For the Intel 82Q45, 82Q43, 82B43, 82G45, 82G43, 82G41 Graphics and Memory Controller Hub (GMCH) and the Intel® 82P45, 82P43 Memory Controller Hub (MCH)*, 2010.
- [20] S. Zhuravlev, S. Blagodurov, and A. Fedorova, "Addressing shared resource contention in multicore processors via scheduling," *SIGPLAN Not.*, vol. 45, no. 3, pp. 129–142, 2010.
- [21] D. Wentzlauff, P. Griffin, H. Hoffmann, L. Bao, B. Edwards, C. Ramey, M. Mattina, C.-C. Miao, J. F. B. III, and A. Agarwal, "On-chip interconnection architecture of the tile processor," *IEEE Micro*, vol. 27, pp. 15–31, 2007.
- [22] Kalray, "Kalray MPPA 256 ."
<http://www.kalray.eu/products/mppa-manycore/mppa-256/>.
- [23] Intel, "Intel Xeon Phi Coprocessor ."
<http://www-ssl.intel.com/content/dam/www/public/us/en/documents/datasheets/xeon-phi-coprocessor-datasheet.pdf>.
- [24] Intel, "The single-chip-cloud computer," 2010.
<http://www.intel.com/content/dam/www/public/us/en/documents/technology-briefs/intel-labs-single-chip-cloud-article.pdf>.
- [25] L. Benini and G. De Micheli, "Networks on chips: a new soc paradigm," *Computer*, vol. 35, pp. 70 –78, jan 2002.
- [26] "Market Applications of Phase Change Memory (PCM)."
<http://ovonyx.com/technology/market-applications-of-phase-change-memory-pcm.html>.

- [27] S. Mohan, M. Caccamo, L. Sha, R. Pellizzoni, G. Arundale, R. Kegley, and D. de Niz, "Using multicore architectures in cyber-physical systems," *Workshop on Developing Dependable and Secure Automotive Cyber-Physical Systems from Components.*, 2011.
- [28] N. R. Storey, *Safety Critical Computer Systems*. Addison-Wesley Longman Publishing Co., Inc., 1996.
- [29] ISO26262-4, *Road vehicles – Functional safety – Part 4: Product development at the system level*, 1 ed., 2011.
- [30] IEC 61508, *Functional safety of electrical/electronic/programmable electronic safety-related systems*, 2010.
- [31] RECOMP, "Reduced Certification Costs Using Trusted Multi-core Platforms ." <http://atcproyectos.ugr.es/recomp/>.
- [32] MERASA, "Multi-Core Execution of Hard Real-Time Applications Supporting Analysability ." <http://ginkgo.informatik.uni-augsburg.de/merasa-web/>.
- [33] ARAMiS, "Automotive, Railway and Avionics multicore systems." <http://www.projekt-aramis.de/index.php>.
- [34] C. E. Salloum, "A New Generation of Multi-Core Processors Designed for Safety-Critical Embedded Systems ." <http://www.across-project.eu/>.
- [35] CESAR, "Cost-efficient methods and processes for safety relevant embedded systems ." <http://www.cesarproject.eu/index.php?id=6>.
- [36] J. Gustafsson and A. Ermedahl, "Experiences from applying wcet analysis in industrial settings," in *ISORC*, pp. 382–392, IEEE Computer Society, 2007.
- [37] Rapita Systems Ltd., "Rapitime explained." http://www.rapitasystems.com/downloads/rapitime_explained_white_paper".

- [38] P. Lokuciejewski and P. Marwedel, “Summary and future work,” in *Worst-Case Execution Time Aware Compilation Techniques for Real-Time Systems*, Embedded Systems, pp. 229–234, Springer Netherlands, 2011.
- [39] C. Ferdinand, R. Heckmann, and B. Franzen, “Static memory and timing analysis of embedded systems code,” in *Proceedings of VVSS2007 - 3rd European Symposium on Verification and Validation of Software Systems, 23rd of March 2007, Eindhoven* (P. Groot, ed.), 2007.
- [40] N. Holsti and S. Saarinen, “Status of the Bound-T WCET tool,” in *2nd International Workshop on Worst-Case Execution Time Analysis (WCET’2002)*, 2002.
- [41] X. Li, Y. Liang, T. Mitra, and A. Roychoudhury, “Chronos: A timing analyzer for embedded software,” in *Science of Computer Programming*, 2007.
- [42] “Heptane.”
<http://www.irisa.fr/aces/work/heptane-demo/heptane.html>.
- [43] A. Ermedahl, *A Modular Tool Architecture for Worst-Case Execution Time Analysis*. VDM Verlag, 2008.
- [44] R. Kirner, P. Puschner, and I. Wenzel, “Measurement-based worst-case execution time analysis using automatic test-data generation,” in *Proc. 4th Euromicro International Workshop on WCET Analysis*, pp. 67–70, June 2004.
- [45] “Bus Computing.”
[http://en.wikipedia.org/wiki/Bus_\(computing\)](http://en.wikipedia.org/wiki/Bus_(computing)).
- [46] “Bus and Bits.”
<http://blog.teachbook.com.au/index.php/computer-science/1-0-hardware-overview/bus-bits/>.
- [47] D. J. Sorin, M. D. Hill, and D. A. Wood, *A Primer on Memory Consistency and Cache Coherence*. Morgan & Claypool Publishers, 1st ed., 2011.
- [48] *Optimizing Application Performance on Intel Core Microarchitecture Using Hardware-Implemented Prefetchers*.

- [49] T. Noergaard, *Embedded Systems Architecture: A Comprehensive Guide for Engineers and Programmers*. Newnes, 2005.
- [50] R. Wilhelm, D. Grund, J. Reineke, M. Schlickling, M. Pister, and C. Ferdinand, “Memory hierarchies, pipelines, and buses for future architectures in time-critical embedded systems,” *IEEE Transactions on Computer-Aided Design of Integrated Circuits and Systems*, vol. 28, pp. 966–978, July 2009.
- [51] J. Reineke, D. Grund, C. Berg, and R. Wilhelm, “Timing predictability of cache replacement policies,” *Real-Time Systems*, vol. 37, pp. 99–122, Nov. 2007.
- [52] C. Ferdinand and R. Wilhelm, “Efficient and precise cache behavior prediction for real-time systems,” *Real-Time Systems*, vol. 17, pp. 131–181, 1999.
- [53] T. King, “Cache partitioning increases CPU utilization for safety-critical multicore applications.”
<http://mil-embedded.com/articles/cache-utilization-safety-critical-multicore-applications/#>.
- [54] JEDEC Solid State Technology Association, *DDR3 SDRAM Specification*, JESD79-3E ed., July 2010.
- [55] B. Jacob, N. G. Spencer, and D. Wang, *Memory Systems Cache, DRAM, Disk*, pp. 497–520. Morgan Kaufmann, 2007.
- [56] S. Rixner, W. J. Dally, U. J. Kapasi, P. Mattson, and J. D. Owens, “Memory access scheduling,” in *ISCA '00: Proceedings of the 27th annual international symposium on Computer architecture*, pp. 128–138, 2000.
- [57] B. Akesson and K. Goossens, “Architectures and modeling of predictable memory controllers for improved system integration,” in *Design, Automation Test in Europe Conference Exhibition (DATE), 2011*, pp. 1–6, 2011.
- [58] M. Paolieri, E. Quinones, F. Cazorla, and M. Valero, “An Analyzable Memory Controller for Hard Real-Time CMPs,” *Embedded Systems Letters, IEEE*, vol. 1, no. 4, pp. 86–90, 2009.

- [59] J. Reineke, I. Liu, H. Patel, S. Kim, and E. A. Lee, "PRET DRAM Controller: Bank Privatization for Predictability and Temporal Isolation," in *CODES+ISSS '11: Proceedings of the IEEE/ACM international conference on Hardware/software codesign and system synthesis*, pp. 99–108, Oct. 2011.
- [60] J. Dodd, "Adaptive page management," July 2006. US Patent 7,076,617.
- [61] S. Goossens, B. Akesson, and K. Goossens, "Conservative Open-page Policy for Mixed Time-Criticality Memory Controllers," in *Proc. Design, Automation and Test in Europe Conference and Exhibition (DATE)*, pp. 525–530, 2013.
- [62] O. Mutlu and T. Moscibroda, "Parallelism-Aware Batch Scheduling: Enabling High-Performance and Fair Shared Memory Controllers," *IEEE Micro*, vol. 29, no. 1, pp. 22–32, 2009.
- [63] J. Shao and B. Davis, "A burst scheduling access reordering mechanism," in *Proceedings of the 13th International Symposium on High-Performance Computer Architecture*, pp. 285–294, 2007.
- [64] S. Heithecker and R. Ernst, "Traffic shaping for an FPGA based SDRAM controller with complex QoS requirements," pp. 575–578, 2005.
- [65] S. Whitty and R. Ernst, "A bandwidth optimized SDRAM controller for the MORPHEUS reconfigurable architecture," in *Proceedings of the Parallel and Distributed Processing Symposium (IPDPS)*, 2008.
- [66] A. Burchard, E. Hekstra-Nowacka, and A. Chauhan, "A real-time streaming memory controller," pp. 20–25, 2005.
- [67] C. Macian, S. Dharmapurikar, and J. Lockwood, "Beyond performance: Secure and fair memory management for multiple systems on a chip," in *IEEE International Conference on Field-Programmable Technology (FPT)*, pp. 348–351, 2003.
- [68] W.-D. Weber, *Efficient Shared DRAM Subsystems for SOCs*. Sonics, Inc, 2001. White paper.

- [69] K. Lee, T. Lin, and C. Jen, “An efficient quality-aware memory controller for multi-media platform SoC,” vol. 15, no. 5, pp. 620–633, 2005.
- [70] S. Novak, J. Peck Jr, and S. Waldron, “Method and apparatus for optimizing memory performance with opportunistic refreshing,” Nov. 2000. US Patent 6,147,921.
- [71] S. Biswas, “Refresh-ahead and burst refresh preemption technique for managing dram in computer system,” May 1999. US Patent 5,907,857.
- [72] J. Rosen, A. Andrei, P. Eles, and Z. Peng, “Bus access optimization for predictable implementation of real-time applications on multiprocessor systems-on-chip,” in *RTSS '07: Proceedings of the 28th IEEE International Real-Time Systems Symposium*, pp. 49–60, IEEE Computer Society, 2007.
- [73] S. Chattopadhyay, A. Roychoudhury, and T. Mitra, “Modeling shared cache and bus in multi-cores for timing analysis,” in *Proceedings of the 13th International Workshop on Software & Compilers for Embedded Systems*, pp. 6:1–6:10, 2010.
- [74] T. Kelter, H. Falk, P. Marwedel, S. Chattopadhyay, and A. Roychoudhury, “Bus-Aware Multicore WCET Analysis through TDMA Offset Bounds,” in *Proceedings of the 2011 Euromicro Conference on Real-Time Systems*, pp. 3 –12, 2011.
- [75] A. Schranzhofer, J.-J. Chen, and L. Thiele, “Timing analysis for TDMA arbitration in resource sharing systems,” in *16th IEEE Real-Time and Embedded Technology and Applications Symposium*, pp. 215–224, 2010.
- [76] A. Schranzhofer, R. Pellizzoni, J.-J. Chen, L. Thiele, and M. Caccamo, “Timing analysis for resource access interference on adaptive resource arbiters,” in *Real-Time and Embedded Technology and Applications Symposium*, 2011.
- [77] M. Lv, W. Yi, N. Guan, and G. Yu, “Combining abstract interpretation with model checking for timing analysis of multicore software,” in *Proceedings of the 2010 31st IEEE Real-Time Systems Symposium*, RTSS '10, pp. 339–349, 2010.
- [78] A. Gustavsson, A. Ermedahl, B. Lisper, and P. Pettersson, “Towards WCET analysis of multicore architectures using UPPAAL,” in *WCET*, pp. 101–112, 2010.

- [79] R. Pellizzoni, A. Schranzhofer, J.-J. Chen, M. Caccamo, and L. Thiele, “Worst case delay analysis for memory interference in multicore systems,” in *Conference on Design, Automation and Test in Europe*, pp. 741–746, 2010.
- [80] S. Schliecker, M. Negrean, and R. Ernst, “Bounding the shared resource load for the performance analysis of multiprocessor systems,” in *Proceedings of the Conference on Design, Automation and Test in Europe*, pp. 759–764, 2010.
- [81] M. A. Marsan, G. Balbo, G. Conte, and F. Gregoretti, “Modeling bus contention and memory interference in a multiprocessor system,” *IEEE Trans. Comput.*, vol. 32, no. 1, pp. 60–72, 1983.
- [82] M. Paolieri, E. Qui nones, F. J. Cazorla, G. Bernat, and M. Valero, “Hardware support for wcet analysis of hard real-time multicore systems,” in *ISCA '09: Proceedings of the 36th annual international symposium on Computer architecture*, pp. 57–68, ACM, 2009.
- [83] J. Yan and W. Zhang, “WCET analysis for multi-core processors with shared L2 instruction caches,” in *RTAS '08: Proceedings of the 2008 IEEE Real-Time and Embedded Technology and Applications Symposium*, pp. 80–89, 2008.
- [84] Y. Ding and W. Zhang, “Static analysis of worst-case inter-core communication latency in cmps with 2d-mesh noc,” in *Proceedings of the 2012 WiP session of LCTES*, 2012.
- [85] Y. Li, V. Suhendra, Y. Liang, T. Mitra, and A. Roychoudhury, “Timing analysis of concurrent programs running on shared cache multi-cores,” in *Real-Time Systems Symposium, 2009, RTSS 2009. 30th IEEE*, pp. 57–67, dec. 2009.
- [86] V. Suhendra and T. Mitra, “Exploring locking & partitioning for predictable shared caches on multi-cores,” in *DAC '08: Proceedings of the 45th annual Design Automation Conference*, pp. 300–303, ACM, 2008.
- [87] N. Guan, M. Stigge, W. Yi, and G. Yu, “Cache-aware scheduling and analysis for multicores,” in *Proceedings of the seventh ACM international conference on Embedded software*, pp. 245–254, 2009.

- [88] G. Taylor, P. Davies, and M. Farmwald, "The tlb slice—a low-cost high-speed address translation mechanism," in *ISCA '90: Proceedings of the 17th annual international symposium on Computer Architecture*, pp. 355–363, ACM, 1990.
- [89] D. Hardy, T. Piquet, and I. Puaut, "Using bypass to tighten WCET estimates for multi-core processors with shared instruction caches," in *Proceedings of the 2009 30th IEEE Real-Time Systems Symposium*, pp. 68–77, 2009.
- [90] J. Rosén, A. Andrei, P. Eles, and Z. Peng, "Bus access optimization for predictable implementation of real-time applications on multiprocessor systems-on-chip," in *Proceedings of the Real-Time Systems Symposium*, pp. 49–60, 2007.
- [91] D. Dasari, B. Andersson, V. Nelis, S. M. Petters, A. Easwaran, and J. Lee, "Response time analysis of COTS-based multicores considering the contention on the shared memory bus," in *IEEE 10th International Conference on Trust, Security and Privacy in Computing and Communications*, pp. 1068–1075, nov. 2011.
- [92] R. J. Bril, J. J. Lukkien, and W. F. Verhaegh, "Worst-case response time analysis of real-time tasks under fixed-priority scheduling with deferred preemption," *Real-Time Systems*, vol. 42, pp. 63–119, August 2009.
- [93] K. Tindell, A. Burns, and A. Wellings, "Calculating controller area network (can) message response times," *Control Engineering Practice*, vol. 3, no. 8, pp. 1163–1169, 1995.
- [94] B. Sprunt, "The basics of performance-monitoring hardware," *IEEE Micro*, vol. 22, no. 4, pp. 64–71, 2002.
- [95] K. W. Tindell, A. Burns, and A. J. Wellings, "An extendible approach for analyzing fixed priority hard real-time tasks," *Real-Time Systems*, vol. 6, pp. 133–151, March 1994.
- [96] A. V. Goldberg and A. Marchetti-Spaccamela, "On finding the exact solution of a zero-one knapsack problem," in *Proceedings of the sixteenth annual ACM symposium on Theory of computing*, STOC '84, pp. 359–368, ACM, 1984.

- [97] T. H. Cormen, C. E. Leiserson, R. L. Rivest, and C. Stein, *Introduction to Algorithms, 2nd Ed.* McGraw-Hill, 2001.
- [98] J. Carpenter, S. Funk, P. Holman, A. Srinivasan, J. Anderson, and S. Baruah, *A Categorization of Real-time Multiprocessor Scheduling Problems and Algorithms*, ch. 30. Chapman & Hall/CRC, 2004.
- [99] C. L. Liu and J. W. Layland, "Scheduling algorithms for multiprogramming in a hard-real-time environment," *J. ACM*, vol. 20, pp. 46–61, Jan. 1973.
- [100] J. Goossens and R. Devillers, "The non-optimality of the monotonic priority assignments for hard real-time offset free systems," *Real-Time Systems*, vol. 13, pp. 107–126, 1997.
- [101] M. Zhou, S. Bock, A. Ferreira, B. Childers, R. Melhem, and D. Mosse, "Real-time scheduling for phase change main memory systems," in *TrustCom, ICCESS11*, pp. 991–998, nov. 2011.
- [102] H. Shah, A. Raabe, and A. Knoll, "Priority division: A high-speed shared-memory bus arbitration with bounded latency," in *Design, Automation Test in Europe Conference Exhibition (DATE), 2011*, pp. 1–4, march 2011.
- [103] S. Raoux, G. W. Burr, M. J. Breitwisch, C. T. Rettner, Y.-C. Chen, R. M. Shelby, M. Salinga, D. Krebs, S.-H. Chen, H.-L. Lung, and C. H. Lam, "Phase-change random access memory: A scalable technology," *IBM Journal of Research and Development*, vol. 52, pp. 465–479, july 2008.
- [104] A. P. Ferreira, B. R. Childers, R. G. Melhem, D. Mossé, and M. Yousif, "Using pcm in next-generation embedded space applications," in *IEEE Real-Time and Embedded Technology and Applications Symposium*, pp. 153–162, 2010.
- [105] B. C. Lee, E. Ipek, O. Mutlu, and D. Burger, "Architecting phase change memory as a scalable dram alternative," in *Proceedings of the 36th annual international symposium on Computer architecture*, ISCA '09, pp. 2–13, ACM, 2009.

- [106] S. Schliecker and R. Ernst, “Real-time performance analysis of multiprocessor systems with shared memory,” *ACM Transactions in Embedded Computing Systems*, vol. 10, pp. 22:1–22:27, 2011.
- [107] Y. Hara, H. Tomiyama, S. Honda, H. Takada, and K. Ishii, “Chstone: A benchmark program suite for practical c-based high-level synthesis,” in *ISCAS*, pp. 1192–1195, 2008.
- [108] *VxWorks Applications Programmers Guide, 6.8*.
- [109] Intel Corp., *Intel 64 and IA-32 Architecture Software Developers Manual Volume 3B: System Programming Guide, Part 2*.
- [110] M. R. Guthaus, J. S. Ringenberg, D. Ernst, T. M. Austin, T. Mudge, and R. B. Brown, “Mibench: A free, commercially representative embedded benchmark suite,” in *WWC '01: Proceedings of the Workload Characterization, 2001. WWC-4. 2001 IEEE International Workshop*, pp. 3–14, IEEE Computer Society, 2001.
- [111] J. Gustafsson, A. Betts, A. Ermedahl, and B. Lisper, “The Mälardalen WCET benchmarks – past, present and future,” pp. 137–147, OCG, July 2010.
- [112] B. Akesson, A. Hansson, and K. Goossens, “Composable resource sharing based on latency-rate servers,” in *Digital System Design, Architectures, Methods and Tools, 2009. DSD'09. 12th Euromicro Conference on*, pp. 547–555, IEEE, Aug. 2009.
- [113] H. Shah, A. Raabe, and A. Knoll, “Bounding wcet of applications using sdram with priority based budget scheduling in mpsoCs,” in *Design, Automation Test in Europe Conference Exhibition (DATE), 2012*, pp. 665–670, 2012.
- [114] Z. P. Wu, Y. Krish, and R. Pellizzoni, “Worst case analysis of dram latency in multi-requestor systems,” in *Proc. of IEEE Real-Time Systems Symposium*, 2013.
- [115] H. Yun, G. Yao, R. Pellizzoni, M. Caccamo, and L. Sha, “Memory access control in multiprocessor for real-time systems with mixed criticality,” in *Real-Time Systems (ECRTS), 2012 24th Euromicro Conference on*, pp. 299–308, 2012.

- [116] M. Behnam, R. Inam, T. Nolte, and M. Sjodin, "Multi-core composability in the face of memory-bus contention," in *Proceedings of the 5th Workshop on Compositional Theory and Technology for Real-Time Embedded Systems (CRTS)*, 2012.
- [117] D. Dasari and V. Nelis, "An analysis of the impact of bus contention on the wcet in multicores," in *IEEE 9th International Conference on Embedded Software and Systems (HPC-ICESS)*, pp. 1450–1457, june 2012.
- [118] T. Austin, E. Larson, and D. Ernst, "SimpleScalar: An infrastructure for computer system modeling," *Computer*, vol. 35, no. 2, pp. 59–67, 2002.
- [119] JEDEC Solid State Technology Association, *DDR3 SDRAM Specification*, JESD79-3F ed., 2012.
- [120] "Phase Change Memory: Altered states."
<http://www.economist.com/node/21560981>.
- [121] J. Handy, "Phase Change Memory will Change Memory System Design."
<http://www.rtcmagazine.com/articles/view/101556>.
- [122] "Phase Change Memory."
<http://www.pdl.cmu.edu/SDI/2009/slides/Numonyx.pdf>.
- [123] C. Lee, M. Potkonjak, and W. Mangione-Smith, "Mediabench: a tool for evaluating and synthesizing multimedia and communications systems," in *Microarchitecture, 1997. Proceedings., Thirtieth Annual IEEE/ACM International Symposium on*, pp. 330–335, dec 1997.
- [124] B. C. Lee, E. Ipek, O. Mutlu, and D. Burger, "Architecting phase change memory as a scalable dram alternative," in *ISCA '09*, pp. 2–13, ACM, 2009.
- [125] M. K. Qureshi, V. Srinivasan, and J. A. Rivers, "Scalable high performance main memory system using phase-change memory technology," ISCA '09.
- [126] A. P. Ferreira, B. Childers, R. Melhem, D. Mosse, and M. Yousif, "Using PCM in next-generation embedded space applications," in *RTAS '10*, IEEE Computer Society, 2010.

- [127] P. Zhou, B. Zhao, J. Yang, and Y. Zhang, “A durable and energy efficient main memory using phase change memory technology,” in *ISCA '09*, pp. 14–23, ACM, 2009.
- [128] W. Zhang and T. Li, “Exploring phase change memory and 3d die-stacking for power/thermal friendly, fast and durable memory architectures,” in *PACT '09*, pp. 101–112, 2009.
- [129] M. K. Qureshi, M. Franceschini, and L. A. Lastras-Montaña, “Improving read performance of phase change memories via write cancellation and write pausing,” in *HPCA*, pp. 1–11, 2010.
- [130] P. S. Magnusson, M. Christensson, J. Eskilson, D. Forsgren, G. Hållberg, J. Högberg, F. Larsson, A. Moestedt, and B. Werner, “Simics: A full system simulation platform,” *Computer*, vol. 35, pp. 50–58, Feb. 2002.
- [131] B. Bishop, T. Kelliher, and M. Irwin, “A detailed analysis of mediabench,” in *Signal Processing Systems, 1999. SiPS 99. 1999 IEEE Workshop on*, pp. 448 –455, 1999.
- [132] W. Dally, “Virtual-channel flow control,” *IEEE Transactions on Parallel and Distributed Systems*, vol. 3, pp. 194 –205, mar 1992.
- [133] W. Dally and C. Seitz, “The torus routing chip,” *Distributed Computing*, vol. 1, pp. 187 –196, 1986.
- [134] J. T. Draper and J. Ghosh, “A comprehensive analytical model for wormhole routing in multicomputer systems,” *J. Parallel Distrib. Comput.*, vol. 23, pp. 202–214, Nov. 1994.
- [135] J. Diemer and R. Ernst, “Back suction: Service guarantees for latency-sensitive on-chip networks,” in *Fourth ACM/IEEE International Symposium on Networks-on-Chip (NOCS)*, pp. 155 –162, 2010.
- [136] Z. Shi and A. Burns, “Real-time communication analysis for on-chip networks with wormhole switching,” in *Networks-on-Chip, 2008. Second ACM/IEEE International Symposium on*, pp. 161 –170, april 2008.

- [137] C. Paukovits and H. Kopetz, "Concepts of switching in the time-triggered network-on-chip," in *14th IEEE International Conference on Embedded and Real-Time Computing Systems and Applications*, pp. 120–129, 2008.
- [138] K. Goossens, J. Dielissen, and A. Radulescu, "Aethereal network on chip: concepts, architectures, and implementations," *Design Test of Computers, IEEE*, vol. 22, no. 5, pp. 414–421, 2005.
- [139] "Survey of network-on-chip proposals," March 2008.
- [140] T. Ferrandiz, F. Frances, and C. Fraboul, "A sensitivity analysis of two worst-case delay computation methods for spacewire networks," in *Euromicro Conference on Real-Time Systems*, pp. 47–56, 2012.
- [141] J.-Y. L. Boudec and P. Thiran, "Network calculus - a theory of deterministic queuing systems for the internet," in *Lecture Notes in Computer Science, LNCS*, Springer Verlag, 2004.
- [142] Y. Qian, Z. Lu, and W. Dou, "Analysis of worst-case delay bounds for on-chip packet-switching networks," *IEEE Transactions on Computer-Aided Design of Integrated Circuits and Systems*, vol. 29, pp. 802–815, may 2010.
- [143] T. Ferrandiz, F. Frances, and C. Fraboul, "Using network calculus to compute end-to-end delays in spacewire networks," *SIGBED Rev.*, vol. 8, pp. 44–47, Sept. 2011.
- [144] S. Lee, "Real-time wormhole channels," *Journal Of Parallel And Distributed Computing*, vol. 63, pp. 299–311, 2003.
- [145] D. Rahmati, S. Murali, L. Benini, F. Angiolini, G. De Micheli, and H. Sarbazi-Azad, "A method for calculating hard QoS guarantees for networks-on-chip," in *Computer-Aided Design - Digest of Technical Papers, IEEE/ACM International Conference on*, pp. 579–586, 2009.
- [146] T. Ferrandiz, F. Frances, and C. Fraboul, "A method of computation for worst-case delay analysis on spacewire networks," in *IEEE International Symposium on Industrial Embedded Systems*, pp. 19–27, 2009.

- [147] Z. Lu, A. Jantsch, and I. Sander, “Feasibility analysis of messages for on-chip networks using wormhole routing,” pp. 960–964, 2005.
- [148] Intel, “SCC External Architecture Specification .”
<http://www.intel.com/content/www/us/en/research/intel-labs-single-chip-cloud-architecture-brief.html/>.
- [149] “Tile processor: user architecture manual,” May 2011.
- [150] J. Hu and R. Marculescu, “Energy-aware mapping for tile-based noc architectures under performance constraints,” in *8th Design Automation Conference*, pp. 233–239, 2003.
- [151] K. Knauber and B. Chen, “Supporting preemption in wormhole networks,” in *The Twenty-Third Annual International Computer Software and Applications Conference, COMPSAC*, pp. 232 –238, 1999.